Cape Peninsula
University of Technology

ANALYSIS OF HYDROMAGNETIC BOUNDARY LAYER FLOW AND HEAT TRANSFER OF NANOFLUIDS

BY

WINIFRED NDUKU MUTUKU
B.Ed(Science)(Kenyatta University), MSc (Kenyatta University)

Thesis submitted in fulfilment of the requirements for the degree Doctor of Technology: Mechanical Engineering
in the faculty of Engineering
at Cape Cape Peninsula University of Technology, South Africa.

Supervisor: Professor O.D. Makinde
Senior Professor & Director, Institute for Advanced Research in Mathematical Modelling & Computations
Cape Cape Peninsula University of Technology, South Africa.

Supervisor: Dr. Bigwen Yan
Mechanical Engineering Department,
Cape Cape Peninsula University of Technology, South Africa.

Bellville Campus
January 2014

CPUT copyright information

The thesis may not be published either in part (in scholarly, scientific or technical journals), or as a whole (as a monograph), unless permission has been obtained from the University.

DECLARATION

I, Winifred Nduku MUTUKU hereby declare that, the contents of this thesis represent my own work and that the thesis has not previously been submitted for academic examination towards any degree or diploma qualification at any other University. Furthermore, it represents my own opinions and not necessarily those of the Cape Peninsula University of Technology.

Signed: _____ **Date:** _____

ABSTRACT

Magnetohydrodynamic (MHD) boundary layer flow of an electrically conducting viscous incompressible fluid with a convective surface boundary condition is frequently encountered in many industrial and technological applications such as extrusion of plastics in the manufacture of Rayon and Nylon, the cooling of reactors, purification of crude oil, textile industry, polymer technology, metallurgy, geothermal engineering, liquid metals and plasma flows, boundary layer control in aerodynamics and crystal growth etc.

Nanofluid is envisioned to describe a fluid in which nanometer-sized particles are suspended in conventional heat transfer base fluids to improve their thermal physical properties. Nanoparticles are made from various materials, such as metals (Cu, Ag, Au, Al, Fe), oxide ceramics (Al_2O_3, CuO, TiO_2), nitride ceramics (AlN, SiN), carbide ceramics (SiC, tiC), semiconductors, carbon nanotubes and composite materials such as alloyed nanoparticles or nanoparticle core–polymer shell composites. It is well known that, conventional heat transfer fluids, such as oil, water, and ethylene glycol, in general, have poor heat transfer properties compared to those of most solids. Nanofluids have enhanced thermophysical properties such as thermal conductivity; thermal diffusivity, viscosity and convective heat transfer coefficients compared with those of base fluids like oil or water. Owing to their enhanced properties, nanofluids can be used in a plethora of technical and biomedical applications such as nanofluid coolant: electronics cooling, vehicle cooling, transformer cooling, computers cooling and electronic devices cooling; medical applications: magnetic drug targeting, cancer therapy and safer surgery by cooling; process industries; materials and chemicals: detergency, food and drink, oil and gas, paper and printing and textiles.

This studies examines the effect of the complex interaction between the electrical conductivity of the conventional base fluid and that of the nanoparticles under the influence of magnetic field in a boundary layer flow with heat transfer over a convectively heated surfaces bearing in mind the engineering and industrial applications.

In chapter one, key terminologies related to fluid flow are given, the thermophysical properties of nanofluids are highlighted in relation to the convectional base fluids and finally the applications of both nanofluids and MHD are discussed. Chapter two lays the foundation for basic fundamental equations governing fluid flow.

Chapter three explores the magnetohydrodynamics (MHD) boundary layer flow of nanofluids past a permeable moving flat plate with convective heating at the plate surface. The nanofluids considered contain water as the base fluid with copper (Cu) or Alumina (Al_2O_3) as the nanoparticles. The influence of pertinent parameters on velocity, temperature, skin friction and Nusselt number are investigated.

In chapter four, the effect of the complex interaction between the electrical conductivity of the conventional base fluid and that of the nanoparticles under the influence of magnetic field in a boundary layer flow with heat transfer over a convectively heated flat surface is examined. Three types of water based nanofluids containing metallic or nonmetallic nanoparticles such as copper (Cu), Alumina (Al_2O_3) and Titania (TiO_2) are investigated and the effects of various thermophysical parameters on the boundary layer flow characteristics are displayed graphically and discussed quantitatively.

A numerical analysis is performed in chapter five on the buoyancy and magnetic effects on a steady two-dimensional boundary layer flow of an electrically conducting water-based nanofluid containing three different types of nanoparticles: copper (Cu), aluminium oxide (Al_2O_3), and titanium dioxide (TiO_2) past a convectively heated porous vertical plate with variable suction. The effects of the type of nanoparticle, solid volume fraction φ, Hartmann number *Ha*, Grashof number *Gr*, Eckert number *Ec*, suction/injection parameter F_w, and Biot number *Bi* on the flow field, temperature, skin friction coefficient and heat transfer rate are presented graphically and then discussed quantitatively.

Chapter six examines the effect of magnetic field on boundary layer flow of an incompressible electrically conducting water based nanofluids past a convectively heated vertical porous plate with Navier slip boundary condition. Three different water-based nanofluids containing copper (Cu), Aluminium oxide (Al_2O_3), and Titanium dioxide (TiO_2) are utilised. Graphical results are presented and discussed quantitatively with respect to the influence of pertinent parameters such as, solid volume fraction of nanoparticles(φ), magnetic field parameter(*Ha*), buoyancy effect(*Gr*), Eckert number (*Ec)*, suction/injection parameter (f_w), Biot number (*Bi*) and slip parameter (β), on the dimensionless velocity, temperature, skin friction coefficient and heat transfer rate.

It is noted that the presence of nanoparticles greatly enhance the magnetic susceptibility of nanofluids as compared to the convectional base fluids. Increasing the magnetic field strength retards the fluid velocity while increasing the thermal boundary layer thickness, which from the application point of view, it is obvious the surface cooling effect is enhanced, thus nanofluids are appropriate as heat transfer fluids.

ACKNOWLEDGEMENTS

I wish to express my sincere gratitude to my supervisor, Prof. O.D. Makinde who shepherded me thorough the bulk of the work. This thesis would not have been successfully completed without his valuable intellectual tutelage, words of encouragement, push for tenacity and opportunity to gain from his wealth of knowledge.

I wish to acknowledge the moral support from my family who did not at any one-time hold any reservations to my undertaking this study. I sincerely thank them for believing in my capabilities and encouraging me untiringly especially in difficult circumstances during the period of my study.

I would like to express a special word of thanks to my friends, especially, Ananda and Ambrose for their encouragement and readily stepping in whenever I needed assistance back home in Kenya.

The financial assistance of the Organization for Women in Science for the Developing World (OWSDW) and Swedish International Development Cooperation Agency (SIDA) towards this research is sincerely acknowledged.

To my angelic children; Ronnie and Torrie, a special heartfelt thank you. I know it was not easy for both of you for mom to leave you behind as she went to pursue her studies. Thank you for your understanding, love and encouragement. Thank you for the numerous reminders that you wanted mom to become a ‘Doctor’.

To those I may not have mentioned by name, there are many more people to thank, but like stars, some shine bright for all to see and others fade in the background aiding in the beauty of the night sky. Thank you all very much.

Finally my heartfelt thanks go to the Giver of Life without whose grace, blessings and love this would not have been achievable.

DEDICATION

I would like to dedicate my thesis work to my late father, Peter Mutuku and my lovely children; Ronnie and Torrie.

PREFACE

This thesis contains the result of research undertaken at the Department of Mechanical Engineering, Cape Peninsula University of Technology, and is an original intellectual product of the author, WN Mutuku-Njane. This research was realized within the framework of the PhD programme: funded by the Organization for Women in Science for the developing World (OWSDW) and the Swedish International Development Cooperation Agency (SIDA). Certainly, I would never have reached the point of finishing my thesis without the expert couching and support by my supervisor, O.D. Makinde.

In chapter one and two, concepts tackled in the study are introduced. This includes; definition of key terminologies, applications of the study, literature review, statement of problem and objectives of the study. Subsequent chapters (chapter three to six) consist of journal articles, submitted and accepted for publication. Chapter Seven summarises the thesis and gives the major conclusions accruing from the entire research.

NOMECLATURE

(u,v)	Velocity components
(x,y)	coordinates
B_0	Constant applied magnetic field
C_p	Specific heat at constant pressure
Nu	Local Nusselt number
Pr	Prandtl number
Br	Brinkmann number
Ec	Eckert number
Gr	Grashof number
Bi	Local Biot Number
Ha	Hartmann Number
q_w	Dimensional heat flux
Re_x	Local Reynolds number
T	temperature
T_∞	Free stream temperature
U_∞	Free stream velocity
f_w	Suction/injection parameter
k	Thermal conductivity
h_f	Heat transfer coefficient

Greek symbols

ψ	Stream function
θ	Dimensionless temperature
η	Similarity variable
β	Thermal expansion coefficient
α	Thermal diffusivity
φ	Solid volume fraction
μ	Dynamic viscosity
υ	Kinematic viscosity
σ	Electrical conductivity
ρ	Density
τ_w	Skin friction or shear stress
λ	Slip Coefficient

Subscripts

f	Fluid
s	Solid
nf	Nanofluid

TABLE OF CONTENTS

LIST OF FIGURES

LIST OF TABLES

CHAPTER ONE
INTRODUCTION

In this chapter, the main terminologies used in the thesis are defined. The synthesis of nanofluids and their thermal properties are quantitatively discussed. A detailed review of the applications of MHD and nanofluids is given. The statement of the problem, aims and objectives of the study and the methodology are also discussed.

1.1 Magnetohydrodynamics (MHD)

Magnetohydrodynamics (MHD) is the academic discipline concerned with the dynamics of electrically conducting fluids in a magnetic field. These fluids include salt water, liquid metals (such as Mercury, gallium, molten Iron) and ionized gases or plasmas (such as solar atmosphere). The term MHD is comprised of the words magneto – meaning magnetic, hydro – meaning fluids, and dynamics – meaning movement. Synonyms of MHD that are less frequently used are the terms magnetofluiddynamics and hydromagnetics. The field of MHD was initiated by the Swedish Physicist Hannes Alfvén (1908-1995), who received the Nobel Prize in Physics in 1970 for fundamental work and discoveries in magnetohydrodynamics with fruitful applications in different parts of plasma physics .

MHD covers those phenomena, where, in an electrically conducting fluid, the velocity field **V** and the magnetic field **B** are coupled. The magnetic field induces an electric current of density **j** in the moving conductive fluid (electromagnetism). The induced current creates forces on the liquid and also changes the magnetic field. Each unit volume of the fluid having magnetic field **B** experiences an MHD force **j** x **B** known as Lorentz force.

The set of equations which describe MHD flows are a combination of Navier-Stokes equation of fluid dynamics and Maxwell's equation of electromagnetism. These differential equations are solved simultaneously either analytically or numerically.

1.2 Heat Transfer

Temperature variations may exist within a fluid due to temperature differences between boundaries or between a boundary and an ambient fluid. Temperature variations can also arise from a variety of causes such as radioactivity, absorption of thermal radiation and release of latent heat as fluid vapor condenses. Heat transfer is the generation, use, conversion and exchange of thermal energy and heat between the physical systems which

occurs as a result of a a temperature gradient. This energy transfer is defined as heat. Heat transfer is commonly encountered in engineering systems and daily aspects of life.

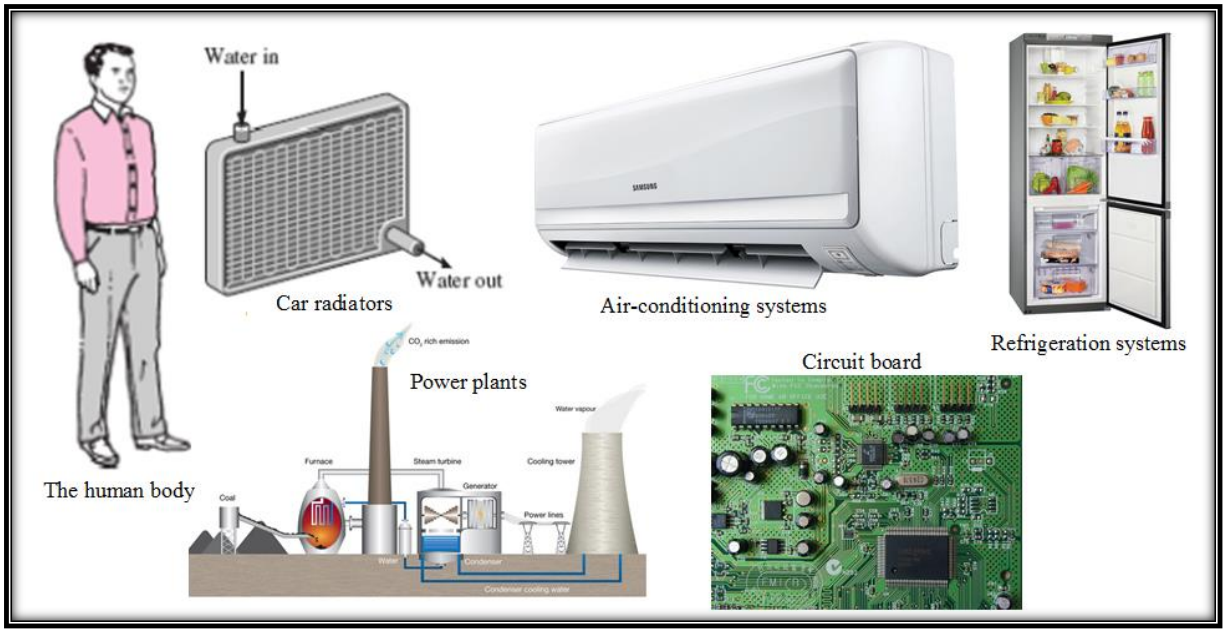

Figure 1.1: Energy Transfer in Daily life

There are three modes of heat transfer: conduction, convection and radiation. In our study we consider convection.

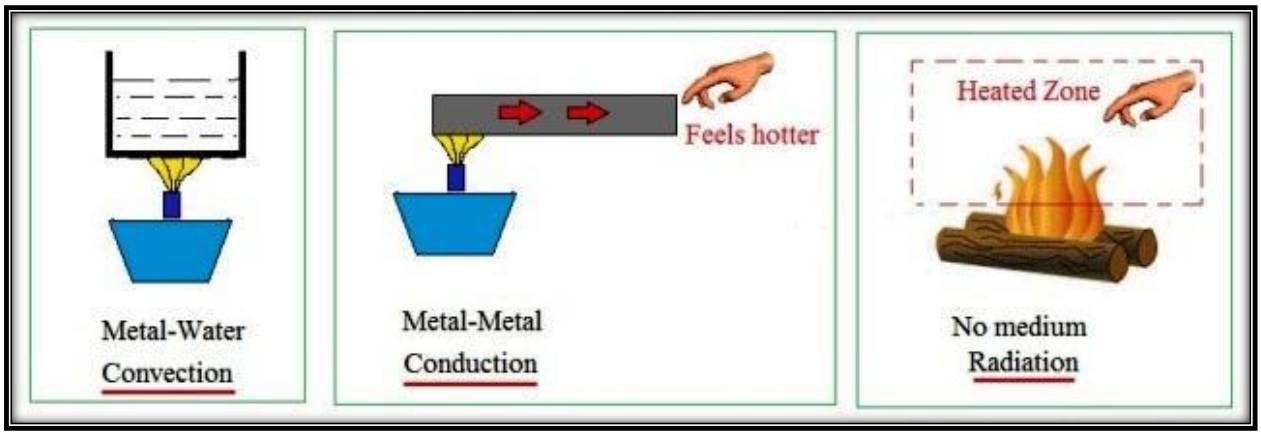

Figure 1.2: Modes of Heat Transfer (Image Source: India Study Channel Website)

1.3 Convection

Convection refers to heat transfer that will occur between a surface and a moving fluid when they are at different temperatures. The convection heat transfer mode is sustained both by random molecular motion and by the bulk motion of a fluid within the boundary layer. The contribution due to random molecular motion (diffusion) generally dominates near the

surface where the fluid velocity is low. The contribution due to bulk fluid motion originates from the fact that boundary layer grows as the flow progresses. Convection heat depends on viscosity, thermal conductivity, specific heat and density of the fluid. Viscosity also influences the velocity profile of the fluid flow.

In convection heat transfer, the transfer of heat is between a surface and a moving fluid (liquid or gas), when they are at different temperatures. The rate of transfer is given by **Newton's Law of Cooling.**

$$q'' = h\left(T_w - T_\infty\right), \tag{1.1}$$

where,

h is the convective heat transfer coefficient (w/m^2.k)

T_w is surface temperatures of the wall (°C)

T_∞ is the bulk fluid temperature (°C)

Table 1.1 Typical values of convective heat transfer coefficients

Type of Convection	**h(W/m2.K)**
Natural convection (air)	5 – 15
Natural convection (water)	500 – 1000
Force convection (oil)	20 – 2000
Force convection (air)	10 – 200
Force convection (water)	300 – 20000
Water boiling	100000
Water condensing	5000- 10000

Heat transfer has a wide spectrum of application ranging flow situations where heat transfer is to be maximized such as heat exchangers to situations where heat transfer is to be minimized such as steam pipes. The application of heat transfer has become more intense in modern technology in areas such as energy production, heat exchangers (which are used in refrigeration, air conditioning, space heating and power generation), nuclear reactors.

1.4 Boundary Layer

The concept of boundary layer in fluid flow over a surface is attributed primarily to Ludwig Prandtl (1874-1953). His 1904 paper on the subject formed the basis for future work on skin friction, heat transfer, and separation. Due to viscous shearing, the fluid velocity immediately adjacent to the surface is zero and the fluid layer next to the surface becomes attached to the surface (it wets the surface). This is referred to as the 'no slip condition'. The layers of fluid above the surface are moving, hence there is shearing taking place

between the layers of the fluid. The shear stress acting between the wall and the first moving layer next to it is called the wall shear stress and is denoted by τ_w. This thin layer adjacent to the surface of a body or a solid wall in which viscous forces affect the flow is called the boundary layer (or shear layer). The fluid velocity u increases with height y. The boundary layer thickness δ is defined as the distance from the boundary to the height above the surface at which the velocity becomes 99% of the free stream velocity u_o.

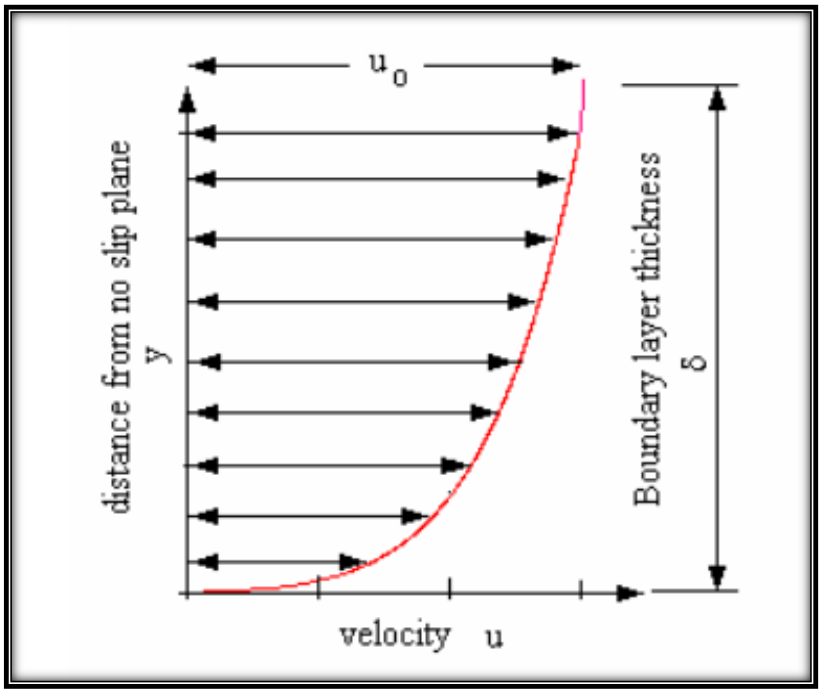

Figure 1.3: Velocity u variation with height y for a typical boundary layer.

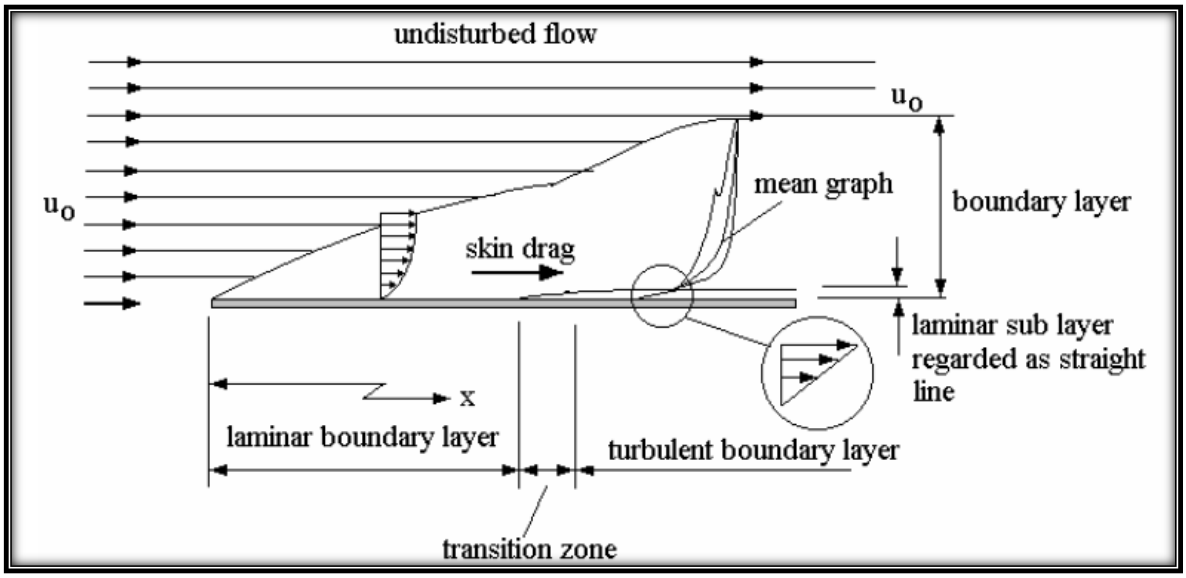

Figure 1.4: Fully Developed Boundary layer thickness

The thickness of the boundary layer is a function of the ratio between inertial forces and viscous forces, that is, the Reynolds number. At low Reynolds number, viscous forces govern the entire boundary layer and the flow is laminar, however for high Reynolds number inertia forces dominate the boundary layer and fluid becomes turbulent.

There are two types of boundary layers; hydrodynamic (velocity) boundary layer and thermal boundary layer. Hydrodynamic boundary layer may be defined as the region in which the fluid velocity changes from its free stream flow value to zero at the body surface. For fluids flowing past heated or cooled bodies, heat transfer takes place by conduction, convection or radiation. Heat will flow between a wall and the fluid adjacent to it when a temperature gradient is established between the wall and the fluid. Just like the fluid velocity increases from zero at the surface to the mainstream, the temperature changes from that at the wall to that in the free stream. The result is that the fluid temperature adjacent to the wall is assumed to be equal to the surface temperature of the wall at the interface and is equal to the bulk fluid temperature at some point in the fluid. This thin layer near the surface of the body is known as the thermal boundary layer.

The problem of thermal boundary layer is classified into forced convection and free (natural) convection. Forced convection occurs when the fluid is forced to flow over a surface by external means such as a pump, fan, wind or a mixer. In contrast, natural convection is caused by buoyancy forces induced by density differences in the fluid as a result of temperature variation within the fluid. The Buoyant force causes denser parts of the fluid to move downwards and less dense part to move upwards. Generally the densities of most fluids decrease with increase in temperature.

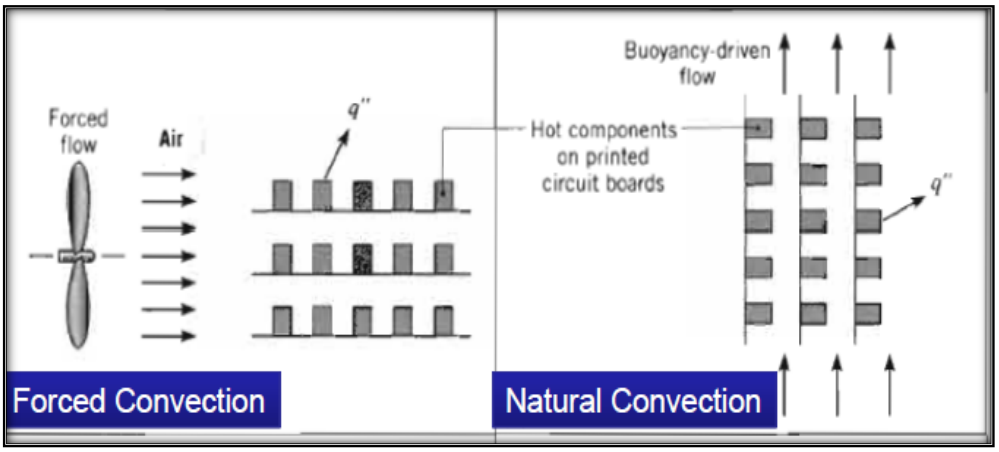

Figure 1.5: Natural and Forces Convection

Natural convection plays an important role in the flow and heat transfer in atmospherical, oceangraphical and geophysical processes in nature, and technological applications. Heat transfer coefficients along the walls from convection flow are of great importance to engineers. Thus information on heat transfer and conditions for transition from laminar to turbulent flows are important. Boundary layer is also applied in the calculation of friction drag of bodies in a flow, such as friction drag of a ship and the body of an aeroplane.

1.5 Mass Transfer

Mass transfer is mass in transit as the result of a species concentration difference in a mixture. Just as the temperature gradient constitutes the driving potential for heat transfer, the species concentration gradient in a mixture provides the driving potential for mass transfer. Mass transfer encompasses both mass diffusion on a molecular scale and the bulk mass transport from convection process. Mass transfer may also result from a temperature gradient in a system and this is known as *thermal diffusion*. Similarly the concentration gradient can give rise to the temperature gradient and thus heat transfer. These two effects are termed as *coupled phenomena*.

In industrial processes, mass transfer operations include separation of chemical components in distillation columns, absorbers such as scrubbers, adsorbers such as activated carbon beds, and liquid-liquid extraction. Mass transfer is often coupled to additional transport processes in industrial cooling towers. In many technical applications, heat transfer processes occur simultaneously with mass transfer processes.

1.6 Nanofluids

Fluid is a substance that deforms continuously under the application of shear stress (tangential force per unit area). Convectional heat transfer fluids such as water, minerals oil and ethylene glycol play an important role in many industrial sectors including power generation, chemical production, air-conditioning, transportation and microelectronics. Although various techniques have been applied to enhance their heat transfer, their performance is often limited by their low thermal conductivities which obstruct the performance enhancement and compactness of heat exchangers. With the rising demands of modern technology for process intensification and device miniaturization, there is need to develop new types of fluids that are more effective in terms of heat exchange performance. In order to achieve this, it has been recently proposed to disperse small amounts of

nanometer-sized (10–50 nm) solid particles (nanoparticles) in base fluids, resulting into what is commonly known as nanofluids. The term “nanofluid” was coined by Choi [1] who was working with the group at the Argonne National Laboratory(ANL), USA, in 1995. The nanoparticles used are ultrafine, therefore, nanofluids appear to behave more like a single-phase fluid than a solid–liquid mixture. The commonly used materials for nanoparticles made of chemically stable metals (Al, Cu, Ag, Au, Fe), nonmetals (graphite, carbon nanotubes), oxides ceramics (Al_2O_3, CuO, TiO_2, SiO_2), carbides (SiC), nitrides (AlN, SiN), layered (Al+ Al_2O_3, Cu+C), PCM and functionalized nanoparticles. The base fluids is usually a conductive fluid, such as water, (or other coolants), oil (and other lubricants), polymer solutions, bio-fluids and other common fluids, such as paraffin. Investigations have shown that nanofluids possess enhanced thermophysical properties such as thermal conductivity, thermal diffusivity, viscosity and convective heat transfer coefficients compared to those of base fluids like oil or water [2–7].

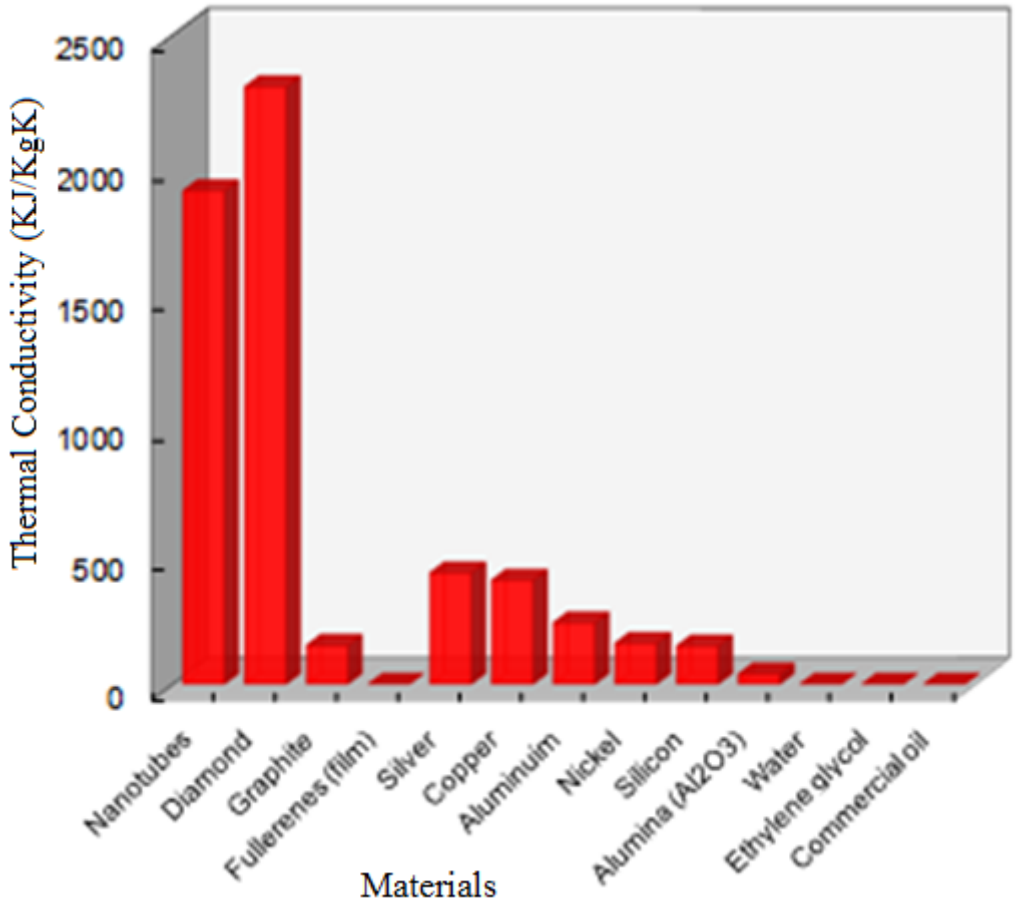

Figure 1.6: Thermal Conductivity of Materials (Image Source: Thermal Interface Materials website)

1.6.1 Synthesis of Nanofluids

There are two techniques used in the production of nanofluids; the single-step method in which in nanoparticles are evaporated directly into the base fluid and the 2-step method in which nanoparticles are first prepared by either the inert gas-condensation technique or chemical vapor deposition method and then dispersed into the base fluid.

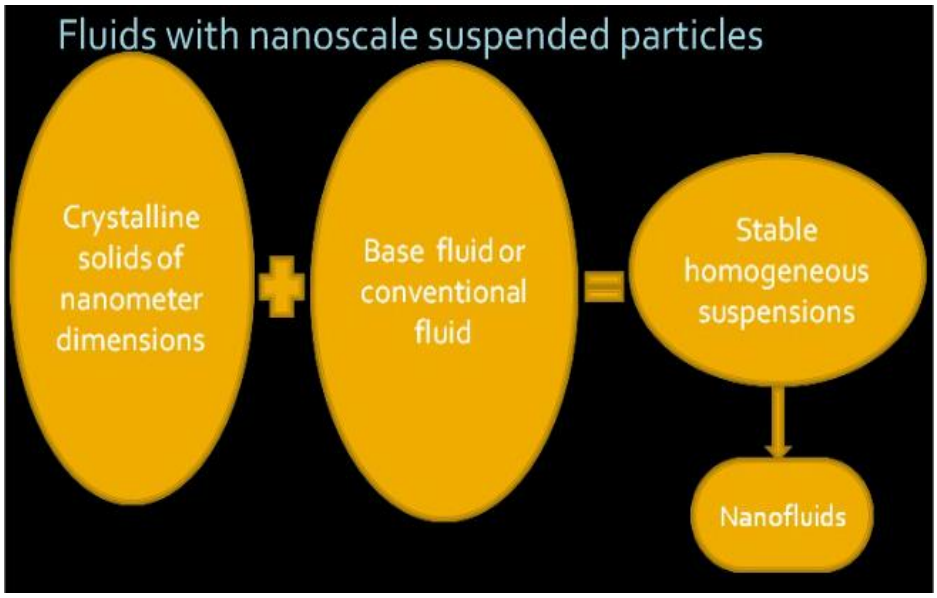

Figure 1.7: Nanofluid Synthesis

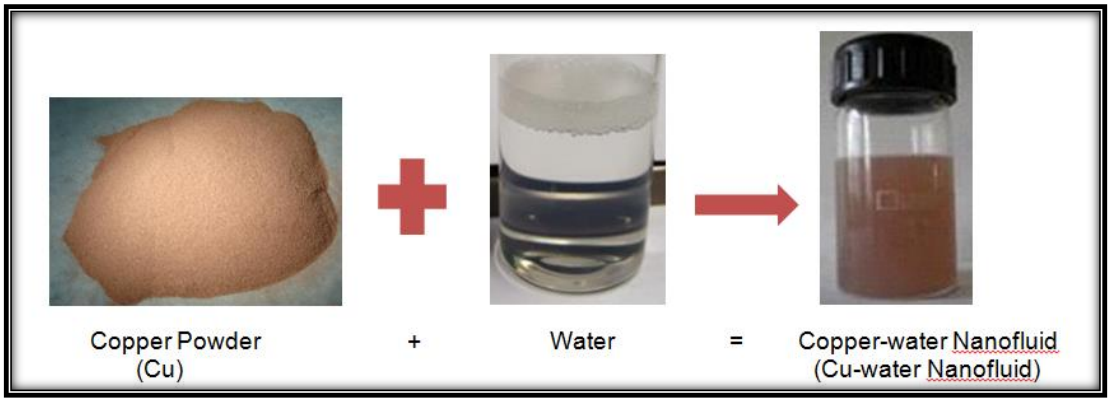

Figure 1.8: Cu-water nanofluid

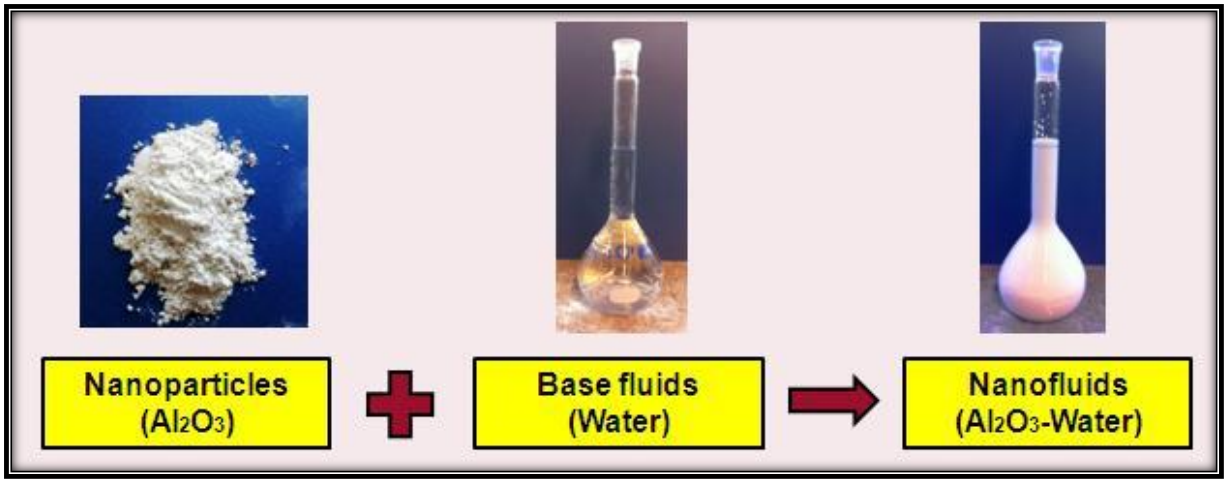

Figure 1.9: Al_2O_3-water nanofluid

1.6.2 Two-step method

The two-step method is the most widely used method for preparing nanofluids. Nanoparticles, nanofibers, nanotubes, or other nanomaterials used in this method are first produced as dry powders, often by inert gas condensation [8]. Chemical vapor deposition has also been used to produce materials for use in nanofluids, particularly the carbon multiwalled nanotubes (CMWNT) [9]. The nanosized powder is then dispersed into a fluid in a second processing step with the help of intensive magnetic force agitation, ultrasonic agitation, high-shear mixing, homogenizing, and ball milling, used to minimize particle aggregation and improve dispersion behavior. To enhance the stability of nanoparticles in fluids surfactants are added to the fluids. However, the functionality of the surfactants under high temperature is also a big concern, especially for high-temperature applications. The two-step process works well in some cases, such as nanofluids consisting of oxide nanoparticles dispersed in deionized water [10]. Less success has been found when producing nanofluids containing heavier metallic nanoparticles [11]. The Two-step method is the most economic method for producing nanofluids in large scale, because nanopowder synthesis techniques have already been scaled up to industrial production levels. A key problem of two-step processes is that nanoparticles are in an aggregated state after many hours of sonication. Due to the difficulty in preparing stable nanofluids by two-step method, several advanced techniques are developed to produce nanofluids, including one-step method.

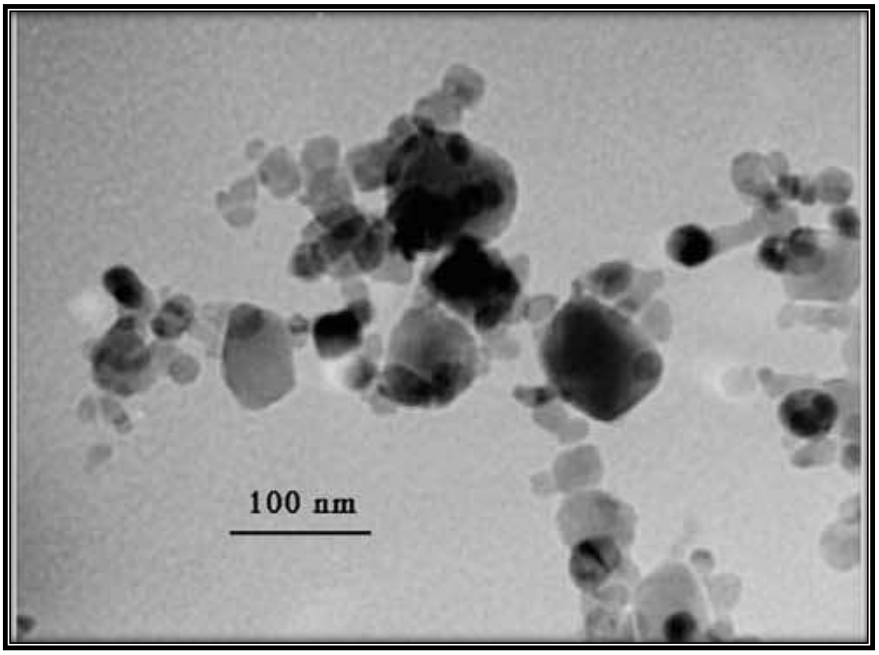

Figure 1.10: TEM image of CuO-EG nanofluid after 9hours of sonification [15]

1.6.3 One-Step Method

To reduce the agglomeration of nanoparticles, the one-step physical vapor condensation method to prepare Cu/ethylene glycol nanofluids was developed [12]. The one-step process consists of simultaneously making and dispersing the particles in the base fluid. In this method the processes of drying, storage, transportation, and dispersion of nanoparticles are avoided, so the agglomeration of nanoparticles is minimized and the stability of fluids is increased [13]. The one-step method produces uniformly dispersed nanoparticles and the particles are stably suspended in the base fluid. However the one-step method has the disadvantages in that the residual reactants are left in the nanofluids due to incomplete reaction or stabilization and that only low vapor pressure fluids are compatible with the process.

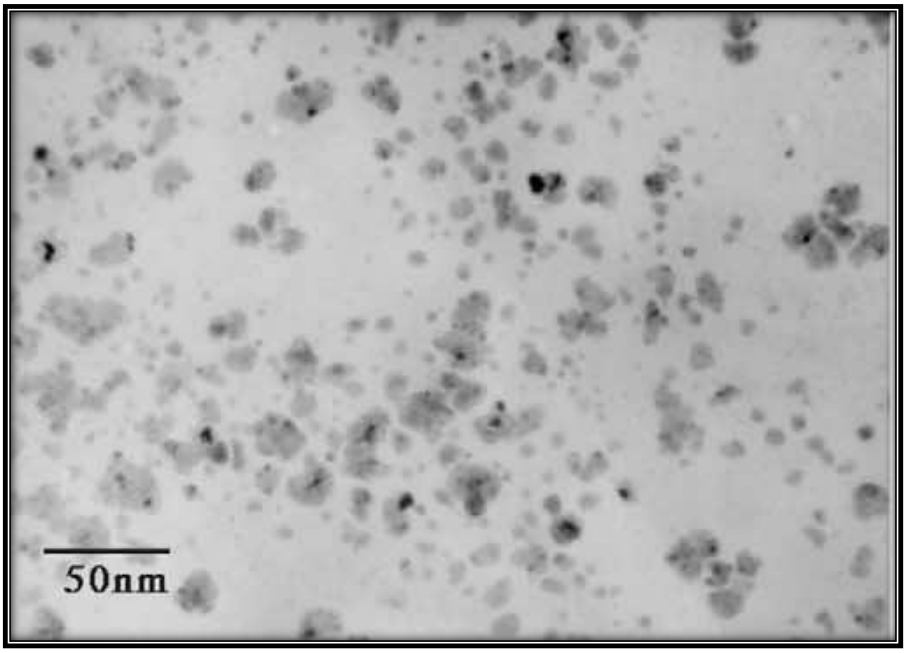

Figure 1.11: TEM Image of Cu-EG by 1-step Method Little agglomeration occurs [15]

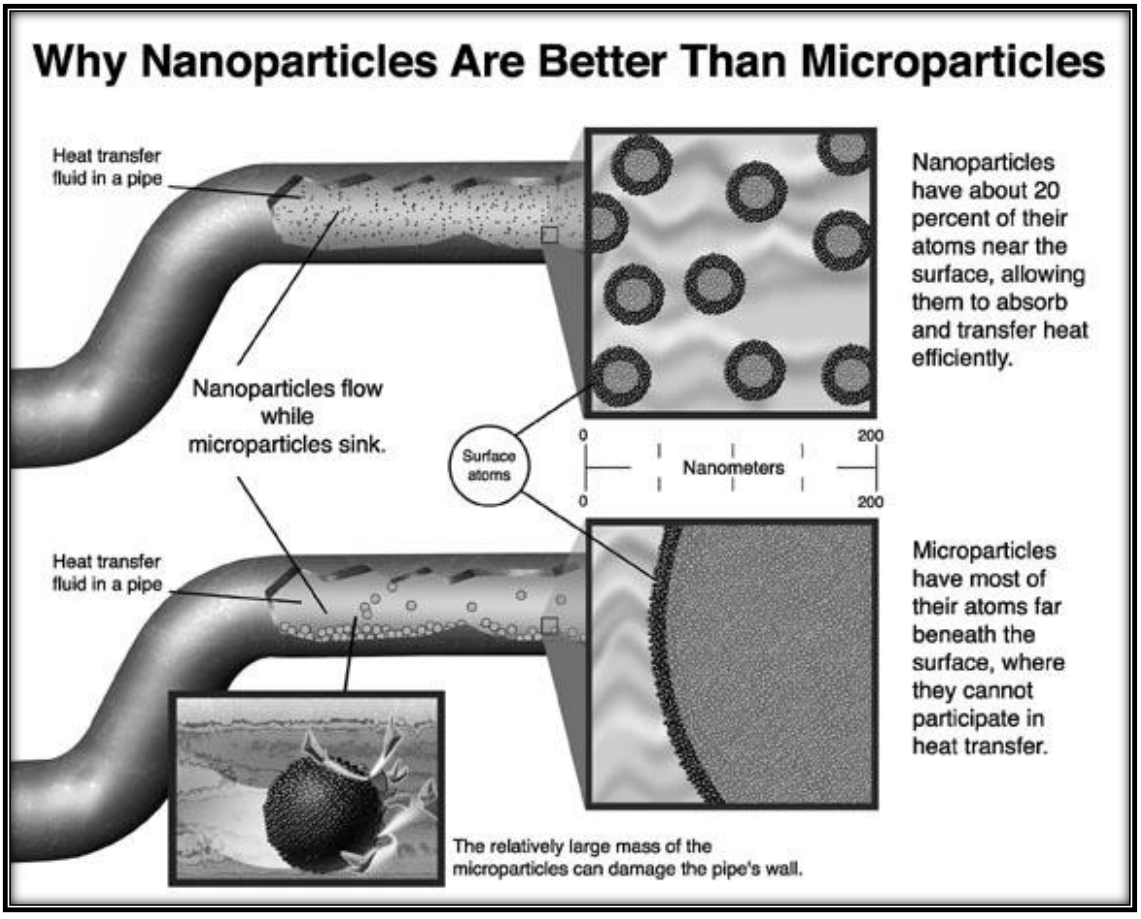

Figure 1.12: Image source: ANL Media Center Website

Spherical particles are mostly used in nanofluids. However, rod-shaped, tube-shaped, cylindrical and disk-shaped nanoparticles are also used. The suspended metallic or

nonmetallic nanoparticles change the transport properties and heat transfer characteristics of the base fluid, hence enhance the heat transfer of the base fluid. [16]. This can be explained theoretically, at room temperature, metals in solid form have higher thermal conductivity than fluids. Thermal conductivity of metallic liquids is much greater than that of non-metallic liquids. It is then expected that the thermal conductivities of the fluids with metallic nanoparticles should be significantly higher. Experiments have showed that the thermal conductivities of nanofluids depend on the thermal conductivities of both the base fluid and the nanoparticles. The properly prepared nanofluids are expected to give the benefits of (i) higher heat conduction, (ii) more stability, (iii) microchannel cooling without clogging, (iv) reduced chances of erosion and (v) reduction in pumping power [17]. Choi who coined the term nanofluid proposed that the thermal conductivity of the base fluid can be increased by adding low concentration of nanoparticles of materials having higher thermal conductivity than the base fluid. Masuda et al. [18] showed that different nanofluids (*i.e.*, Al_2O_3-water, SiO_2-water, and TiO_2-water combinations) generated a *thermal conductivity* increase of up to 30% at volume fractions of less than 4.3%. Such an enhancement phenomenon was also reported by Eastman and Choi [19] for CuO-water, Al_2O_3-water and Cu-Oil nanofluids. Experimental studies have shown that the thermal conductivity of nanofluids depends on several parameters; nanoparticle material, particle volume fraction, spatial distribution, particle size, particle shape, base-fluid type, temperature, and pH value.

Table 1.2: Thermophysical properties of water and nanoparticles [20-25]

Material	ρ (kg/m^3)	C_p (J/Kg K)	K(W/m K)	$\beta \times 10^{-5}$ (K^{-1})	$\sigma(s/m)$
Pure Water	997.1	4179	0.613	21	5.5x10^{-6}
Ethylene glycol	1114	2415	0.252	57	1.07x10^{-6}
Engine oil (EO)	884	1909	0.145	70	1.00x10^{-7}
Mineral Oil	920	1670	0.138	64	1.00x10^{-7}
Blood	1063	3594	0.492	0.18	6.67x10^{-1}
Silver (Ag)	10500	235	429	1.89	6.3x10^{7}
Copper (Cu)	8933	385	401	1.67	5.96x10^{7}
Iron	7870	460	80	58	1.00x10^{7}
Aluminium	2701	902	237	2.31	3.5x10^{7}
Copper Oxide (CuO)	6510	540	18	0.85	5.96x10^{7}
Alumina (Al_2O_3)	3970	765	40	0.85	3.5x10^{7}
Titanium Oxide(TiO_2)	4250	686.2	8.9538	0.9	2.38x10^{6}
Iron Oxide(Fe_3O_4)	5180	670	80.4	20.6	1.12 x10^{5}

Note:SI units for electrical conductivity is Siemens per metre (Sm^{-1})

1.6.4 Thermal Conductivity and Particle Volume Fraction

Studies have shown that the particle volume fraction, which is the volumetric concentration of the nanoparticle in the nanofluid has effects on the thermal conductivity of the nanofluid. Experimental results of nanofluids with small nanoparticle volume fractions showed that thermal conductivity significantly increased when compared to the base fluid. Masuda et al. [19] measured the thermal conductivity of nanofluids containing Al_2O_3 (13 nm), SiO_2 (12 nm), and TiO_2 (27 nm) nanoparticles, with water as the base fluid. They observation an enhancement of 32.4% for the effective thermal conductivity of 4.3 vol. % Alumina-water nanofluid at 31.85°C. In their studies Lee and Choi [26] based on CuO-water/ethylene glycol nanofluids with particle diameters 18.6 and 23.6 nm as well as Al_2O_3-water/ethylene glycol nanofluids with particle diameters 24.4 and 38.4 nm they discovered a 20% thermal

conductivity increase at a volume fraction of 4%. In both cases it was found that thermal conductivity enhancement increases linearly with particle volume fraction. Wang et al.[27] showed a 12% increase in thermal conductivity for 28-nm-diameter Al_2O_3-water and 23 nm CuO-water nanofluids with 3% volume fraction. For the case of 8 vol. % Al_2O_3-water nanofluid, thermal conductivity enhancement as high as 40% was achieved. From his results, Murshed et al. [28] showed a 27% increase in 4% TiO_2-water nanofluids with particle size 15 nm and 20% increase for Al_2O_3-water nanofluids. The use of copper nanoparticles and carbon nanotubes (CNT) has shown the most promising thermal conductivity enhancement of 40% and 160% respectively in relation to the base fluid. Khanafer et al.[29] developed a stream function vorticity based numerical algorithm based on the thermal dispersion model. They found that the nanofluid heat transfer rate increases with increase in nanofluid volume fraction.

1.6.5 Thermal Conductivity and Particle Material

In their work, Das et al. [30] and Abareshi et al. [31] noted a significant increase in thermal conductivity with increase in temperature. In their study Das et al., they used Al_2O_3 (38.4 nm)/water and CuO (28.6 nm)/water nanofluids at different temperatures ranging from 21 to 51°C. It was observed that for 1 vol. % Al_2O_3/water nanofluid, thermal conductivity enhancement increased from 2% at 21°C to 10.8% at 51°C, and for 4vol%, thermal conductivity enhancement increased from 9.4% at 21°C to 24.4% at 51°C. Theoratically, this is expected, since, with the increment of the nanofluid's bulk temperature T, molecules and nanoparticles are more active due to enhanced Brownian motion and are able to transfer more energy from one location to another per unit time.

1.6.6 Thermal Conductivity and Base Fluid

According to the conventional thermal conductivity models such as the Maxwell model [32], as the base fluid thermal conductivity of a mixture decreases, the thermal conductivity ratio (thermal conductivity of nanofluid divided by the thermal conductivity of base fluid) increases. Wang et al. [27] used Al_2O_3 and CuO nanoparticles to prepare nanofluids with several base fluids; water, ethylene glycol, vacuum pump fluid, and engine oil. Al_2O_3 - ethylene glycol nanofluid had the highest thermal conductivity ratio. Engine oil showed somewhat lower thermal conductivity ratios than ethylene glycol. Water and pump fluid showed even smaller ratios, respectively. CuO nanoparticles were used with ethylene glycol and water as the

base fluid and it is interesting to note that they showed exactly the same thermal conductivity ratios for the same particle volume fraction. Xie et al. [33] carried investigations on nanofluids with Al_2O_3 nanoparticles using different base fluids; deionized water, glycerol, ethylene glycol, and pump oil. In addition, ethylene glycol-water and glycerol-water mixtures with different volume fractions were also used as base fluids and the variation of the thermal conductivity ratio with thermal conductivity of the base fluid mixture was examined. It was seen that, thermal conductivity ratio decreased with increasing thermal conductivity of the base fluid. Chopkar et al. [34] also analyzed the effect of base fluid by comparing water and ethylene glycol. They used Al_2Cu and Ag_2Al nanoparticles and found that water-based nanofluids showed a higher thermal conductivity ratio. Liu et al. [35] studies the effect of base fluid effect using MWCNT nanofluids. They used Ethylene glycol and synthetic engine oil as base fluids. 1 vol. % MWCNT/ethylene glycol nanofluid showed 12.4% thermal conductivity enhancement, whereas for 2 vol. % MWCNT/synthetic engine oil nanofluid, enhancement was 30%. It was observed that higher enhancements were achieved with synthetic engine oil as the base fluid.

1.6.7 Thermal Conductivity and Particle Size

Nanoparticles of various sizes, ranging between 5 and 100 nm are produced and it has been observed that the particle size/diameter is an important parameter of thermal conductivity of nanofluids. Chopkar et al. [34] investigated the effect of particle size on the thermal conductivity, by using nanofluids with water and ethylene glycol as the base fluids and Al_2Cu and Ag_2Al nanoparticles. The nanoparticles sizes were varied between 30 and 120 nm. For all the four types of nanofluids, it was observed that thermal conductivity enhancement increased with decreasing particle size. In another study, Chopkar et al. [36] prepared nanofluids by using $Al_{70}Cu_{30}$ nanoparticles into ethylene glycol and varied the particle size between 9 and 83 nm. They showed that thermal conductivity enhancement decreases with increasing particle size. For 0.5 vol. % nanofluid, thermal conductivity enhancement decreased from 38 to 3% by increasing the particle size from 9 to 83 nm. It can be concluded that the thermal conductivity of nanofluids increases with decreasing particle size.Das [26], showed that there is an inverse relationship between the particle size and thermal conductivity enhancement of nanofluids. Moghadassi et al. [37] showed that the thermal conductivity increases with decrease of nanoparticle diameters.

1.6.8 Thermal Conductivity and Particle Shape

Different particle shapes influence the thermal conductivity of nanofluids. Xie et al. [38] investigated the thermal conductivity of SiC/distilled water nanofluid using the spherical particles with 26 nm average diameter and cylindrical particles with 600 nm average diameter. Cylindrical particles usually have a large length-to-diameter ratio. It was found that 4.2 vol. % water-based nanofluids with spherical particles had a thermal conductivity enhancement of 15.8%, whereas 4 vol. % nanofluids with cylindrical particles had a thermal conductivity enhancement of 22.9%. It can be concluded that Spherical particles show slightly less enhancement than those which are nanorods. Murshed et al. [39] studies the thermal conductivity of TiO_2/deionized water nanofluid, using two types of nanoparticles; spherical particles (15 nm) and rod-shaped particles (10 nm in diameter and 40 nm in length). They observed that the nanofluids with spherical particles, had enhancement of 29.7% at 5 vol. %. And the rod-shaped nanoparticles showed an enhancement of 32.8% at the same volume fraction. Nanofluids with carbon nanotubes (which are cylindrical in shape) generally show greater thermal conductivity enhancement than nanofluids with spherical particles. As a result, we conclude that cylindrical nanoparticles provide higher thermal conductivity enhancement than spherical particles. The thermal conductivity of CuO-water-based nanofluids containing shuttle-like-shaped CuO nanoparticles is larger than those for CuO nanofluids containing nearly spherical CuO nanoparticles [40].

1.6.9. Thermal Conductivity and pH value

Murshed et al. [39] investigated the thermal conductivity of TiO_2 /water nanofluid and observed a decrease in the thermal conductivity with increasing pH value. Zhu et al. [41] showed that the pH value of a nanofluid strongly affects the thermal conductivity of suspensions, by influencing the stability of the nanoparticle suspension. They measured the thermal conductivity of nanofluids, which were prepared using Al_2O_3 nanoparticles and water, ethylene glycol, and pump oil. They noted that the thermal conductivity enhancement of 5 vol. % Al_2O_3water nanofluid was 23% when pH is equal to 2.0 and it became 19% when pH is equal to 11.5. This shows a significant decrease in thermal conductivity ratio with increasing pH values.

1.7 Ferrofluids

Magnetic nanofluid, popularly known as ferrofluid, is a magnetic colloidal suspension consisting of base liquid and magnetic nanoparticles with a size range of 5 to 15nm in diameter coated with a surfactant layer. The nanoparticles are suspended by Brownian motion and generally will not settle under normal conditions. The most often used magnetic particle materials are magnetite, iron or cobalt; and the base liquids are water or kerosene. The advantage of the ferrofluids is that the fluid flow and heat transfer may be controlled by an external magnetic field which makes it applicable in various fields such as electronic packing, mechanical engineering, smart fluids, thermal engineering, aerospace and bioengineering [42]. Other applications include magneto-optical wavelength filter, optical modulators, nonlinear optical materials, tunable optical fiber filter, optical grating, optical switches, drug targeting, drug delivery, MRI contrast, and hyperthermia.

Table 1.3: Thermal Conductivity Enhancement of Nanofluids

Author	Particle Type	Base Fluid	Particle Volume Fraction (%)	Particle size (nm)	Maximum Enhancement (%) $\frac{100(K_{nf}-K_f)}{K_f}$	Notes
Masuda et al [19]	Al_2O_3	Water	1.30-4.30	13	32.4	
	SiO_2	Water	1.10-2.40	12	1.1	31.85-86.85°C
	TiO_2	Water	3.10-4.30	27	10.8	
Lee et al. [26]	Al_2O_3	Water/EG	1.00-4.30/1.00-5.00	38.4	10/18	Room Temperature
	CuO	Water/EG	1.00-3.41/1.00-4.00	23.6	12/23	
Wang et al. [27]	Al_2O_3	Water/EG	3.00-5.00/5.00-8.00	28	16/41	
	CuO	EO/PO	2.25-7.40/5.00-7.10	28	30/20	Room Temperature
	CuO	Water/EG	4.50-9.70/6.20-14.80	23	34/54	
Eastman et al [20]	Cu	EG	0.01-0.56	<10	41	Room Temperature
Xie et al. [38]	SiC	Water/EG	0.78-4.18/0.89-3.50	26sphere	17/13	Effect of particle shape and size is examined
	SiC	Water/EG	1.00-4.00	600cylinder	24/23	
Xie et al. [33]	Al_2O_3	Water/EG	5.00	60.4	23/29	Room Temperature
	Al_2O_3	Water/EG	5.00	60.4	38/27	
Das et al. [30]	Al_2O_3	Water	1.00-4.00	38.4	24	21-51°C
	CuO	Water	1.00-4.00	28.6	36	
Murshed et al.[28]	TiO_2 \ TiO_2	Water water	0.50-5.00 0.50-5.00	15 sphere 10x40rod	30 33	Room Temperature
Li and Peterson[43]	Al_2O_3	Water	2.00-10.00	36	29	27.5-34.7°C
	CuO	water	2.00-6.00	29	51	28.9-33.4°C
Chopkar et al.[34]	Al_2Cu	Water/EG	1.00-2.00	31/68/101	96/76/61	Effect of particle size was examined
	Ag_2Al	Water/EG	1.00-2.00	33/80/120	106/93/75	
Beck et al.[44]	Al_2O_3	Water	1.86-4.00	8-2.82	20	Effects of particle size examined
	Al_2O_3	EG	2.00-3.01	12-282	19	
Mintsa et al. [45]	Al_2O_3	Water	0-18	36/47	31/31	20-48°C
	CuO	water	1-16	29	24	
Turgut et al.[46]	TiO_2	Water	0.2-3.0	21	7.4	13-55°C
Choi et al.[47]	MWCNT	PAO	0.04-1.02	25x50000	57	Room Temp
Liu et al.[35]	MWCNT	EG/EO	0.20-1.00/ 1.00-2.00	20~50 (diameter)	12/30	Room Temperature
Ding et al.[48]	MWCNT	Water	0.05-0.49	40 (diameter)	79	20-30°C

Note: EG: Ethylene glycol, EO: Engine oil, PO: Pump oil, PAO: Polyalphalefin.

1.8 Application of MHD

Many natural phenomena and engineering problems are susceptible to MHD analysis. In natural phenomena, since magnetic field exists everywhere in the world, it follows that MHD phenomena must occur whenever conducting fluids are available. Electrically conducting

fluids are abundant in nature, although their conductivities vary greatly. On the other hand, MHD is of special technical significance because of its frequent occurrence in many industrial applications such as MHD generators, pumps, cooling of nuclear reactors, geothermal energy extractors, thermal insulators, nuclear waste disposal, heat exchangers, petroleum and polymer technology, and heat transfers involving metallurgical processes.

1.8.1 MHD Pump

One of the more practical uses of the MHD force is in pumping systems, where electrical energy is converted directly into force on the working liquid. “EM pumps” (as they are commonly known) have been in existence for many years, and many different designs have been successfully developed and employed. The first MHD pump prototype was built in 1907 [49]. The pump consists of mutually perpendicular magnetic and electric fields arranged normally to the axis of a duct. The duct is filled with a conducting liquid. As current flows, the resulting Lorentz force provides the necessary pumping action. With the advent of micro-electro-mechanical systems (MEMS) technology, a lot of research efforts have been made in microvalves, micropumps, and flow sensors in microfluidics[50]. Micropumps are required in chemical, medical, and biological applications such as microsyringes for diabetics since they are able to handle small and precise volumes[51]. In microfluidic devices, the MHD pump is so far the most effective for producing a continuous, nonpulsating flow in a complex microchannel design. MHD micropump has several advantages, such as simple fabrication process, and bidirectional pumping ability. It can be constructed with no moving parts and no direct contact with the working liquid. This is a distinct advantage if high temperature and/or corrosive liquids must be handled. The absence of seals or moving parts leads to a highly reliable system. In addition, EM pumps are typically controllable, and even reversible, by varying the magnitude and direction of the applied current.

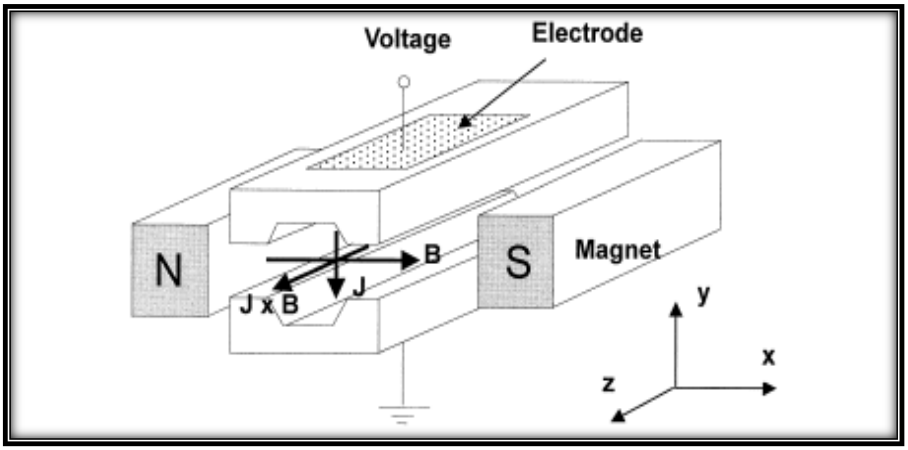

Figure 1.13: MHD micropump with Lorentz force as the driving force

1.8.2 MHD Generators

Michael Faraday created the first MHD generator in 1831. This type of generator creates electrical power by using an electrically conducting fluid with a magnetic field. In effect, it changes thermal or kinetic energy into electricity. There are several ways to achieve electrical conductivity with an MHD generator. The conducting fluids that are usually considered are all gases that are made from alkali metal vapors, noble gases and combustion. When combustion gases are chosen as the conducting fluid, then potassium carbonate is added to the flow in tiny amounts. It is thermally ionized and makes up the electron density necessary for conductivity. Cesium is used in the case of monatomic gases, and the electron temperature is raised above the gas, which makes electrical conductivity possible at a lower temperature than would be the case with thermal ionization. Finally, in the case of liquid metal, electrical conductivity happens when the liquid metal is injected directly into the vapor or gas stream. This makes a continuous liquid phase possible. MHD power generation provides a way of generating electricity directly from a fast moving stream of ionized gases without the need for any moving mechanical parts - no turbines and no rotary generators. The flow of the conducting plasma through a magnetic field causes a voltage to be generated (and an associated current to flow) across the plasma, perpendicular to both the plasma flow and the magnetic field according to Fleming's Right Hand Rule. The MHD generator needs a high temperature gas source, which could be the coolant from a nuclear reactor or more likely high temperature combustion gases generated by burning fossil fuels, including coal, in a combustion chamber. Gas-phase MHD is probably best known in MHD power generation. Since 1959 [52,53], major efforts have been carried out around the world to develop this technology in order to improve electric

conversion efficiency, increase reliability by eliminating moving parts, and reduce emissions from coal and gas plants.

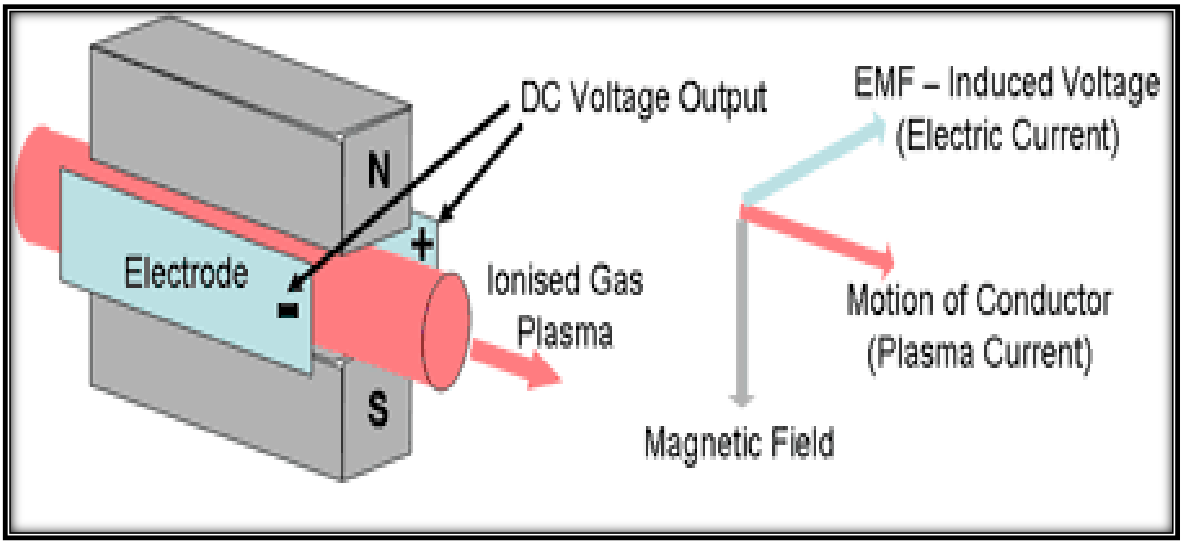

Figure 1.14: MHD Power Generation Principle (Image Source: Electropaedia website)

1.8.3 MHD Flow Meters

Another common MHD device is the EM flow meter, where the potential induced by fluid motion is measured and used to infer the average flow rate of a conducting liquid. It is an electromagnetic flow measurement method that is based on exposing a flow to a magnetic field and measuring the force acting on the magnetic field generating system [54]. Flow measurement using magnetic fields has a long history. It started in 1832 when Michael Faraday attempted to determine the velocity of the Thames river [55]. Faraday's method which consisted of exposing a flow to a magnetic field and measuring the induced voltage using two electrodes has evolved into a successful commercial application known as the inductive flowmeter. The theory of such devices has been developed and comprehensively summarized by [56]. While inductive flowmeters are widely used for flow measurement in fluids at low temperatures such as beverages, chemicals and wastewater, they are not suited for flow measurement in metallurgy. Since they require electrodes to be inserted into the fluid, their use is limited to applications at temperatures far below the melting points of practically relevant metals. Consequently there have been several attempts to develop flow measurement methods which do not require any mechanical contact with the fluid. Among them is the eddy current flowmeter [57] which measures flow-induced changes in the electric impedance of coils interacting with the flow. More recently, a noncontact method was proposed [58,59] in which a magnetic field is applied to the flow and the velocity is

determined from measurements of flow-induced deformations of the applied field. MHD can also be used to create a flowmeter for blood. The has been a number of successful attempts at applying MHD methods of velocity measurement to physiology and in particular to monitor fluctuations in the rate of blood flows in arteries [60]. The use of flow meters to study blood flows was initiated by Kolin [61].

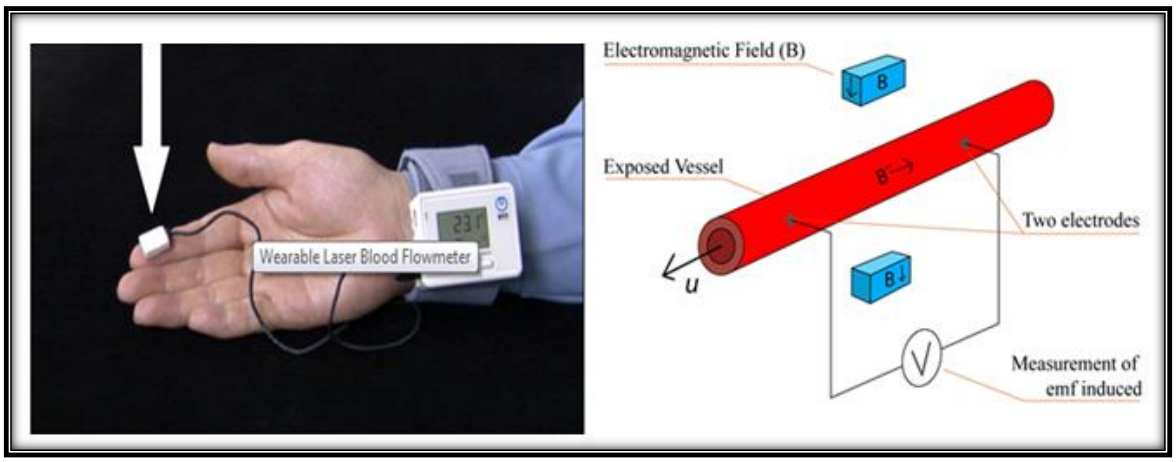

Figure 1.15: MHD Blood Flow Meter

The basic idea is that a conducting fluid flowing through a magnetic field produces an EMF. So by measuring an EMF, a flow rate can be determined. Two electrodes are attached along the length of a vessel, and an electromagnetic field is applied perpendicular to the flow. The emf between the two electrodes can be measured and gives a continuous result proportional to the flow velocity. The blood flowmeter is used during vascular surgery to measure the quantity of blood passing through a vessel or graft, before during or after surgery.

1.8.4 Metallurgy

More recently, MHD devices have been used for stirring, levitating, and controlling flows of liquid metals for metallurgical processing and other applications [62]. High-level requirements to metal works production determine a transit to a tangibly advanced level of melting, pouring and semi-finished products primary processing performance technology. Therefore, the task of metal ingots and blanks quality should be solved on a comprehensive basis, i.e. the alloy quality should be controlled at the stage of preparation, intermediate processing and pouring. To realize these tasks within melting casting units incorporating melting furnaces, mixers, ladders, refining installations and continuous pouring machines, an efficient method is electric conductive metal melt electromagnetic stirring [63].

Electromagnetic stirring (EMS) improves quality and productivity in continuous casting. The rotating field induces magnetodynamic forces in the liquid steel producing rotational flow, thereby providing better heat transfer and gas release, improved equiaxed zone, and

minimizing carbon segregation, inclusions, porosity, surface and internal cracks. In this connection, magneto-dynamic (MHD) technologies and devices are wider applied in ferrous and non-ferrous metal works.

1.8.5 MHD Propulsion

MHD propulsion is a method for propelling seagoing vessels using only electric and magnetic fields with no moving part using MHD. An electric current is passed through the seawater in the presence of an intense magnetic field, which interacts with the magnetic field of the current through the water. The Lorentz force created in the sea water accelerates it away from the ship hence the ship moves in the opposite direction. MHD is attractive because it has no moving parts, which means that a good design might be silent, reliable, efficient, and inexpensive. A number of experimental methods of spacecraft propulsion are based on magnetohydrodynamic principles. In these the working fluid is usually a plsma or a thin cloud of ions. Some of the techniques include various kinds of ion thruster, the magntoplasma dynamic thruster, and the variable specific impulse magnetoplasma rocket. The first ship to be propelled this was the Mitsubishi built boat 'Yamoto' in 1991.

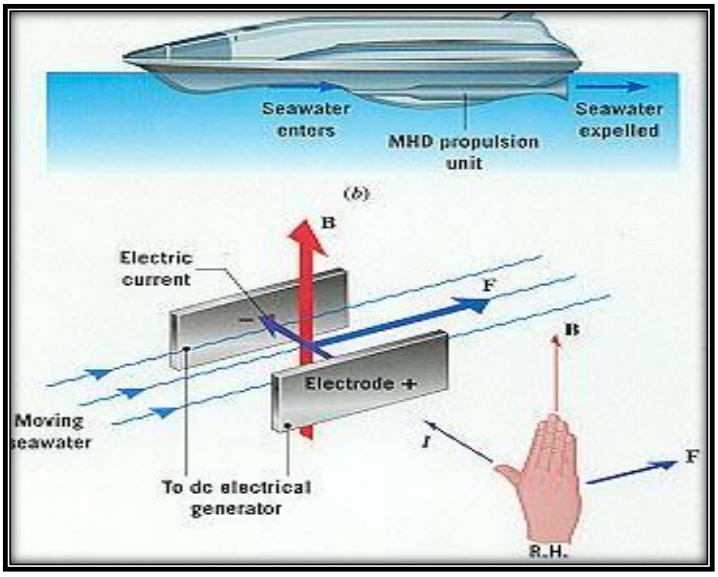

Figure 1.16: Generation of Propulsion Force in Jamato (Mitsubishi 1991)

1.9 Application of Nanofluids

Nanofluids have an unprecedented combination of the four characteristic features desired in energy systems (fluid and thermal systems); Increased thermal conductivity at low

nanoparticle concentrations, Strong temperature-dependent thermal conductivity, non-linear increase in thermal conductivity with nanoparticle concentration and increase in boiling critical heat flux. These distinctive features enhance nanofluid's potential applications to improve heat transfer and energy efficiency in industrial and engineering areas including industrial coolants, smart fluids, nuclear reactors coolant, extraction of geothermal power, nanofluids in automobile fuels, brake fluids, car radiator coolant, microelectronics cooling, bio and pharmaceutical industry [64-66].

1.9.1 Heat Transfer Applications

Since the advent of nanofluids almost two decades ago, the potential of nanofluids in heat transfer applications has been highlighted in many publications [67-71]. These include industrial coolants, smart fluids, nuclear reactors, extraction of geothermal power. Electronic Applications.

1.9.1.1 Industrial Cooling Application

According to Routbort et al. [72], the use of nanofluids for industrial cooling will result in great energy savings and emissions reductions. For instance, in tyre plants, the productivity of many industrial processes is constrained by the lack of facility to cool the rubber efficiently as it is being processed, and as a result lots of heat transfer fluids are required. The use of water-based nanofluids can reduce the cost of production of the tyres and result in an increase in profit margins.

For US industry, the replacement of cooling and heating water with nanofluids has the potential to conserve 1 trillion Btu of energy [72]. For the US electric power industry, using nanofluids in closed loop cooling cycles could save about 10–30 trillion Btu per year (equivalent to the annual energy consumption of about 50,000–150,000 households)[24]. The associated emissions reductions would be approximately 5.6 million metric tons of carbon dioxide, 8,600 metric tons of nitrogen oxides, and 21,000 metric tons of sulfur dioxide [21]

Nelson et al [73] performed a flow-loop experiment to investigate the performance of polyalphaolefin nanofluids containing exfoliated graphite nanoparticle fibers in cooling, showed that, the specific heat of the nanofluids was 50% higher and the convective heat transfer was enhanced by 10% compared to those of the polyalphaolefin. It was also noted that both the specific heat capacity and the rate of heat transfer increased with increase in temperature. Ma et al. [74] proposed the concept of nanoliquid-metal fluid, as a promising

engineering possibility for making the highest conductive coolant whose thermal conductivity is several times higher than that of convective base fluids.

Generally, industrial coolants are used in public utilities; the oil and gas industry; the food and beverage processing industry; the chemicals and plastics industry; solar energy conversion to electricity and in buildings for heating, ventilation, and air conditioning (HVAC) systems.

1.9.1.2 Smart Fluid

In this era of energy saving and the widespread use of battery operated devices, such as cellphones and laptops, have accented the necessity for a smart technological handling of energetic resources. Smart materials have one or more properties that can be dramatically altered, eg, smart material with variable viscosity may turn from a fluid which flows easily to a solid. Nanofluids have been demonstrated to be able to handle this role in some instances as a smart fluid.

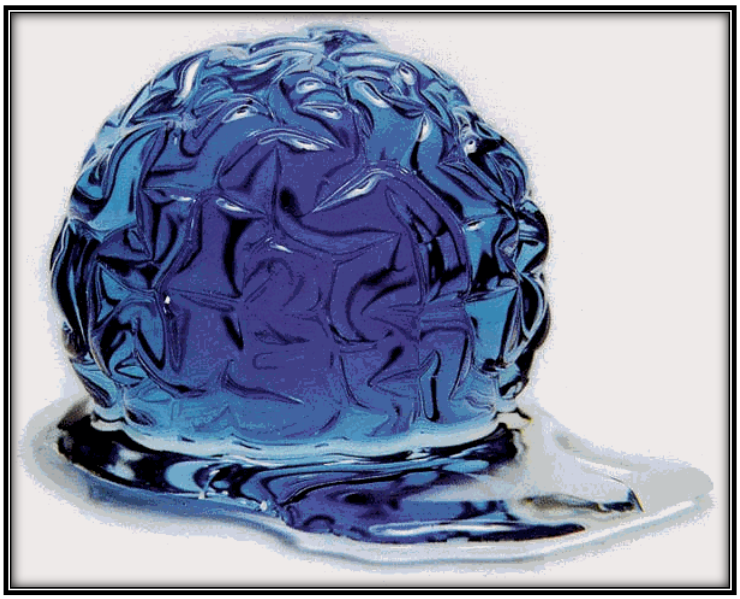

Figure 1.17: A smart fluid developed in labs at the Michigan Institute of Technology

[2001 SMA/MEMS Research Group]

Nanofluids can be used as a smart material working as a heat valve to control the flow of heat, where heat transfer can be reduced or enhanced at will [75]. The nanofluid can be readily configured either in a “low” state, where it conducts heat poorly, or in a “high” state, where the dissipation is more efficient. This shows that nanofluids can be used as a double

edged sword to provide heating or cooling technologies as required. In particular, Magneto-rheostatic (MR) materials is a nanofluid, which consists of tiny iron particles suspended in oil. It changes from a thick fluid (similar to motor oil) to nearly a solid substance within the span of a millisecond when exposed to a magnetic field, and the effect is completely reversed when the field is removed.

MR fluids are being developed for use in car shocks, damping washing machine vibration, prosthetic limbs, exercise equipment, and surface polishing of machine parts.

Figure1.18: The MR Fluid is liquid on the left, and as a solid in magnetics field on the right[2001 SMA/MEMS Research Group]

1.9.1.3 Nuclear Reactors

A nuclear reactor is a system that contains and controls sustained nuclear chain reactions. Reactors are used for generating electricity, moving aircraft carriers and submarines, producing medical isotopes for imaging and cancer treatment, and for conducting research. Fuel with heavy atoms are placed in a reactor vessel with neutrons. The neutrons start a chain reaction where each atom splits releasing more neutrons that cause other atoms to split. This produces large amounts of energy in form of heat. The heat is carried to coolants, which heat up and go off to a turbine to spin a generator, thus producing electricity. This provided clean energy alternative that frees us from the shackles of fossil fuel dependence. Kim et al. [76,77], at the Nuclear Science and Engineering Department of the Massachusetts

Institute of Technology (MIT),carried feasibility studies on the use of nanofluids in nuclear energy industry as an alternative to improving the performance of water-cooled nuclear system for heat removal. The studies have shown possible applications in pressurized water reactor (PWR) primary coolant, standby safety systems, accelerator targets, plasma divertors, and so forth [78].

Nanofluids can be used as the main reactor coolant for PWRs, thus enabling significant power uprates the PWRs and enhancing their economic performance. The experiments demonstrated that, the use of nanofluids with at least 32% higher critical heat flux (CHF) enabled a 20% power density uprate in current plants without changing the fuel assembly design and without reducing the margin to CHF.

Nanofluids can also be used as a coolant for the emergency core cooling systems (ECCSs) of both PWRs and boiling water reactors, where they could cool down overheat surfaces more quickly leading to an improvement in power plant safety. The use of a nanofluid in the ECCS accumulators and safety injection can increase the peak-cladding-temperature margins (in the nominal-power core) or maintain them in uprated cores if the nanofluid has a higher post-CHF heat transfer rate.

Another possible application of nanofluids in nuclear systems is the alleviation of postulated severe accidents during which the core melts and relocates to the bottom of the reactor vessel. If such accidents were to occur, it is desirable to retain the molten fuel within the vessel by removing the decay heat through the vessel wall. This process is limited by the occurrence of CHF on the vessel outer surface, but analysis indicates that the use of nanofluid can increase the in-vessel retention capabilities of nuclear reactors by as much as 40% [79]

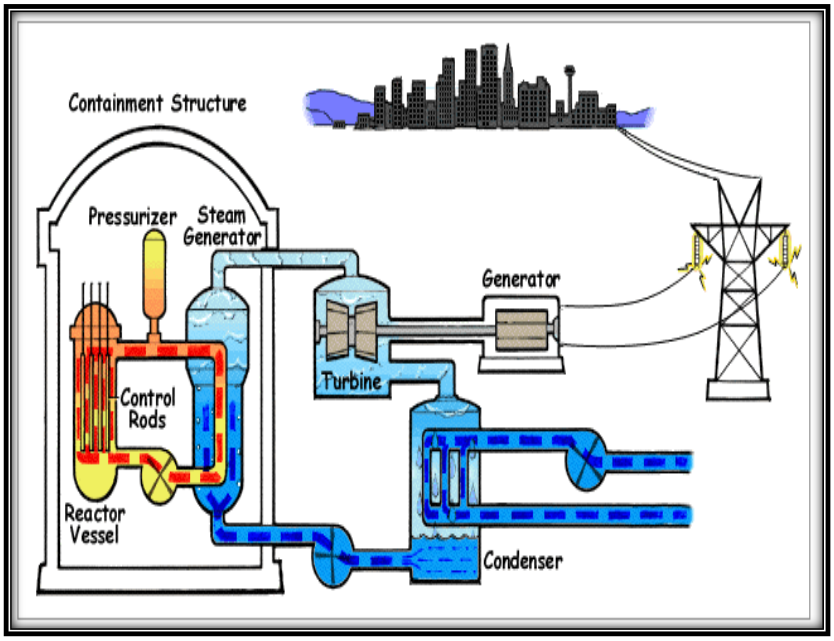

Figure 1.19: Nuclear Reactor Plant (Image Source: http://www.english-online.at/technology/nuclear-power/nuclear-energy.htm, 26th November, 2013)

1.9.1.4 Geothermal Power Extraction

When extracting energy from the earth's crust that varies in length between 5 to 10 km and temperature between 500^{o}C and 1000^{o}C, nanofluids can be employed to cool the pipes exposed to such high temperatures. When drilling, nanofluids can serve in cooling the machinery and equipment working in high friction and high temperature environment. As a "fluid superconductor," nanofluids could be used as a working fluid to extract energy from the earth core and processed in a pressurized water reactor(PWR) power plant system producing large amounts of work energy [80]. In drilling technology, which in vital in geothermal power, the use of nanofluids can ensure improved sensors and electronics capable of operating at higher temperature. Such improvements will enable access to deeper and hotter regions. Nanofluids can be used as a highly specialized drilling fluid that has superior performance in high temperature drilling.

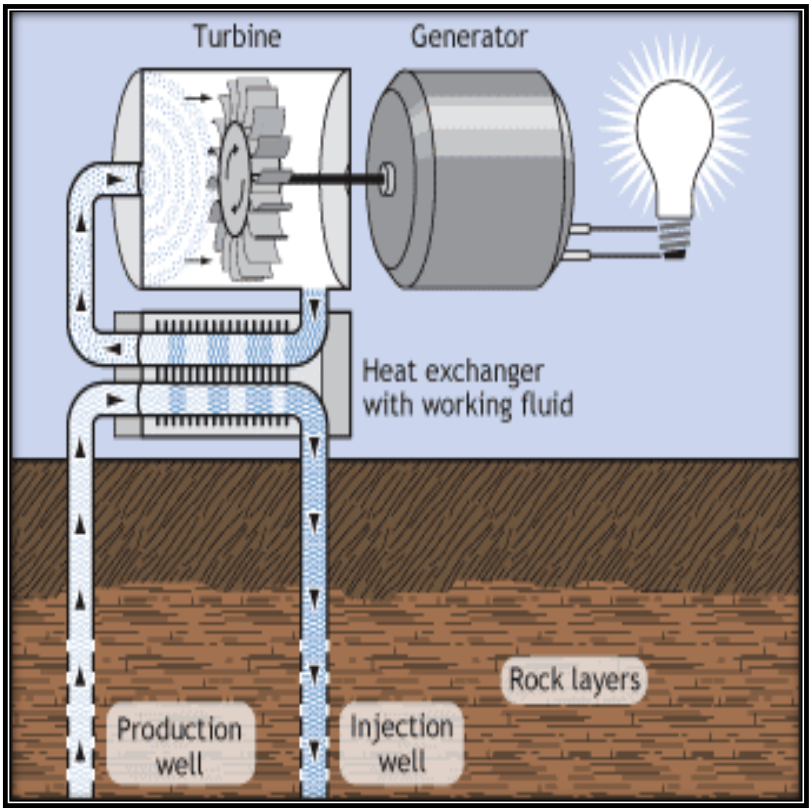

Figure 1.20: Binary Cycle Power Plant (Image Source: EERE, Courtesy of the U.S. Dept. of Energy).

1.10 Electronic Applications

Nanofluids are used for cooling of microchips in computers as well as in other electronic applications which use microfluidic applications. Due to rapid development in modern technology, current electronic systems generate a huge amount of heat, which deteriorates the performance of the devices and decreases their reliability [81].

1.10.1 Cooling of Personal Computers and Microchips

A principal limitation on developing smaller high density microchips is the heat dissipation problem. Advanced electronic devices face thermal management challenges from the high level of heat generation and the reduction of available surface area for heat removal. This challenge can be overcome either by finding an optimum geometry of cooling devices or increasing the heat transfer capacity. Nanofluids can be used for liquid coolant of computer processors due to their high thermal conductivity and increased heat transfer coefficient. A study by Jang and Choi [82] illustrated that a combined microchannel heat sink with nanofluids had the potential as the next-generation cooling devices for removing ultrahigh heat flux.

With increased thermal dissipation of the computer processing unit (CPU), the thermal dissipation requirements on the personal computer have become more challenging. One of the methods employed to overcome this challenge is the use of heat pipes with nanofluids as the working medium for enhanced thermal performances. At a same charge volume, there is a significant reduction in thermal resistance of heat pipe with nanofluids containing gold nanoparticles as compared with water [83]. Investigations on various nanoparticles have shown that nanofluids containing silver or titanium nanoparticles could be used as an efficient cooling fluid for devices with high energy density.

Figure 1.21: Computer Microchip and Laptop

1.10.2 Microscale Fluidic Applications

The manipulation of small volumes of liquid is necessary in fluidic digital display devices, optical devices, and microelectromechanical systems(MEMS) such as lab-on-chip analysis systems. This can be achieved by electrowetting, or reducing the contact angle by an applied voltage, the small volumes of liquid. One of most useful methods of microscale liquid manipulation is Electrowetting on dielectric (EWOD) actuation. Vafaei et al. [84] discovered that nanofluids are effective in engineering the wettability of the surface and possibly of surface tension. Dash et al. [85] demonstrated that the use of nanofluids in EWOD resulted in increased performance and stability when exposed to electric fields. Since the contact angle of droplets of nanofluids can be changed has potential applications for efficiently moving liquids in microsystems, allowing for new methods for focusing lenses in miniature cameras as well as for cooling computer chips.

1.11 Automotive Applications

Nanofluids are been used in automobile for applications such as coolant, fuel additives, lubricant, shock absorber and refrigerant. The current engine oils, automatic transmission fluids, coolants, lubricants, and other synthetic high-temperature heat transfer fluids found in conventional truck thermal systems radiators, engines, heating, ventilation and air-conditioning (HVAC)—have inherently poor heat transfer properties. These could benefit from the high thermal conductivity offered by nanofluids. Nanofluids are commonly used in cooling radiators for automobiles and trucks, and power electronics for hybrid electric vehicles.

1.11.1 Nanofluid Coolant

In order to improve the aerodynamic designs of vehicles, and subsequently the fuel economy, manufacturers must reduce the amount of energy needed to overcome wind resistance on the road. At high speeds, approximately 65% of the total energy output from a truck is expended in overcoming the aerodynamic drag [65]. This fact is partly due to the large radiator in front of the engine positioned to maximize the cooling effect of oncoming air. The use of nanofluids as coolants would allow for smaller size and better positioning of the radiators. Owing to the fact that there would be less fluid due to the higher efficiency, coolant pumps could be shrunk and truck engines could be operated at higher temperatures

allowing for more horsepower while still meeting stringent emission standards. Future engines designed using nanofluids' cooling properties will run at more optimal temperatures allowing for increased power output. With a nanofluids engine, components would be smaller and weigh less allowing for less fuel consumption, saving consumers money and resulting in fewer emissions for a cleaner environment. Singh et al. [86], researchers at Argonne National Laboratory assessing the applications of nanofluids for transportation, determined that the use of high-thermal conductive nanofluids in radiators can lead to a reduction in the frontal area of the radiator by up to 10%. This new aerodynamic automotive designs which minimizes the aerodynamics drag not only leads to fuel saving of up to 5% but reduces emissions as well. The use of nanofluid also lead to a reduction of friction and wear, reducing parasitic losses, operation of components such as pumps and compressors, hence more than 6% fuel savings.

It can be concluded that the use of nanofluids will enhance the efficiency and economic performance of car engines, as well as greatly influence the structure design of automotives, such as smaller and lighter engine radiators cooled by a nanofluids which can be placed elsewhere in the vehicle as opposed to the front of the car. By reducing the size and repositioning the radiator, a reduction in weight and wind resistance could enable greater fuel efficiency and subsequently lower exhaust emissions.

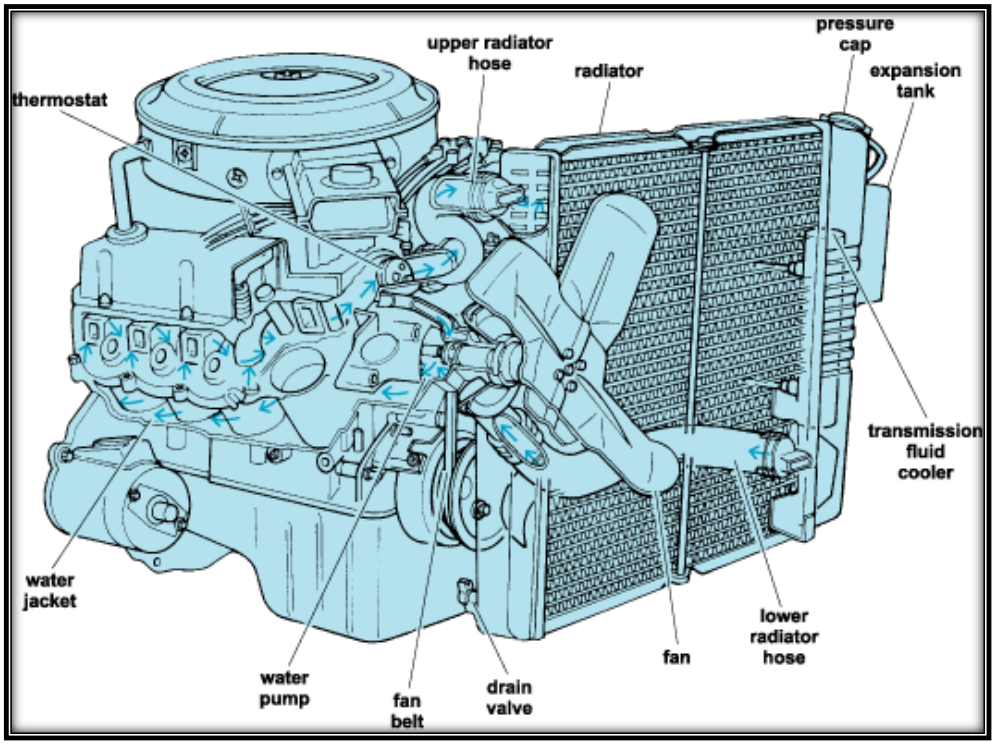

Figure 1.22: Engine Cooling System(Image Source: crankshaftcoalition website)

1.11.2 Nanofluid in Fuel

The aluminium nanoparticles, produced using a plasma arc system, are covered with thin layers of aluminium oxide, owing to the high oxidation activity of pure aluminium, thus creating a larger contact surface area with water and allowing for increased decomposition of hydrogen from water during the combustion process. During this combustion process, the alumina acts as a catalyst and the aluminium nanoparticles then serve to decompose the water to yield more hydrogen. It was shown that the combustion of diesel fuel mixed with aqueous aluminium nanofluid increased the total combustion heat while decreasing the concentration of smoke and nitrous oxide in the exhaust emission from the diesel engine [87,88].

1.11.3 Brake and Other Vehicular Nanofluids

As vehicle aerodynamics is improved and drag forces are reduced, there is a higher demand for braking systems with higher and more efficient heat dissipation mechanisms and properties such as brake nanofluid. A vehicle's kinetic energy is dispersed through the heat produced during the process of braking and this is transmitted throughout the brake fluid in the hydraulic braking system. If the heat causes the brake fluid to reach its boiling point, a vapor-lock is created that retards the hydraulic system from dispersing the heat caused from braking. Such an occurrence will in turn will cause a brake malfunction and pose a safety hazard in vehicles. Since brake oil is easily affected by the heat generated from braking, nanofluids will maximize performance in heat transfer as well as remove any safety concerns [65]

1.12 Heating Buildings and Reducing Pollution

In cold regions, ethylene or propylene glycol mixed with water in different proportions is commonly uses as a heat transfer fluid. Kulkarni et al. [89] showed that using nanofluids in heat exchangers could reduce volumetric and mass flow rates, resulting in an overall pumping power savings. They demonstrated that nanofluids made it possible to have less expensive smaller heating systems, which are capable of delivering the same amount of thermal energy as larger heating systems. This will also reduce environmental pollutants, because smaller heating units use less power, and the heat transfer unit has less liquid and material waste to discard at the end of its life cycle.

1.13 Biomedical Applications

1.13.1 Magnetic Drug Targeting

Magnetism plays an important role in living beings metabolism. For example, the haemoglobin in our blood is an iron complex and is magnetic in nature. Magnetite, Fe_3O_4, is a biocompatible structure and therefore it is one of the most extensively used biomaterials for different biological and medical applications from cell separation and drug delivery to hyperthermia [90]. One of the main problems of chemotherapy is often not the lack of efficient drugs, but the inability to precisely deliver and concentrate these drugs in affected areas. Failure to provide localized targeting results is an increase of toxic effects on neighboring organs and tissues. One promising methods to accomplish precise targeting is magnetic drug delivery. Medicine is bound to magnetic particles (ferrofluids) which are biologically compatible and injected into the blood stream. The targeted areas are subjected to an external magnetic field that is able to affect the blood stream by reducing its flow rate. In these regions the drug is slowly released from the magnetic carriers. Consequently, relatively small amounts of a drug magnetically targeted to the localized disease site can replace large amounts of the freely circulating drug. At the same time, drug concentrations at the targeted site will be significantly higher compared to the ones delivered by standard (systemic) delivery methods. When magnetic fluids are used as a delivery system for anticancer agents in localized region tumor therapy it minimizes undesirable side effects in the organism and to increase its localized effectiveness [91]. Very encouraging findings have been recently reported in the clinical application of magnetic drug targeting including patients with an advanced and unsuccessfully pre-treated cancer or sarcoma [92]. Interactions between the magnetic particles passing through the blood with the external magnetic field are studied using MHD equations and Finite Element analysis. Thus efficacy of such treatments can be estimated. New applications are concerning the use of injectable magnetic fluids in the eye tissues since they could be capable of repairing all areas of the damaged retina [92]. The researchers speculate that use of a magnetized version of the conventional silicone fluid technique would facilitate tissue repairs and make the process more precise due to the possibility of the magnetic fluid driving toward those areas of the eye that are more difficult to reach.

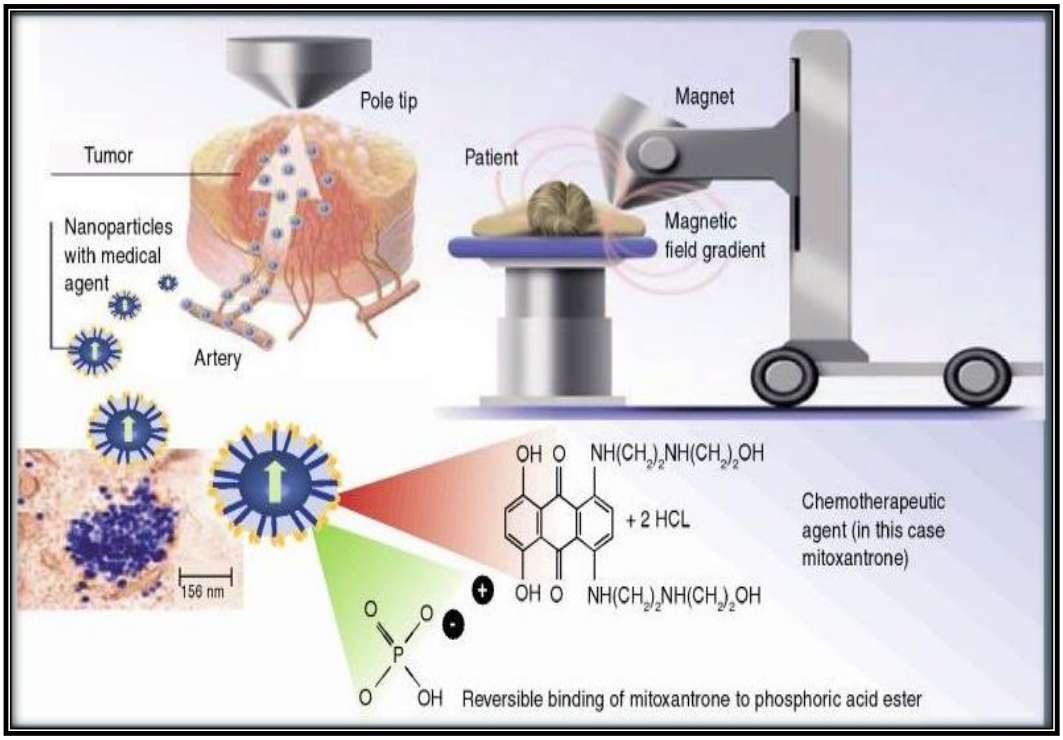

Figure 1.23: Magnetic Drug Targeting (Source: Nanomedicine ©2009 Future Medicine Ltd)

1.13.2 Nanodrug Delivery

Modern technology advancement has resulted to the recent development in bio-microelectromechanical systems(MEMS), such as; electronically activated drug delivery microchip[93] - a controlled delivery system via integration of silicon and electroactive polymer technologies; a MEMS-based DNA sequence developed by Cepheid [94], in-plane and out-of-plane hollow micro-needles for dermal/transdermal drug delivery [95,96] and nanomedicine applications of nanogels or gold-coated nanoparticles [97]. The development of the integrated micro- or nanodrug delivery has led to easy monitoring and controlling target-cell responses to pharmaceutical stimuli, better understanding of biological cell activities, and drug development processes. While conventional drug delivery is characterized by uncertainity, microdevices facilitate precise drug delivery by both implanted and transdermal techniques. Employing nanodrug delivery (ND) systems, controlled drug release takes place over an extended period of time. Thus, the desired drug concentration will be sustained within the therapeutic window as required.

1.13.3 Nanocryosurgery

Cryosurgery is a procedure that uses freezing to destroy undesired tissues. Although, its cannot be regarded as a routine method for cancer treatment, Cryosurgery is becoming a popular alternative to traditional therapies because of its important clinical advantages. According to simulations performed by Yan and Liu [98], intentional loading of nanoparticles with high thermal conductivity into the target tissues can reduce the final temperature, increase the maximum freezing rate, and enlarge the ice volume obtained in the absence of nanoparticles. Also, introduction of nanoparticle enhanced freezing could also make conventional cyrosurgery more flexible in many aspects such as artificially interfering in the size, shape, image and direction of iceball formation. The concepts of nanocyrosurgery may offer new opportunities for future tumor treatment. Magnetite (Fe_3O_4) and diamond are perhaps the most popular and appropriate choice for enhancing freezing because of their good biological compatibility.

1.13.4 Nanofluid-based optical filter optimization for PV/T systems

Optical filters can be created from specialized nanoparticle suspensions, for instance, nanofluid-based filters for hybrid solar photovoltaic/thermal (PV/T) applications. This particular application is suitable because nanofluids can be utilized as both volumetric solar absorbers and flowing heat transfer mediums.

Well-designed PV/T systems provide significant financial savings for residential and industrial applications where demands for both electrical and thermal energy are presented. Most commonly PV/T systems put the working fluid directly in contact with the PV system, thereby removing excess heat. This type of design necessitates a compromise between the drop in efficiency with temperature for PV cells and the value of higher output temperatures from the thermal system. However, the use of nanofluids provide a solution to this challenge, thus improve the performance of solar thermal systems. The advantage of using nanofluids is that they can easily be pumped in and out of a system or controlled by magnetic/electric fields, making them ideal for applications where dynamic optical switching is desired. For solar energy harvesting applications, this is especially advantageous because a nanofluid-based filter can also be used as the heat transfer and thermal storage medium. Thus, with a nanofluid filter, it is possible to de-couple the PV and thermal systems so that each can operate at optimum temperature. Nanofluid-based filters provide superior solar-weighted efficiency to pure fluids and comparable efficiency to conventional optical filters over the solar wavelengths—ultraviolet to near infrared.

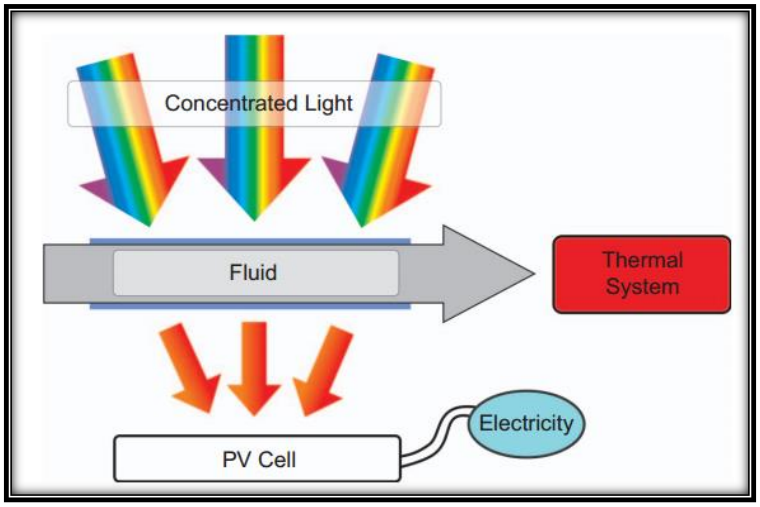

Figure 1.24: De-coupled PV/T system (Image Source: Natural Journal website)

1.14 Other Applications

1.14.1 Nanofluid Detergent

The unique behaviour of Nanofluids in classical concepts of spreading and adhesion on solid surfaces, opens up the possibility of nanofluids being excellent candidates in the processes of soil remediation, lubrication, oil recovery and detergency. Future engineering applications could abound in such processes [85].

1.14.2 Literature Review

The laws of magnetism and fluid flow are hardly a 20th century innovation yet MHD became a fully - fledged subject only in the late 30's or early 40's. Thus while there were a few isolated experiments in 19th century by Physicists such as faraday (1832)[99], who tried to measure the voltage across the Thames, induced by its motion through the earth's magnetic field, the subject languished until the turn of the century, when Astrophysicists realized how ubiquitous magnetic fields and plasmas are throughout the universe. In 1942, an engineer – astrophysicist Alfven [100] coined the term MHD in his classical paper, and this marked the emergence of a full-pledged MHD. He discovered the MHD wave known as Alfven w, which has a number of applications of MHD in astrophysical problems. Around the same time, geophysicists began to suspect that the earth's magnetic field was generated by a dynamo action within the liquid metals of its core, a hypothesis first put forward in 1919 by Larmor [101]. MHD flow between two parallel plates is a classical problem that has importance in many applications such as; MHD power generators and pumps, cooling of nuclear reactors,

geothermal systems, nuclear waste disposal, petroleum and polymer technology and others [102]. The experimental investigations of modern MHD flow in a laboratory was carried out by Hartmann and Lazarus [103]. They analyzed the influence of the effects of a transverse uniform magnetic field on the flow of a viscous incompressible electrically conducting fluid exiting through parallel stationary plates that are insulated. This culminated with the design of a mercury pump to put mercury in motion in the presence of a transverse magnetic field. Plasma physicists, on the other hand, acquired an interest in MHD and in 1950 thermonuclear research began with the work of Sakharov et al [104]. They formulated the principles of magnetic confinement of high temperature plasmas that would allow the development of a thermonuclear reactor. Development of MHD in Engineering was pioneered by Hartman, who invented the electromagnetic pump 1n 1918 [105]. He undertook theoretical and experimental investigations of the flow of mercury in a homogenous magnetic field (1837). In 1958 Rosson, investigated flow of electrically conducting fluids over a flat plate in the presence of transverse magnetic field[106].The impetus for change came in 1960s largely as a result of i) fast breeder reactors using sodium as a coolant and this needed to be pumped. ii) Controlled thermonuclear fusion which required hot plasma to be confined away from material surface by magnetic forces. iii) MHD generators in which ionized gas needed to be propelled through a magnetic field to offer improved power stations efficiencies. This lead to research in metallurgical MHD. Magnetic fields are used to heat, pump, stir, and levitate liquid metals in metallurgical industries. This uses the Lorentz force to provide non-intrusive means of controlling the flow of metals. With constant pressure to produce cheaper, better and more consistent materials, MHD, provides a unique means of exercising greater control over casting and refining processes. Laminar boundary layer behavior over a moving continuous and linearly stretching surface is a significant type of flow has considerable practical applications in engineering, electrochemistry, and polymer processing. Samad, and Mohebujjaman [107] investigated MHD boundary-layer flow and mass transfer past a vertical plate in a porous medium with constant heat flux. Sakiadis [108] numerically studied the boundary layer flow over a stretching surface moving with a constant velocity, while Tsou et al. [109], confirmed the results of Sakiadis experimentally by analyzing the effects of heat transfer on a continuously moving surface with constant velocity. Ibrahim et al. [110] investigated the combined effect of wall suction and magnetic field on boundary layer flow with heat and mass transfer over an accelerating vertical plate. Makinde [111] analysed the magnetohydrodynamics boundary layer flow with heat and mass transfer over a moving vertical plate in the presence of magnetic field and a convective heat exchange at the surface with the surrounding.

Mixed convection flow with simultaneous heat and mass transfer from different geometrics embedded in porous media has many engineering and geophysical applications such as geothermal reservoirs, drying of porous solids, thermal insulation, enhanced oil recovery, packed-bed catalytic reactors, cooling of nuclear reactors and underground energy transport [112].Singh et al. [113] studied the transient free convection flow of a viscous incompressible fluid in a vertical parallel plate channel, when the walls are heated asymmetrically. Jha [114] studied the combined effect of natural convection and uniform transverse magnetic field on the unsteady couette flow. Makinde [115], studied Free-convection flow with thermal radiation and mass transfer past a moving vertical porous plate. The effect of suction and injection on ordinary fluid flow and heat transfer as well as skin friction coefficients for the steady, laminar, free convection boundary layer flow generated above a heated horizontal rectangular surface was studied by Hossain and Mojumder [116]. Researchers in heat transfer have been carried out over the previous several decades, leading to the development of the currently used heat transfer techniques such as MHD generator channels, nuclear reactors, geothermal energy extractions, heat transfer involving metallurgical and metal working processes and others.

Many numerical studies on the various aspects of boundary layer flow with heat transfer over surfaces have been carried. Ibrahim and Makinde [117], investigated the chemically reacting MHD boundary layer flow of heat and mass transfer over a moving vertical plate with suction. The velocity and heat transfer in a boundary layer flow with thermal radiation past a moving vertical porous plate was examined by Makinde et al. [118]. Ali [119] studied the thermal boundary layer of a continuous stretching surface.

Till today, there has been many studies regarding heat transfer of fluids other than nanofluids. However, the number of articles related to nanofluids has increased exponentially, since the discovery of the term nanofluid by Choi in 1995 [1]. The research on nanofluids has mainly focused on the prediction and measurement techniques in order to evaluate their thermal conductivity. Some experimental investigations [27,28,120,121] have revealed that the nanofluids have remarkably higher thermal conductivities than those of conventional pure fluids and shown that the nanofluids have great potential for heat transfer enhancement. It incurs little or no penalty in pressure drop because the nanoparticles are so small that the nanofluid behaves like a pure fluid. Nanofluids are expected to be suitable for the engineering application without severe problems in pipeline and with little or no pressure drop. Jang et al. [122] carried studies on the role of Brownian motion in the enhancement of thermal conductivity of nanofluids. The role of Brownian motion hydrodynamics on

nanofluid thermal conductivity was explained by Evans [123]. Most studies of the transport properties of the nanofluids were focused on the thermal conductivity.

Convective heat transfer in nanofluids has received much attention in recent years. Chang et al. [124], Putra et al. [125], Bernaz et al. [126], Khanafer et al.[127], Wen and Ding [128], Rong et al. [129], Chen et al. [130], Xuan and Li [131], Pak and Cho [132], Tahery et al. [133] and Hakan [134] numerically investigated heat transfer performance of nanofluids. Most of the studies were on free convection, however, Maïga et al. [135] carried out studies on forced convection of alumina particles suspended in water and ethylene glycol in a uniformly heated tube. They found that the heat transfer coefficient and the wall shear stress increase with increasing nanoparticle volume fraction and Reynolds number. Peyghambarzadeh et al. [136] carried out experiments on forced convective heat transfer in a car radiator using water or a mixture of water and anti-freezing material like ethylene glycol. They noted that the nanofluids significantly increased the heat transfer rates, and the heat transfer rates depended on particle concentration, flow conditions(rate of fluid flow) and weakly depended on temperature. This shows that nanofluids are highly suited for use in effective radiators for cars. These research findings, erases any doubts that, that adding nanoparticles to a base fluid will increase its thermal conductivity. It can be concluded that improving the thermal conductivity is the key to improving heat transfer characteristics of convectional fluids. However, it has been observed that, The natural convective heat transfer coefficient decrease systematically with increasing nanoparticle concentration, and the deterioration is partially attributed to the high viscosity of nanofluids [137]. Lee and Choi [26] applied the nanofluid as the coolant to a microchannel heat exchanger for cooling crystal silicon mirrors used in high-intensity X-ray sources and pointed out that the nanofluid dramatically enhanced cooling rates compared with the conventional water-cooled and liquid-nitrogen-cooled microchannel heat exchangers.

The problem of incompressible, viscous, forced convective laminar boundary layer flow of copper water and alumina water nanofluid over a flat plate was investigated by Anjali and Andrews [138]. Using nanofluids strongly influences the boundary layer thickness by modifying the viscosity of the resulting mixture leading to variations in the mass transfer in the vicinity of walls in external boundary-layer flows[139]. More recently, heat transfer problems for boundary layer flow with a convective boundary condition for nanofluids were investigated by Aziz [140], Makinde and Aziz [141], and Ishak [142]. There has been little research on MHD boundary layer flow and heat transfer of nanofluids. Nourazar et al. [143] carried studies on the two-dimensional forced convection boundary layer MHD

incompressible flow of nanofluid over a horizontal stretching flat plate with variable magnetic field including the viscous dissipation effect, and solved the resulting non linear partial equations using the homotopy perturbation method (HPM). Hamad et al. [144] investigated the steady laminar two-dimensional flow of water based nanofluid (with copper, alumina and silver as nanoparticles) past a vertical semi-infinite flat plate in the presence of an applied magnetic field. A convective flow and heat transfer of an incompressible viscous nanofluid past a semi-infinite vertical stretching sheet in the presence of a magnetic field was investigated by Hamad [145]. The study natural convection in an enclosure filled with a water-Al_2O_3 nanofluid under the influenced of a magnetic field was carried out by Ghasemi et al. [146].

There has been lots of research on heat transfer of fluids in general but not of nanofluids. There is need for more research in the heat transfer of nanofluids especially with metal nanoparticles, some of which possess magnetic properties.

The impact of heat transfer technology is vital, since heat exchangers are ubiquitous in all types of industrial applications. Model studies of MHD with heat transfer and boundary layer have been many. Despite the fact that there has been numerous research on MHD of base fluids and the research on nanofluids characteristics has escalated exponentially, there is little study, which combines both areas to find the characteristics of nanofluids flow in a magnetic field. There has been lots of research on thermal conductivity and heat transfer characteristics of nanofluids, and the few done under the influence of a magnetic field, do not put into consideration the different electrical conductivity of the nanoparticles and base fluids, hence the nanofluid.

The motivation behind our study is to contribute towards this gap in numerical study on boundary heat transfer and boundary layer problem of MHD flows using nanofluids.

1.14.3 Statement of the Problem

Different convectional heat transfer fluids and nanoparticles have different electrical conductivities, and behave differently in the presence of a magnetic field. It is then expected that Nanofluids (which is a mixture of base fluids and nanoparticle) to be electrically conducting and hence susceptible to MHD. The flow of electrically conducting fluids in the presence of a magnetic field has many industrial and engineering applications. Thus, the influence of a magnetic field on nanofluids flow cannot be overlooked and requires investigation.

1.15 Research Objectives

1) To formulate mathematical models for different flow geometries of nanofluids under the influence of a magnetic field.
2) To develop numerical algorithms for solving the model problems.
3) To find the differences in flow behavior of convectional fluids and nanofluids in a magnetic field.
4) To investigate the effects of magnetic field on heat transfer characteristics of nanofluids compared to base fluids.
5) To investigate the effects of magnetic field on the skin friction due to nanofluids compared to base fluids.

1.16 Significance of the Study

Many natural phenomena and engineering problems are susceptible to MHD analysis. In natural phenomena, since magnetic field exists everywhere in the world, it follows that MHD phenomena must occur whenever conducting fluids are available. It is useful in astrophysics because much of the universe is filled with widely spaced, charged particles permeated by magnetic fields. Geophysics encounter MHD phenomena when dealing with the presence of conducting fluids and magnetic fields in and around the earth. On the other hand, MHD is of great significance because its principles are employed by engineers in the design of many industrial applications such as MHD generators, pumps, flow meters, cooling of nuclear reactors, geothermal energy extractors, nuclear waste disposal, heat exchangers, in solving space vehicle propulsion. MHD devices have been used for stirring, levitating, and controlling flows of liquid metals for metallurgical processing and other applications. Further importance of MHD is illustrated by the recent advancement of its application in plasma confinement. This innovation which is partially a MHD problem which will free mankind of energy shortage, by providing much more energy for a given weight of fuel than any technology in use and at the same time reducing thermal pollution.

The study of MHD flows with heat transfer has also received considerable attention due to its wide application in astrophysical problems such as sun-spot theory, motion of inter-stellar gas, re-entry problem of inter-continental ballistic missiles. Laws governing heat transmission are important to the engineer for metal-working processes, operation of heat-exchange apparatus, nuclear reactors, such to mention a few.

A more recent promising discovery is the application of MHD in drug targeting for the treatment of cancer. Suspensions of metal nanoparticles are being developed for medical applications including cancer therapy. One of the main problems of chemotherapy is often not the lack of efficient drugs, but the inability to precisely deliver and concentrate these drugs in affected areas. Failure to provide localized targeting results is an increase of toxic effects on neighboring organs and tissues. Medicine is bound to magnetic particles (ferrofluids) which are biologically compatible and injected into the blood stream. The targeted areas are subjected to an external magnetic field that is able to affect the blood stream by reducing its flow rate. In these regions the drug is slowly released from the magnetic carriers. This procedure ensures that drug concentrations at the targeted site is significantly higher compared to the ones delivered by standard (systemic) delivery methods. Interactions between the magnetic particles passing through the blood with the external magnetic field are studied using MHD equations and Finite Element analysis. Thus efficacy of such treatments can be estimated.

Miniaturization has been a major trend in modern science and technology. This trend has gone from the earlier millimeter scale to the present atomic scale. This trend is being actualized by the rapidly emerging microelectromechanical systems(MEMS) technology. Microscale products such as miniaturized sensors, motors, heat exchangers, pumps, medical devices have great advantage over the conventional systems. Since they are extremely compact and light weight, their manufacturing costs are lower, their fuel consumption is low and they need less space in buildings and engineering plants. These devices require ultra high performance cooling, which is crucial technical challenge facing many industrial and engineering applications. The conventional method for increasing heat transfer is to increase the area available for exchanging heat with a heat transfer fluid. Unfortunately the convectional heat transfer fluids used have low thermal conductivity, hence, there is an urgent need for new and innovative coolants with improved performance. The recent discovery of nanofluids, provides a solution to cooling technology. This is because nanofluids have fascinating features; high thermal conductivity at very low nanoparticles concentration and considerable enhancement of forced convective heat transfer. Nanofluids are also used as coolants for computers and nuclear reactors. Their cooling properties are used in many industrial applications. The main driving force for nanofluids research lies in a wide range of applications.

Most of these industrial and engineering applications using fluids, have a magnetic fields acting on the fluids. Current trend clearly shows that the convectional fluids are rapidly being replaced by nanofluids. The nanofluids will have to be used in magnetic fields since most of these applications have magnetic fields within them. There is then an urgent need to

investigate electrical conductivity, and heat transfer characteristics of nanofluids in the presence of a magnetic field.

1.17 Research Methodology

We employed a computational approach to solve the model problem which are boundary value problems (BVPs). The method is adequately explained in literature and gives accurate results for boundary layer equations. It involves, transforming the BVPs into a set of initial value problems(IVP) which contain unknown initial values that need to be determined by guessing, after which the fourth order Runge–Kutta Fehlberg iteration scheme is employed to integrate the set of IVPs until the given boundary conditions are satisfied. The entire computation procedure is implemented using a program which uses symbolic and computational computer language MAPLE. Being a BVP, the equations are automatically solved by the dsolve command by applying the appropriate algorithm. This involves solving the model problem numerically using the Newton–Raphson shooting method coupled with fourth-order Runge–Kutta integration scheme.

1.18 The Shooting Method

Many important physical problems always lead to boundary value problems(BVPs). The shooting method is one among the commonly used powerful numerical methods for solving boundary value problems for ordinary differential equations. In our study, we choose the shooting method to solve the boundary value problem, since it has many advantages such as ease of programming in a general form, less storage is required, and its suitability for automatic procedures. The shooting method is an iterative algorithm that reformulates the original boundary value problem to a related initial value problem (IVPs) with its appropriate initial conditions. The new problem requires the solution of the IVP with the initial conditions arbitrary chosen to approximate the boundary conditions at the end points. If these boundary conditions are not satisfied to the required accuracy, the procedure is repeated again with a new set of initial conditions until the required accuracy is acquired or a limit to the iteration is reached. The resultant IVP is solved numerically using any appropriate method for solving linear ordinary differential equations. In our case we use the 4^{th} order Runge-Kutta method, which provides high accuracy results. The solution of the IVP should converge to that of the BVP. The algorithm for the above procedure is achieved by using Maple programming language. The computed results are presented in graphical form.

We consider a two-point boundary value problem,

$$y'' = f(x, y, y'), \quad y(a) = \alpha \text{ and } y(b) = \beta \tag{1.2}$$

where $a < b$ and $x \in [a, b]$.

The requirement of the shooting method is to convert the BVP to an IVP with appropriate initial condition. Thus we have,

$$y'' = f(x, y, y'), \; y(a) = \alpha, \; y'(a) = s. \tag{1.3}$$

Introducing the notations $u(x;s) = y(x;s)$, $v(x;s) = \frac{\partial}{\partial x} y(x;s)$, equation (1.2) can be rewritten as a system of first order ODEs,

$$\begin{aligned} &\frac{\partial}{\partial x} u(x;s) = v(x;s), \quad u(a;s) = \alpha \\ &\frac{\partial}{\partial x} v(x;s) = f\left(x, u(x;s), v(x,s)\right), \quad v(a;s) = \beta. \end{aligned} \tag{1.4}$$

The solution $u(x;s)$ of the IVP (1.4), will coincide with the solution $y(x)$ of the BVP (1.2), as long as a value for s is found, such that,

$$\varphi(s) = u(b;s) - \beta = 0. \tag{1.5}$$

Equation (1.5) is solvable if and only if there exists $s \in R$, so that $\phi(s) = 0$ [122].

The essence of the shooting method for the solution of the BVP (1.2) is to find a root to the equation (1.5). A standard root-finding technique such as Bisection method or Newton-Raphson method is used.

1.18. 1 The Bisection Method

Suppose the two numbers s_1 and s_2 are known such that $\phi(s_1) < 0$ and $\phi(s_2) > 0$, we also assume that $s_1 < s_2$. Since the solution of the IVP depends on the initial conditions there exists at least one value of s in the interval $[s_1, s_2]$ such that $\phi(s) = 0$. Thus the interval $[s_1, s_2]$ contains a root of the equation (1.5). The method of bisection can then be used to approximate the root of (1.5).

We take the midpoint s_3 of the interval $[s_1, s_2]$, compute $u(b, s_3)$ and consider whether $\phi(s_3) = u(b; s_3) - \beta$ is positive or negative.

If $\phi(s_3) > 0$, then its in the interval $[s_1, s_3]$ that contain the root of ϕ, whereas if $\phi(s_3) < 0$ then it is in the interval $[s_3, s_2]$. Repeating this procedure generates a sequence of numbers $\{s_n\}_{n=1}^{\infty}$ converging the s. The process is terminated after a finite number of steps when the length of the interval containing s has become sufficiently small.

1.18.2 Newton-Raphson Method

This will help compute a sequence $\{s_n\}_{n=1}^{\infty}$ generated by $s_{n+1} = s_n - \dfrac{\varphi(s_n)}{\varphi'(s_n)}$. (1.6)

Starting with a value s_0 arbitrary chosen. To calculate $\phi'(s_n)$ we introduce new independent variables, $\xi(x;s) = \dfrac{\partial u(x;s)}{\partial x}$, $\eta(x;s) = \dfrac{\partial v(x;s)}{\partial x}$ and differentiate the IVP (1.4) with respect to *s* to obtain a 2nd IVP,

$$\begin{aligned} &\frac{\partial \xi(x;s)}{\partial x} = \eta(x;s), \qquad \xi(a;s) = 0, \\ &\frac{\partial \eta(x;s)}{\partial x} = p(x;s)\xi(x;s) + q(x;s)\eta(x;), \qquad \eta(a;s) = 1. \end{aligned} \quad , \tag{1.7}$$

where,

$$p(x;s) = \frac{\partial f\left(x, u(x;s), v(x;s)\right)}{\partial u}, \quad q(x;s) = \frac{\partial f\left(x, u(x;s), v(x;s)\right)}{\partial v} \tag{1.8}$$

We assign the value s_n to s, $n \geq 0$, then the IVP (1.4) and (1.7) can be solved using an numerical method for IVPs such as the 4th order Runge-Kutta method in the interval $[a,b]$. Thus an approximation of $u(b;s_n)$ is obtained to calculate $\phi(s_n) = u(b;s_n) - \beta$ and we also obtain an approximation $\xi(b;s_n) = \phi'(s_n)$. The values $\phi(s_n)$ and $\phi'(s_n)$ give the next Newton-Raphson iterate s_{n+1} from (1.6). The process is repeated until the iterate s_n settle to a fixed number of digits.

The problem with the shooting method is that it assumes that the BVP has a unique solution and also there is no guarantee that the IVP has a solution in the interval $[a,b]$.

1.18.3 The Runge-Kutta Method

The Runge-Kutta method is a numerical technique used to solve ordinary differential equations. It is based on the first five terms of the Taylors series. The scheme for the fourth order Runge-Kutta is;

$$y_{i+1} = y_i + \frac{1}{6}\left(k_1 + 2k_2 + 2k_3 + k_4\right), \tag{1.9}$$

where

$$k_1 = f\left(x_i, y_i\right), \tag{1.10a}$$

$$k_2 = f\left(x_i + \frac{1}{2}h, y_i + \frac{1}{2}k_1 h\right), \tag{1.10b}$$

$$k_3 = f\left(x_i + \frac{1}{2}h, y_i + \frac{1}{2}k_2 h\right), \tag{1.10c}$$

$$k_4 = f\left(x_i + h, y_i + k_3 h\right). \tag{1.10d}$$

A numerical code that incorporate the methods described above, using maple was developed to tackle the problems.

CHAPTER TWO

GOVERNING EQUATIONS OF FLUID DYNAMICS

2.1 Introduction

The basis of computational fluid dynamics is the fundamental of fluid dynamics governing equations, viz.; the continuity, momentum (Navier-Stokes equation) and the energy equations. These equations depict the physics of various flows. They are the mathematical statements of the three fundamental laws or principles upon which fluid dynamics is based:

(1) Mass is conserved for a system;

(2) Newton's Second Law: $F = ma$;

(3) First law of Thermodynamics: Energy is conserved.

The purpose of this chapter is to derive these equations.

2.2 The Continuity Equation

The continuity equation is based on the mass conservation principle or law, which states that *mass can neither be created nor be destroyed*. Conservation of mass is inherent to a control mass system (closed system). Mathematically the above law is stated as:

$$\Delta m/\Delta t = 0,$$

where m = mass of the system.

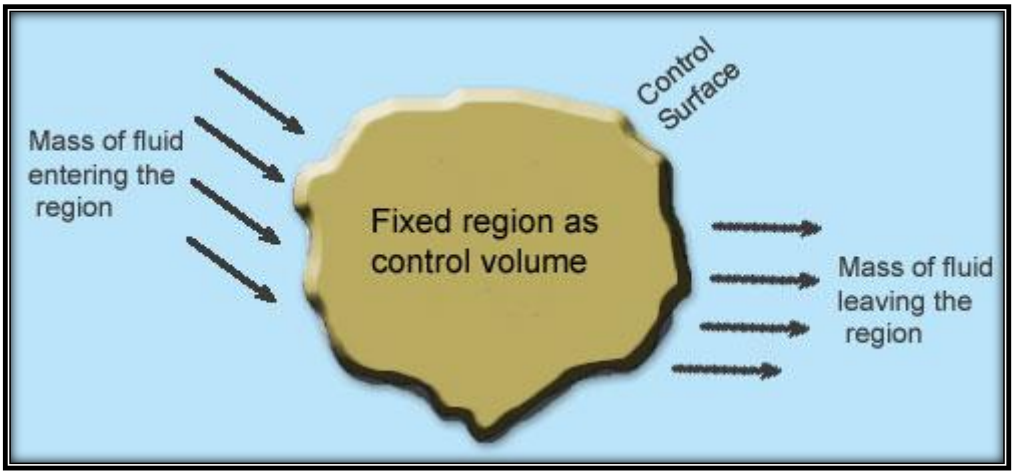

Figure 2.1: A Control Volume in a Flow Field

For a control volume (figure 2.1), the principle of conservation of mass requires that the net flow through the control volume is zero, that is, all fluid that is accumulated inside the control

volume plus all the fluid that is flowing into the control volume must be equal to the amount of fluid flowing out of the control volume.

Accumulation + Flow In = Flow Out

OR

Rate at which mass enters = Rate at which mass leaves the region + Rate of accumulation of mass in the region

OR

Rate of accumulation of mass in the control volume

+ Net rate of mass efflux from the control volume = 0. (2.1)

The above statement expressed analytically in terms of velocity and density field of a flow is known as the equation of continuity.

2.2.1 Continuity Equation: Differential Approach

Consider a small fluid element (control volume) where density and velocity in x, y, z directions are ρ, u, v, w respectively, thus, the volume is *dV = dxdydz*.

The mass within the control volume is;

$$\rho dV = \rho dx dy dz \; . \qquad (2.2)$$

According to the principle of conservation of mass, the rate at which mass increase within the fluid element is equal to the rate at which mass enters or leaves the fluid element through its six faces. The inflows (positive) and outflows (negative) are indicated on the fluid element using the first 2 terms of Taylors series expansion.

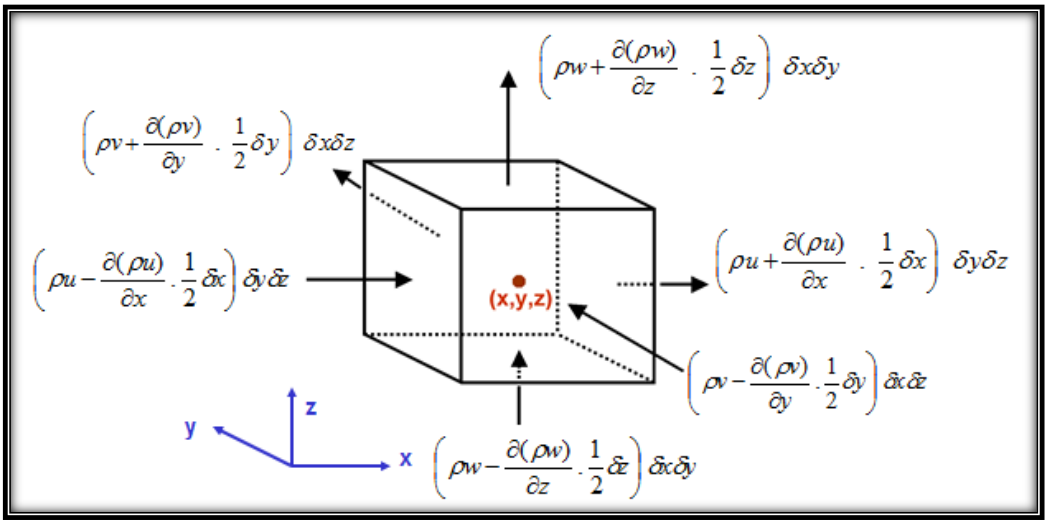

Figure 2.2: A Control Volume for Rectangular Cartesian Coordinate System

The net flow rate through the control volume for the *x*-direction is;

$$=\left(\rho u+\frac{\partial(\rho u)}{\partial x}\frac{\delta x}{2}\right)\delta y\delta z-\left(\rho u-\frac{\partial(\rho u)}{\partial x}\frac{\delta x}{2}\right)\delta y\delta z=\frac{\partial \rho u}{\partial x}\delta x\delta y\delta z\,, \quad (2.3)$$

Similarly, the net flow through the *y* and *z* faces are respectively;

$$\frac{\partial \rho v}{\partial y}\delta x\delta y\delta z\,,\ \ \frac{\partial \rho w}{\partial z}\delta x\delta y\delta z\,. \quad (2.4)$$

The time rate of change of mass inside the control volume is;

$$\frac{\partial}{\partial t}\left(\rho\partial x\partial y\partial z\right)=\frac{\partial \rho}{\partial t}\partial x\partial y\partial z. \quad (2.5)$$

Adding up the resulting net flow and diving by the volume of the fluid element (*dxdydz*),

$$\frac{\partial \rho}{\partial t}+\frac{\partial(\rho u)}{\partial x}+\frac{\partial(\rho v)}{\partial y}+\frac{\partial(\rho w)}{\partial z}=0. \quad (2.6)$$

This is the Continuity Equation for a compressible fluid in a rectangular Cartesian coordinate system.

2.2.2 Continuity Equation: Integral Approach

Consider a control volume, V, bounded by the control surface S.

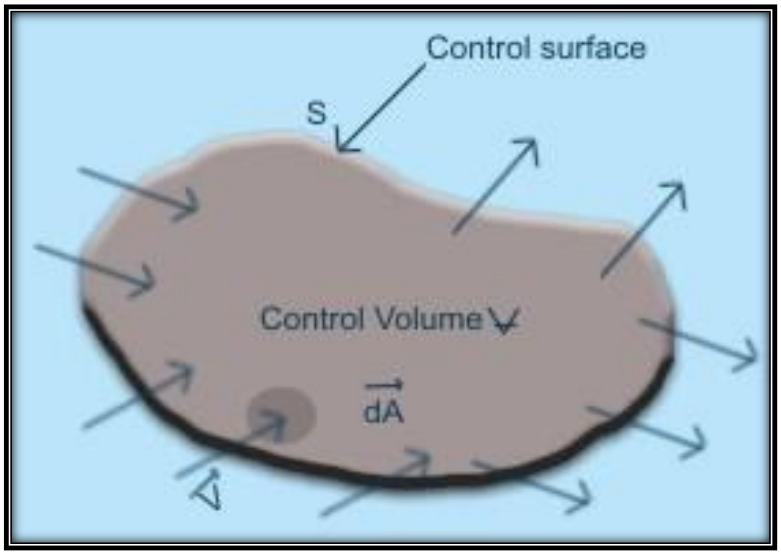

Figure 2.3: Control Volume

The net rate of mass efflux across the control surface, S , velocity vector $\vec{V}$ at an elemental area $d\vec{A}$ is;

$$\iint_s \rho\vec{V}d\vec{A}. \quad (2.7)$$

Mass accumulation rate within the control volume is therefore;

$$\frac{\partial}{\partial t}\iiint_v \rho dV. \tag{2.8}$$

where V is the total volume, the principle of conservation of mass states that, the rate of accumulation of mass in the control volume together with the rate of mass efflux from the control volume must be zero. Hence;

$$\frac{\partial}{\partial t}\iiint_v \rho dV + \iint_s \rho \vec{V} d\vec{A} = 0. \tag{2.9}$$

Applying Gauss's divergence theorem on the second expression on the left hand, then

$$\iint_s \rho \vec{V} d\vec{A} = \iiint_v div\left(\rho \vec{V}\right) dV = \iiint_v \nabla \cdot \left(\rho \vec{V}\right) dV. \tag{2.10}$$

Substituting equation (2.10) to (2.9), we have;

$$\frac{\partial}{\partial t}\iiint_v \rho dV + \iiint_v \nabla \cdot \left(\rho \vec{V}\right) dV = 0. \tag{2.11}$$

Hence,

$$\frac{\partial \rho}{\partial t} + \nabla \cdot \left(\rho \vec{V}\right) = 0. \tag{2.12}$$

The continuity equation (2.12) can be written in a vector form as;

$$\frac{\partial \rho}{\partial t} + \left(\frac{\partial}{\partial x}\hat{i} + \frac{\partial}{\partial y}\hat{j} + \frac{\partial}{\partial z}\hat{k}\right).\left[\rho u\hat{i} + \rho v\hat{j} + \rho w\hat{k}\right] = 0 \tag{2.13}$$

where $\vec{V} = u\hat{i} + v\hat{j} + w\hat{k}$ is the velocity of the point.

For a steady flow, $\frac{\partial \rho}{\partial t} = 0$, thus,

$$\frac{\partial(\rho u)}{\partial x} + \frac{\partial(\rho v)}{\partial y} + \frac{\partial(\rho w)}{\partial z} = 0,$$

or

$$\nabla \cdot \left(\rho \vec{V}\right) = 0. \tag{2.14}$$

For incompressible fluid flow, $\rho = \text{constant}$, hence $\frac{\partial \rho}{\partial t} = 0$, therefore, the continuity equation for an incompressible flow becomes;

$$\frac{\partial u}{\partial x} + \frac{\partial v}{\partial y} + \frac{\partial w}{\partial z} = 0,$$

or (2.15)

$$\nabla \cdot \left(\vec{V} \right) = 0.$$

where $\nabla \cdot \left(\vec{V} \right)$ is called divergence of the velocity, which physically, is the rate of change of volume of a moving fluid element, per unit volume.

2.3 The Momentum Equation (Navier-Stokes Equation)

This equation is derived by applying another fundamental physical principle to a model of the flow, namely:

Physical Principle: $\vec{F} = m\vec{a}$ (Newton's 2nd law)

We consider a small fixed volume of fluid element with dimensions dx, dy, dz moving in a stream (see figure 2.3 below).

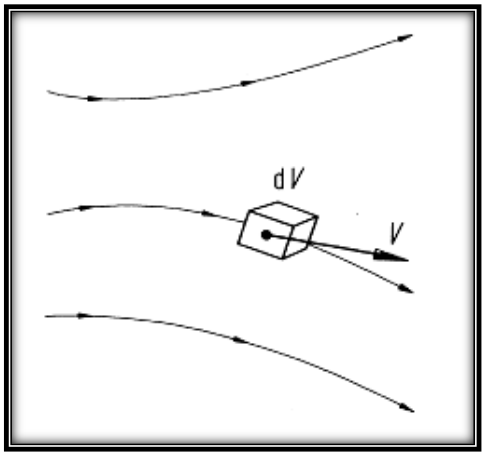

Figure 2.3: Fluid Element

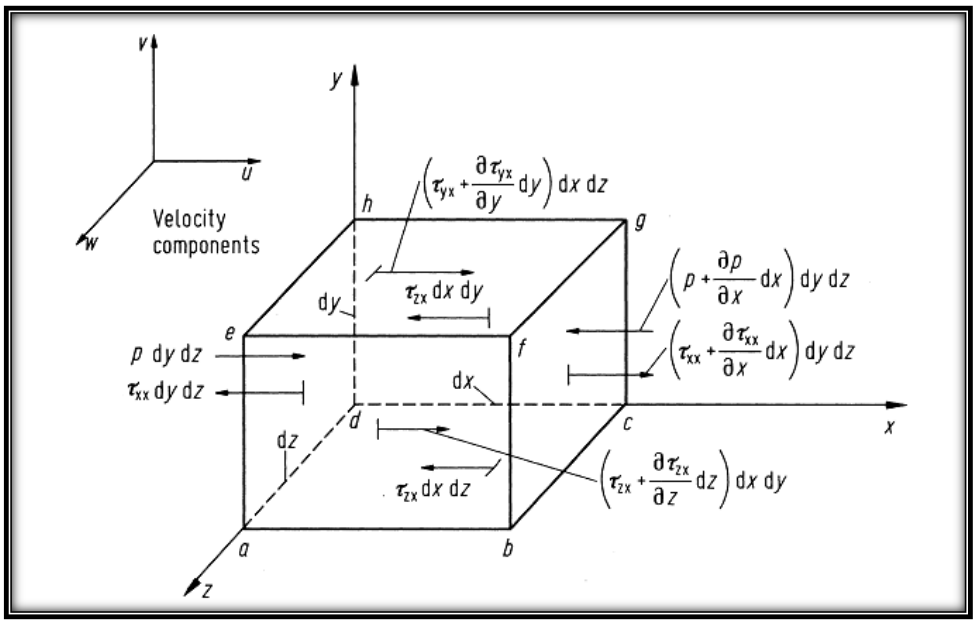

Figure 2.4: Infinitesimally small, moving fluid element showing forces in the x direction.

Newton's 2nd law on the moving fluid element in figure 2.4, states that the net force on the fluid element equals its mass times the acceleration of the element. This is a vector relation, thus it can be split into three scalar relations along the x, y, and z-axes.

We consider only the x-component of Newton's 2nd law,

$$F_x = ma_x . \tag{2.16}$$

where F_x and a_x are the scalar x-components of the force and acceleration respectively.
Next we take into consideration the forces acting on the moving fluid element the x-direction. There are two types of forces;

(a) ***Body forces*** (F_B), which act directly throughout the volumetric mass of the fluid element, for example, gravitational, electric and magnetic forces.

(b) ***Surface forces*** (F_s), which act directly on the surface of the fluid element, for example, pressure and the stress. They are due to only two sources: (*i*) the pressure distribution acting on the surface, imposed by the outside fluid surrounding the fluid element, and (*ii*) the stress distributions acting on the surface, also imposed by the outside fluid 'tugging' or 'pushing' on the surface by means of friction.

(c) ***Line surface*** (F_L), which act along a line and have a magnitude proportional to the extent of the line and they usually appear at the interface between a liquid and a gas or at the interface between two immiscible liquids, for example, surface tension.

The only body force taken into consideration is the weight of the fluid element which acts in transverse direction. Let $\vec{g}$ denote the body force per unit mass acting on the fluid element, with g_x as its x-component. The volume of the fluid element is ($dx\,dy\,dz$); hence,

$$\left\{\begin{matrix} Body \text{ force on the} \\ \text{fluid element acting} \\ \text{in the x-direction} \end{matrix}\right\} = \rho g_x \left(dx \text{ dy dz}\right). \tag{2.17}$$

The surface forces due to stress exerted on the sides of the fluid element are of two kinds; Normal stress and shear stress. Along the x –direction, the two types of stresses; Shear stress and Normal stress are denoted as $\left(\tau_{xy}\right)$ and $\left(\tau_{xx}\right)$ respectively. The convention used to name the stresses is $\left(\tau_{ij}\right)$, where i refer to the axis normal to the surface and j represent the direction of the stress.

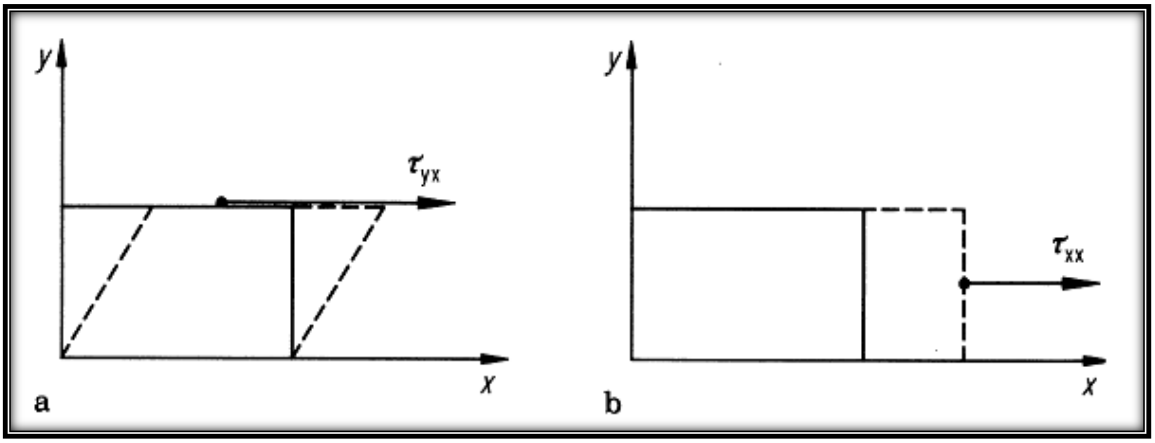

Figure 2.5: Shear and Normal stresses

The shear stress, denoted by (τ_{xy}) in figure 2.5a, is related to the time rate-of-change of the shearing deformation of the fluid element, whereas the normal stress, denoted by (τ_{xx}) figure 2.5b, is related to the time-rate-of-change of volume of the fluid element. Thus, both shear and normal stresses depend on velocity gradients in the flow. In most viscous flows, normal stresses are much smaller than shear stresses, and many times are neglected. Normal stresses become important when the normal velocity gradients (say *∂u/∂x*) are very large, such as inside a shock wave.

The surface forces (normal stress, shear stress and pressure) in the x-direction exerted on the fluid element are sketched in figure 2.4. On the '*abcd*' face, there is only one force in the negative x-direction which is shear stress defined as, $\tau_{yx}dxdz$. At a distance dy above '*abcd*' face , we have the '*efgh*' face with a shear force of $\tau_{yx}+\left(\frac{\partial \tau_{yx}}{\partial y}dy\right)dxdz$ in the positive

x-direction. Considering the face '*dcgh*' $\tau_{zx}dxdy$ which acts in the negative x-direction, whereas on the face 'abfe', $\tau_{zx}+\left(\frac{\partial \tau_{zx}}{\partial z}dz\right)dxdy$ which acts in the positive x-direction. On face '*adhe*', which is perpendicular to the x-axis, the only forces in the x-direction are the pressure force $pdydz$ which always acts in the positive x-direction into the fluid element and the normal stress $\tau_{xx}dydz$ in the negative x-direction. In the opposite '*bcgf*' face which is dx from '*adhe*' face the

forces acting on it are the pressure, $\left(p + \frac{\partial p}{\partial x} dx \right) dydz$, which acts against the fluid element flow and the normal shear $\left(\tau_{xx} + \frac{\partial \tau_{xx}}{\partial x} dx \right) dydz$ that acts in the positive x-direction.

Therefore for the moving fluid element;

$$\begin{aligned} \left\{ \begin{matrix} \text{Net surface force} \\ \text{in the x-direction} \end{matrix} \right\} = & \left[p - \left(p + \frac{\partial p}{\partial x} dx \right) \right] dydz \\ & + \left[\left(\tau_{xx} + \frac{\partial \tau_{xx}}{\partial x} dx \right) - \tau_{xx} \right] dydz \\ & + \left[\left(\tau_{yx} + \frac{\partial \tau_{yx}}{\partial y} dy \right) - \tau_{yx} \right] dxdz \\ & + \left[\left(\tau_{zx} + \frac{\partial \tau_{zx}}{\partial z} dz \right) - \tau_{zx} \right] dxdy. \end{aligned} \qquad (2.18)$$

The total force in the x-direction, F_x is given by summing of Eqs. (2.17) and (2.18). On simplification we have,

$$F_x = \left(-\frac{\partial p}{\partial x} + \frac{\partial \tau_{xx}}{\partial x} + \frac{\partial \tau_{yx}}{\partial y} + \frac{\partial \tau_{zx}}{\partial z} \right) dx \text{ dy dz } + \rho f_x \text{dx dy dz.} \quad (2.19)$$

Considering the right-hand side of Eq. (2.6), the mass of the fluid element is fixed and is equal to;

$$m = \rho \text{ dx dy dz.} \qquad (2.20)$$

If we consider a 2D flow with axial and transverse velocities denoted by $u(x, y, t)$, and $v(x, y, t)$ respectively. The total differentials of these fields are:

$$\left. \begin{aligned} du &= \frac{\partial u}{\partial x} dx + \frac{\partial u}{\partial y} dy + \frac{\partial u}{\partial t} dt \\ dv &= \frac{\partial v}{\partial x} dx + \frac{\partial v}{\partial y} dy + \frac{\partial v}{\partial t} dt \end{aligned} \right\}. \qquad (2.21)$$

Dividing both equations by dt , we get,

$$\left. \begin{aligned} \frac{du}{dt} &= \frac{\partial u}{\partial x} \frac{dx}{dt} + \frac{\partial u}{\partial y} \frac{dy}{dt} + \frac{\partial u}{\partial t} \\ \frac{dv}{dt} &= \frac{\partial v}{\partial x} \frac{dx}{dt} + \frac{\partial v}{\partial y} \frac{dy}{dt} + \frac{\partial v}{\partial t} \end{aligned} \right\}. \qquad (2.22)$$

But, $\frac{dx}{dt} = u$, $\frac{dy}{dt} = v$, thus equations (2.12) become

$$\left.\begin{aligned} \frac{du}{dt} &= u\frac{\partial u}{\partial x} + v\frac{\partial u}{\partial y} + \frac{\partial u}{\partial t} \\ \frac{dv}{dt} &= u\frac{\partial u}{\partial x} + v\frac{\partial u}{\partial y} + \frac{\partial v}{\partial t} \end{aligned}\right\} \qquad (2.23)$$

Equation (2.13) is the acceleration of the fluid element.

Substituting equsation (2.9), (2.10) and (2.11) into (2.6), and dividing by $dxdydz$ we have,

$$\rho\left(\frac{\partial u}{\partial t} + u\frac{\partial u}{\partial x} + v\frac{\partial u}{\partial y}\right) = -\frac{\partial p}{\partial x} + \frac{\partial \tau_{xx}}{\partial x} + \frac{\partial \tau_{yx}}{\partial y} + \frac{\partial \tau_{zx}}{\partial z} + \rho g_x. \qquad (2.24a)$$

which is the x-component of the momentum equation for a viscous flow.

Similarly, the *y* component of the flow is by,

$$\rho\left(\frac{\partial v}{\partial t} + u\frac{\partial v}{\partial x} + v\frac{\partial v}{\partial y}\right) = -\frac{\partial p}{\partial y} + \frac{\partial \tau_{xy}}{\partial x} + \frac{\partial \tau_{yy}}{\partial y} + \frac{\partial \tau_{zy}}{\partial z} + \rho g_y. \qquad (2.24b)$$

We note that the x and y components of the momentum equation are partial differential equations obtained directly by the application of the fundamental physical principle to an infinitesimal fluid element. They equations are called the **Navier–Stokes equations** in honour of two men—the Frenchman M. Navier and the Englishmen G. Stokes, who independently obtained the equations in the first half of the nineteenth century.

The left hand side of the Navier–Stokes equations can be rewritten by introducing the vector operator,

$$\nabla \equiv \vec{i}\frac{\partial}{\partial x} + \vec{j}\frac{\partial}{\partial y} + \vec{k}\frac{\partial}{\partial z}. \qquad (2.25)$$

Thus the Left Hand Side of equation (2.24a) an be written as

$$\rho\left(\frac{\partial V}{\partial t} + \left(\vec{V}.\nabla\right)V\right). \qquad (2.26)$$

where $\frac{\partial V}{\partial t}$ is the local derivative and $\left(\vec{V}.\nabla\right)V$ is the convective derivative.

Substituting equation (2.26) into equation (2.24a) we have

$$\frac{\partial(\rho u)}{\partial t} + \nabla\cdot\left(\rho u\vec{V}\right) = -\frac{\partial p}{\partial x} + \frac{\partial \tau_{xx}}{\partial x} + \frac{\partial \tau_{yx}}{\partial y} + \frac{\partial \tau_{zx}}{\partial z} + \rho g_x. \qquad (2.27a)$$

Similarly for the y and z components of the navier stokes equation,

$$\frac{\partial(\rho v)}{\partial t} + \nabla\cdot\left(\rho v\vec{V}\right) = -\frac{\partial p}{\partial y} + \frac{\partial \tau_{xy}}{\partial x} + \frac{\partial \tau_{yy}}{\partial y} + \frac{\partial \tau_{zy}}{\partial z} + \rho g_y. \qquad (2.27b)$$

$$\frac{\partial(\rho w)}{\partial t}+\nabla\cdot\left(\rho w\vec{V}\right)=-\frac{\partial p}{\partial z}+\frac{\partial\tau_{xz}}{\partial x}+\frac{\partial\tau_{yz}}{\partial y}+\frac{\partial\tau_{zz}}{\partial z}+\rho g_z. \qquad (2.27c)$$

Equation (2.27a-c) are the Navier-Stokes equations in *conservation* form.

For Newtonian fluids (water, oil, air), shear stress α rate of shear strain, thus,

$$\tau_{xy}=\tau_{yx}=\mu\left(\frac{\partial v}{\partial x}+\frac{\partial u}{\partial y}\right),$$
$$\tau_{yz}=\tau_{zy}=\mu\left(\frac{\partial w}{\partial y}+\frac{\partial v}{\partial z}\right),$$
$$\tau_{zx}=\tau_{xz}=\mu\left(\frac{\partial u}{\partial z}+\frac{\partial w}{\partial x}\right). \qquad (2.28)$$

On the other hand, normal viscous stress α volumetric strain rate, thus,

$$\tau_{xx}=2\mu\frac{\partial u}{\partial x},\qquad \tau_{yy}=2\mu\frac{\partial v}{\partial y},\qquad \tau_{zz}=2\mu\frac{\partial w}{\partial z}, \qquad (2.29)$$

$$\tau_{xx}=\lambda\nabla\cdot\vec{V}+2\mu\frac{\partial u}{\partial x},$$
$$\tau_{yy}=\lambda\nabla\cdot\vec{V}+2\mu\frac{\partial v}{\partial y},$$
$$\tau_{zz}=\lambda\nabla\cdot\vec{V}+2\mu\frac{\partial w}{\partial z}. \qquad (2.30)$$

where μ is the molecular viscosity coefficient and λ is the bulk viscosity coefficient of the fluid.

Stokes made the hypothesis that, $\lambda=-\frac{2}{3}\mu,$

Thus,

$$\frac{\partial\tau_{xx}}{\partial x}+\frac{\partial\tau_{yx}}{\partial y}+\frac{\partial\tau_{zx}}{\partial z}=\frac{\partial}{\partial x}\left(2\mu\frac{\partial u}{\partial x}\right)+\frac{\partial}{\partial y}(\mu)\left(\frac{\partial v}{\partial x}+\frac{\partial u}{\partial y}\right)+\frac{\partial}{\partial z}(\mu)\left(\frac{\partial u}{\partial z}+\frac{\partial w}{\partial x}\right)$$
$$=2\mu\frac{\partial^2 u}{\partial x^2}+\mu\left(\frac{\partial}{\partial y}\frac{\partial u}{\partial x}+\frac{\partial}{\partial y}\frac{\partial v}{\partial x}\right)+\mu\left(\frac{\partial}{\partial z}\frac{\partial u}{\partial z}+\frac{\partial}{\partial x}\frac{\partial w}{\partial x}\right)$$
$$=2\mu\frac{\partial^2 u}{\partial x^2}+\mu\frac{\partial^2 u}{\partial y^2}+\mu\frac{\partial^2 u}{\partial z^2}+\underbrace{\mu\left(\frac{\partial}{\partial y}\frac{\partial v}{\partial x}+\frac{\partial}{\partial z}\frac{\partial w}{\partial x}\right)}_{0}.$$

Thus equation (2.27a) becomes

$$\frac{\partial(\rho u)}{\partial t}+\nabla\cdot\left(\rho u\vec{V}\right)=\rho g_x-\frac{\partial p}{\partial x}+\mu\left(\frac{\partial^2 u}{\partial x^2}+\frac{\partial^2 u}{\partial y^2}+\frac{\partial^2 u}{\partial z^2}\right). \qquad (2.31)$$

In vector form the Navier-Stokes equation is

$$\rho\left(\frac{\partial V}{\partial t}+(V\cdot\nabla)V\right)=\rho g-\nabla p+\mu\nabla^2 V. \qquad (2.32)$$

2.4 The Energy Equation

The energy equation is derived from the 1st law of thermodynamics which states that the amount of heat added to a system *dQ* is equal to change in internal energy *dE* plus the amount of energy lost due to work done on the system *dW*. This implies that energy can neither be created nor destroyed, it can only change in form.

Thus,

$$\left\{\begin{matrix}\text{Rate of change of}\\ \text{energy inside the}\\ \text{fluid element}\end{matrix}\right\}=\left\{\begin{matrix}\text{Net flux of}\\ \text{heat into}\\ \text{the element}\end{matrix}\right\}+\left\{\begin{matrix}\text{Rate of working done on}\\ \text{the element due to body}\\ \text{and surface forces}\end{matrix}\right\} \qquad (2.33)$$

We start by evaluating the rate of work done on the moving fluid element due to body and surface forces. It can be shown that the rate of doing work by a force exerted on a moving body is equal to the product of the force and the component of velocity in the direction of the force.

Hence the rate of work done by the body force acting on the fluid element moving at a velocity **V** is $\rho\,\vec{f}\cdot\vec{V}(dx\,\mathrm{dy}\,\mathrm{dz})$.

We consider the surface forces (pressure plus shear and normal stresses), acting in the x-direction, as shown in Figure 2.4. The rate of work done on the moving fluid element by the surface forces in the x-direction is the x-component of velocity *u*, multiplied by the forces, e.g. on face `*abcd*` the rate of work done by $\tau_{yx}dxdz$ is $u\tau_{yx}dxdz$ with similar expressions for the other faces. To emphasize these energy considerations, the moving fluid element is redrawn in Figure 2.6 below, where the rate of work done on each face by surface forces in the x-direction is shown explicitly. To obtain the net rate of work done on the fluid element by the surface forces, note that forces in the positive x-direction do positive work and that forces in the negative x-direction do negative work.

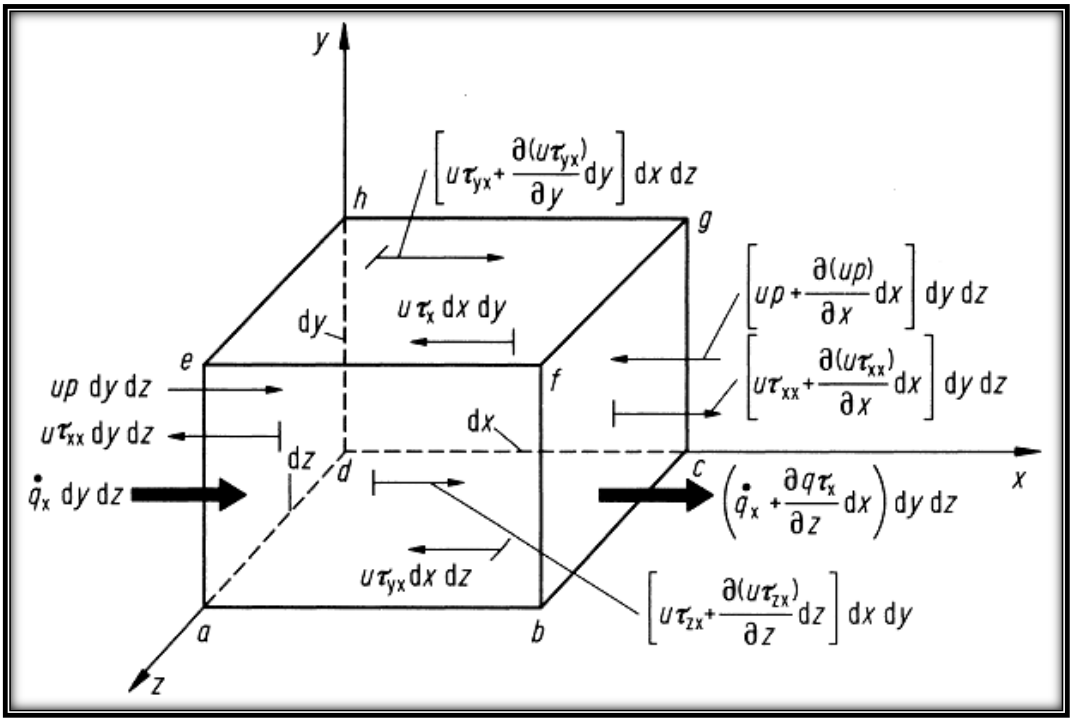

Figure 2.6: Energy fluxes associated with an infinitesimally small, moving fluid element.

Considering the pressure forces on face '*adhe*' and '*bcgf*' in figure 2.6, the net rate of work done by pressure and the shear stresses in the x-direction is given by

$$\left[up-\left(up+\frac{\partial(up)}{\partial x}\right)\right]\mathrm{dy\ dz} = -\frac{\partial(up)}{\partial x}\mathrm{dx\ dy\ dz},$$

and

$$\left[\left(u\tau_{yx}+\frac{\partial(u\tau_{yx})}{\partial y}\right)-u\tau_{yx}\right]\mathrm{dx\ dz} = -\frac{\partial(u\tau_{yx})}{\partial y}\mathrm{dx\ dy\ dz},$$

Considering all the surface forces shown in figure 2.6, the net rate of work done on the moving fluid element due to these forces is;

$$\left[-\frac{\partial(up)}{\partial x}+\frac{\partial(u\tau_{xx})}{\partial x}+\frac{\partial(u\tau_{yx})}{\partial y}+\frac{\partial(u\tau_{zx})}{\partial y}\right]dx\ dy\ dz.$$

The above expression gives only surface forces in the x-direction, similar expressions can be obtained for the y- and z-directions. Considering all the surface forces and incorporating the body force contribution we get the net rate of work done on the moving fluid element as,

$$\left\{\begin{array}{l}\text{Rate of work done}\\ \text{onthe element due}\\ \text{to the body and}\\ \text{surface forces}\end{array}\right\}=\left[\begin{array}{l}\left(\dfrac{\partial(up)}{\partial x}+\dfrac{\partial(vp)}{\partial y}+\dfrac{\partial(wp)}{\partial z}\right)+\\ \dfrac{\partial(u\tau_{xx})}{\partial x}+\dfrac{\partial(u\tau_{yx})}{\partial y}+\dfrac{\partial(u\tau_{zx})}{\partial y}\\ +\dfrac{\partial(v\tau_{xy})}{\partial x}+\dfrac{\partial(v\tau_{yy})}{\partial y}+\dfrac{\partial(v\tau_{zy})}{\partial y}\\ +\dfrac{\partial(w\tau_{xz})}{\partial x}+\dfrac{\partial(w\tau_{yz})}{\partial y}+\dfrac{\partial(w\tau_{zz})}{\partial y}\end{array}\right]dxdydz+\rho\,\vec{f}\cdot\vec{V}\,dxdydz. \qquad (2.34)$$

We now turn to the second term of equation (2.33), i.e. the net flux of heat into the element. This heat flux is due to: volumetric heating such as absorption or emission of radiation, heat transfer across the surface due to temperature gradients, i.e. thermal conduction.

We define $\dot{q}$ as the rate of volumetric heat addition per unit mass. As earlier defined the mass of the moving fluid element in ***ρdxdydz***, thus, we then obtain;

$$\left\{\begin{array}{l}\text{Volemetric heating}\\ \text{of the element}\end{array}\right\}=\rho\,\dot{q}\,\mathrm{dx\ dy\ dz}. \qquad (2.35)$$

In Figure 2.6, the heat transferred by thermal conduction into the moving fluid element across face '*adhe*' is $\dot{q}_x\,\mathrm{dx\ dy\ dz}$ where $\dot{q}_x$ is the heat transferred in the x-direction per unit time per unit area by thermal conduction. The heat transferred out of the element across face '*bcgf*' is,

$$\left[\dot{q}_x+\left(\partial\dot{q}_x/\partial x\right)\mathrm{dx}\right]\mathrm{dy\ dz},$$

Thus, the net heat transferred in the x-direction into the fluid element by thermal conduction is;

$$\left[\dot{q}_x-\left(\dot{q}_x+\frac{\partial\dot{q}_x}{\partial x}\right)\mathrm{dx}\right]\mathrm{dy\ dz}=-\frac{\partial\dot{q}_x}{\partial x}\mathrm{dx\ dy\ dz}.$$

Taking into account heat transfer in the y- and z-directions across the other faces in figure 2.6, we obtain,

$$\left\{\begin{matrix}\text{Heating of the}\\ \text{fluid element by}\\ \text{thermal conduction}\end{matrix}\right\} = -\left(\frac{\partial \dot{q}_x}{\partial x} + \frac{\partial \dot{q}_y}{\partial y} + \frac{\partial \dot{q}_z}{\partial z}\right) \text{dx dy dz.} \qquad (2.36)$$

Summing up equations (2.35) and (2.36), gives the net flux of heat into the element;

$$\left\{\begin{matrix}\text{Heating of the}\\ \text{fluid element by}\\ \text{thermal conduction}\end{matrix}\right\} = \left[\rho \dot{q} - \left(\frac{\partial \dot{q}_x}{\partial x} + \frac{\partial \dot{q}_y}{\partial y} + \frac{\partial \dot{q}_z}{\partial z}\right)\right] \text{dx dy dz.} \quad (2.37)$$

Heat transfer by thermal conduction is proportional to the local temperature gradient;

$$\dot{q}_x = -k\frac{\partial T}{\partial x}; \qquad \dot{q}_y = -k\frac{\partial T}{\partial y}; \qquad \dot{q}_z = -k\frac{\partial T}{\partial z};$$

where *k* is the thermal conductivity.

Substituting these in equation (2.37) we have,

$$\left\{\begin{matrix}\text{Heating of the}\\ \text{fluid element by}\\ \text{thermal conduction}\end{matrix}\right\} = \left[\rho \dot{q} - \frac{\partial}{\partial \text{x}}\left(k\frac{\partial T}{\partial x}\right) + \left(k\frac{\partial T}{\partial y}\right) + \left(k\frac{\partial T}{\partial z}\right)\right] \text{dx dy dz.} \quad (2.38)$$

Finally, we consider the time-rate-of-change of energy of the fluid element. The total energy of a moving fluid per unit mass is the sum of its internal energy per unit mass, *e*, and its kinetic energy per unit mass, $V^2/2$. Hence, the total energy is $e + V^2/2$. Since it is a moving fluid element, the time-rate-of-change of energy per unit mass is given by the substantial derivative. Taking the mass of the fluid element as *ρdxdydz*, we have;

$$\left\{\begin{matrix}\text{Rate of change of'}\\ \text{energy inside}\\ \text{the fluid element}\end{matrix}\right\} = \rho\frac{D}{Dt}\left(e + \frac{V^2}{2}\right) dx\ dy\ dz. \qquad (2.39)$$

The final form of the energy equation is obtained by substituting equations (2.34), (2.38) and (2.39) into equation (2.33), obtaining;

$$\rho\frac{D}{Dt}\left(e+\frac{V^2}{2}\right)=\rho\dot{q}+\frac{\partial}{\partial x}\left(k\frac{\partial T}{\partial x}\right)+\frac{\partial}{\partial y}\left(k\frac{\partial T}{\partial y}\right)+\frac{\partial}{\partial z}\left(k\frac{\partial T}{\partial z}\right)$$
$$-\left(\frac{\partial(up)}{\partial x}+\frac{\partial(vp)}{\partial y}+\frac{\partial(wp)}{\partial z}\right)+\frac{\partial(u\tau_{xx})}{\partial x}+\frac{\partial(u\tau_{yx})}{\partial y}$$
$$+\frac{\partial(u\tau_{zx})}{\partial y}+\frac{\partial(v\tau_{xy})}{\partial x}+\frac{\partial(v\tau_{yy})}{\partial y}+\frac{\partial(v\tau_{zy})}{\partial y}+\frac{\partial(w\tau_{xz})}{\partial x}$$
$$+\frac{\partial(w\tau_{yz})}{\partial y}+\frac{\partial(w\tau_{zz})}{\partial y}+\rho\vec{f}\cdot\vec{V}. \qquad (2.40)$$

This is the non-conservation form of the energy equation; also note that it is in terms of the total energy, ($e+V^2/2$). The non-conservation form results from the application of the fundamental physical principle to amoving fluid element. The left-hand side of equation (2.30) involves the total energy ($e+V^2/2$). Frequently, the energy equation is written in a form that involves just the internal energy *e*. The derivation is as follows;

Rewriting equations 2.24a – b, in non-conservative form and including the equation in z-direction, we have;

$$\rho\frac{Du}{Dt}=-\frac{\partial p}{\partial x}+\frac{\partial\tau_{xx}}{\partial x}+\frac{\partial\tau_{yx}}{\partial y}+\frac{\partial\tau_{zx}}{\partial z}+\rho f_x,$$

$$\rho\frac{Dv}{Dt}=-\frac{\partial p}{\partial y}+\frac{\partial\tau_{xy}}{\partial x}+\frac{\partial\tau_{yy}}{\partial y}+\frac{\partial\tau_{zy}}{\partial z}+\rho f_y, \qquad (2.41)$$

$$\rho\frac{Dw}{Dt}=-\frac{\partial p}{\partial z}+\frac{\partial\tau_{xz}}{\partial x}+\frac{\partial\tau_{yz}}{\partial y}+\frac{\partial\tau_{zz}}{\partial z}+\rho f_z.$$

Multiplying each of the equations, equation (2.41) by *u*, *v*, and *w* respectively,

$$\rho\frac{D\left(\frac{u^2}{2}\right)}{Dt}=-u\frac{\partial p}{\partial x}+u\frac{\partial\tau_{xx}}{\partial x}+u\frac{\partial\tau_{yx}}{\partial y}+u\frac{\partial\tau_{zx}}{\partial z}+\rho u f_x, \qquad (2.42a)$$

$$\rho\frac{D\left(\frac{v^2}{2}\right)}{Dt}=-v\frac{\partial p}{\partial y}+v\frac{\partial\tau_{xy}}{\partial x}+v\frac{\partial\tau_{yy}}{\partial y}+v\frac{\partial\tau_{zy}}{\partial z}+\rho v f_y, \qquad (2.42b)$$

$$\rho \frac{D\left(\frac{w^2}{2}\right)}{Dt} = -w\frac{\partial p}{\partial z} + w\frac{\partial \tau_{xz}}{\partial x} + w\frac{\partial \tau_{yz}}{\partial y} + w\frac{\partial \tau_{zz}}{\partial z} + \rho w f_z. \qquad (2.42c)$$

Adding equations (2.42a, b,and c), and noting that $u^2+v^2+w^2 = V^2$, we obtain;

$$\begin{aligned}\rho \frac{DV^2/2}{Dt} = &-u\frac{\partial p}{\partial x} - v\frac{\partial p}{\partial y} - w\frac{\partial p}{\partial z} + u\left(\frac{\partial \tau_{xx}}{\partial x} + \frac{\partial \tau_{yx}}{\partial y} + \frac{\partial \tau_{zx}}{\partial z}\right) \\ &+ v\left(\frac{\partial \tau_{xy}}{\partial x} + \frac{\partial \tau_{yy}}{\partial y} + \frac{\partial \tau_{zy}}{\partial z}\right) + w\left(\frac{\partial \tau_{xz}}{\partial x} + \frac{\partial \tau_{yz}}{\partial y} + \frac{\partial \tau_{zz}}{\partial z}\right) \\ &+ \rho\left(uf_x + vf_y + wf_z\right).\end{aligned} \qquad (2.43)$$

Subtracting equation (2.43) from equation (2.40), noting that $\rho \vec{f}.\vec{V} = \rho\left(uf_x + vf_y + wf_z\right)$ we have;

$$\begin{aligned}\rho \frac{D}{Dt} = &\rho \dot{q} + \frac{\partial}{\partial x}\left(k\frac{\partial T}{\partial x}\right) + \frac{\partial}{\partial y}\left(k\frac{\partial T}{\partial y}\right) + \frac{\partial}{\partial z}\left(k\frac{\partial T}{\partial z}\right) \\ &- p\left(\frac{\partial u}{\partial x} + \frac{\partial v}{\partial y} + \frac{\partial w}{\partial z}\right) + \tau_{xx}\frac{\partial u}{\partial x} + \tau_{yx}\frac{\partial u}{\partial y} + \tau_{zx}\frac{\partial u}{\partial x} \\ &+ \tau_{xy}\frac{\partial v}{\partial x} + \tau_{yy}\frac{\partial v}{\partial y} + \tau_{zy}\frac{\partial w}{\partial x} + \tau_{xz}\frac{\partial w}{\partial x} + \tau_{yz}\frac{\partial w}{\partial y} + \tau_{zz}\frac{\partial w}{\partial z}.\end{aligned} \qquad (2.44)$$

Equation (2.44) is the energy equation in terms of internal energy *e*. Note that the body force terms have cancelled; the energy equation when written in terms of *e* does not explicitly contain the body force. Equation (2.44) is still in non-conservation form. We note that $\tau_{xy} = \tau_{yx} = \tau_{xz} = \tau_{zx} = \tau_{yz} = \tau_{zy}$, thus equation(2.44) can be rewritten as,

$$\begin{aligned}\rho \frac{D}{Dt} = &\rho \dot{q} + \frac{\partial}{\partial x}\left(k\frac{\partial T}{\partial x}\right) + \frac{\partial}{\partial y}\left(k\frac{\partial T}{\partial y}\right) + \frac{\partial}{\partial z}\left(k\frac{\partial T}{\partial z}\right) \\ &- p\left(\frac{\partial u}{\partial x} + \frac{\partial v}{\partial y} + \frac{\partial w}{\partial z}\right) + \tau_{xx}\frac{\partial u}{\partial x} + \tau_{yy}\frac{\partial v}{\partial y} + \tau_{zz}\frac{\partial w}{\partial z} \\ &+ \tau_{yx}\left(\frac{\partial u}{\partial y} + \frac{\partial v}{\partial x}\right) + \tau_{zx}\left(\frac{\partial u}{\partial z} + \frac{\partial w}{\partial x}\right) + \tau_{zy}\left(\frac{\partial v}{\partial z} + \frac{\partial w}{\partial y}\right).\end{aligned} \qquad (2.45)$$

Using the definitions of normal the viscous stress and shear stress given by equations (2.28) and (2.29), equation (2.45) becomes,

$$\rho\frac{D}{Dt}=\rho\dot{q}+\frac{\partial}{\partial x}\left(k\frac{\partial T}{\partial x}\right)+\frac{\partial}{\partial y}\left(k\frac{\partial T}{\partial y}\right)+\frac{\partial}{\partial z}\left(k\frac{\partial T}{\partial z}\right)$$
$$-\mathrm{p}\left(\frac{\partial u}{\partial x}+\frac{\partial v}{\partial y}+\frac{\partial w}{\partial z}\right)+\lambda\left(\frac{\partial u}{\partial x}+\frac{\partial v}{\partial y}+\frac{\partial w}{\partial z}\right)^2$$
$$+\ \mu\left[\begin{array}{l}2\left(\frac{\partial u}{\partial x}\right)^2+2\left(\frac{\partial v}{\partial y}\right)^2+2\left(\frac{\partial w}{\partial z}\right)^2\\+\left(\frac{\partial u}{\partial y}+\frac{\partial v}{\partial x}\right)^2+\left(\frac{\partial u}{\partial z}+\frac{\partial w}{\partial x}\right)^2+\left(\frac{\partial v}{\partial z}+\frac{\partial w}{\partial y}\right)^2\end{array}\right]. \qquad (2.46)$$

Equation (2.46) is a form of the energy equation completely in terms of the flow-field variables. A similar substitution can be made into equation (2.40).

The energy equation in conservation form can be obtained as follows;

Considering the left-hand side of equation (2.46) and from the definition of the substantial derivative:

$$\rho\frac{De}{Dt}=\rho\frac{\partial e}{\partial t}+\rho\vec{V}\cdot\nabla e, \qquad (2.47)$$

$$\frac{\partial(\rho e)}{\partial t}=\rho\frac{\partial e}{\partial t}+e\frac{\partial\rho}{\partial t} \qquad \text{or} \qquad \rho\frac{\partial e}{\partial t}=\frac{\partial(\rho e)}{\partial t}-e\frac{\partial\rho}{\partial t}. \qquad (2.48)$$

From the vector identity concerning the divergence of the product of a scalar times a vector,

$$\nabla\cdot\left(\rho e\vec{V}\right)=e\nabla\cdot\left(\rho\vec{V}\right)+\rho\vec{V}\cdot e\nabla. \qquad (2.49)$$

Substituteequations (2.48) and (2.49) into equation (2.47) we have;

$$\rho\frac{De}{Dt}=\frac{\partial(\rho e)}{\partial t}-e\left[\frac{\partial\rho}{\partial t}+\nabla\cdot\left(\rho\vec{V}\right)\right]+\nabla\cdot\left(\rho e\vec{V}\right). \qquad (2.50)$$

From the continuity equation, equation (2.3), the term in square brackets in equation (2.50) is zero,

thus, equation (2.50) becomes;

$$\rho \frac{De}{Dt} = \frac{\partial (\rho e)}{\partial t} + \nabla \cdot \left(\rho e \vec{V} \right). \tag{2.51}$$

Substituting equation (2.51) into equation (2.46), we obtain;

$$\begin{aligned} \frac{\partial (\rho e)}{\partial t} + \nabla \cdot \left(\rho e \vec{V} \right) = \rho \dot{q} + \frac{\partial}{\partial x}\left(k \frac{\partial T}{\partial x} \right) + \frac{\partial}{\partial y}\left(k \frac{\partial T}{\partial y} \right) + \frac{\partial}{\partial z}\left(k \frac{\partial T}{\partial z} \right) \\ - \mathrm{p}\left(\frac{\partial u}{\partial x} + \frac{\partial v}{\partial y} + \frac{\partial w}{\partial z} \right) + \lambda \left(\frac{\partial u}{\partial x} + \frac{\partial v}{\partial y} + \frac{\partial w}{\partial z} \right)^2 \\ + \mu \left[\begin{array}{l} 2\left(\frac{\partial u}{\partial x} \right)^2 + 2\left(\frac{\partial v}{\partial y} \right)^2 + 2\left(\frac{\partial w}{\partial z} \right)^2 + \left(\frac{\partial u}{\partial y} + \frac{\partial v}{\partial x} \right)^2 \\ + \left(\frac{\partial u}{\partial z} + \frac{\partial w}{\partial x} \right)^2 + \left(\frac{\partial v}{\partial z} + \frac{\partial w}{\partial y} \right)^2 \end{array} \right]. \end{aligned} \tag{2.52}$$

Equation (2.52) is the conservation form of the energy equation, written in terms of the internal energy.

Similarly, the conservation form of the energy equation in terms of total energy can be written as;

$$\begin{aligned} \frac{\partial}{\partial t}\left[\rho \left(e + \frac{V^2}{2} \right) \right] + \nabla \cdot \left[\rho \left(e + \frac{V^2}{2} \vec{V} \right) \right] = \rho \dot{q} + \frac{\partial}{\partial x}\left(k \frac{\partial T}{\partial x} \right) + \frac{\partial}{\partial y}\left(k \frac{\partial T}{\partial y} \right) + \frac{\partial}{\partial z}\left(k \frac{\partial T}{\partial z} \right) \\ - \frac{\partial (up)}{\partial x} - \frac{\partial (vp)}{\partial y} - \frac{\partial (wp)}{\partial z} + \frac{\partial (u\tau_{xx})}{\partial x} + \frac{\partial (u\tau_{yx})}{\partial y} \\ + \frac{\partial (u\tau_{zx})}{\partial z} + \frac{\partial (v\tau_{xy})}{\partial x} + \frac{\partial (v\tau_{yy})}{\partial y} + \frac{\partial (v\tau_{zy})}{\partial z} \\ \frac{\partial (w\tau_{xz})}{\partial x} + \frac{\partial (w\tau_{yz})}{\partial y} + \frac{\partial (w\tau_{zz})}{\partial z} + \rho \vec{f} \cdot \vec{V}. \end{aligned} \tag{2.53}$$

The Governing Equations for Fluid Flow in Cartesian Coordinate System

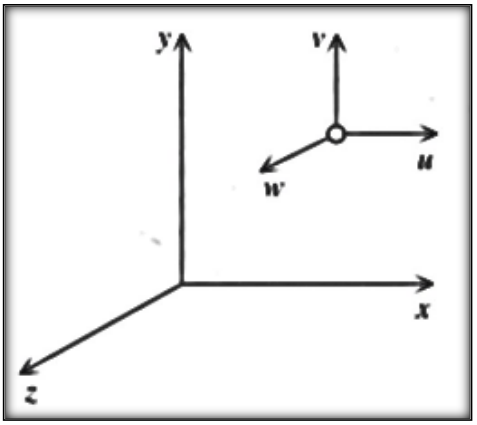

Figure 2.7: Cartesian Coordinate System.

Mass Conservation (Continuity) Equation

$$\frac{\partial \rho}{\partial t}+\frac{\partial(\rho u)}{\partial x}+\frac{\partial(\rho v)}{\partial y}+\frac{\partial(\rho w)}{\partial z}=0.$$

For incompressible fluid flow is; $\frac{\partial u}{\partial x}+\frac{\partial v}{\partial y}+\frac{\partial w}{\partial z}=0.$

Momentum (Navier Stokes) Equations

x-direction: $$\frac{\partial u}{\partial t}+u\frac{\partial u}{\partial x}+v\frac{\partial u}{\partial y}+w\frac{\partial u}{\partial z}=-\frac{\partial p}{\partial x}+\mu\left(\frac{\partial^2 u}{\partial x^2}+\frac{\partial^2 u}{\partial y^2}+\frac{\partial^2 u}{\partial z^2}\right)+\text{ Body Forces.}$$

y-direction: $$\frac{\partial u}{\partial t}+u\frac{\partial u}{\partial x}+v\frac{\partial u}{\partial y}+w\frac{\partial u}{\partial z}=-\frac{\partial p}{\partial x}+\mu\left(\frac{\partial^2 v}{\partial x^2}+\frac{\partial^2 v}{\partial y^2}+\frac{\partial^2 v}{\partial z^2}\right)+\text{ Body Forces.}$$

z-direction: $$\frac{\partial u}{\partial t}+u\frac{\partial u}{\partial x}+v\frac{\partial u}{\partial y}+w\frac{\partial u}{\partial z}=-\frac{\partial p}{\partial x}+\mu\left(\frac{\partial^2 w}{\partial x^2}+\frac{\partial^2 w}{\partial y^2}+\frac{\partial^2 w}{\partial z^2}\right)+\text{ Body Forces.}$$

Energy Equation

$$\rho C_p\left(\frac{\partial T}{\partial t}+u\frac{\partial T}{\partial x}+v\frac{\partial T}{\partial y}+w\frac{\partial T}{\partial z}\right)=k\left(\frac{\partial^2 T}{\partial x^2}+\frac{\partial^2 T}{\partial y^2}+\frac{\partial^2 T}{\partial z^2}\right)+\dot{q}+\mu\Phi,$$

where, $\Phi=2\left[\left(\frac{\partial u}{\partial x}\right)^2+\left(\frac{\partial v}{\partial x}\right)^2+\left(\frac{\partial w}{\partial x}\right)^2\right]+\left(\frac{\partial u}{\partial y}+\frac{\partial v}{\partial x}\right)^2+\left(\frac{\partial v}{\partial z}+\frac{\partial w}{\partial y}\right)^2+\left(\frac{\partial w}{\partial x}+\frac{\partial u}{\partial z}\right)^2.$

The Governing Equations for Fluid Flow in Cylindrical Polar Coordinate System

The transformation between the Cartesian and the polar system is given by the relations,

$$r = \sqrt{x^2 + y^2}, \quad \theta = \tan^{-1}\frac{y}{x}, \quad z = z$$

and the del operator as

$$\nabla\rho = \frac{1}{r}\frac{\partial}{\partial r}(\rho r) + \frac{1}{r}\frac{\partial}{\partial \theta}(\rho) + \frac{\partial}{\partial z}(\rho)$$

thus the continuity equation;

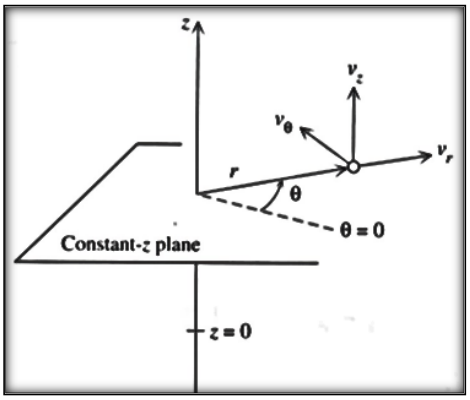

Figure 2.8: Cylindrical Polar Coordinate system.

Mass Conservation (Continuity) Equation

$$\frac{\partial\rho}{\partial t} + \frac{1}{r}\frac{\partial}{\partial r}(\rho v_r r) + \frac{1}{r}\frac{\partial}{\partial \theta}(\rho v_\theta) + \frac{\partial}{\partial z}(\rho v_z) = 0.$$

For incompressible fluid flow is; $\frac{\partial v_r}{\partial r} + \frac{v_r}{r} + \frac{1}{r}\frac{\partial v_\theta}{\partial \theta} + \frac{\partial v_z}{\partial z} = 0.$

where v_r, v_θ and v_z are the velocity components in their respective directions.

Momentum (Navier Stokes) Equations

x-direction:

$$\rho\left(\frac{\partial v_r}{\partial t} + v_r\frac{\partial v_r}{\partial r} + \frac{v_\theta}{r}\frac{\partial v_r}{\partial \theta} - \frac{v^2_\theta}{r} + v_z\frac{\partial v_r}{\partial z}\right) = -\frac{\partial P}{\partial r} + \mu\left(\frac{\partial^2 v_r}{\partial r^2} + \frac{1}{r}\frac{\partial v_r}{\partial r} - \frac{v_r}{r^2} + \frac{1}{r^2}\frac{\partial^2 v_r}{\partial \theta^2} - \frac{2}{r^2}\frac{\partial v_\theta}{\partial \theta} + \frac{\partial^2 v_r}{\partial z^2}\right) + F_r.$$

y-direction:

$$\rho\left(\frac{\partial v_\theta}{\partial t} + v_r\frac{\partial v_\theta}{\partial r} + \frac{v_\theta}{r}\frac{\partial v_\theta}{\partial \theta} - \frac{v_r v_\theta}{r} + v_z\frac{\partial v_\theta}{\partial z}\right) = -\frac{1}{r}\frac{\partial P}{\partial \theta} + \mu\left(\frac{\partial^2 v_\theta}{\partial r^2} + \frac{1}{r}\frac{\partial v_r}{\partial r} - \frac{v_\theta}{r^2} + \frac{1}{r^2}\frac{\partial^2 v_\theta}{\partial \theta^2} + \frac{2}{r^2}\frac{\partial v_r}{\partial \theta} + \frac{\partial^2 v_\theta}{\partial z^2}\right) + F_\theta.$$

z-direction:

$$\rho\left(\frac{\partial v_z}{\partial t} + v_r\frac{\partial v_z}{\partial r} + \frac{v_\theta}{r}\frac{\partial v_z}{\partial \theta} + v_z\frac{\partial v_z}{\partial z}\right) = -\frac{\partial P}{\partial z} + \mu\left(\frac{\partial^2 v_z}{\partial r^2} + \frac{1}{r}\frac{\partial v_z}{\partial r} + \frac{1}{r^2}\frac{\partial^2 v_z}{\partial \theta^2} + \frac{\partial^2 v_z}{\partial z^2}\right) + F_z.$$

Energy Equation

$$\rho c_p\left(\frac{\partial T}{\partial t} + v_r\frac{\partial T}{\partial r} + \frac{v_\theta}{r}\frac{\partial T}{\partial \theta} + v_z\frac{\partial T}{\partial z}\right) = k\left[\frac{1}{r}\frac{\partial}{\partial r}\left(r\frac{\partial T}{\partial r}\right) + \frac{1}{r^2}\frac{\partial^2 T}{\partial \theta^2} + \frac{\partial^2 T}{\partial z^2}\right] + \dot{q} + \mu\Phi.$$

where,

$$\Phi = 2\left[\left(\frac{\partial v_z}{\partial r}\right)^2 + \left(\frac{1}{r}\frac{\partial v_\theta}{\partial \theta} + \frac{v_r}{r}\right)^2 + \left(\frac{\partial v_r}{\partial z}\right)^2\right] + \left(\frac{\partial v_\theta}{\partial r} - \frac{v_\theta}{r} + \frac{1}{r}\frac{\partial v_r}{\partial \theta}\right)^2 + \left(\frac{1}{r}\frac{\partial v_z}{\partial \theta} + \frac{\partial v_\theta}{\partial z}\right)^2 + \left(\frac{\partial v_r}{\partial z} + \frac{\partial v_z}{\partial r}\right)^2.$$

The Governing Equations for Fluid Flow in Spherical Polar Coordinate System

Mass Conservation (Continuity) Equation

$$\frac{\partial \rho}{\partial t}+\frac{1}{r^2}\frac{\partial}{\partial r}\left(r^2\rho V_r\right)+\frac{1}{r\sin\phi}\frac{\partial\left(\rho V_\theta\right)}{\partial\theta}+\frac{1}{r\sin\phi}\frac{\partial\left(\rho V_\phi\sin\phi\right)}{\partial\phi}=0\,,$$

For incompressible fluid flow is;

$$\frac{1}{r}\frac{\partial}{\partial r}\left(r^2V_r\right)+\frac{1}{\sin\phi}\frac{\partial V_\theta}{\partial\theta}+\frac{1}{\sin\phi}\frac{\partial\left(V_\phi\sin\phi\right)}{\partial\phi}=0,$$

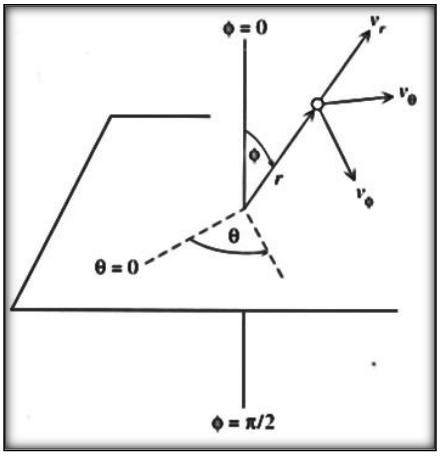

Figure 2.9: Spherical Polar Coordinate System.

Momentum (Navier Stokes) Equations

x-direction: $$\rho\left(\frac{Dv_r}{Dt}-\frac{v_\phi^2+v_\theta^2}{r}\right)=-\frac{\partial P}{\partial r}+\mu\left(\nabla^2v_r-\frac{2v_r}{r^2}-\frac{2}{r^2}\frac{\partial v_\phi}{\partial\phi}-\frac{2v_\phi\cot\phi}{r^2}-\frac{2}{r^2\sin\phi}\frac{\partial v_\theta}{\partial\theta}\right)+F_r.$$

y-direction: $$\rho\left(\frac{Dv_\phi}{Dt}+\frac{v_rv_\phi}{r}-\frac{v_\theta^2\cot\phi}{r}\right)=-\frac{1}{r}\frac{\partial P}{\partial\phi}+\mu\left(\nabla^2v_\phi+\frac{2}{r^2}\frac{\partial v_r}{\partial\phi}-\frac{v_\phi}{r^2\sin^2\phi}-\frac{2\cos\phi}{r^2\sin^2\phi}\frac{\partial v_\theta}{\partial\theta}\right)+F_\phi.$$

z-direction:

$$\rho\left(\frac{Dv_\theta}{Dt}+\frac{v_\theta v_r}{r}+\frac{v_\phi\,v_\theta\cot\phi}{r}\right)=-\frac{1}{r\sin\phi}\frac{\partial P}{\partial\theta}+\mu\left(\nabla^2v_\theta-\frac{v_\theta}{r^2\sin^2\phi}+\frac{2}{r^2\sin\phi}\frac{\partial v_r}{\partial\theta}+\frac{2\cos\phi}{r^2\sin^2\phi}\frac{\partial v_\phi}{\partial\theta}\right)+F_\theta.$$

where,

$$\frac{D}{Dt}=\frac{\partial}{\partial t}+v_r\frac{\partial}{\partial r}+\frac{v_\phi}{r}\frac{\partial}{\partial\phi}+\frac{v_\theta}{r\sin\phi}\frac{\partial}{\partial\theta}\ \text{ and }\ \nabla^2=\frac{1}{r^2}\frac{\partial}{\partial r}\left(r^2\frac{\partial}{\partial r}\right)+\frac{1}{r^2\sin\phi}\frac{\partial}{\partial\phi}\left(\sin\phi\frac{\partial}{\partial\phi}\right)+\frac{1}{r^2\sin^2\phi}\frac{\partial^2}{\partial\theta^2}.$$

Energy Equation

$$\rho c_p\left(\frac{\partial T}{\partial t}+v_r\frac{\partial T}{\partial r}+\frac{v_\phi}{r}\frac{\partial T}{\partial\phi}+\frac{v_\theta}{r\sin\phi}\frac{\partial T}{\partial\theta}\right)=k\left[\frac{1}{r^2}\frac{\partial}{\partial r}\left(r^2\frac{\partial T}{\partial r}\right)+\frac{1}{r^2\sin\phi}\frac{\partial}{\partial\phi}\left(\sin\phi\frac{\partial T}{\partial\phi}\right)+\frac{1}{r^2\sin^2\phi}\frac{\partial^2T}{\partial\theta^2}\right]+\dot{q}+\mu\Phi.$$

where,

$$\Phi=2\left[\left(\frac{\partial v_r}{\partial r}\right)^2+\left(\frac{1}{r}\frac{\partial v_\phi}{\partial\phi}+\frac{v_r}{r}\right)^2+\left(\frac{1}{r\sin\phi}\frac{\partial v_\theta}{\partial\theta}+\frac{v_r}{r}+\frac{v_\phi\cot\phi}{r}\right)^2\right]+\left[r\frac{\partial}{\partial r}\left(\frac{v_\phi}{r}\right)+\frac{1}{r}\frac{\partial v_r}{\partial\phi}\right]^2$$
$$+\left[\frac{\sin\phi}{r}\frac{\partial}{\partial\phi}\left(\frac{v_\theta}{r\sin\phi}\right)+\frac{1}{r\sin\phi}\frac{\partial v_\theta}{\partial\theta}\right]^2+\left[\frac{1}{r\sin\phi}\frac{\partial v_r}{\partial\theta}+r\frac{\partial}{\partial r}\left(\frac{v_\theta}{r}\right)\right]^2.$$

2.5 General Equations Governing MHD Nanofluids Flow

Taking into consideration the Boussineq approximations; (*i*) Density changes in a fluid can be neglected except in the gravity term where density is multiplied by *g*. (*ii*) All fluid properties e.g. μ, k, C_p are constants, under these approximations the above equations reduce to;

2.5.1 Continuity Equation

The equation of continuity can be written as;

$$\frac{\partial u}{\partial x}+\frac{\partial v}{\partial y}+\frac{\partial w}{\partial z}=0. \tag{2.54}$$

2.5.2 Navier Stoke's (Momentum) Equation

The equation of momentum governing the flow of a nanofluid is;

$$\frac{\partial \mathbf{V}}{\partial t}+(\mathbf{V}.\nabla)\mathbf{V}=\frac{1}{\rho_{nf}}\left[-\nabla p+\mu_{nf}\nabla^2\mathbf{V}\right]+\mathrm{F}. \tag{2.55}$$

where F is other forces acting on the flow.

Taking into account force due to gravity (*g*), thermal expansion and the force per unit volume when an electric current density **j** flows through the fluid (Lorentz force $\mathbf{j}\times\mathbf{B}$), since the fluid flow is in a magnetic field. Then, the Navier-Stokes equation becomes,

$$\frac{\partial \mathbf{V}}{\partial t}+\left(\mathbf{V}.\nabla\right)\mathbf{V}=\frac{1}{\rho_{nf}}\left[-\nabla p+\mu_{nf}\nabla^2\mathbf{V}\right]+\left(\rho\beta\right)_{nf}\,g\Delta T+\frac{1}{\rho_{nf}}\,\mathbf{j}\times\mathbf{B}, \tag{2.56}$$

where, **V** is velocity, p is pressure, ρ_{nf} is density of the nanofluid, μ_{nf} is the dynamic viscosity of the nanofluid, g is force due to gravity and β_{nf} is thermal expansion coefficient of nanofluid.

2.5.3 Energy Equation

This equation is derived from the first law of thermodynamics which states that the amount of heat added to a system dQ equals to the change in internal energy dE plus the work done dW, that is $dQ=dE+dW$. In other words if a net energy transfer to a system occurs, the energy contained/stored in the system must increase by an amount equal to the energy transferred. The First Law of Thermodynamics requires that,

$$\left(\rho C_p\right)\left(\frac{\partial T}{\partial t}+\left(\mathbf{V}.\nabla\right)T\right)=K_{nf}\nabla^2 T+q'''. \tag{2.57}$$

Putting in consideration joule heating, the energy equation becomes,

$$\tau_w=\mu_{nf}\left.\frac{\partial u}{\partial y}\right|_{y=0},\quad q_w=-k_{nf}\left.\frac{\partial T}{\partial y}\right|_{y=0}. \tag{2.58}$$

where V is velocity, T is local Temperature of nanofluid, $\left(\rho C_p\right)_{nf}$ is heat capacitance of a nanofluid , σ_{nf} is electrical conductivity, K_{nf} is thermal conductivity of the nanofluid, q''' is heat flux.

Following [147], the relationship between the thermophysical properties of the nanofluid and its conventional base fluid together with nanoparticles are given as:

$$\begin{aligned}
&\mu_{nf}=\frac{\mu_f}{(1-\phi)^{2.5}},\quad \rho_{nf}=(1-\phi)\rho_f+\phi\rho_s,\quad \beta_{\mathrm{nf}}=\left(1\text{-}\phi\right)\beta_f+\phi\beta_s\\
&\left(\rho C_p\right)_{nf}=\left(1-\varphi\right)\left(\rho C_p\right)_f+\varphi\left(\rho C_p\right)_s,\quad \sigma_{nf}=(1-\phi)\sigma_f+\phi\sigma_s,\\
&\frac{k_{nf}}{k_f}=\frac{(k_s+2k_f)-2\phi(k_f-k_s)}{(k_s+2k_f)+\phi(k_f-k_s)}.
\end{aligned} \tag{2.59}$$

where; ρ_f density of the base fluid, ρ_s is density of the nanoparticle, ϕ is the volume fraction of the nanoparticle, β_f is the base fluid thermal expansion coefficient, β_s is the nanoparticle thermal expansion coefficient, μ_f is dynamic viscosity of the base fluid, K_f is the thermal conductivity of the base fluid, σ_f is electric conductivity of base fluid, K_s is the thermal conductivity of the nanoparticle, σ_s is electric conductivity of nanoparticle, $\left(\rho C_p\right)_s$ is the heat capacitance of the nanoparticle and $\left(\rho C_p\right)_f$ is the heat capacitance of the base fluid.

2.5.4 Maxwell's Equations

These are related through Maxwell's equations, the equations governing the evolution of electric and magnetic fields are;

$$\nabla\times\mathbf{B}=\mu_o\mathbf{j}\ \text{(Ampere's Law)}. \tag{2.60}$$

$$\frac{\partial\mathbf{B}}{\partial t}=-\nabla\times\mathbf{E}\ \text{(Faraday's Law)}. \tag{2.61}$$

$$\mathbf{j}=\sigma\left(\mathbf{E}+\mathbf{V}\times\mathbf{B}\right)\text{(Ohm's Law)}. \tag{2.62}$$

where, μ_o is magnetic permeability, **B** is Magnetic field, **j** is electric current density, **E** is electric field.

CHAPTER THREE

ON HYDROMAGNETIC BOUNDARY LAYER FLOW OF NANOFLUIDS OVER A PERMEABLE MOVING SURFACE WITH NEWTONIAN HEATING[1]

3.0 Abstract

In this paper, the magnetohydrodynamics (MHD) boundary layer flow of nanofluids past a permeable moving flat plate with convective heating at the plate surface has been studied. The nanofluids considered contain water as the base fluid with copper (Cu) or Alumina (Al_2O_3) as the nanoparticles. The model equations are obtained and solved numerically by applying shooting iteration technique together with the fourth order Runge-Kutta-Fehlberg integration scheme. The influence of pertinent parameters on velocity, temperature, skin friction and Nusselt number are investigated. The obtained results are presented graphically and the physical aspects of the problem discussed quantitatively.

3.1 Introduction

The study of the flow of an electrically conducting fluids past permeable walls not only possesses a theoretical appeal but also model many biological and engineering problems such as MHD generators, nuclear reactors, geothermal energy extraction, drag reduction in aerodynamics, blood flow problems among others [102]. In metallurgy, the quality of the final product depends mainly on the cooling liquid used and the cooling rate. The combined effects of heat transfer and MHD are useful in achieving the desired characteristics of the final product. Experimental and theoretical studies on convectional electrically conducting fluids indicate that magnetic field markedly changes their transport and heat transfer characteristics. In a pioneering work, Sakiadis [108] investigated the boundary layer flow induced by a moving plate in a quiescent ambient fluid. Suction of a fluid on the boundary surface, can significantly change the flow field and, as a consequence, affect the heat transfer rate at the surface [148-150]. Various aspects of boundary layer flow problem have

[1]*This chapter is a journal paper:* W.N. Mutuku-Njane and O. D. Makinde, On Hydromagnetic Boundary Layer Flow of Nanofluids Over a Permeable Moving Surface With Newtonian Heating*, Latin American Applied Research Journal, Vol 44, No. 1, 2014.*

been investigated by several authors [111,112,141,151]. Convectional heat transfer fluids such as water, mineral oil and ethylene glycol have poor heat transfer properties compared to those of most solids. An innovative way of improving the heat transfer of fluids is to suspend small amounts of nanometer-sized (10–50 nm) particles and fibers in the fluids. This new kind of fluids named as “nanofluids” was introduced by Choi [1]. The nanoparticles are made of metals such as aluminium, copper, gold, iron, titanium or their oxides and the most commonly used base fluids are water, ethylene glycol, toluene and oil. The choice of base fluid-particle combination depends on the application for which the nanofluid is intended. Nanofluids, with their various potential applications in industrial, engineering and biomedicine have recently attracted intensive studies [20,121,128,138,147,152,153]. The remarkably improved convective heat transfer coefficient makes the nanofluid a superior heat transfer medium for cooling application.

Most convectional fluids used for producing nanofluids are liquids and their electrical conductivity properties are lower than that of the metallic or nonmetallic nanoparticles. The presence of the nanoparticles enhance the electrical conductivity property of the nanofluids, hence are more susceptible to the influence of magnetic field than the convectional base fluids. Recently, several authors [143-146] numerically investigated the natural convection of nanofluids under the influence of a magnetic field. Their theoretical studies on magnetic nanofluids assumed that both the nanoparticles and the convectional base fluids have equal electrical conductivity properties. In reality, this is not the case and ignoring the difference in electrical conductivity property of both the nanoparticles and the convectional base fluids may affect the outcome of the investigations carried out. To our knowledge, no attempt has been made in the past to study the effects of the complex interaction between the electrical conductivity of the convectional base fluids and that of the nanoparticles on the hydromagnetic flow with Newtonian heating. The main objective of this paper is to numerically investigate the change in the electrical conductivity of the convectional base fluids as a result of the nanoparticles and the subsequent interaction with the magnetic field at the boundary layer flow over a flat permeable surface with convective heating. The set of coupled non-linear ordinary differential equations for momentum and energy balance are solved numerically by applying shooting iteration technique together with fourth order Runge –Kutta integration scheme. Several results showing velocity and temperature profiles, skin friction and Nusselt number are presented graphically and discussed quantitatively.

3.2. Mathematical formulation

We consider a steady unidirectional boundary layer flow of an electrically conducting nanofluid (Cu-water and Al_2O_3-water) past a semi-infinite permeable moving flat plate in the presence of a uniform transverse magnetic field of strength B_0 applied parallel to the y-axis (figure 3.1). It is assumed that the induced magnetic field and the external electric field are negligible. At the boundary, the permeable plate is moving at a velocity U_o with a hot convectional fluid of temperature T_f flowing below it and a cold nanofluid of temperature $T < T_f$ flowing above the plate. Far away from the plate, $u = 0$, $T = T_\infty$.

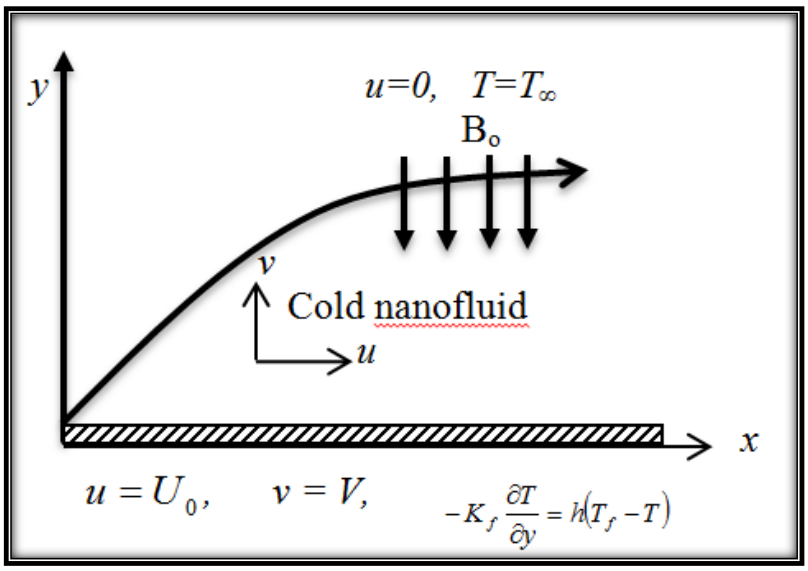

Figure 3.1. Flow configuration and coordinate system.

Table 3.1: Thermophysical properties of water, Copper and Alumina [151]

Physical properties	Fluid phase (water)	Cu	Al_2O_3
C_p ($J.kg^{-1}K^{-1}$)	4179	385	765
ρ($kg.m^{-3}$)	997.1	8933	3970
k($W.m^{-1}K^{-1}$)	0.613	400	40
σ(S/m)	$5.5x10^{-6}$	$58x10^{6}$	$35x10^{6}$

The x-axis is taken along the direction of plate and y-axis normal to it. The surface temperature is assumed to be maintained by convective heat transfer at a constant temperature T_f. The general equations governing the nanofluid flow are:

$$\frac{\partial u}{\partial x}+\frac{\partial v}{\partial y}=0, \tag{3.1}$$

$$u\frac{\partial u}{\partial x}+v\frac{\partial u}{\partial y}=-\frac{1}{\rho_{nf}}\frac{\partial p}{\partial x}+\frac{\mu_{nf}}{\rho_{nf}}\frac{\partial^2 u}{\partial y^2}-\frac{\sigma_{nf}B_o^2 u}{\rho_{nf}}, \tag{3.2}$$

$$u\frac{\partial T}{\partial x}+v\frac{\partial T}{\partial y}=\frac{K_{nf}}{\left(\rho c_p\right)_{nf}}\frac{d^2T}{dy^2}+\frac{\mu_{nf}}{\left(\rho c_p\right)_{nf}}\left(\frac{du}{dy}\right)^2+\frac{\sigma_{nf}B_o^2u^2}{\left(\rho c_p\right)_{nf}}, \tag{3.3}$$

where (u, v) are the velocity components of the nanofluid in the (x, y) directions respectively, p is the fluid pressure, μ_{nf} is the dynamic viscosity of the nanofluid, ρ_{nf} is the density of the nanofluid, σ_{nf} is the electrical conductivity of the nanofluid, $(\rho c_p)_{nf}$ is the heat capacitance of the nanofluid and k_{nf} is the thermal conductivity of the nanofluid which are defined as;

$$\mu_{nf}=\frac{\mu_f}{(1-\phi)^{2.5}},\quad \rho_{nf}=(1-\phi)\rho_f+\phi\rho_s,\quad \sigma_{nf}=(1-\phi)\sigma_f+\phi\sigma_s,$$

$$(\rho c_p)=(1-\phi)(\rho c_p)_f+\phi(\rho c_p)_s,\qquad \frac{k_{nf}}{k_f}=\frac{(k_s+2k_f)-2\phi(k_f-k_s)}{(k_s+2k_f)+\phi(k_f-k_s)}. \tag{3.4}$$

Under the boundary-layer approximation the nanofluid equations for continuity, momentum and energy balance governing the problem under consideration in one dimension are written as;

$$\frac{\partial u}{\partial y}=0, \tag{3.5}$$

$$-V\frac{du}{dy}=-\frac{1}{\rho_{nf}}\frac{dp}{dx}+\frac{\mu_{nf}}{\rho_{nf}}\frac{d^2u}{dy^2}-\frac{\sigma_{nf}B_o^2u}{\rho_{nf}}, \tag{3.6}$$

$$-V\frac{dT}{dy}=\frac{K_{nf}}{\left(\rho c_p\right)_{nf}}\frac{d^2T}{dy^2}+\frac{\mu_{nf}}{\left(\rho c_p\right)_{nf}}\left(\frac{du}{dy}\right)^2+\frac{\sigma_{nf}B_o^2u^2}{\left(\rho c_p\right)_{nf}}, \tag{3.7}$$

with boundary conditions,

$$\begin{aligned} &u(x,0)=U_0, \qquad -\mathrm{k_f}\frac{\partial T}{\partial y}(x,0)=h_f\left[T_f-T(x,0)\right],\\ &u(x,\infty)=0, \qquad \mathrm{T}(x,\infty)=T_\infty. \end{aligned} \tag{3.8}$$

Introducing the following dimensionless variables and quantities into the governing conservation equations (3.5)-(3.7) :

$$\eta = \frac{yU_0}{\upsilon_f}, \quad W = \frac{u}{U_0}, \quad S = \frac{V}{U_0}, \quad \theta = \frac{T - T_\infty}{T_f - T_\infty},$$
$$\Pr = \frac{\upsilon_f}{\alpha_f}, \quad Bi = \frac{h\upsilon_f}{U_0 k_f}, \quad Ha = \frac{\sigma_f B_0^2 \upsilon_f}{\rho_f U_0^2}, \quad Br = \frac{\mu_f U_0^2}{k_f (T_f - T_\infty)}, \tag{3.9}$$

we obtain,

$$\frac{d^2W}{d\eta^2} + S(1-\varphi)^{2.5}(1-\varphi+\varphi\rho_s/\rho_f)\frac{dW}{d\eta} - Ha(1-\varphi)^{2.5}(1-\varphi+\varphi\sigma_s/\sigma_f)W = 0, \tag{3.10}$$

$$\frac{d^2\theta}{d\eta^2} + \frac{S\,\Pr\, k_f}{k_{nf}}(1-\phi+\phi(\rho c_p)_s/(\rho c_p)_f)\frac{d\theta}{d\eta} + \frac{k_f Br}{k_{nf}(1-\phi)^{2.5}}\left(\frac{dW}{d\eta}\right)^2 + \frac{HaBrk_f}{k_{nf}}(1-\phi+\phi\sigma_s/\sigma_f)W^2 = 0. \tag{3.11}$$

with the boundary conditions;

$$\begin{aligned} &W = 1, \quad \frac{d\theta}{d\eta} = Bi(\theta - 1) && \text{at } \eta = 0, \\ &W = 0, \quad \theta = 0 && \text{as } \eta \to \infty. \end{aligned} \tag{3.12}$$

where *W* and θ are the dimensionless nanofluid velocity and temperature respectively, *Pr* represents the Prandtl number, *Br* is the Brinkmann number, *S* is the suction velocity parameter, *Ha* is the Hartmann number, *Bi* is the Biot number, φ is the solid volume fraction parameter of the nanofluid, μ_f is the viscosity of the base fluid, ρ_f and ρ_s are the densities of the base fluid and nanoparticle respectively, k_f and k_s are the thermal conductivities of the base fluid and nanoparticle respectively, $(\rho c_p)_f$ and $(\rho c_p)_s$ are the heat capacitance of the base fluid and the nanoparticle respectively, σ_f and σ_s are the electrical conductivities of the base fluid and the nanoparticle respectively. It is important to take note that φ = 0 correspond to a regular fluid scenario with magnetic field effect.

The physical quantities of practical significance in this work are skin friction coefficient and the local Nusselt number *Nu*, which are defined as

$$C_f = \frac{\tau_w}{\rho_f U_0^2}, \quad Nu = \frac{xq_w}{k_f(T_f - T_\infty)}, \tag{3.13}$$

where τ_w is the skin friction and q_w is the heat flux from the plate which are given by

$$\tau_w = \mu_{nf} \left.\frac{\partial u}{\partial y}\right|_{y=0}, \quad q_w = -k_{nf} \left.\frac{\partial T}{\partial y}\right|_{y=0}. \tag{3.14}$$

Substituting equation (3.14) into equation (3.13), we obtain;

$$C_f = \frac{1}{(1-\varphi)^{2.5}} W'(0), \quad \mathrm{Re}_x^{-1} Nu = -\frac{k_{nf}}{k_f}\theta'(0), \tag{3.15}$$

where Rex = U∞x/υf is the local Reynolds number and the prime symbol denotes derivatives with respect to η. The set of equations (3.10) – (3.11) under the boundary conditions (3.12) have been solved numerically using Runge-Kutta-Fehlberg method with shooting technique implemented on Maple 12. From the numerical computations, the local skin-friction coefficient and the local Nusselt number in equation (3.15) are also worked out and their numerical values depicted graphically.

3.3 Results and discussion

The effects of various dimensionless parameters on the velocity, temperature, skin friction and Nusselt's number are illustrated by the set of Figures 3.2 – 3.15. The Prandt number is kept constant at 6.2 [154]. The values of the Magnetic parameter *Ha* considered range from 10^{-10} to 10^{-13} and the nanoparticle volume fraction parameter φ is varied from 0 to 0.2. *Ha* = 0 corresponds to absence of magnetic field and φ = 0 is regular fluid. In order to benchmark our numerical results, the special case of heat transfer in MHD flow of convectional fluid (i.e. φ =0) over a moving permeable surface is compared with that of [153] as shown in the table 2 below:

Table 3.2: Computations showing comparison with [153] for *Br*=0.1, *Pr*=0.72, φ =0, *Bi*=0.1, *S*=1

Ha	θ(0) [153]	$-\theta'(0)$ [153]	$W'(0)$ [153]	θ(0) Present	$\theta'(0)$ Present	$W'(0)$ Present
0.1	0.1939	0.0806	1.0916	0.1939	0.0806	1.0916
0.5	0.2273	0.0772	1.3660	0.2273	0.0772	1.3660
1	0.2581	0.0742	1.6180	0.2581	0.0742	1.6180

It is noteworthy that the numerical results in Table 3.2 shows perfect agreement, hence validate the accuracy of our numerical procedure and the MHD nanofluids results obtained thereafter.

3.3.1 Velocity profiles

Figures 3.2 – 3.5 depicts the effects of various physical parameters on the nanofluid velocity profiles. It is noted that for all the pertinent parameters, the velocity is maximum at the moving plate surface but decreases gradually to zero at the free stream far away from the plate surface thus satisfying the boundary conditions. Figure 3.2 shows that the momentum boundary thickness for Cu-water nanofluid is smaller than that of Al_2O_3-water nanofluid, consequently, Cu-water nanofluid tends to flow closer to the convectively heated plate surface and serve as a better coolant than Al_2O_3-water nanofluid. It is observed in Figure 3.3, an increase in the magnetic parameter *Ha* pushes the fluid towards the plate surface hence decreasing both the momentum boundary layer thickness and the fluid velocity. This is in agreement with the physics of the problem in that, an increase in the magnetic field intensity leads to an increase in the Lorentz force thus producing more resistance to the transport phenomena. A similar trend is observed with increase in the nanoparticle volume fraction φ and suction parameter *S* as ascertained in Figures 3.4 and 3.5.

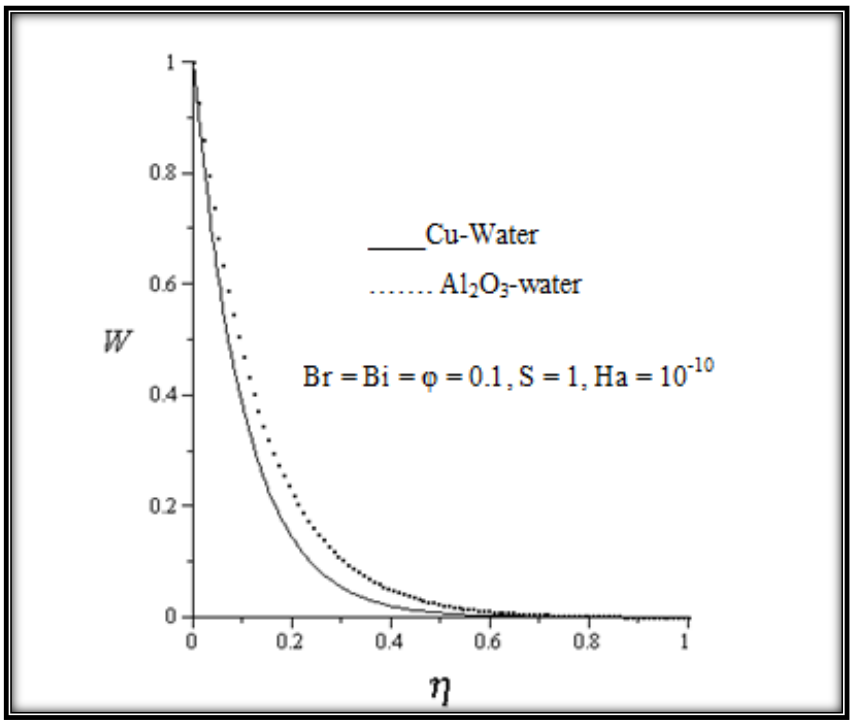

Figure 3.2: Velocity profiles for different nanofluids

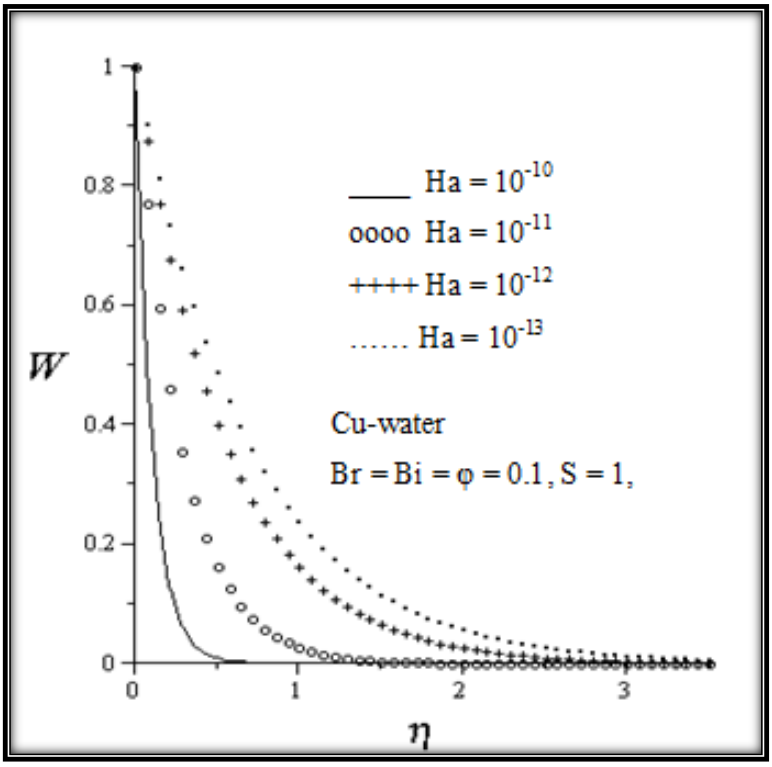

Figure 3.3: Velocity profiles for increasing magnetic field intensity.

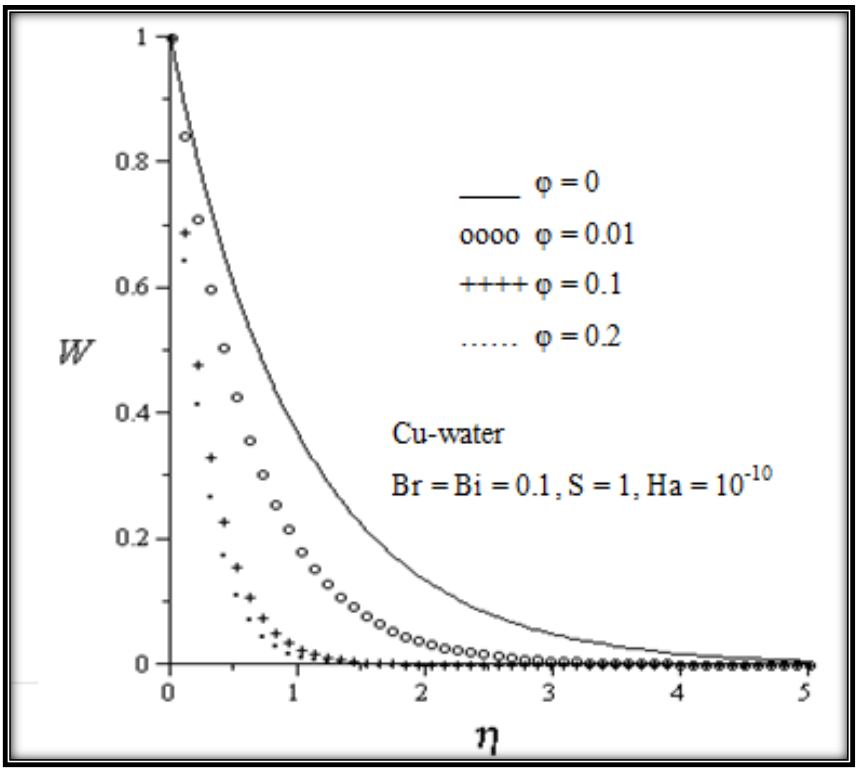

Figure 3.4: Velocity profiles for increasing nanoparticle concentration.

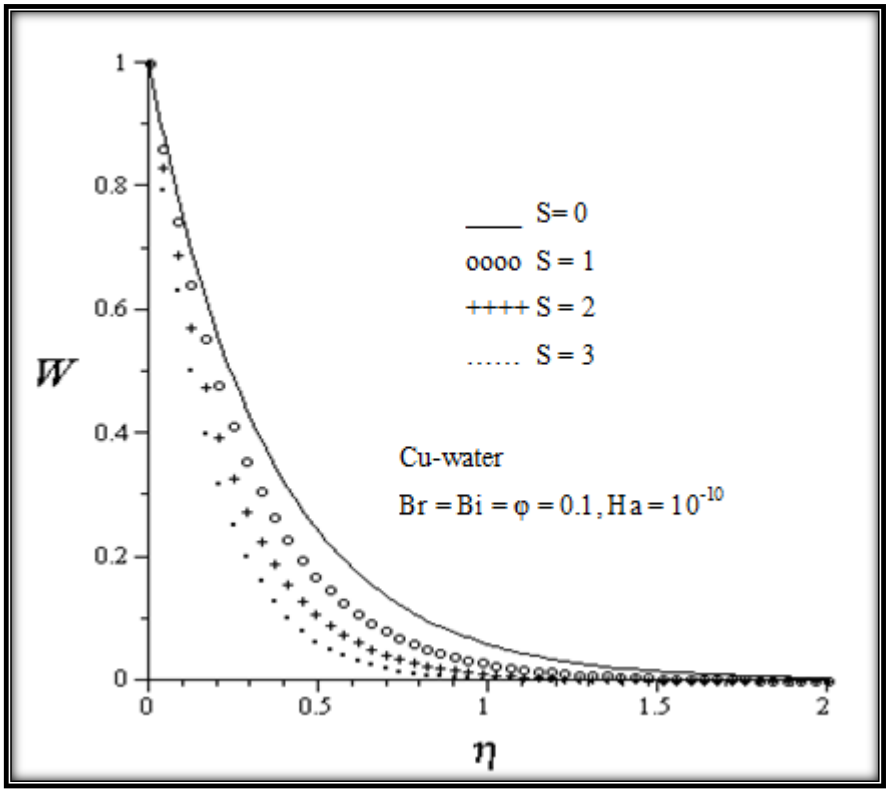

Figure 3.5: Velocity profiles for increasing suction.

3.3.2 Temperature profiles

Figure 3.6 – 3.11 shows the effects of various parameter on the temperature profile. It is observed that the temperature gradually decreases from a maximum value near the plate surface to zero far away from the plate satisfying the free stream conditions. Figure 3.6 shows that Cu-water nanofluid thermal boundary layer thickness is greater than that of Al_2O_3-water nanofluid as expected. This is in accordance with the earlier observation, since the Cu-water nanofluid tends to absorb more heat from the plate surface owing to its close proximity to the hot surface. In Figure 3.7, it is noted that an increase in *Ha* leads to an increase in the temperature, and as a result, the thermal boundary layer thickness increases. Increasing the *Bi* increases the temperature and the thermal boundary layer thickness, a fact attributed to an increase in the convective heating as shown in Figure 3.8. Similar results are observed with an increase in φ and *Br* as shown in Figures 3.9 – 3.10. This agrees with the physical behaviour in that when the volume fraction of copper increases the thermal conductivity increases as well, and as a result the thermal boundary layer thickness increases. This observation shows that using nanofluids changes the temperature, thus the use of nanofluids will be of significance in the cooling and heating processes. Figure 3.11

shows that an increase in $S > 0$ means more nanofluid is sucked out of the porous plate leading to a decrease in the temperature and subsequently, a decrease in the thermal boundary layer thickness. This is expected since increasing S implies that more fluid is sucked out of the permeable plate surface.

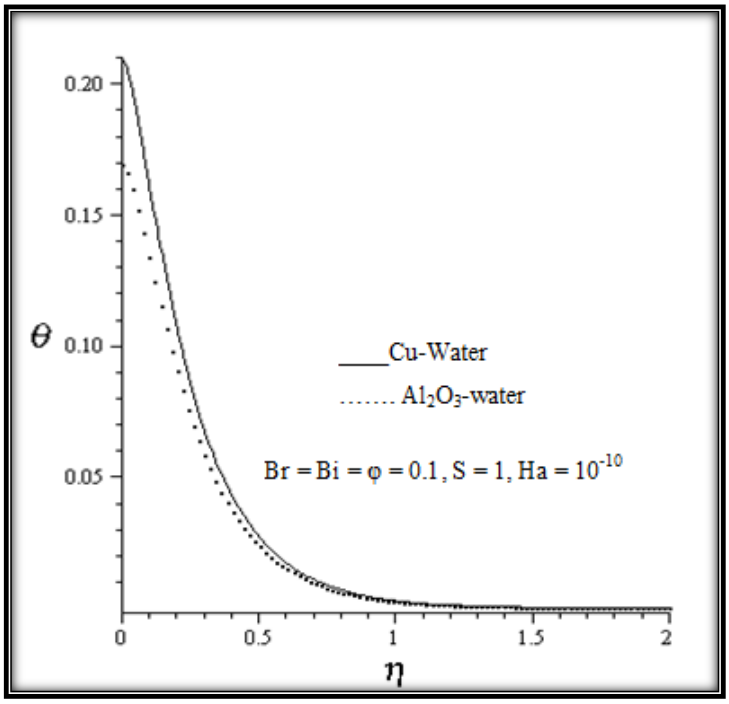

Figure 3.6: Temperature profiles for different nanofluids

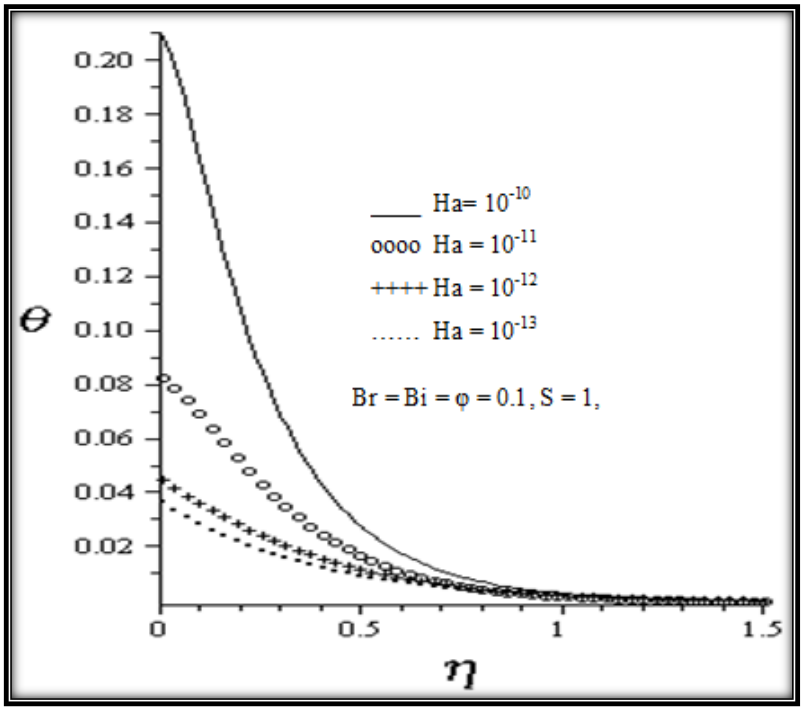

Figure3.7: Temperature profiles for increasing magnetic field intensity

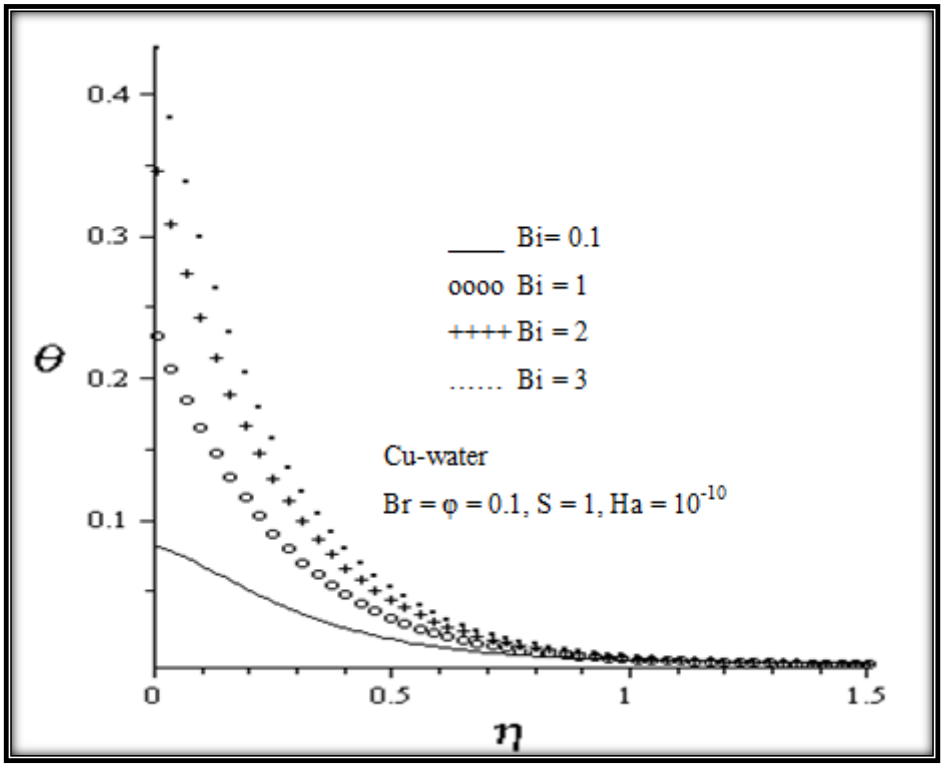

Figure 3.8: Temperature profiles for increasing Biot number

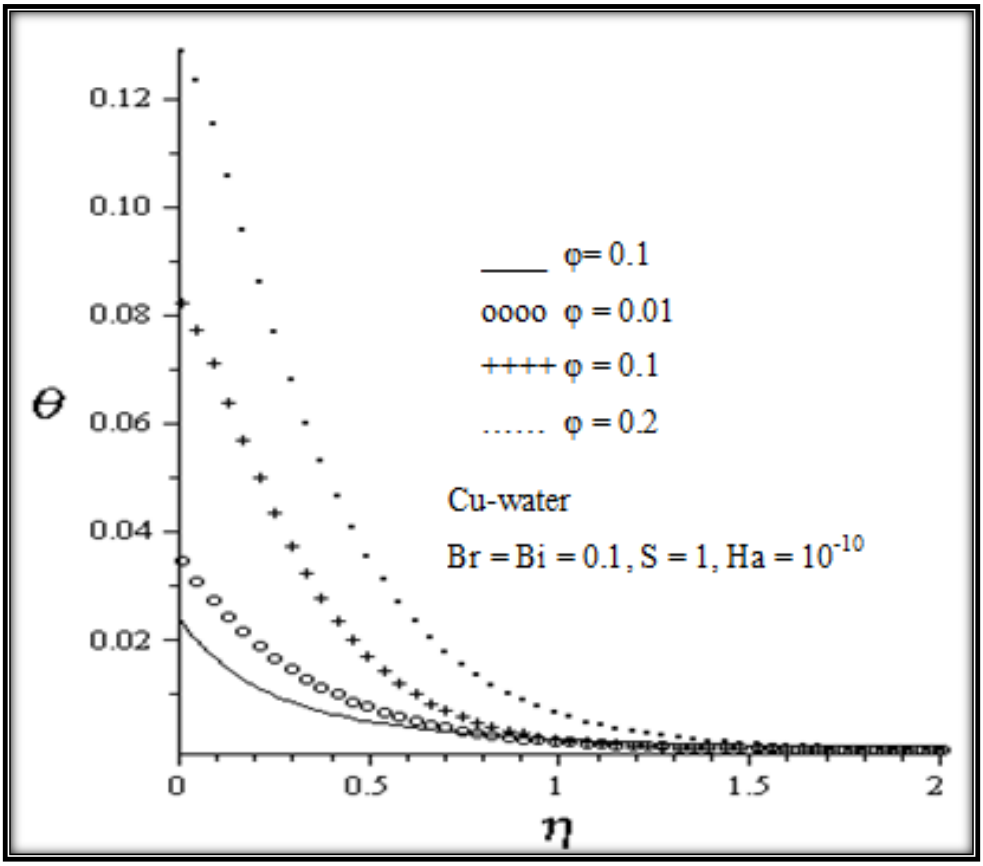

Figure 3.9: Temperature profiles for increasing nanoparticle concentration

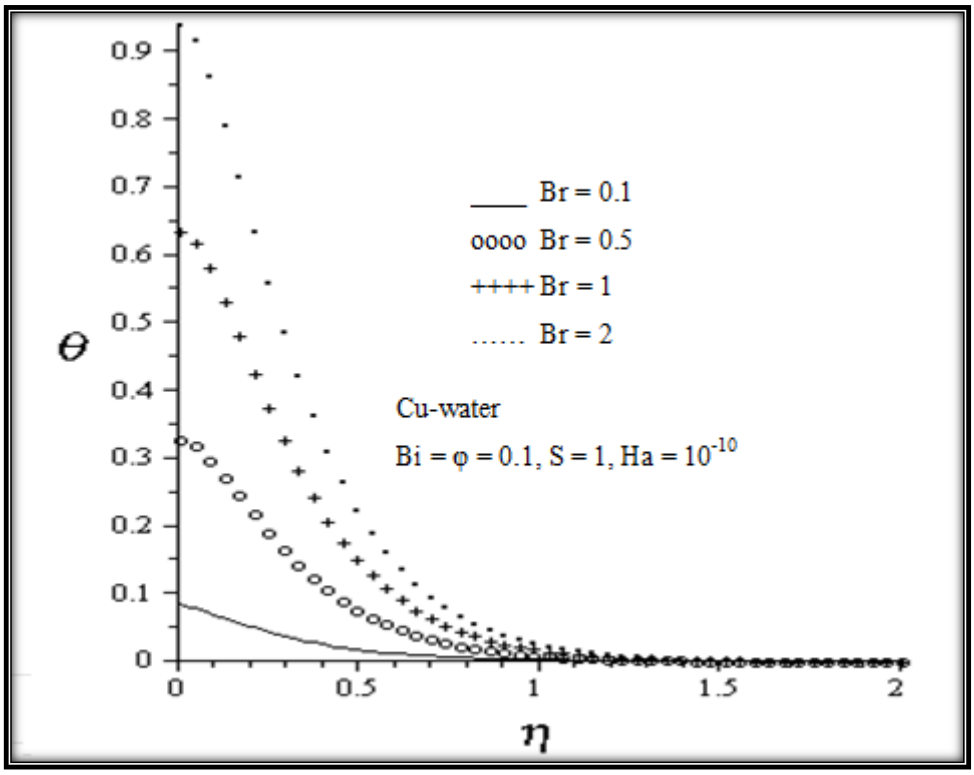

Figure 3.10: Temperature profiles for increasing Brinkmann number

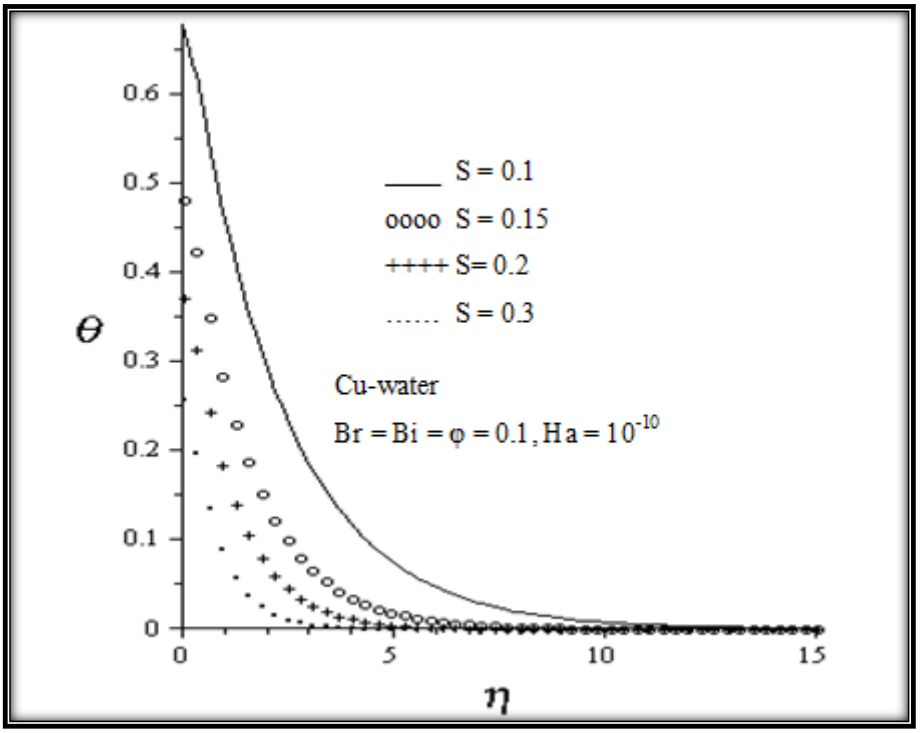

Figure 3.11: Temperature profiles for increasing suction

3.3.3 Skin Friction

Figures 3.12-3.13 shows the variation of the skin friction or the shear stress with φ and *Ha*. It is noted that for high value of φ, the skin friction coefficient becomes higher. Cu-water nanofluid has a higher skin friction compared to Al_2O_3-water nanofluid as shown in Figure 3.12. This is also expected, since Cu-water moves closer to the plate surface leading to an elevation in the velocity gradient at the plate surface. Figure 3.13 illustrates that decreasing the magnetic field strength decreases the skin friction.

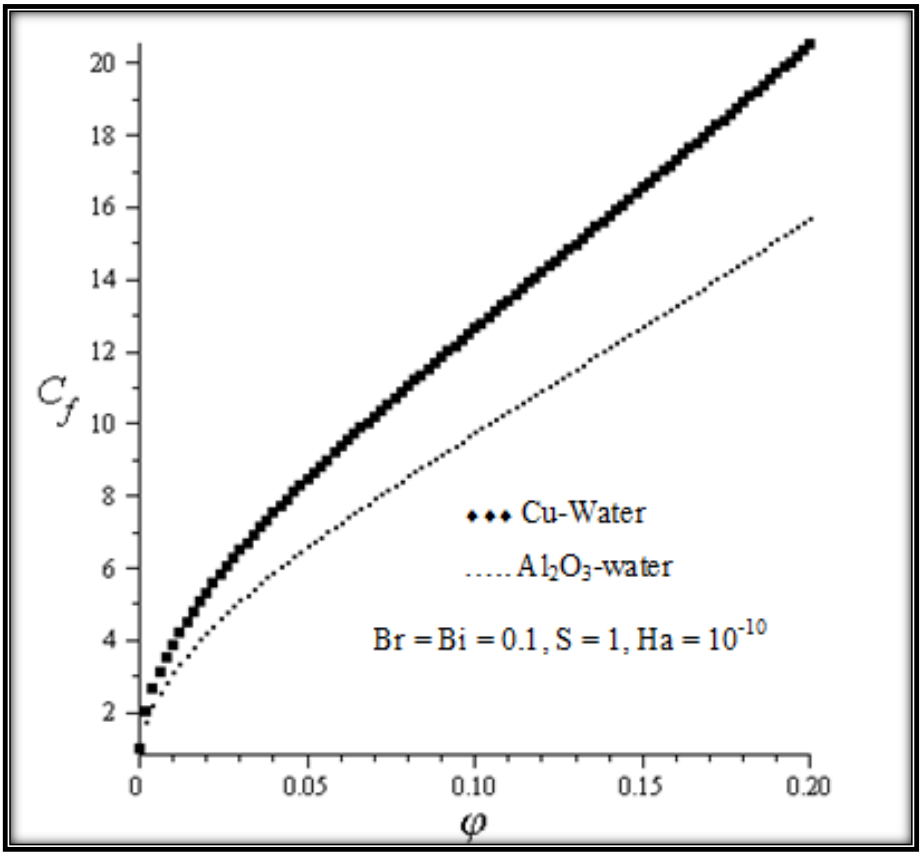

Figure 3.12: Skin friction for different nanofluids.

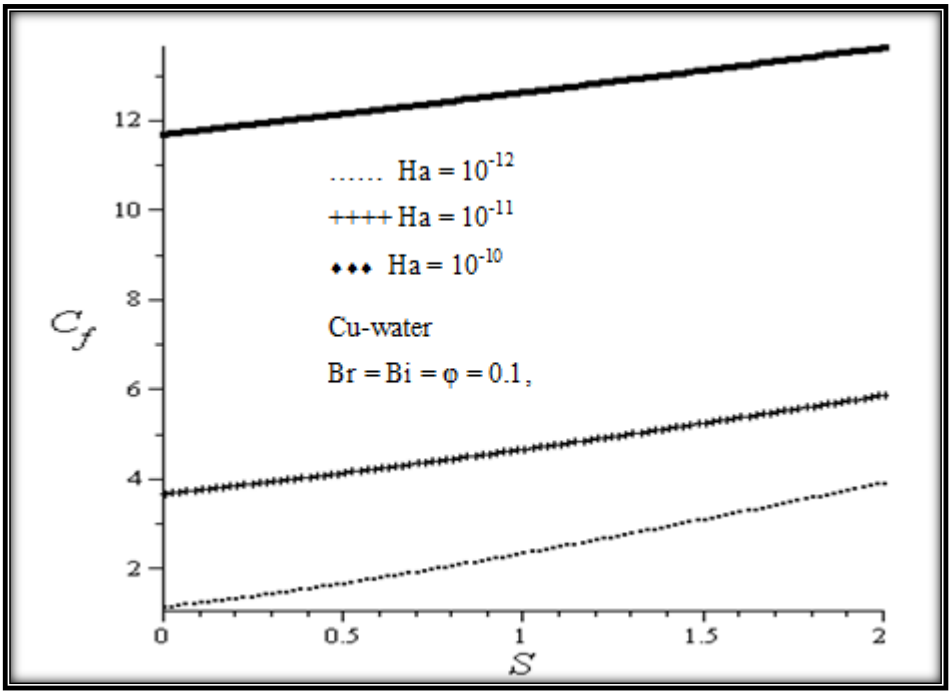

Figure 3.13: Skin friction coefficient for increasing suction and magnetic field intensity.

3.3.4 Nusselt number

Figures 3.14 – 3.16 show the variation of Nusselt number versus different nanofluids, *Ha* and *Bi*. It is noted from Figure 3.14 that the heat transfer rates increases with the increase in φ, although the heat transfer rate at the plate surface for Al_2O_3-water nanofluid is higher compared to Cu-water nanofluid. A decrease in *Ha* leads to an increase in the rate of heat transfer at the plate surface as seen in Figure 3.15. Figure 3.16 illustrates that increasing the *Br*, reduces the rate of heat transfer rate, while increasing the *Bi* increases the rate of heat transfer.

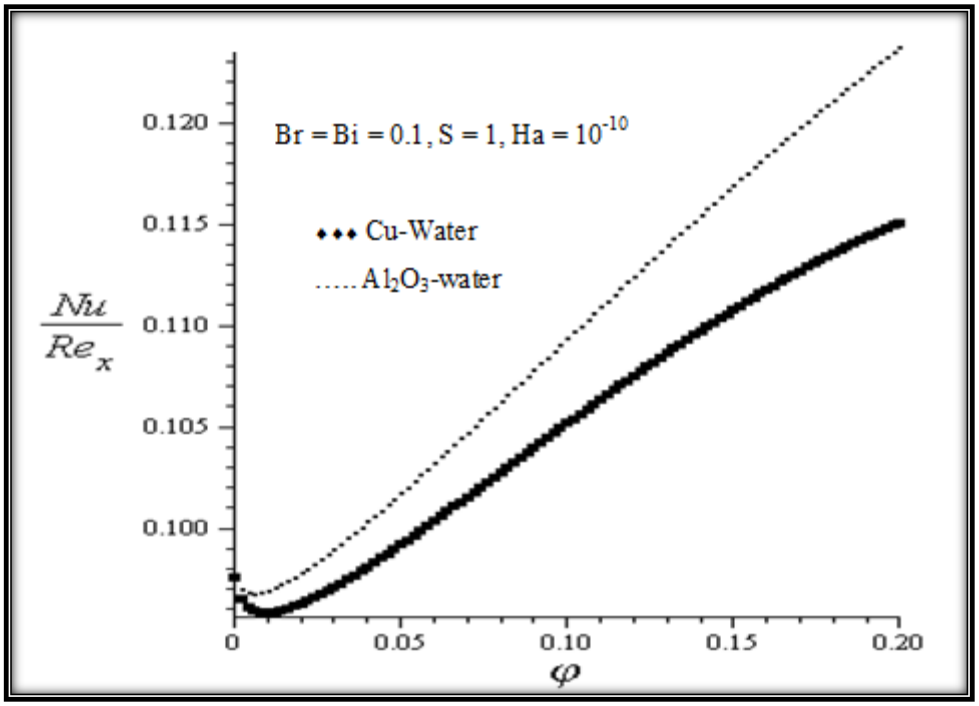

Figure 3.14: Nusselt number for different nanofluids

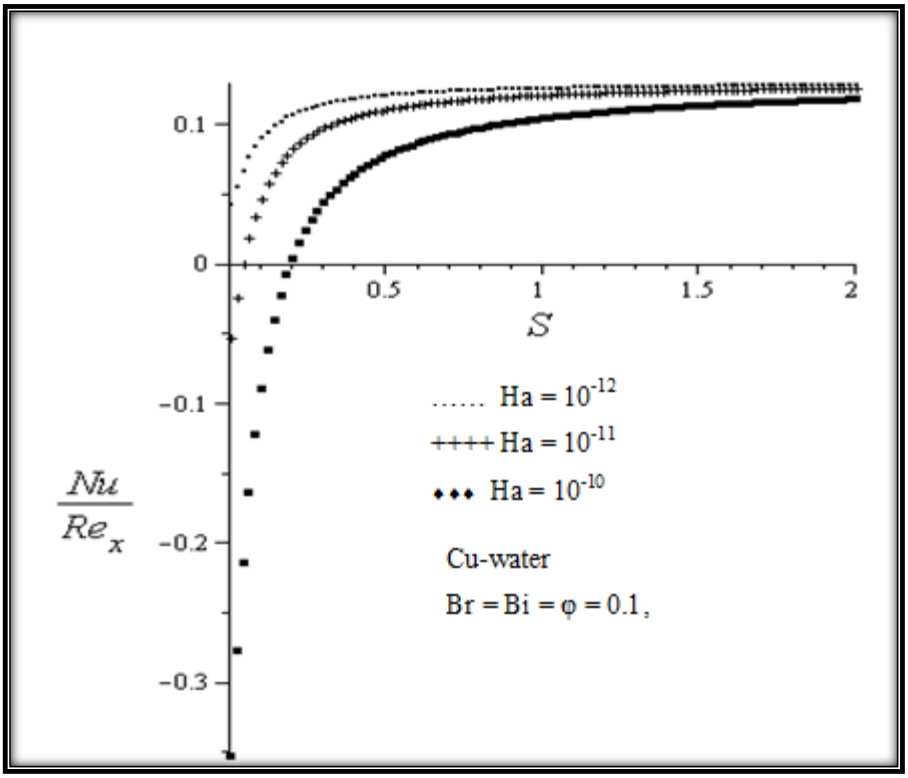

Figure 3.15: Nusselt number for increasing suction and magnetic field intensity

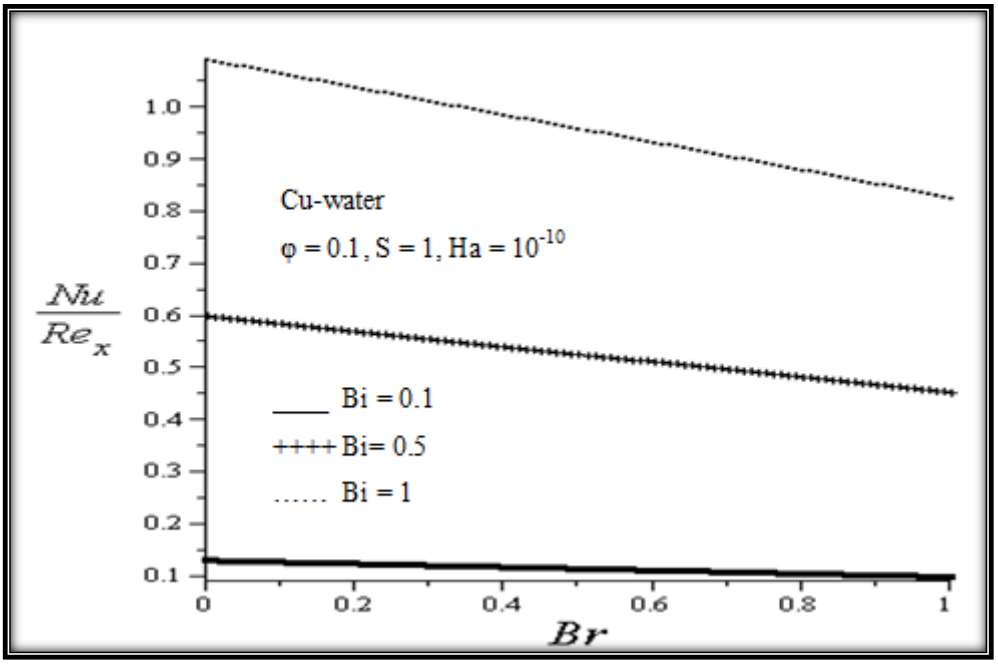

Figure 3.16: Nusselt number for increasing Brinkmann and Biot number

3.4 Conclusion

In the present study, we have theoretically studied the effects of magnetic field on the boundary layer flow of Cu-water and Al_2O_3-water nanofluids past a semi-infinite permeable moving flat plate with a convective heat exchange at the surface. The coupled nonlinear governing equations were derived, non-dimensionalised and solved numerically using fourth-order Runge-Kutta -Fehlberg method with shooting technique, putting into consideration the enhanced electrical conductivity of the convectional base fluid due to the presence of the nanoparticles. The effects of *Ha,* φ*, S* and *Bi* on velocity, temperature, skin friction and local Nusset number are investigated. It is shown that, increasing the values of *Ha*, φ and *S* lead to a decrease in the momentum boundary layer thickness and an increase in the thermal boundary layer thickness. From the application point of view, it is obvious that the cooling effect on the convectively heated plate surface is enhanced with increasing values *Ha*, φ and *S* while an increase in *Bi* decreases the cooling effect. The skin friction increases with increase in both the magnetic parameter and φ, while the Nusset number increases with increase in φ and *Bi*, but with a decrease in *Ha* and *Br*. The results obtained herein justify the physics of the problem, however, experimental data are yet to be found to further validate the formulation of this problem. It is hoped that work such as this will encourage further work in area involving electrically conducting nanofluids and the authors will highlight the interaction between the electrical conductivity of both the convectional base fluid and the nanoparticle in the presence of a magnetic field.

It is evident from the above findings that the present study has numerous industrial, engineering and biomedical applications such as heat transfer applications: industrial cooling, smart fluids; nanofluid coolant: vehicle cooling, electronics cooling; medical applications: magnetic drug targeting and nanocryosurgery.

CHAPTER FOUR

HYDROMAGNETIC THERMAL BOUNDARY LAYER OF NANOFLUIDS OVER A CONVECTIVELY HEATED FLAT PLATE WITH VISCOUS DISSIPATION AND OHMIC HEATING[2]

4.0 Abstract

This paper examines the effect of the complex interaction between the electrical conductivity of the conventional base fluid and that of the nanoparticles under the influence of magnetic field in a boundary layer flow with heat transfer over a convectively heated flat surface. Three types of water based nanofluids containing metallic or nonmetallic nanoparticles such as copper (Cu), Alumina (Al_2O_3) and Titania (TiO_2) are investigated. Using a similarity analysis of the model transport equations followed by their numerical computations, the results for the nanofluids velocity, temperature, skin-friction and Nusselt number are obtained. The effects of various thermophysical parameters on the boundary layer flow characteristics are displayed graphically and discussed quantitatively. It is observed that the presence of nanoparticles greatly enhance the magnetic susceptibility of nanofluids as compared to the convectional base fluid.

4.1 Introduction

Studies related to hydromagnetic boundary layer flows of nanofluids have a wide range of industrial, engineering and biological applications. These include; magnetics drug targeting, MHD blood flow meters, production of magneto-rheostatic (MR) materials known as smart fluids, boundary layer control in aerodynamic and crystal growth [102]. In recent years, we find several applications in polymer industries, cooling of metallurgical materials, cooling of microchips in computers and other electronics which use microfluidic applications, cooling of automobile engine, wire drawing, glass-fiber production. The nanofluid containing magnetic nanoparticles also acts as a super-paramagnetic fluid, which, in an alternating electromagnetic field, absorbs energy and produces a controllable hyperthermia. Choi [1] pioneered the study of nanofluids. The term nanofluid describes a solid liquid mixture which consists of base liquid with low volume fraction of high conductivity solid nanoparticles. The particles are usually of nanometer-size (10–50nm) and are made by a high-energy-pulsed

[2] *This chapter consists of a paper which was accepted for publication on 15/7/2013 in University Politehnica of Bucharest Scientific Bulletin – series A – Applied mathematics and physics journal.*

process from a conductive material. They include particles of metals such aluminium, copper, gold, iron and or their oxides like titanium. Moreover, it is well known that the heat transfer properties of the conventional base fluids such as water, mineral oil and ethylene glycol are very poor compared to that of most solids. A comprehensive survey of convective transport in nanofluids was presented by Buongiorno [155]. He reported that a satisfactory explanation for the abnormal increase in the thermal conductivity and viscosity of nanofluids was yet to be found. Li and Xuan [120] experimentally investigated the various transport properties of nanofluids. Kuznetsov and Nield [147] examined the influence of nanoparticles on the natural convection boundary-layer flow past a vertical plate. Thereafter, several researchers [20, 121, 135, 152] have investigated convention flows of nanofluids under various physical conditions. Ahmad et al. [154] extended the well known Blasius and Sakiadis boundary layer flow problems to include the nanofluids. Makinde and Aziz [153] presented a similarity solution for boundary layer flows of nanofluids over a convectively heated stretching sheet. The effects of thermal radiation and viscous dissipation on boundary layer flow of nanofluids over a permeable moving flat plate were reported by Motsumi and Makinde [156]. Recently, the influence of magnetic field on the boundary layer flow of electrically conducting nanofluids was investigated in some studies [144, 145]. However, in their theoretical analysis, the complex interaction of the nanoparticles electrical conductivities with that of conventional base fluids was ignored. In reality, the electrical conductivities of nanoparticles are not equal to that of conventional base fluid and therefore cannot be ignored in order to obtain a realistic solution to the problem.

In this study, our objective is to investigate the combined effects of magnetic field, viscous dissipation and Ohmic heating on the boundary layer flow of nanofluids over a convectively heated flat plate. The complex interaction of the electrical conductivities of metallic or nonmetallic nanoparticles such as copper (Cu), Alumina (Al_2O_3) and Titania (TiO_2) with that of conventional base fluid (water) is taken into consideration. Using an appropriate similarity transformation, the well-known governing partial differential equations are reduced to ordinary differential equations. The resulting problems are solved numerically using the Runge–Kutta–Fehlberg method with the shooting technique. The effects of various thermophysical parameters on velocity, temperature, skin friction and Nusselt number are discussed in detail. A comparative study between the previously published results and the present results in a limiting sense reveals excellent agreement between them. The organization of the paper is as follows: Problem is formulated and solved in section 4.2. Numerical results and discussion are given in Section 4.3. The conclusions have been summarized in Section 4.4.

4.2 Mathematical Formulation

We consider a steady boundary layer flow of an electrically conducting nanofluid past a semi-infinite convectively heated flat plate in the presence of a uniform transverse magnetic field of strength B_0 applied parallel to the y-axis (Figure 4.1). It is assumed that the induced magnetic field and the external electric field are negligible. The nanofluid on the upper surface of the plate is made up of water as base fluid with copper (Cu), Alumina (Al_2O_3) or Titania (TiO_2) as the nanoparticles. The lower side of the plate is convectively heated by a hot conventional fluid of temperature T_f such that the nanofluid $T < T_f$.

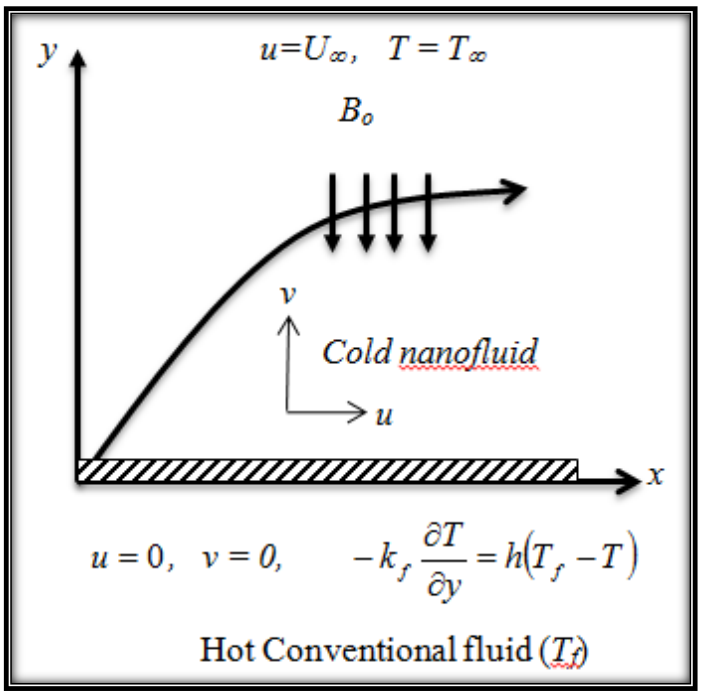

Figure 4.1: Schematic diagram of the problem.

Under the usual boundary layer approximations, the flow is governed by the following equations [10-14];

$$\frac{\partial u}{\partial x}+\frac{\partial v}{\partial y}=0, \tag{4.1}$$

$$u\frac{\partial u}{\partial x}+v\frac{\partial u}{\partial y}=\frac{\mu_{nf}}{\rho_{nf}}\frac{\partial^2 u}{\partial y^2}-\frac{\sigma_{nf}B_0^2(u-U_\infty)}{\rho_{nf}}, \tag{4.2}$$

$$u\frac{\partial T}{\partial x}+v\frac{\partial T}{\partial y}=\alpha_{nf}\frac{\partial^2 T}{\partial y^2}+\frac{\mu_{nf}}{(\rho c_p)_{nf}}\left(\frac{\partial u}{\partial y}\right)^2+\frac{\sigma_{nf}B_0^2}{(\rho c_p)_{nf}}(u-U_\infty)^2, \tag{4.3}$$

where (u, v) are the velocity components of the nanofluid in the (x, y) directions respectively, U_∞ is the free stream velocity, T is the temperature of the nanofluid, μ_{nf} is the dynamic viscosity of the nanofluid, ρ_{nf} is the density of the nanofluid, α_{nf} is the thermal diffusivity of the nanofluid, σ_{nf} is the electrical conductivity of the nanofluid, and $(\rho c_p)_{nf}$ is the heat capacitance of the nanofluid which are given by [20, 135, 154];

$$\begin{aligned}
&\mu_{nf} = \frac{\mu_f}{(1-\varphi)^{2.5}}, \quad \rho_{nf} = (1-\varphi)\rho_f + \varphi\rho_s, \\
&\alpha_{nf} = \frac{k_{nf}}{(\rho c_p)_{nf}}, \frac{k_{nf}}{k_f} = \frac{(k_s + 2k_f) - 2\varphi(k_f - k_s)}{(k_s + 2k_f) + \varphi(k_f - k_s)}, \\
&(\rho c_p)_{nf} = (1-\varphi)(\rho c_p)_f + \varphi(\rho c_p)_s, \sigma_{nf} = (1-\varphi)\sigma_f + \varphi\sigma_s.
\end{aligned} \tag{4.4}$$

The thermal conductivity of the nanofluid is represented by k_{nf}, φ is the solid volume fraction parameter of the nanofluid, ρ_f is the reference density of the fluid fraction, ρ_s is the reference density of the solid fraction, σ_f is the electrical conductivity of the fluid fraction, σ_s is the electrical conductivity of the solid fraction, μ_f is the viscosity of the fluid fraction, k_f is the thermal conductivity of the fluid fraction, c_p is the specific heat at constant pressure and k_s is the thermal conductivity of the solid volume fraction. The boundary conditions at the plate surface and far into the cold nanofluid may be written as [153];

$$u(x,0) = 0,\ v(x,0)=0,\ -k_f \frac{\partial T}{\partial y}(x,0) = h_f[T_f - T(x,0)],\ u(x,\infty) = U_\infty,\ T(x,\infty) = T_\infty, \tag{4.5}$$

where is the h_f plate heat transfer coefficient.

The stream function ψ, satisfies the continuity equation (4.1) automatically with

$$u = \frac{\partial \psi}{\partial y} \text{ and } v = -\frac{\partial \psi}{\partial x}. \tag{4.6}$$

A similarity solution of equations (4.1)–(4.5) is obtained by defining an independent variable η and a dependent variable f in terms of the stream function ψ as [144, 145, 153, 154, 156,]

$$\begin{aligned}
&\eta = y\sqrt{\frac{U_\infty}{\upsilon_f x}} = \frac{y}{x}\sqrt{\mathrm{Re}_x}, \quad \psi = \sqrt{\upsilon_f x U_\infty}\, f(\eta),\ u = U_\infty f'(\eta), \\
&v = \frac{1}{2}\sqrt{\frac{U_\infty \upsilon_f}{x}}\left(\eta f' - f\right), \quad \theta = \frac{T - T_\infty}{T_f - T_\infty},
\end{aligned} \tag{4.7}$$

where a prime symbol denotes differentiation with respect to η and Re_x is the local Reynolds number (=$U_\infty x/\upsilon_f$). After introducing equation (6) into equation (4.1) - (4.5), we obtain;

$$\begin{aligned}
&f''' + \frac{(1-\varphi)^{2.5}(1-\varphi+\varphi\rho_s/\rho_f)}{2} ff'' \\
&\quad - Ha(1-\varphi)^{2.5}(1-\varphi+\varphi\sigma_s/\sigma_f)(f'-1) = 0,
\end{aligned} \tag{4.8}$$

$$\theta''+\frac{k_f\,\mathrm{Pr}[1-\varphi+\varphi(\rho c_p)_s/(\rho c_p)_f]}{2k_{nf}}f\theta' + \frac{k_f Br}{k_{nf}(1-\varphi)^{2.5}}(f'')^2+\frac{HaBrk_f}{k_{nf}}(1-\varphi+\varphi\sigma_s/\sigma_f)(f'-1)^2=0, \tag{4.9}$$

$$\begin{aligned} &f(0)=0,\quad f'(0)=0,\quad \theta'(0)=Bi[\theta(0)-1],\\ &f'(\infty)=1,\quad \theta(\infty)=0, \end{aligned} \tag{4.10}$$

where

$$Bi=\frac{h_f}{k_f}\sqrt{\frac{\upsilon_f x}{U_0}},\quad Ha=\frac{\sigma_f B_o{}^2 x}{\rho_f U_\infty},\quad Br=\frac{\mu_f U_o{}^2}{k_f\left(T_f-T_\infty\right)},\quad \mathrm{Pr}=\frac{\upsilon_\mathrm{f}}{\alpha_\mathrm{f}}. \tag{4.11}$$

represents Biot number, magnetic field parameter, Brinkmann number and Prandtl number respectively. When φ = 0, we obtain the conventional fluid scenario. *Bi* and *Ha* in equations (4.8)-(4.10) are functions of *x* and in order to have a similarity solution, all the parameters must be constant. Following [153] we therefore assume that

$$h_f=ax^{-\frac{1}{2}},\quad \sigma_f=bx^{-1}. \tag{4.12}$$

where *a* and *b* are constants. The quantities of practical interest in this study are the skin friction coefficient C_f and the local Nusselt number *Nu*, which are defined as

$$C_f=\frac{\tau_w}{\rho_f U_0^2},\quad Nu=\frac{xq_w}{k_f(T_f-T_\infty)}, \tag{4.13}$$

where τ_w is the skin friction and q_w is the heat flux from the plate which are given by

$$\tau_w=\mu_{nf}\left.\frac{\partial u}{\partial y}\right|_{y=0},\quad q_w=-k_{nf}\left.\frac{\partial T}{\partial y}\right|_{y=0}, \tag{4.14}$$

Substituting equation (14) into (13), we obtain,

$$\mathrm{Re}_x^{1/2}C_f=\frac{1}{(1-\varphi)^{2.5}}f''(0),\quad \mathrm{Re}_x^{-1/2}Nu=-\frac{k_{nf}}{k_f}\theta'(0). \tag{4.15}$$

The above set of equations (4.8)–(4.9) subject to the boundary conditions (4.10)-(4.11) were solved numerically by the Runge-Kutta-Fehlberg method with shooting technique [157]. Both velocity and temperature profiles were obtained and utilized to compute the skin-friction coefficient and the local Nusselt number in equation (4.15).

4.3 Results and Discussion

Numerical evaluation of the model equations is performed for three types of water based Newtonian and electrically conducting nanofluids containing metallic or nonmetallic nanoparticles such as copper (Cu), Alumina (Al_2O_3) and Titania (TiO_2). The solid volume fraction φ of the nanoparticles is investigated in the range of $0 \leq \varphi \leq 0.2$ and the Prandtl number of the based fluid (water) is kept constant at 6.2. The thermophysical properties of water and the nanoparticles Cu, Al_2O_3 and TiO_2 are shown in the Table 4.1 below,

Table 4.1: Thermophysical Properties of Water and Nanoparticles [120, 121, 135, 152]

Materials	$\rho(kg/m^3)$	c_p (J/kgK)	k (W/mK)	σ (S/m)
Pure water	997.1	4179	0.613	$5.5x10^{-6}$
Copper (Cu)	8933	385	401	$59.6x10^{6}$
Alumina (Al_2O_3)	3970	765	40	$35x10^{6}$
Titania (TiO_2)	4250	686.2	8.9538	$2.6x10^{6}$

In order to validate the accuracy of our numerical procedure, the special case of infinite Biot number in the absence of viscous dissipation and magnetic field effects is considered as shown in table (4.2), our results agreed perfectly with the one reported by Ahmad et al. [154].

Table 4.2:Computations of C_f showing the comparison with [154] results for *Ha=0, Br=0, Bi* = ∞.

φ	Cu-water [10]	Al_2O_3–water [10]	TiO_2 –water [10]	Cu –water (Present)	Al_2O_3–water (Present)	TiO_2 –water (Present)
0	0.3321	0.3321	0.3321	0.3321	0.3321	0.3321
0.002	0.3355	0.3339	0.3340	0.3355	0.3339	0.3340
0.004	0.3390	0.3357	0.3359	0.3390	0.3357	0.3359
0.008	0.3459	0.3394	0.3398	0.3459	0.3394	0.3398
0.01	0.3494	0.3412	0.3417	0.3494	0.3412	0.3417
0.012	0.3528	0.3431	0.3436	0.3528	0.3431	0.3436
0.014	0.3563	0.3449	0.3456	0.3563	0.3449	0.3456
0.016	0.3597	0.3468	0.3476	0.3597	0.3468	0.3476
0.018	0.3632	0.3487	0.3495	0.3632	0.3487	0.3495
0.02	0.3667	0.3506	0.3515	0.3667	0.3506	0.3515
0.1	0.5076	0.4316	0.4362	0.5076	0.4316	0.4362
0.2	0.7066	0.5545	0.5642	0.7066	0.5545	0.5642

4.3.1 Effects of parameters variation on the velocity profiles

The nanofluids velocity profiles are shown in Figures 4.2-4.4. Generally, the flow over a stationary convectively heated plate surface are driven by the combined action of magnetic field, Newtonian heating and free stream velocity. The nanofluid's velocity is zero at the plate surface and increases gradually until it attains the free stream value far away from the plate, satisfying the prescribed boundary conditions. It is interesting to note that of TiO_2-water nanofluid produced a thicker momentum boundary layer thickness than Al_2O_3–water and Cu-water nanofluids under the influence of magnetic field as illustrated in Figure 4.2. In Figure 4.3, it is observed that the momentum boundary layer thickness decreases with increasing magnetic field intensity. The application of a magnetic field normal to the flow direction has the tendency to slow down the movement of the nanofluids because it gives rise to a resistive force called the Lorentz force which acts opposite to the flow direction. Similar trend is observed in Figure 4.4 with increasing nanoparticles volume fraction. As the φ increases, the momentum boundary layer thickness decreases.

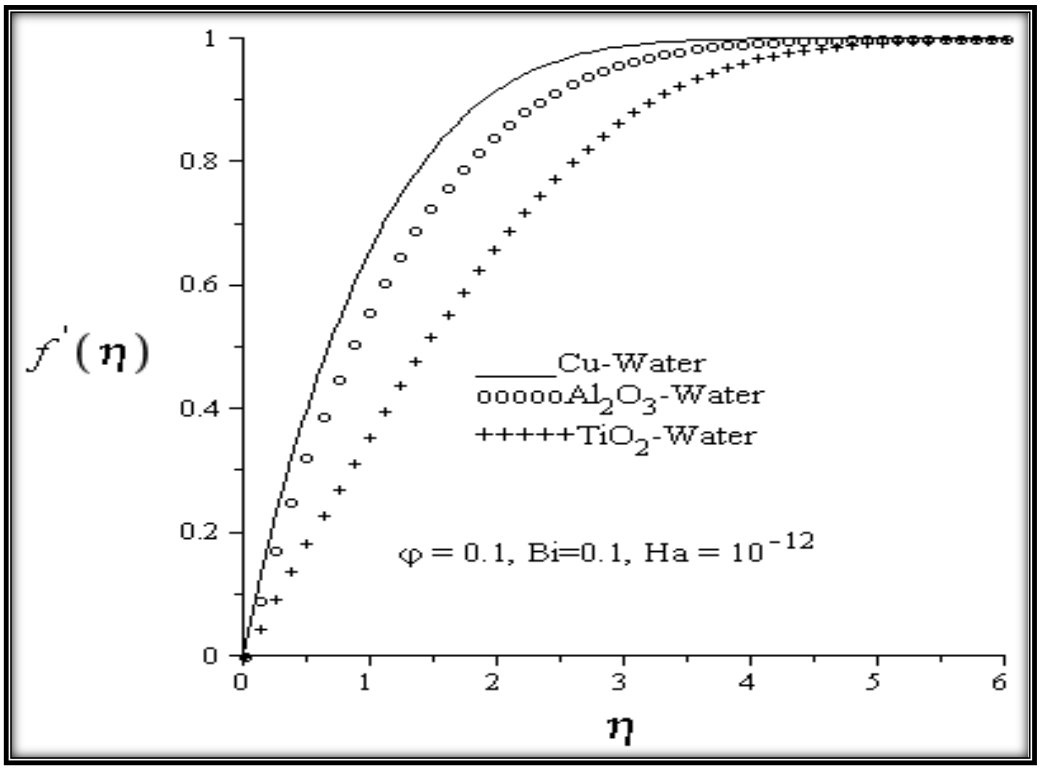

Figure 4.2: Velocity profiles for different nanofluids

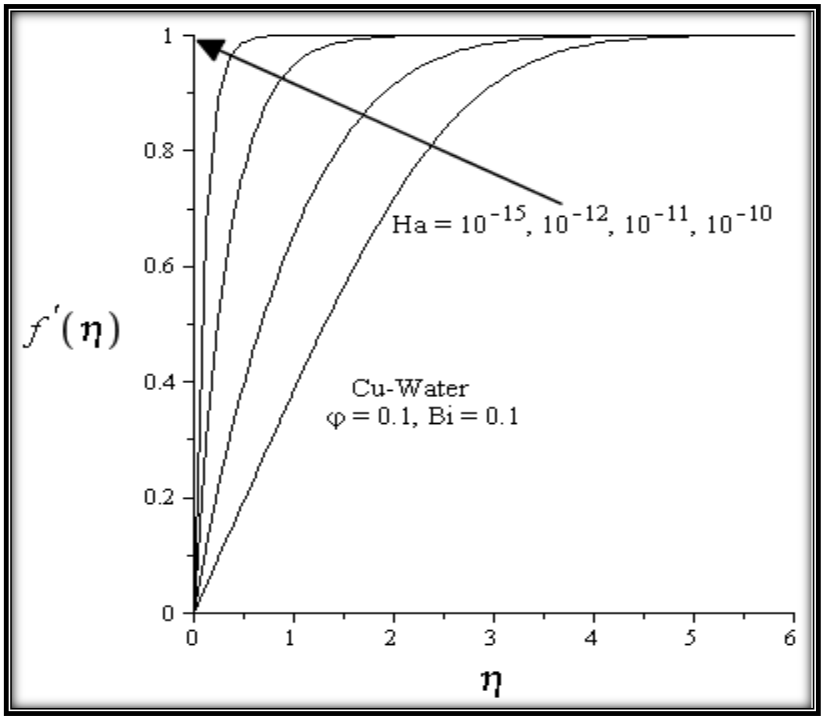

Figure 4.3: Velocity profiles with increasing magnetic field intensity.

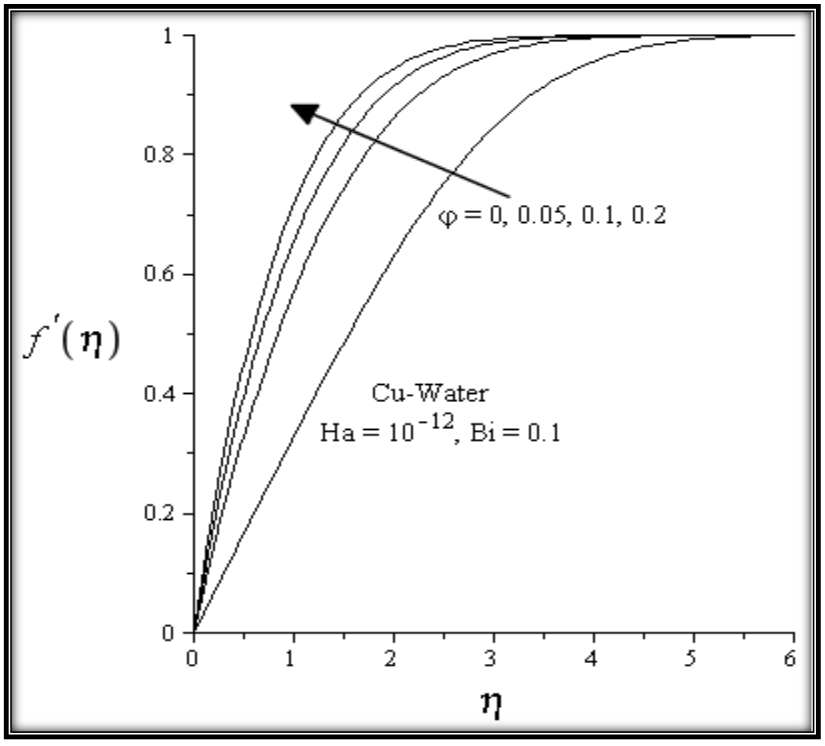

Figure 4.4: Velocity profiles with increasing nanoparticles volume fraction

4.3.2 Effects of parameters variation on the temperature profiles

Effects of various thermophysical parameters on the nanofluid's temperature profiles are displayed in Figures 4.5-4.9. The temperature is highest at the plate surface due to Newtonian heating and decreases to zero far away from the plate satisfying the free stream conditions. It is notde that the plate surface temperature is highest with Cu-water nanofluid followed by Al_2O_3-water nanofluid while TiO_2-water nanofluid produced the lowest plate surface temperature as shown in Figure 4.5. Meanwhile, the thermal boundary layer thickness increases with an increase in the magnetic field intensity as illustrated in Figure 4.6, consequently, the plate surface temperature increases as well. This can be attributed to the influence of Ohmic heating due to magnet field in the flow system. Figure 4.7 depicts the effect of increasing the nanoparticles solid fraction for Cu-water on the temperature profiles. As expected, the thermal boundary layer thickness increases with increasing values of nanoparticle volume fraction (φ), leading to an increase in the plate surface temperature and thermal boundary layer thickness. Moreover, as the values of Biot number (*Bi*) increase, the rate of convective heat transfer from the hot conventional fluid below the plate surface to the nanofluid above the plate surface increases, leading to an increase in the thermal boundary layer thickness and the plate surface temperature as shown in Figure 4.8. Similar trend is observed with increasing values of Brinkmann number (*Br*) as shown in Figure 4.9. This can be attributed to the additional heating in the flow system due to viscous dissipation.

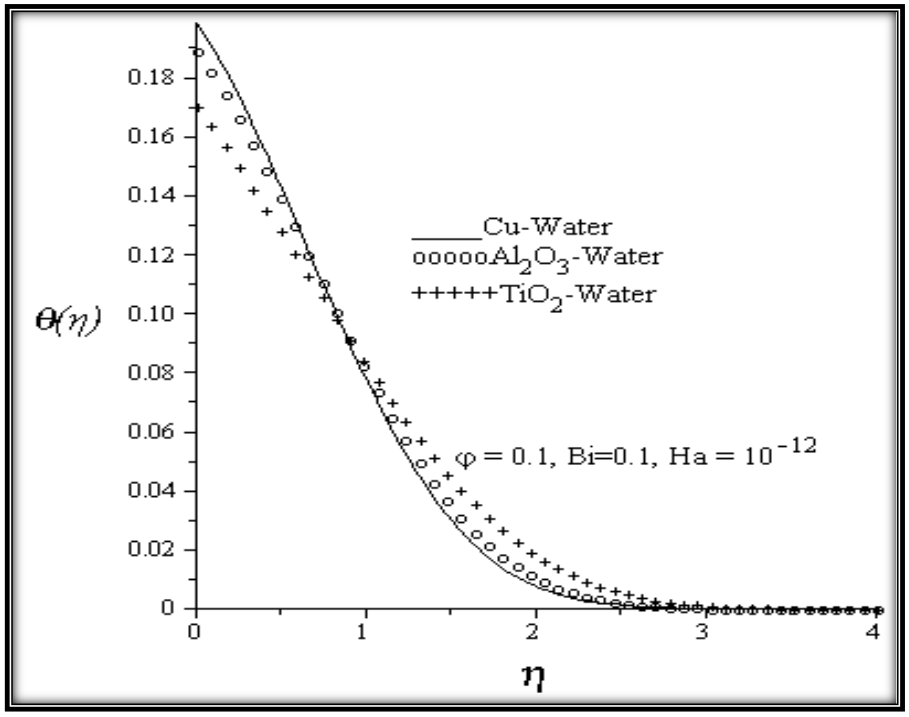

Figure 4.5: Temperature profiles for different nanofluids

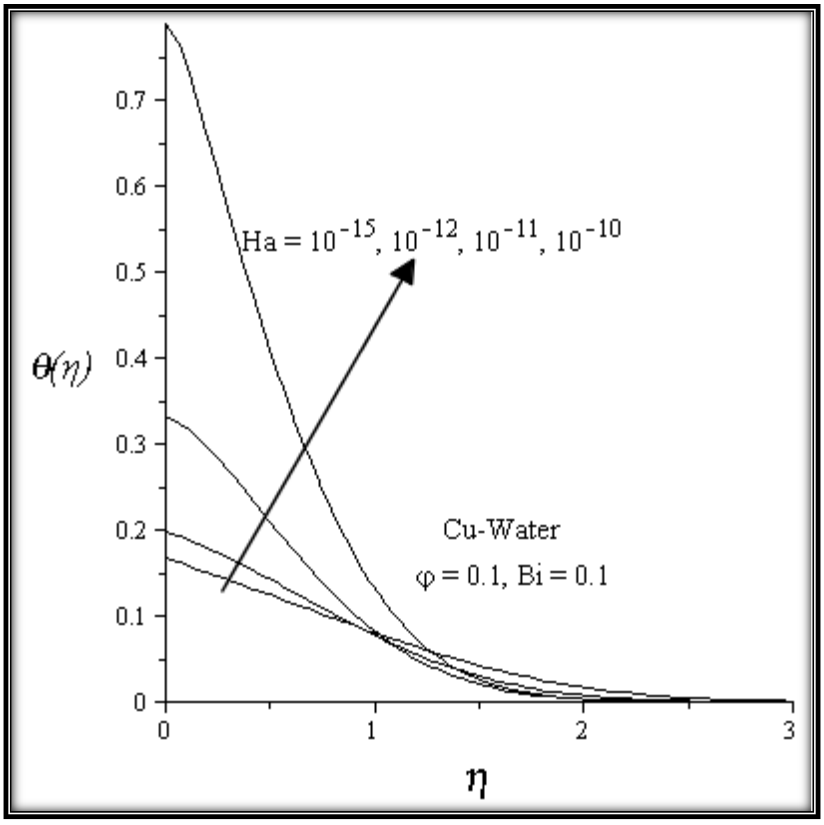

Figure 4.6: Temperature profiles with increasing magnetic field intensity.

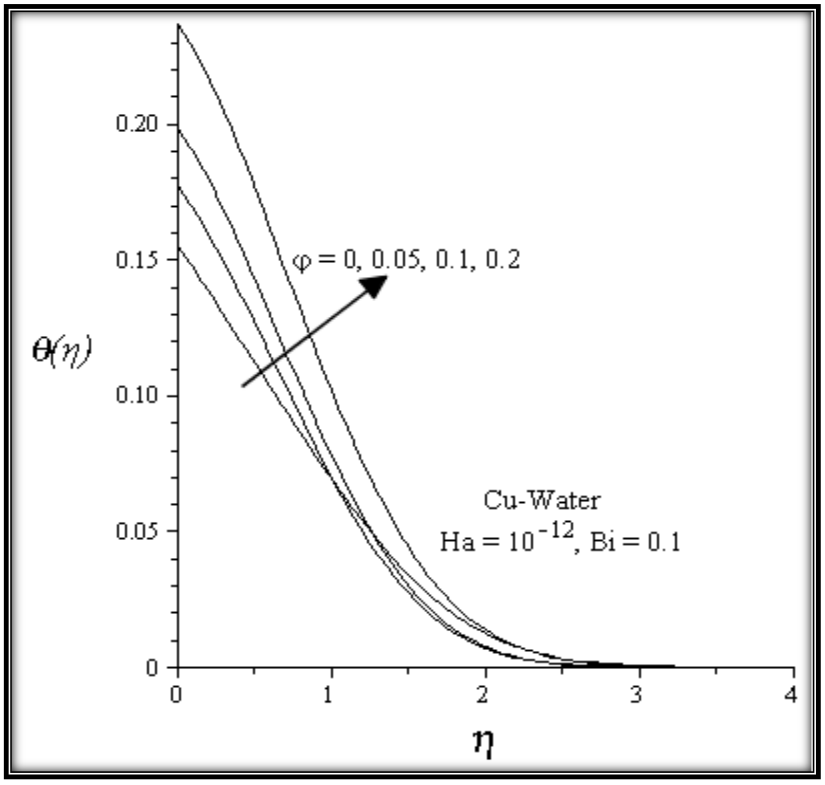

Figure 4.7: Temperature profiles with increasing nanoparticles volume fraction

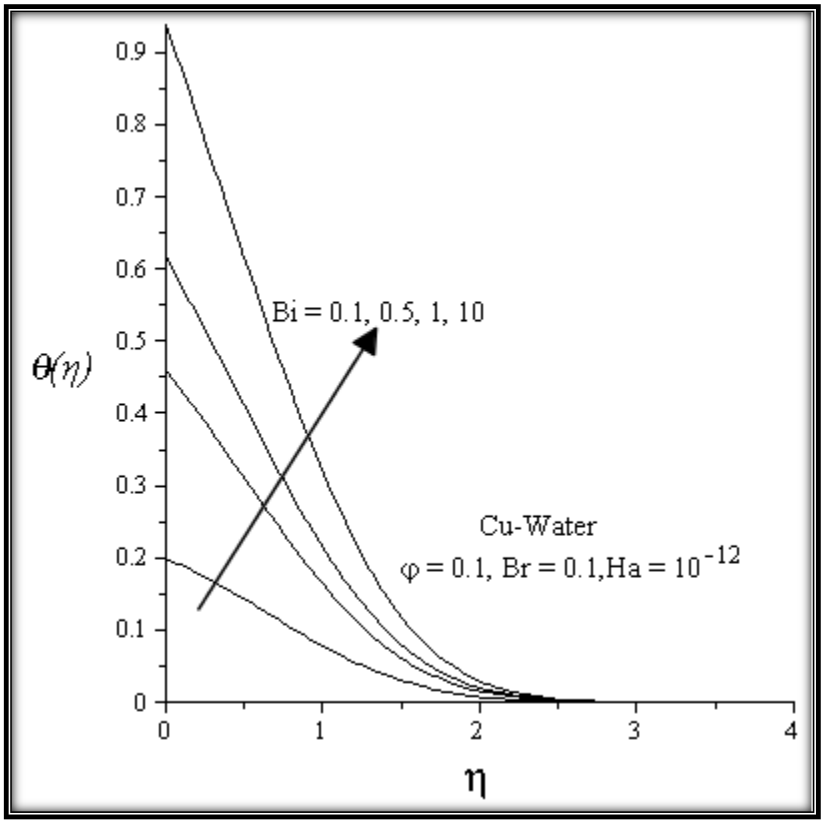

Figure 4.8: Temperature profiles with increasing Biot number

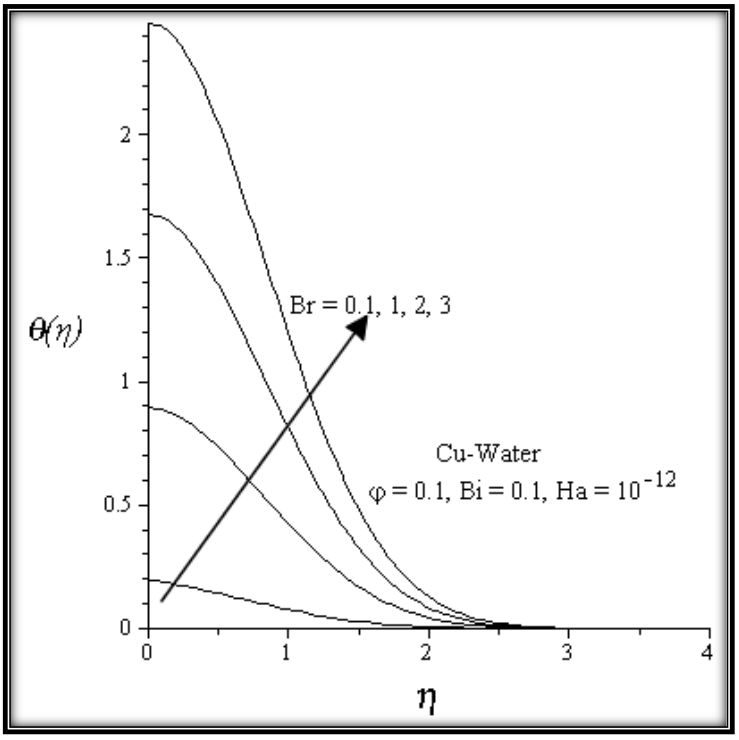

Figure 4.9: Temperature profiles with increasing Brinkmann number

4.3.3 Effects of parameters variation on the skin friction and Nusselt number

Figures 4.10 – 4.14 illustrate the effects of parameter variation on the skin friction and the Nusselt number. As seen in figure 4.10, the skin friction grows with an increase in the nanoparticle volume fraction. Cu-Water nanofluid shows faster growth than Al_2O_3-water while TiO_2-water nanofluid produced the lowest skin friction. Moreover, an increase in the magnetic field intensity (*Ha*), leads to a further increase in the skin friction as shown in Figure 4.11 with Cu-Water as the working nanofluid. In Figure 4.12, it is observed that the Nusselt number increases with an increase in the nanoparticle volume fraction, with Cu-water showing a plate surface higher heat transfer rate than Al_2O_3-water while TiO_2-water nanofluid produced the lowest heat transfer rate at the plate surface. An increase in magnetic field intensity decreases the heat transfer rate at the plate surface as shown in Figure 4.13. As Biot number (*Bi*) increases, the heat transfer rate at the plate surface increases (see Figure 4.14). Meanwhile, an increase in Brinkmann number (*Br*) due to viscous heating decreases the heat transfer rate at the plate surface.

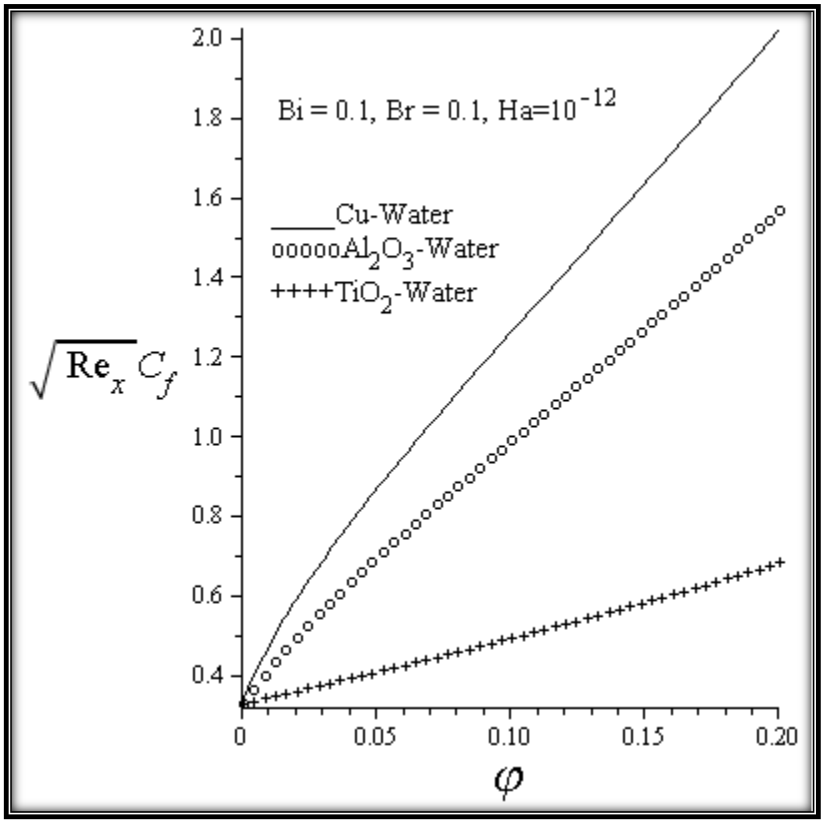

Figure 4.10: Skin friction profiles for different nanofluids

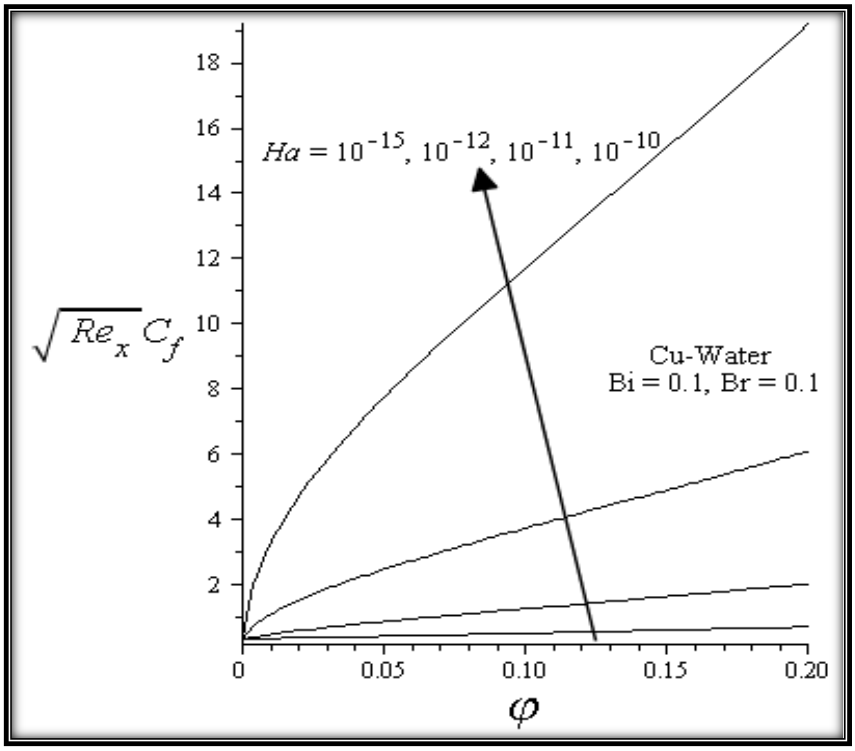

Figure 4.11: Skin friction with increasing magnetic field intensity

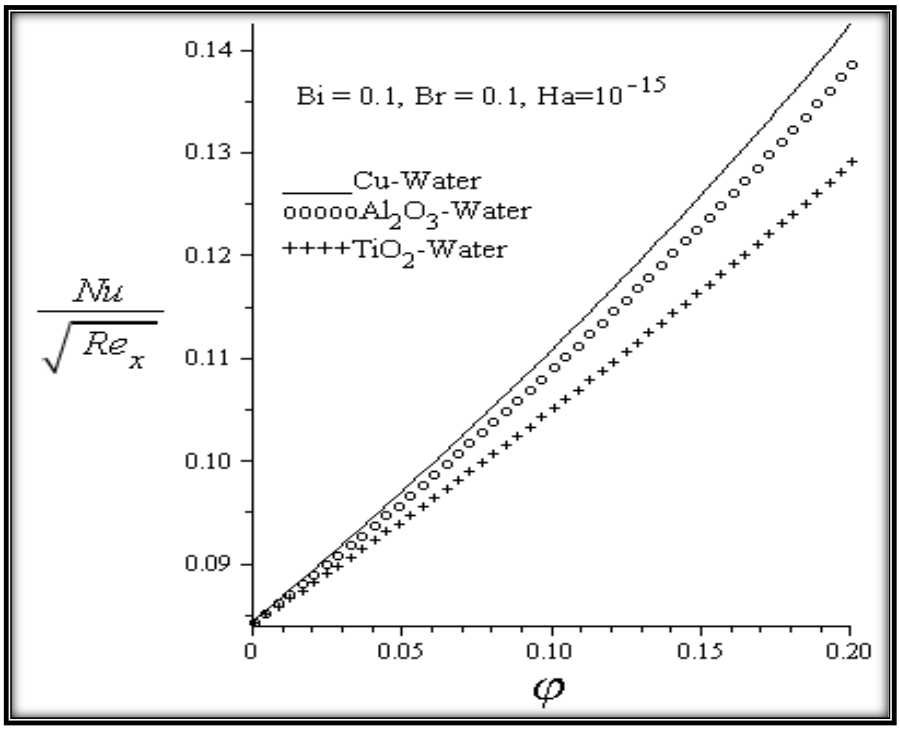

Figure 4.12: Reduced Nusselt number for different nanofluids

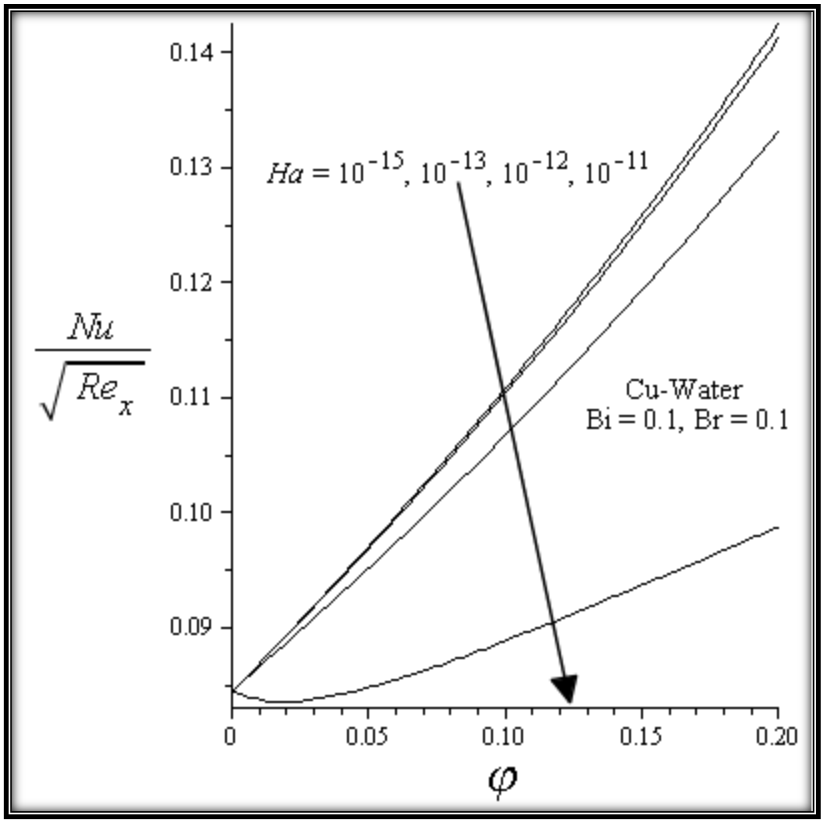

Figure 4.13: Nusselt number with increasing magnetic field intensity

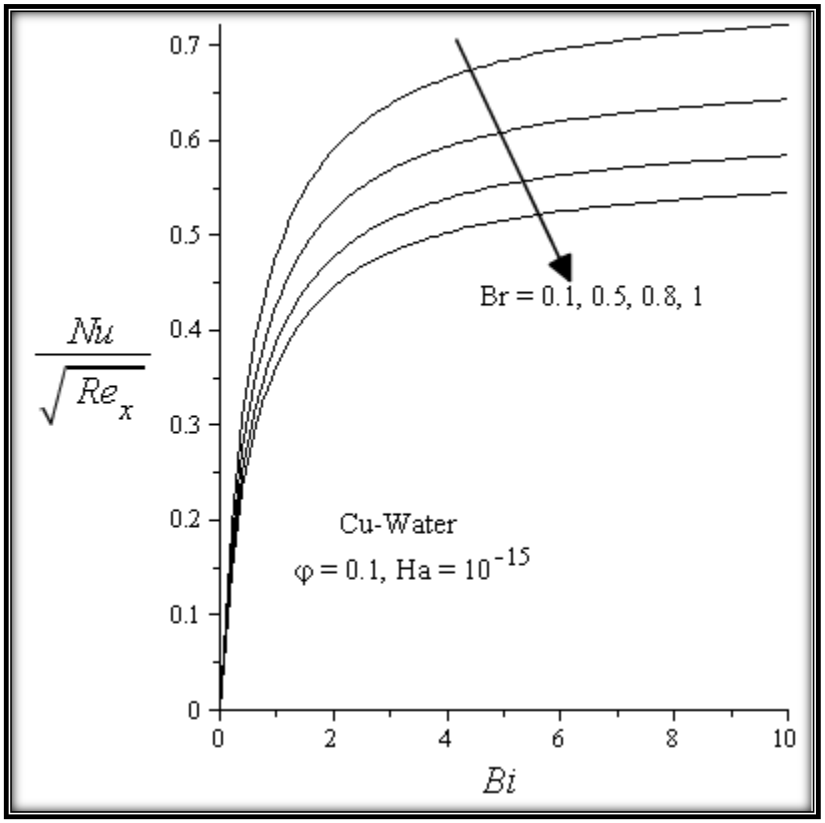

Figure 4.14: Nusselt number with increasing Biot number and Brinkmann number

4.4 Conclusions

The combined effects of magnetic field, viscous dissipation and Ohmic heating on the thermal boundary layer of water-based nanofluids containing Cu, Al_2O_3 and TiO_2 as nanoparticles are investigated theoretically, taking into consideration the complex interaction between the electrical conductivity of the base fluid and that of the nanoparticles. The governing nonlinear partial differential equations were transformed into ordinary differential equations using the similarity approach and solved numerically using the Runge–Kutta–Fehlberg method coupled with the shooting technique. Generally, our results revealed that the susceptibility of nanofluids to the influence of magnetic field is extremely high compared to conventional base fluid due to the complex interaction of electrical conductivity of nanoparticles with that of base fluid. Some other results are as follows;

TiO_2 – water shows a thicker momentum boundary layer than Al_2O_3 –water while Cu-water momentum boundary layer is the thinnest. As *Ha* and φ increase, the momentum boundary layer thickness decreases.

TiO_2 – water produced highest plate surface temperature followed by Al_2O_3 –water while Cu-water produced the lowest surface temperatutre. As Ha, φ, Bi, Br increase, the thermal boundary layer thickness increases.

Cu-water produced the highest skin friction followed by Al_2O_3 –water while TiO_2 – water produced lowest skin friction. As φ and Ha increase, the skin friction increases.

Cu-water produced the highest Nusselt number followed by Al_2O_3 –water while TiO_2 – water produced lowest Nusselt number. The heat transfer rate at the plate surface decreases with increasing Brinknann number values (*Br*) and magnetic field intensity (*Ha*), whereas it increases with increasing values of Biot number (*Bi*) and nanoparticle volume fraction(φ).

CHAPTER FIVE

MHD NANOFLUID FLOW OVER A PERMEABLE VERTICAL PLATE WITH CONVECTIVE HEATING[3]

5.0 Abstract

A numerical analysis is performed on buoyancy and magnetic effects on a steady two-dimensional boundary layer flow of an electrically conducting water-based nanofluid containing three different types of nanoparticles: copper (Cu), aluminium oxide (Al_2O_3), and titanium dioxide (TiO_2) past a convectively heated porous vertical plate with variable suction. A similarity transformation was used to convert the governing partial differential equations to a system of nonlinear ordinary differential equations. A numerical shooting technique with a fourth-order Runge-Kutta-Fehlberg integration scheme was used to solve the boundary value problem. The effects of the type of nanoparticle, solid volume fraction φ, Hartmann number Ha, Grashof number Gr, Eckert number Ec, suction/injection parameter F_w, and Biot number Bi on the flow field, temperature, skin friction coefficient and heat transfer rate are presented graphically and then discussed quantitatively.

5.1 Introduction

The concept of natural convection has many applications in physics, chemistry and engineering such as cooling systems for electronic devices [158], furnace engineering [159], solar energy collectors [160], phase change material and building energy systems [161], non-Newtonian chemical processes [162, 163], electromagnetic fields applications [164] among others. In all these systems, heat transfer enhancement is of a major contemporary interest from an energy saving perspective. An innovative technique to improve heat transfer is the use of nanofluids, a term coined by Choi [1] referring to a liquid containing a suspension of submicronic solid particles (nanoparticles). The characteristic feature of

---

[3] *This chapter consists of a journal article:* Mutuku-Njane, W.N.; Makinde, O. D., MHD Nanofluids Flow over a Permeable Vertical Plate with Convective heating, Journal of Computational and Theoratical Nanoscience, Volume 11, No. 3, 667-675, 2014.

nanofluids is enhancement of the thermophysical properties of the base fluid used. Usage of nanofluids present a unique approach for ensuring a more effective heat removal in any thermal-fluid system. The combination of nanofluids with biotechnological components, have a wide range of practical applications such as agriculture, pharmaceuticals and biological sensors [165]. The industrial applications of nanofluids include electronic cooling, automotive and nuclear applications. Nanobiotechnology is rapidly been adapted in many domains such as medicine, pharmacy and agro-industry [166].

MHD flow past a flat surface is of a special technical significance because of its frequent occurrence in many technological and industrial applications such as MHD pumps, micro-mixing of physiological samples, biological transportation and drug delivery [167, 168]. The flow and heat transfer in any electrically conducting fluid flow system may be controlled by the application of an external magnetic field. The presence of the nanoparticles enhance the electrical conductivity property of nanofluids, hence making them more susceptible to the influence of the magnetic field as compared to the conventional base fluids. Studies on MHD free convective boundary-layer flow of nanofluids [144, 169-174], autonomously pointed out that, magnetic nanofluids have many industrial, engineering and biomedical applications such as magnetofluidic leakage free seals, magnetogravimetric separations, aerodynamic sensors, smartfluids for vibration damping, MHD blood flow meters, magnetic drug targeting, nanodrug delivery, and nanocryosurgery. The natural convective flow of a nanofluid past a vertical plate under different boundary condition has been investigated by several researchers [147, 153,166, 175]. Recently, Motsumi and Makinde [156] investigated the effects of thermal radiation and viscous dissipation on a boundary layer flow of nanofluids over a moving flat plate with varying permeability.

In this present study, we extend the work of Motsumi and Makinde [156] to include the combined effects of buoyancy force and magnetic field, taking into account the complex interaction of the electric conductivities of the nanoparticles (Cu, Al_2O_3, and TiO_2) and the base fluid (water). In the following sections, the model problem is formulated, analysed and solved numerically. Pertinent results are displayed graphically and discussed quantitatively.

5.2 Model Formulation

We consider a steady, incompressible, laminar, two-dimensional (x, y) boundary layer flow of an electrically conducting water-based nanofluid past a vertical semi-infinite flat plate under the influence of a transversely imposed magnetic field as illustrated in Figure 5.1. The nanofluids contain three different types of nanoparticles: Cu, Al_2O_3, and TiO_2. It is assumed that the left side of the plate is heated by convection from a hot fluid at temperature T_f with a heat transfer coefficient h_f. A transverse magnetic field with variable strength B_0 is applied

parallel to the y- axis. There is no applied voltage and the magnetic Reynolds number is small, hence the induced magnetic field and Hall effects are negligible.

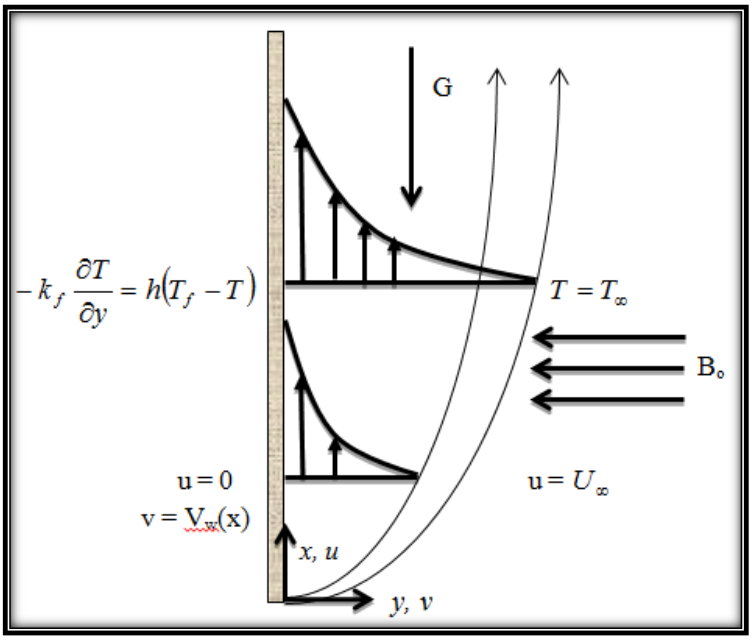

Figure 5.1. Problem geometry

Considering the nanofluid as a continuous media with thermal equilibrium and no slip occurring between the base fluid and the solid nanoparticles, the governing equations of continuity, momentum and energy balance with Boussinesq approximation for buoyancy term are given as;

$$\frac{\partial u}{\partial x} + \frac{\partial v}{\partial y} = 0, \tag{5.1}$$

$$u\frac{\partial u}{\partial x} + v\frac{\partial u}{\partial y} = \frac{\mu_{nf}}{\rho_{nf}}\frac{\partial^2 u}{\partial y^2} + \beta_{nf} g(T - T_\infty) - \frac{\sigma_{nf} B_0^2 (u - U_\infty)}{\rho_{nf}}, \tag{5.2}$$

$$u\frac{\partial T}{\partial x} + v\frac{\partial T}{\partial y} = \frac{k_{nf}}{(\rho c_p)_{nf}}\frac{\partial^2 T}{\partial y^2} + \frac{\mu_{nf}}{(\rho c_p)_{nf}}\left(\frac{\partial u}{\partial y}\right)^2 + \frac{\sigma_{nf} B_0^2}{(\rho c_p)_{nf}}(u - U_\infty)^2, \tag{5.3}$$

subject to the boundary conditions;

$$\begin{aligned} &u(x,0) = 0, \quad v(x,0) = V_w(x), \quad -k_f \frac{\partial T}{\partial y}(x,0) = h_f[T_f - T(x,0)] \\ &u(x,\infty) = U_\infty, \quad T(x,\infty) = T_\infty, \end{aligned} \tag{5.4}$$

where (x, y) are the Cartesian coordinates along the plate and normal to it, (u, v) are the velocity components of the nanofluid in the x- and y-directions respectively, T is the nanofluid temperature, T_∞ is the free stream temperature, μ_{nf} is the nanofluid dynamic viscosity, ρ_{nf} is the nanofluid density, k_{nf} is the nanofluid thermal conductivity, σ_{nf} is the nanofluid electrical conductivity, $(\rho c_p)_{nf}$ is the nanofluid heat capacity at constant pressure and β_{nf} is the nanofluid thermal expansion coefficient. Following [147], the relationship between the thermophysical properties of nanofluid and its conventional base fluid together with nanoparticles are given as;

$$\begin{aligned}
&\mu_{nf} = \frac{\mu_f}{(1-\varphi)^{2.5}}, \quad \rho_{nf} = (1-\varphi)\rho_f + \varphi\rho_s, \beta_{\mathrm{nf}} = (1-\varphi)\beta_f + \varphi\beta_s \\
&\alpha_{nf} = \frac{k_{nf}}{(\rho c_p)_{nf}}, \frac{k_{nf}}{k_f} = \frac{(k_s + 2k_f) - 2\varphi(k_f - k_s)}{(k_s + 2k_f) + \varphi(k_f - k_s)}, \\
&(\rho c_p)_{nf} = (1-\varphi)(\rho c_p)_f + \varphi(\rho c_p)_s, \sigma_{nf} = (1-\varphi)\sigma_f + \varphi\sigma_s,
\end{aligned} \tag{5.5}$$

where φ is the solid volume fraction of the nanoparticle (φ = 0 correspond to a regular fluid), ρ_f and ρ_s are the densities of the base fluid and the nanoparticle respectively, β_f and β_s are the thermal expansion coefficients of the base fluid and the nanoparticle respectively, k_f and k_s are the thermal conductivities of the base fluid and the nanoparticles respectively, $(\rho c_p)_f$ and $(\rho c_p)_s$ are the heat capacitance of the base fluid and the nanoparticle respectively, σ_s and σ_f are the electrical conductivities of the base fluid and the nanofluid respectively.

Table 5.1: Thermophysical Properties of Water and Nanoparticles [20, 120-1, 152, 166]

Materials	ρ(kg/m^3)	c_p (J/kgK)	k (W/mK)	σ (S/m)
Pure water	997.1	4179	0.613	5.5x10^{-6}
Copper (Cu)	8933	385	401	59.6x10^6
Alumina (Al_2O_3)	3970	765	40	35x10^6
Titania (TiO_2)	4250	686.2	8.9538	2.6x10^6

We introduce the stream function ψ, defined as

$$u = \frac{\partial \psi}{\partial y} \text{ and } v = -\frac{\partial \psi}{\partial x}. \tag{5.6}$$

and the non-dimensional variables:

$$\begin{aligned}
&\eta = y\sqrt{\frac{U_\infty}{\upsilon_f x}} = \frac{y}{x}\sqrt{\mathrm{Re}_x}, \quad \psi = \sqrt{\upsilon_f x U_\infty}\, f(\eta), \; u = U_\infty f'(\eta), \\
&v = \frac{1}{2}\sqrt{\frac{U_\infty \upsilon_f}{x}}(\eta f' - f), \quad \theta = \frac{T - T_\infty}{T_f - T_\infty},
\end{aligned} \tag{5.7}$$

into Eqs. (5.1)–(5.4) to reduce the number of equations and number of dependent variables. This gives the following ordinary differential equations,

$$\begin{aligned} & f'''+\frac{1}{2}(1-\phi)^{2.5}(1-\phi+\phi\rho_s/\rho_f)\,ff'' \\ & +\mathrm{Gr}(1-\phi)^{2.5}(1-\phi+\phi\rho_s/\rho_f)(1-\phi+\phi\beta_s/\beta_f)\theta \\ & -Ha(1-\phi)^{2.5}(1-\phi+\phi\sigma_s/\sigma_f)(f'-1)=0, \end{aligned} \tag{5.8}$$

$$\begin{aligned} & \theta''+\frac{k_f\,\mathrm{Pr}[1-\varphi+\varphi(\rho c_p)_s/(\rho c_p)_f]}{2k_{nf}}\,f\theta' \\ & +\frac{k_f\,\mathrm{Pr}\,Ec}{k_{nf}(1-\varphi)^{2.5}}(f'')^2+\frac{Ha\,\mathrm{Pr}\,Eck_f}{k_{nf}}(1-\varphi+\varphi\sigma_s/\sigma_f)(f'-1)^2=0, \end{aligned} \tag{5.9}$$

Taking into account the variable plate surface permeability function given by;

$$V_w(x)=-\frac{f_w}{2}\sqrt{\frac{U_\infty\upsilon_f}{x}} \tag{5.10}$$

the boundary conditions are;

$$\begin{aligned} & f(0)=f_w,\quad f'(0)=0,\quad \theta'(0)=Bi[\theta(0)-1], \\ & f'(\infty)=1,\quad \theta'(0)=0, \end{aligned} \tag{5.11}$$

where a prime symbol denotes differentiation with respect to η, and f_w is a constant with $f_w>0$ representing suction rate at the plate surface, $f_w<0$ corresponds to injection and $f_w=0$ shows an impermeable surface, the Biot number *Bi*, Hartmann number *Ha*, Eckert number *Ec*, Grashof number *Gr*, Prandtl number *Pr*, and local Reynolds number Re_x are defined as;

$$\begin{aligned} & Bi=\frac{h_f}{k_f}\sqrt{\frac{\upsilon_f x}{U_\infty}},\quad \mathrm{Ec}=\frac{U_\infty^{\,2}}{C_{p_f}(T_f-T_\infty)},\ Ha=\frac{\sigma_f B_o^{\,2}x}{\rho_f U_\infty}, \\ & Gr=\frac{\beta_f g(T_f-T_\infty)x}{U_\infty^{\,2}},\ \mathrm{Pr}=\frac{\upsilon_f}{\alpha_f},\ \mathrm{Re}_x=\frac{U_\infty x}{\upsilon_f}. \end{aligned} \tag{5.12}$$

The local Biot number *Bi*, the Hartmann number *Ha* and the Grashof number Gr in Eq. (5.12) are functions of *x* but it is well known that to have a similarity solution, all the parameters must be constant, hence according to [153], we assume

$$h_f = ax^{-\frac{1}{2}},\ \sigma_f = bx^{-1}, \beta_f = cx^{-1}, \tag{5.13}$$

where *a, b* and *c* are constants. We also consider the skin friction coefficient C_f and the local Nusselt number *Nu*, which are defined as;

$$C_f = \frac{\tau_w}{\rho_f U_0^2},\ \ Nu = \frac{xq_w}{k_f(T_f - T_\infty)}, \tag{5.14}$$

where τ_w is the skin friction and q_w is the heat flux from the plate which are given by;

$$\tau_w = \mu_{nf}\left.\frac{\partial u}{\partial y}\right|_{y=0},\ \ q_w = -k_{nf}\left.\frac{\partial T}{\partial y}\right|_{y=0}, \tag{5.15}$$

Putting Eqs. (5.15) into (5.14), we obtain

$$\mathrm{Re}_x^{\frac{1}{2}} C_f = \frac{1}{(1-\varphi)^{2.5}} f''(0),\quad \mathrm{Re}_x^{-\frac{1}{2}} Nu = -\frac{k_{nf}}{k_f}\theta'(0). \tag{5.16}$$

The transformed equations (5.8)–(5.9) which are a highly coupled nonlinear boundary value problems with boundary conditions (5.11) are solved numerically using a shooting technique with the fourth-order Runge-Kutta-Fehlberg integration scheme [176] and the results used to evaluate the skin-friction coefficient and the local Nusselt number in Eq. (5.16). The effects of different parameters on the dimensionless flow and temperature are investigated and presented graphically. The results are obtained up to the desired degree of accuracy, namely 10^{-10}. Computations are carried out for solid volume fraction φ in the range of $0 \le \varphi \le 0.2$, magnetic field strength of $10^{-10} \le Ha \le 10^{-15}$ and the Prandtl number of the based fluid (water) is kept constant at 6.2. It is worth mentioning that this study reduces the governing Equations (5.8)-(5.9) to those of a viscous or regular fluid when $\varphi = 0$.

5.3 Results and Discussion

Three different types of nanoparticles, namely, copper (Cu), alumina (Al_2O_3), and titanium oxide (TiO_2), with water as the base fluid we considered. In the following subsections, the effects of various thermophysical parameters on the nanofluid velocity and temperature profiles as well as the skin friction and the local Nusselt number on the plate surface are highlighted.

5.3.1 Dimensionless Velocity Profiles

Figures 5.2 - 5.7 illustrate the effects of various thermophysical parameters on the nanofluids velocity profiles. Generally, it is noted that there is a gradual increase in the fluid velocity, from a zero at the plate surface to a maximum value as it approaches the free stream far away from the plate surface thus satisfying the boundary conditions. It is observed that Cu-water nanofluid produced the thinnest momentum boundary layer, followed by Al_2O_3-water nanofluid, with TiO_2-water nanofluid exhibiting the largest, as seen from figure 5.2. It is evident, from figure 5.3 that increasing the Hartmann number (*Ha*) retards the fluid velocity and decreases the hydrodynamic boundary layer thickness. This is in accordance to the physics of the problem, since the application of a transverse magnetic field results in a resistive type force (Lorentz force) similar to drag force which tends to resist the fluid flow and thus reducing its velocity. A similar trend is observed from figures 5.4 – 5.7 which depict the effects of nanoparticle volume fraction (φ), Eckert number (*Ec*), Grashof number (*Gr*), and the suction/injection parameter (f_w) on the velocity profiles.

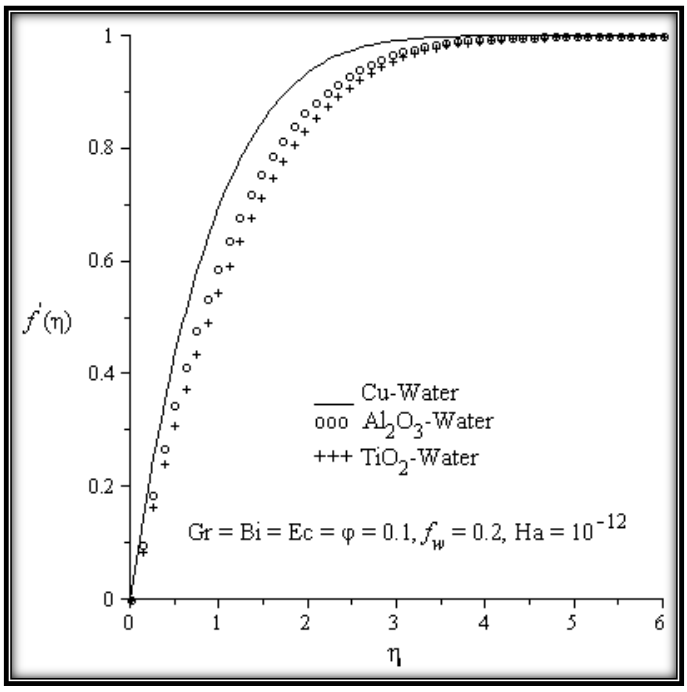

Figure 5.2: Velocity profiles for different nanofluids

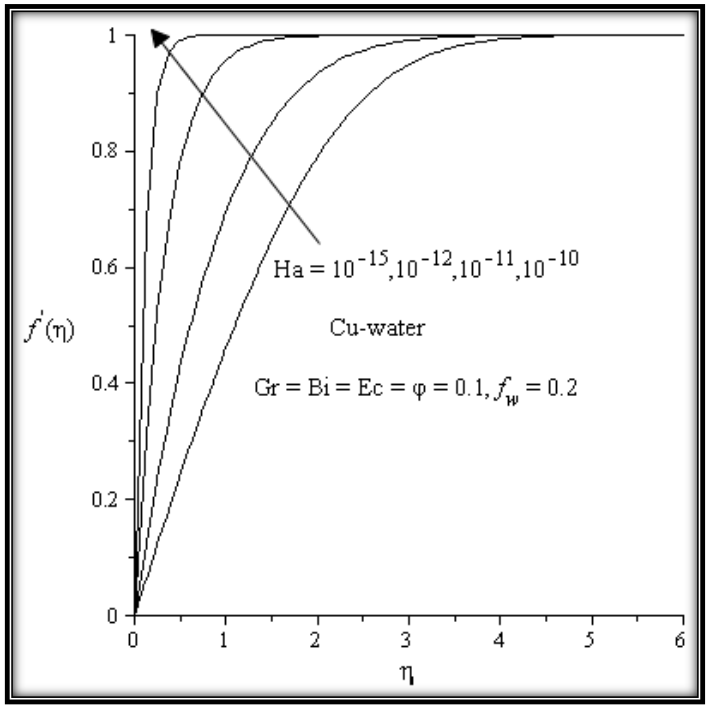

Figure 5.3: Velocity profiles with increasing magnetic field intensity.

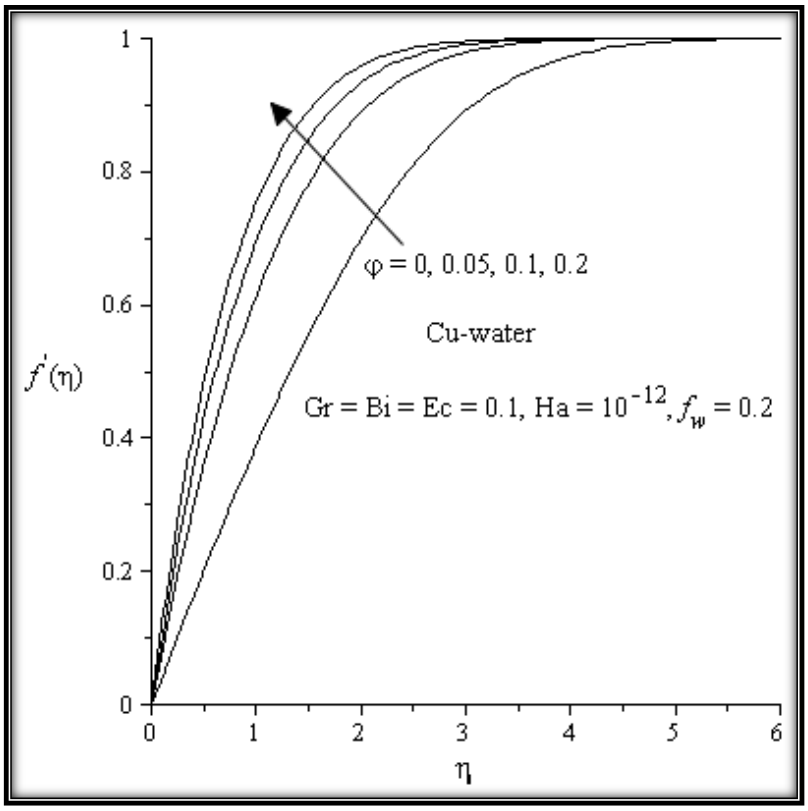

Figure 5.4: Velocity profiles with increasing nanoparticles volume fraction

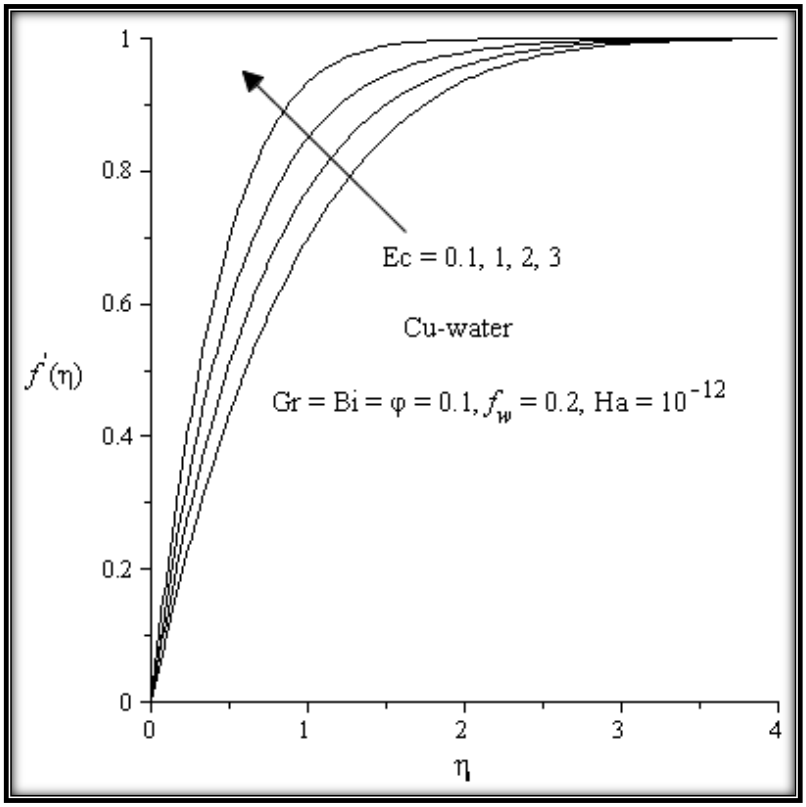

Figure 5.5: Velocity profiles with increasing Eckert number

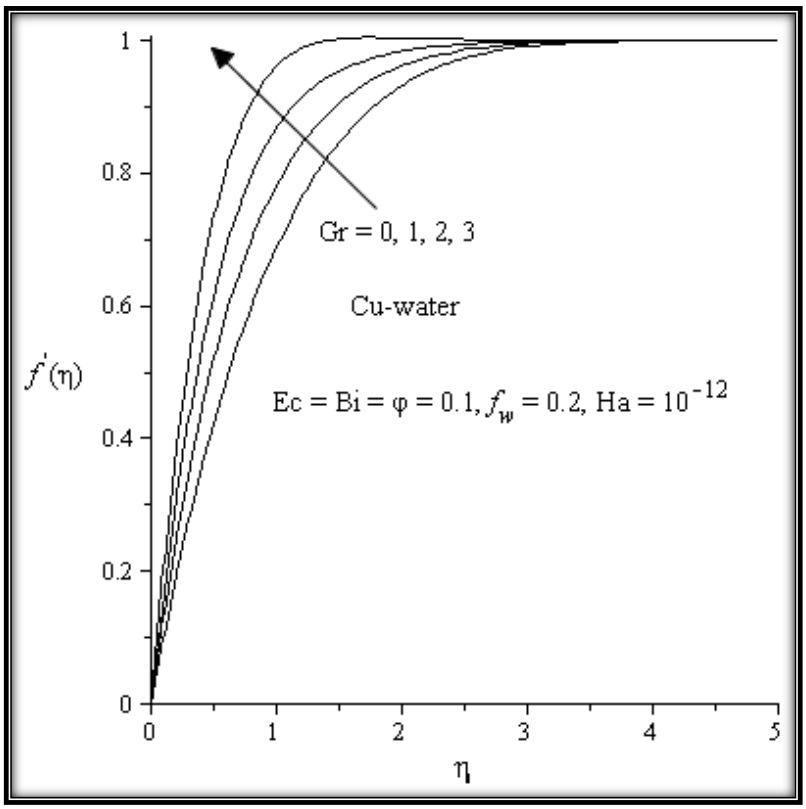

Figure 5.6: Velocity profiles with increasing Grashof number

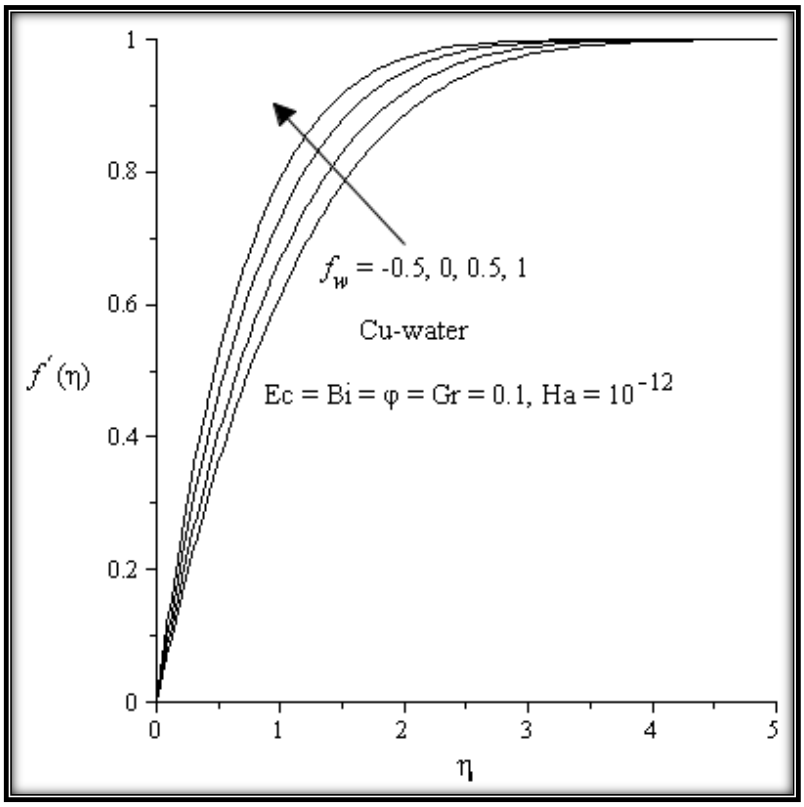

Figure 5.7: Velocity profiles with increasing Suction/Injection Parameter

5.3.2 Dimensionless Temperature Profiles

Figures 5.8 – 5.14 indicate that the temperature is maximum at the plate surface due to the convectional heating but decreases to zero far away from the plate surface satisfying the free stream conditions. It can be seen from figure 5.8, that the plate surface temperature is highest for Cu-water nanofluid followed by Al_2O_3-water nanofluid while TiO_2-water nanofluid exhibited the least temperature at the plate surface. The numerical results obtained show that an increase in the magnetic parameter (*Ha*), nanoparticle volume fraction (φ), Biot number (*Bi*), Eckert number (*Ec*), and Grashof number (*Gr*), leads to an increase in both the temperature and the thermal boundary layer thickness. This can be attributed to the additional heating due resistance of fluid flow as a result of the magnetic field, the presence of the nanoparticle, the increased rate at which the heat moves from the hot fluid to the plate and the additional heating as a result of the viscous dissipation. It is interesting to note that for high Grashof number, although the temperature at the plate surface is high, it rapidly decreases to zero far away from the plate surface compared to cases of low Grashof

number where the initial temperature is low but gradually decreases to zero at the free stream . On the other hand, an increase in the suction/injection parameter (f_w) leads to a decrease in both the temperature and the thermal boundary layer.

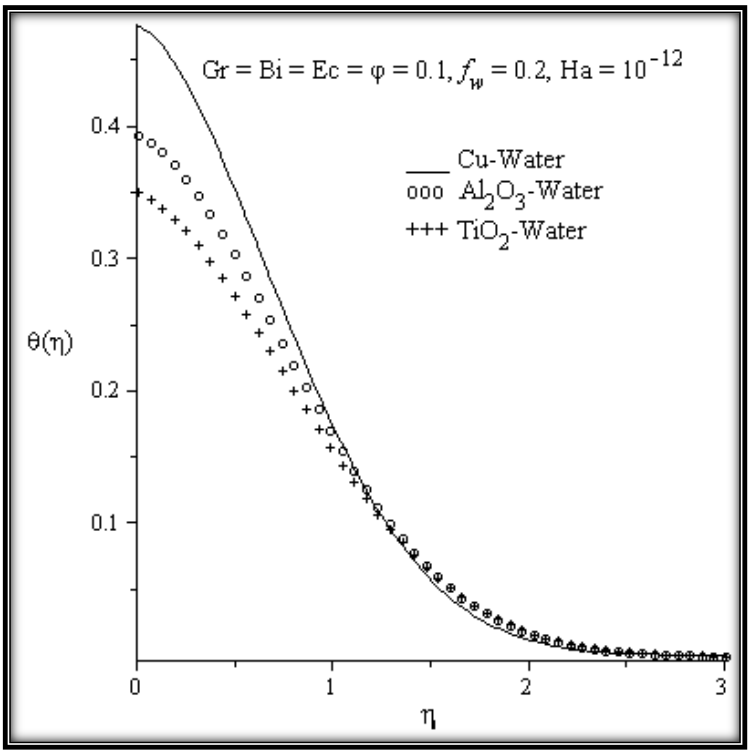

Figure 5.8: Temperature profiles for different nanofluids

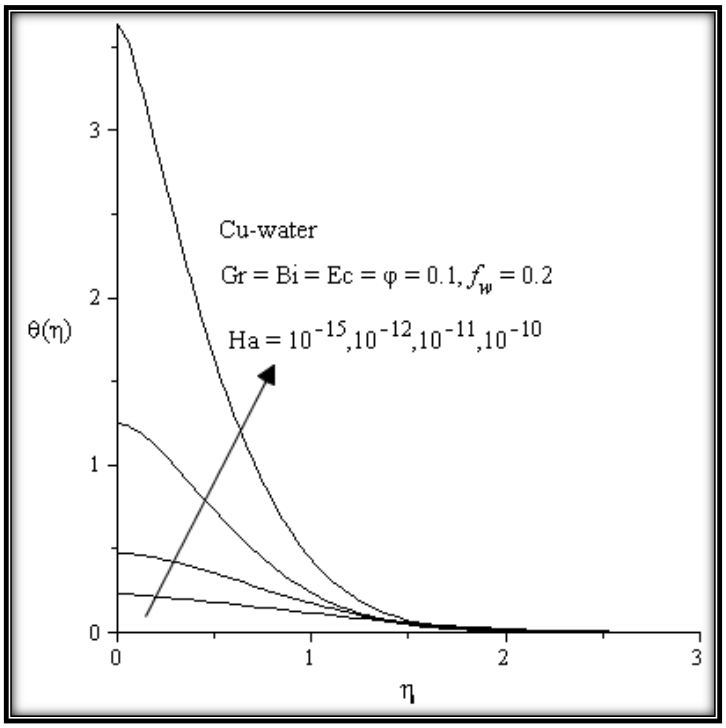

Figure 5.9: Temperature profiles with increasing magnetic field intensity

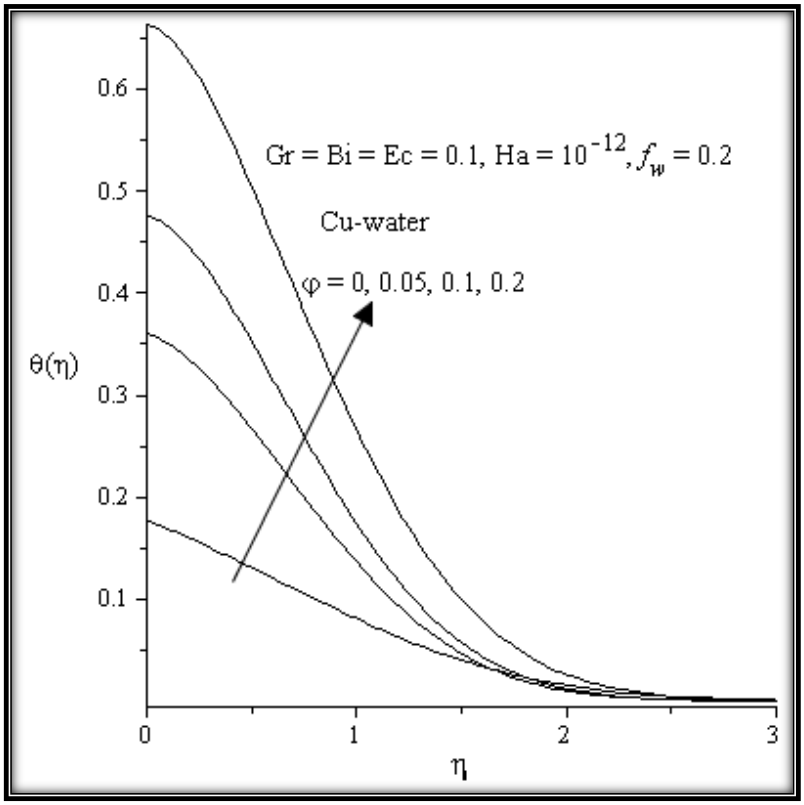

Figure 5.10: Temperature profiles with increasing nanoparticles volume fraction

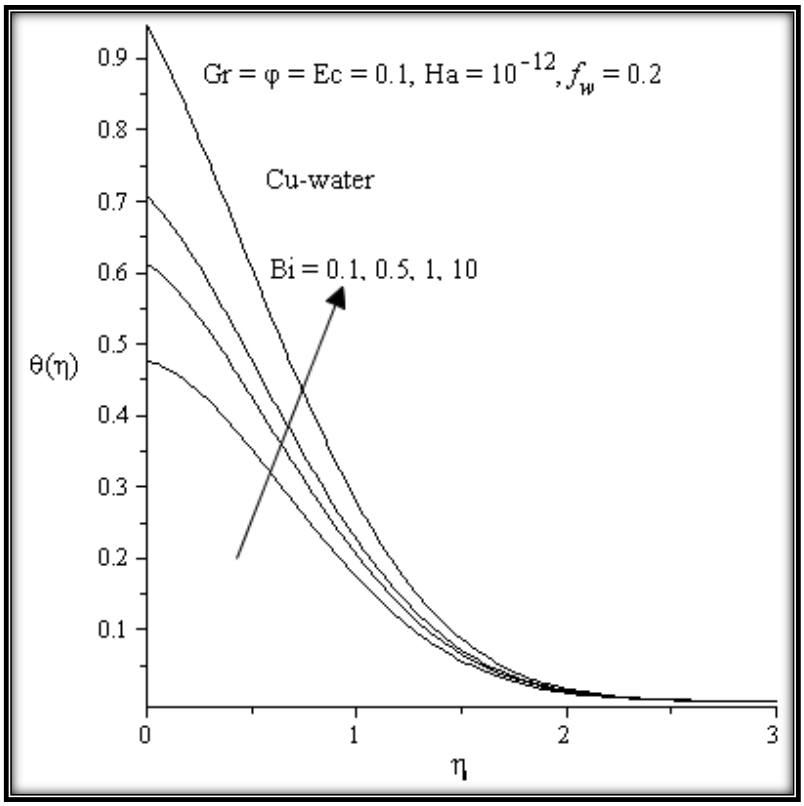

Figure 5.11: Temperature profiles with increasing Biot number

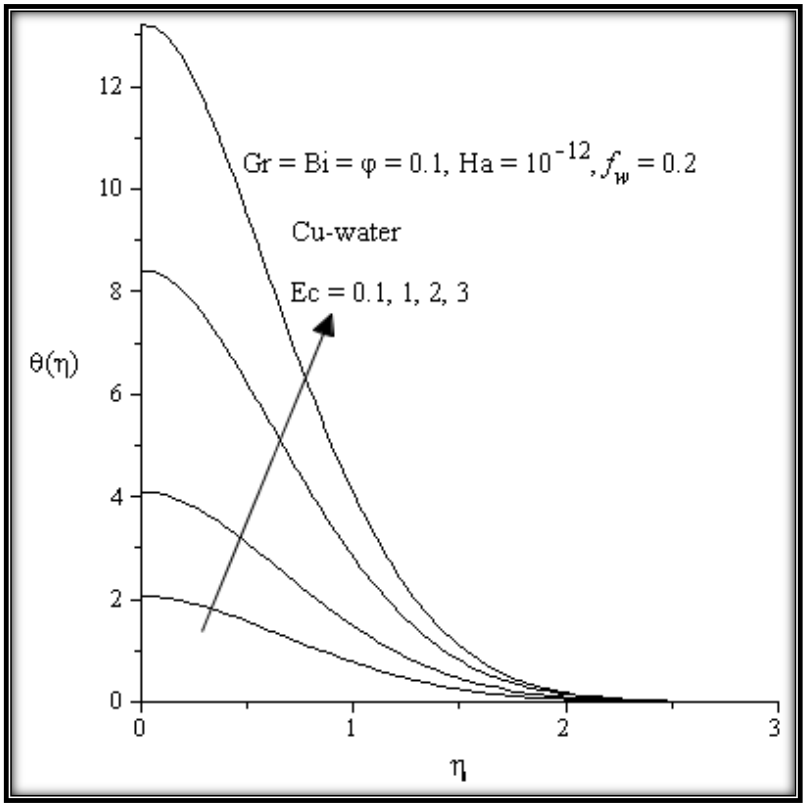

Figure 5.12: Temperature profiles with increasing Eckert number

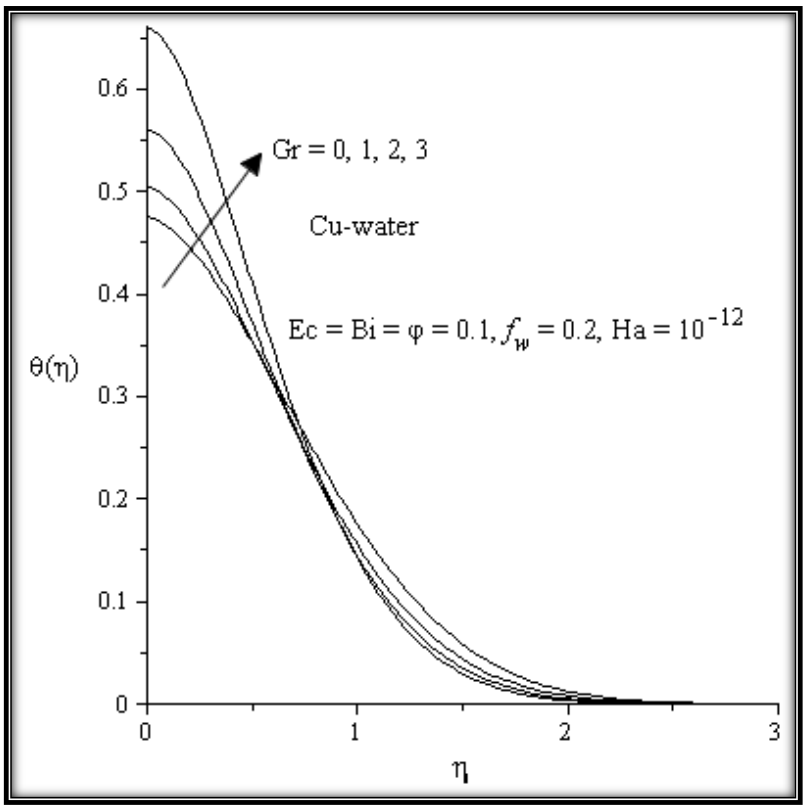

Figure 5.13: Temperature profiles with increasing Grashof number

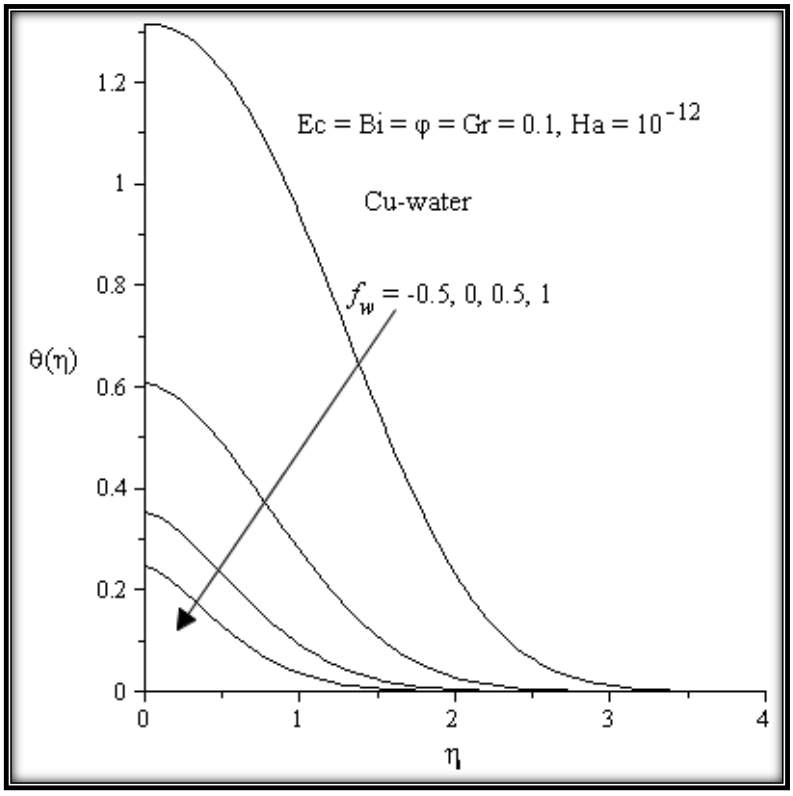

Figure 5.14: Temperature profiles with increasing Suction/Injection parameter

5.3.3 Effects of parameters variation on the skin friction and Nusselt number

Figures 5.15 – 5.23 illustrate the effects of the various pertinent parameters at the plate surface for both the skin friction coefficient and the local Nusselt number (rate of heat transfer). The presence of nanoparticle in the convectional fluid leads to an increase in the skin friction, this is shown in figure 5.15, where increasing the nanoparticle volume fraction increases the skin friction for the three nanoparticles (Cu, Al_2O_3, TiO_2) used, which Cu-water exhibiting the highest increase and TiO_2 the least. As expected, increasing Ha leads to an increase in the skin friction coefficient as shown in figure 5.16. A similar trend is observed in figures 5.17 – 5.18 with increase in *Gr*, F_w and *Ec*. There is an increase in the rate of heat transfer with increasing φ as shown in figure 5.20 and we note that among the three nanofluids used, Al_2O_3 has the highest increment while TiO_2 has the least. Figures 5.21-5.22, shows an increase in Nusselt number with increase in *Ha*, *Bi* and φ. Figure 5.23 is plotted for increasing values of f_w and *Gr*, and it is observed that there is a general decrease in the local Nusselt number with increasing *Gr* while there is an increase in Nusselt number with increasing f_w. We note that increasing *Ec*, leads to a decrease in the rate of heat transfer as illustrated in figure 5.24.

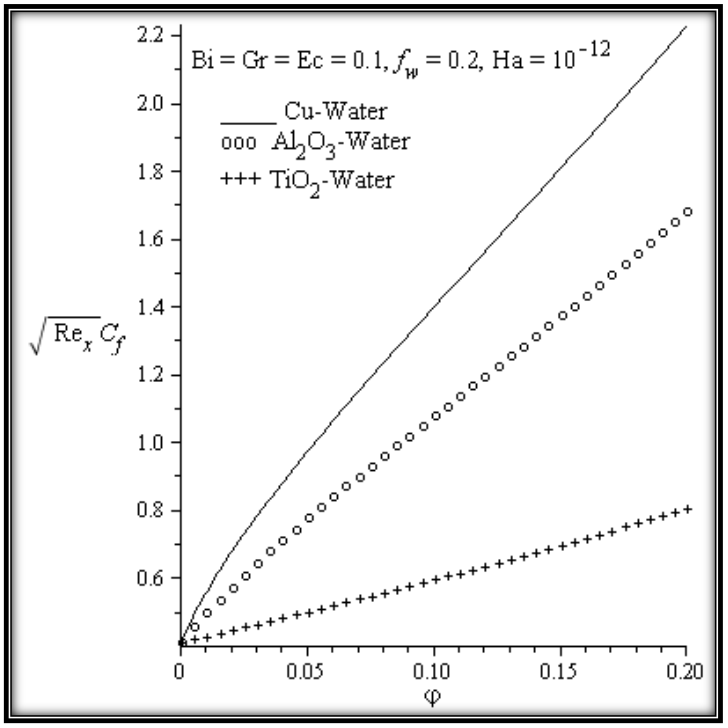

Figure 5.15: Skin friction profiles for different nanofluids

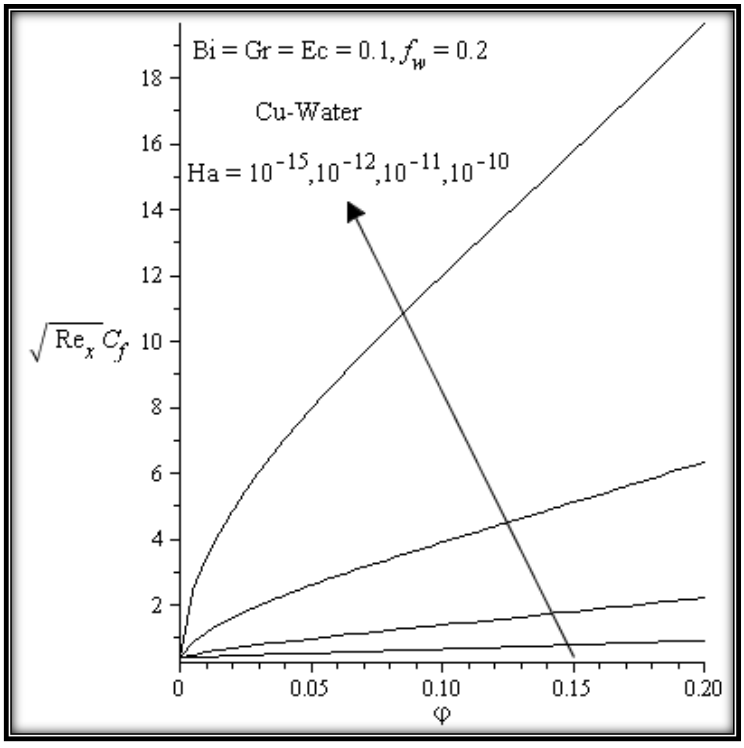

Figure 5.16: Skin friction with increasing magnetic field intensity

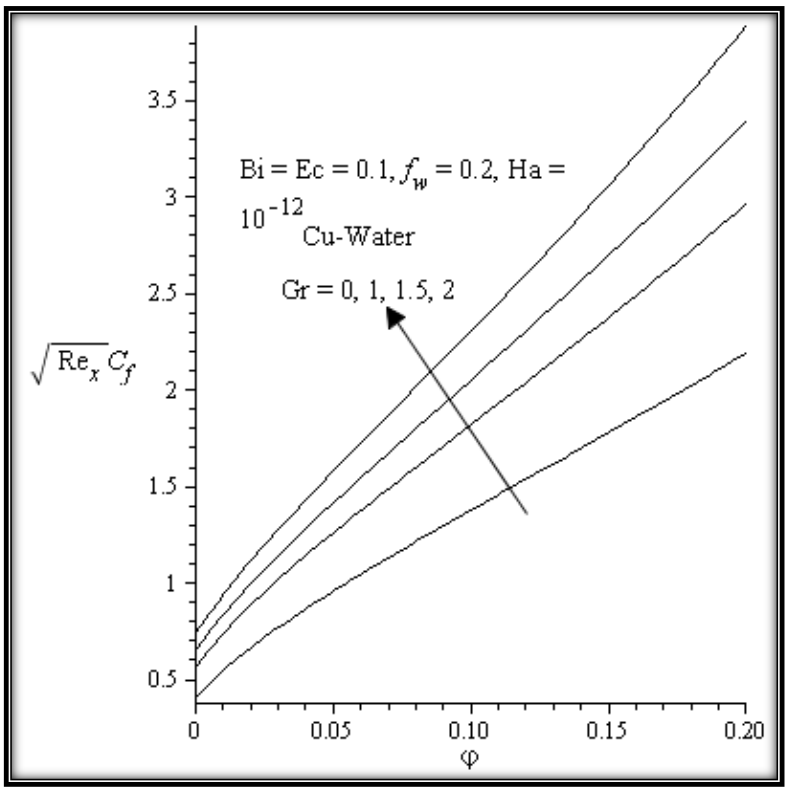

Figure 5.17: Skin friction with increasing Grashof number

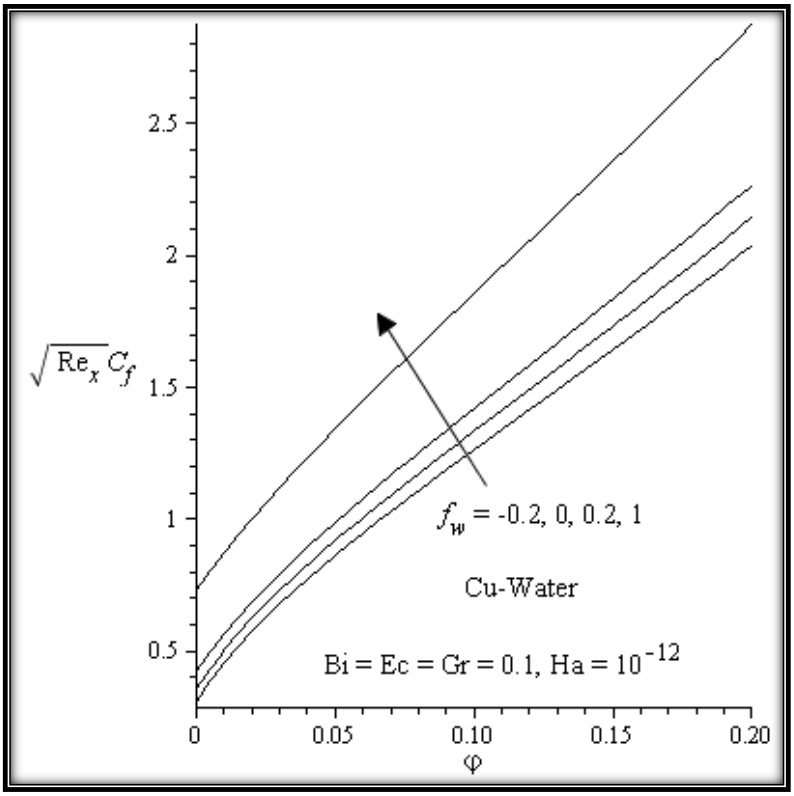

Figure 5.18: Skin friction with increasing Suction/injection parameter

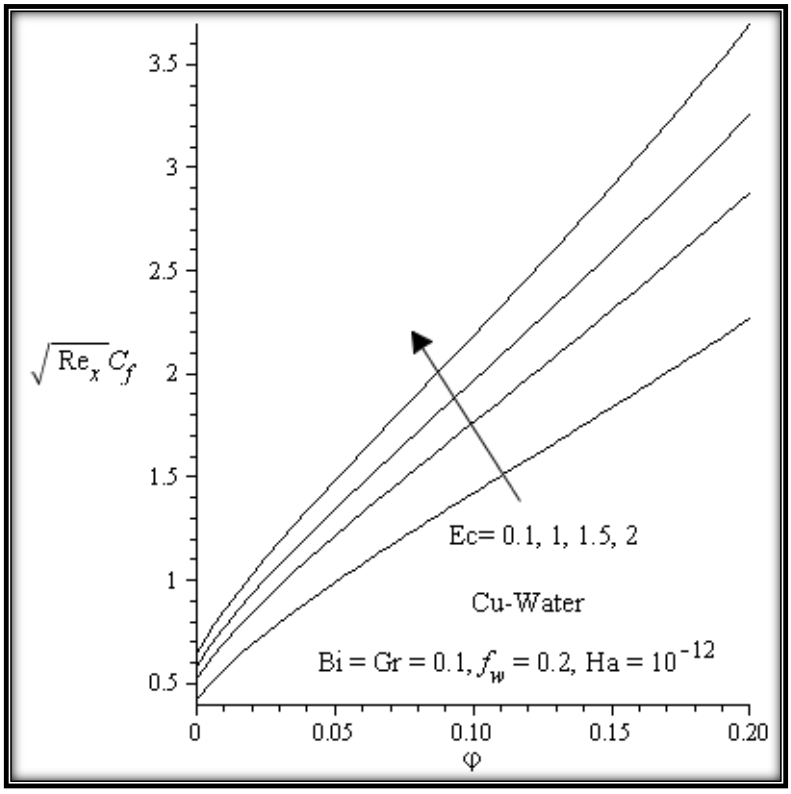

Figure 5.19: Skin friction with increasing Eckert number

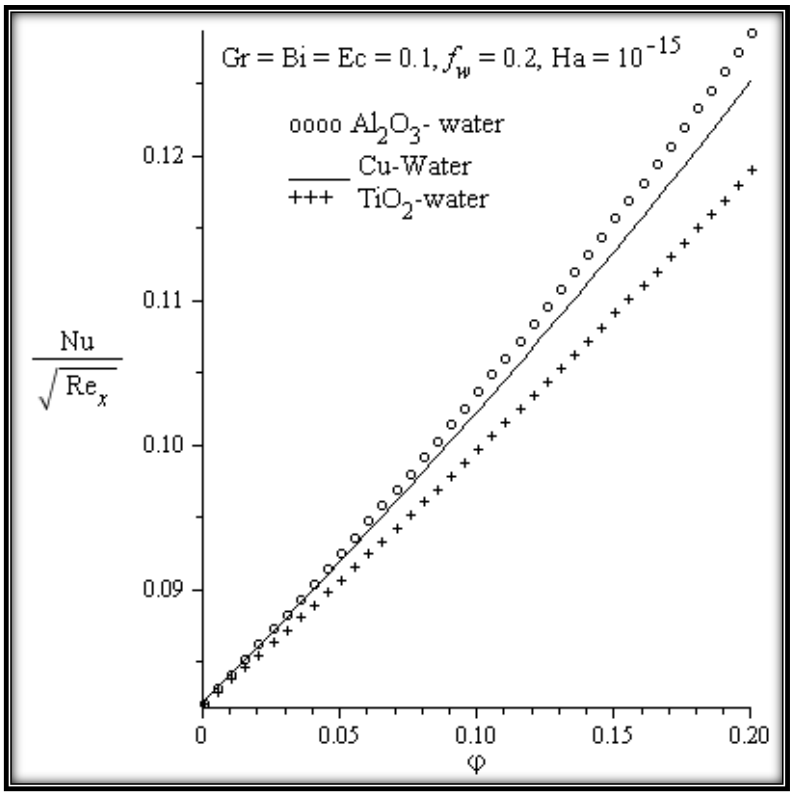

Figure 5.20: Reduced Nusselt number for different nanofluids

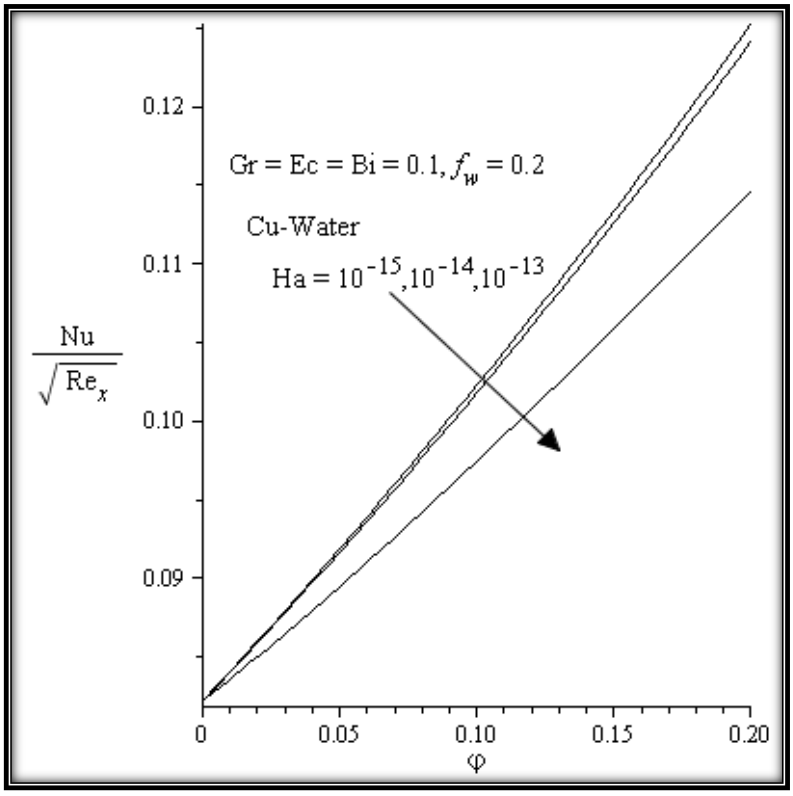

Figure 5.21: Nusselt number with increasing magnetic field intensity

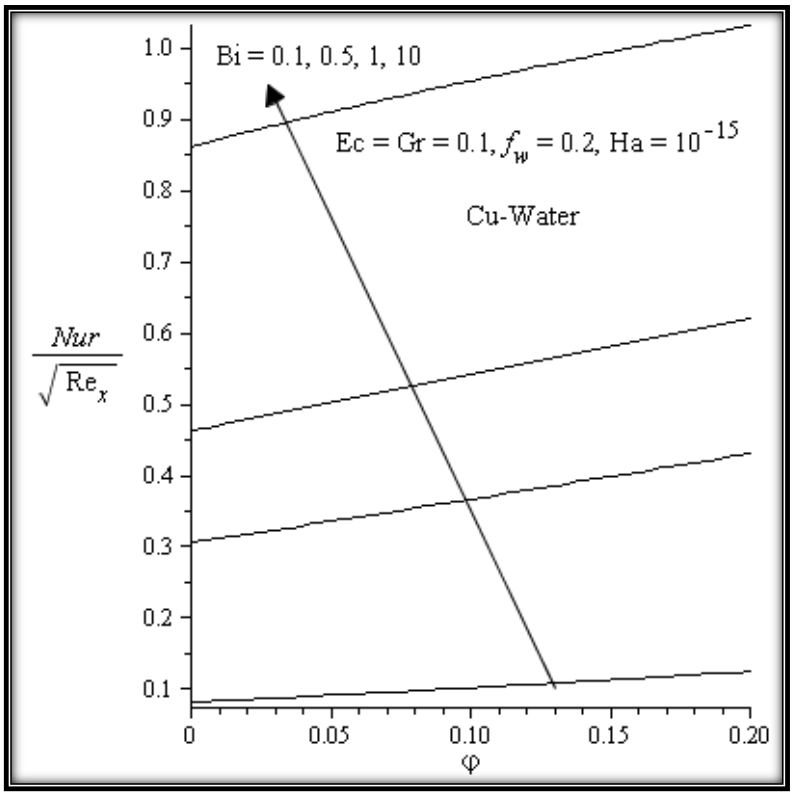

Figure 5.22: Nusselt number with increasing Biot number

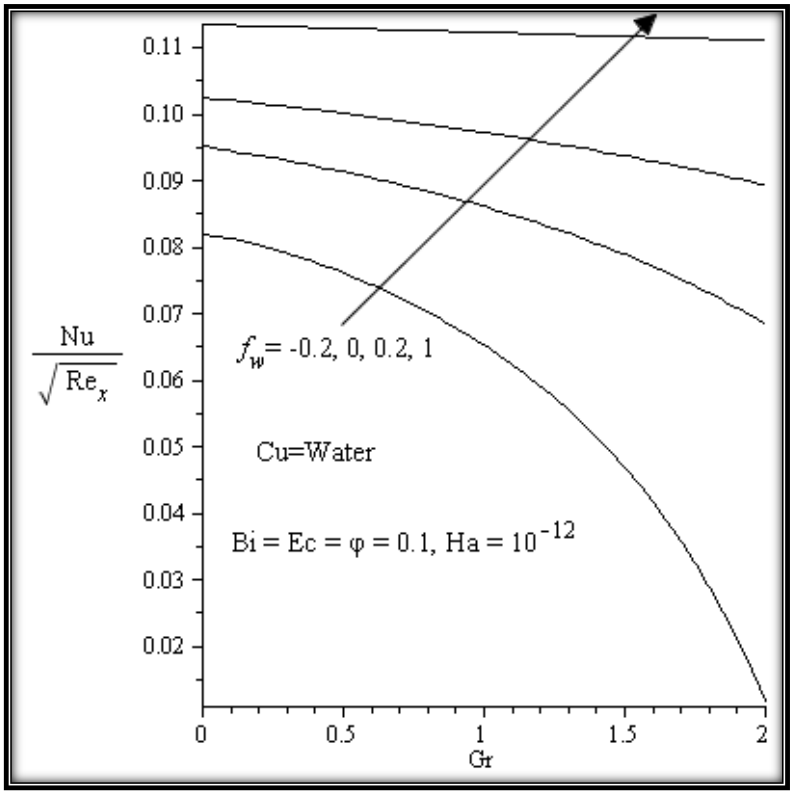

Figure 5.23: Nusselt number with increasing Grashof number and suction/injection parameter

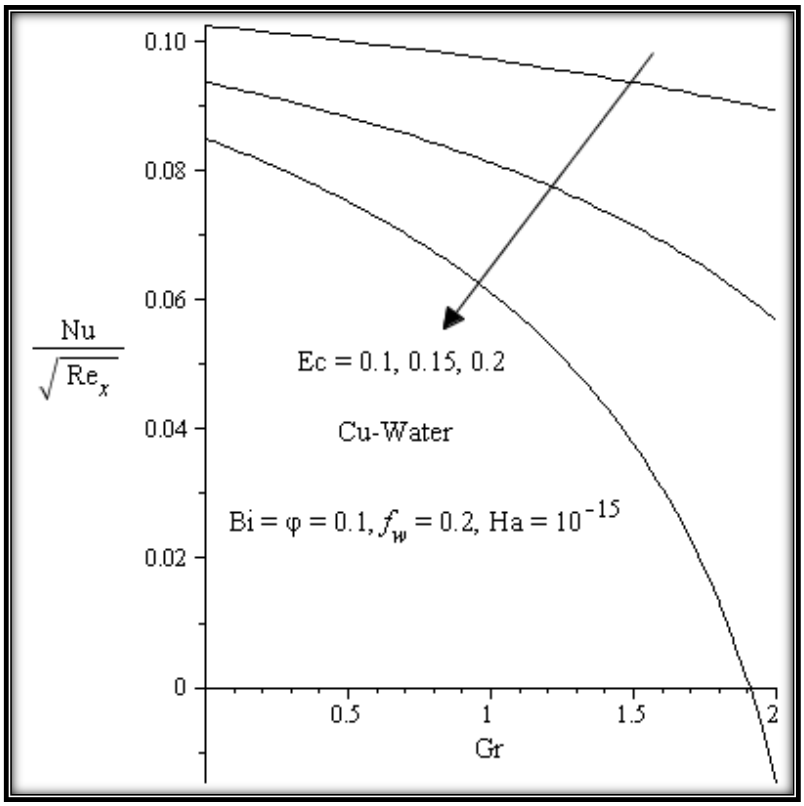

Figure 5.24: Nusselt number with increasing Grashof number and Eckert number

5.4 Conclusions

This paper investigates the combined effects of magnetic field intensity and buoyancy on a steady two-dimensional boundary layer flow of an electrically conducting water-based nanofluid containing three different types of nanoparticles: copper (Cu), aluminium oxide (Al_2O_3), and titanium dioxide (TiO_2) past a convectively heated porous vertical plate with variable suction. The governing nonlinear partial differential equations were transformed into ordinary differential equations using a similarity approach and numerically solved using shooting technique with a fourth-order Runge-Kutta-Fehlberg integration scheme. The Numerical results for dimensionless parameters as well as the skin-friction coefficient and Nusselt number, are presented graphically and analysed quantitatively. Based on the graphical representations, the following important conclusions are summarized:

- Nanofluids are highly susceptible to the effects of magnetic field compared to conventional base fluid due to the complex interaction of the electrical conductivity of nanoparticles with that of base fluid.
- The momentum boundary layer thickness decreases, while the thermal boundary layer thicknesses increase with increase in *Ha, φ, Ec,* and *Gr.*
- An increase in *Ha, φ, Ec, Gr* and suction ($f_w > 0$) increases the local skin friction coefficient, while the opposite is observed with increase in injection ($f_w < 0$).
- Increasing suction and *Bi* leads to an increase in the local Nuselt number, while an increase in *Ha*, injection ($f_w < 0$), *Ec* and *Gr* has the converse effect.

CHAPTER SIX

COMBINED EFFECT OF BUOYANCY FORCE AND NAVIER SLIP ON MHD FLOW OF A NANOFLUID OVER A CONVECTIVELY HEATED VERTICAL POROUS PLATE[4]

In this paper, we examine effect of magnetic field on boundary layer flow of an incompressible electrically conducting water based nanofluids past a convectively heated vertical porous plate with Navier slip boundary condition. A suitable similarity transformation is employed to reduce the governing partial differential equations into nonlinear ordinary differential equations, which are solved numerically by employing fourth order Runge-Kutta with a shooting technique. Three different water-based nanofluids containing copper (Cu), Aluminium oxide (Al_2O_3), and Titanium dioxide (TiO_2) are taken into consideration. Graphical results are presented and discussed quantitatively with respect to the influence of pertinent parameters such as, solid volume fraction of nanoparticles(φ), magnetic field parameter(Ha), buoyancy effect(Gr), Eckert number Ec, suction/injection parameter (f_w), Biot number (Bi) and slip parameter (β), on the dimensionless velocity, temperature, skin friction coefficient and heat transfer rate.

6.1 Introduction

Magnetohydrodynamic (MHD) boundary layer flow of an electrically conducting viscous incompressible fluid with a convective surface boundary condition is frequently encountered in many industrial and technological applications such as extrusion of plastics in the manufacture of Rayon and Nylon, the cooling of reactors, purification of crude oil, textile industry, polymer technology, metallurgy etc. As a result, the simultaneous occurrence of buoyancy and magnetic field forces on fluid flow has been investigated by many researchers [177-181]. In their investigations, all the authors mentioned above, assumed the no slip boundary conditions. However, more recently, researchers have investigated the flow problem taking slip flow condition at the boundary [182-185].

On the other hand, with the advent of nanofluids, there has been wide usage recently discovered smart fluid in many industrial and biomedical applications. Nanofluid concept is employed to designate a fluid in which nanometer-sized particles are suspended in

[4] *This chapter is a published paper: The Scientific World Journal, Volume 2013, Article ID 725643,8pages, http://dx.doi.org/10.1155/2013/725643.*

conventional heat transfer base fluids to improve their thermal physical properties. Nanoparticles are made from various materials, such as metals (Cu, Ag, Au, Al, Fe), oxide ceramics (Al_2O_3, CuO, TiO_2), nitride ceramics (AlN, SiN), carbide ceramics (SiC, tiC), semiconductors, carbon nanotubes and composite materials such as alloyed nanoparticles or nanoparticle core–polymer shell composites. It is well known that, conventional heat transfer fluids, such as oil, water, and ethylene glycol, in general, have poor heat transfer properties compared to those of most solids. Nanofluids have enhanced thermophysical properties such as thermal conductivity; thermal diffusivity, viscosity and convective heat transfer coefficients compared with those of base fluids like oil or water [65]. Several authors [9, 14, 27, 121] have conducted theoretical and experimental investigations to demonstrate that nanofluids distinctly exhibit enhanced heat transfer properties which goes up with increasing volumetric fraction of nanoparticles. Further studies on nanofluids are currently being undertaken by scientists and engineers due to their diverse technical and biomedical applications such as nanofluid coolant: electronics cooling, vehicle cooling, transformer cooling, computers cooling and electronic devices cooling; medical applications: magnetic drug targeting, cancer therapy and safer surgery by cooling; process industries; materials and chemicals: detergency, food and drink, oil and gas, paper and printing and textiles.

According to Aziz [186], the concept of no slip condition at the boundary layer is no longer valid for fluid flows in micro electro mechanical systems and must be replaced by slip condition. The slip flow model states a proportional relationship between the tangential components of the fluid velocity at the solid surface to the shear stress on the fluid–solid interface [187]. The proportionality is called the slip length, which describes the slipperiness of the surface [183]. Many researchers studied the effect of linear momentum and nonlinear slip on the MHD boundary layer flow with heat/mass transfer of free / forced / combined convection past different geometries [188-191]. In spite of the importance of MHD related studies on boundary layer flow problems, the possibility of fluid exhibiting apparent slip phenomenon on the solid surface has received little attention.

The aim of the present study is to investigate the combined effects of buoyancy, magnetic field, suction, Navier slip and convective heating on a steady boundary layer flow over a flat surface. In the subsequent sections the boundary layer partial differential equations first transformed into a system of nonlinear ordinary differential equations, before being solved numerically using a shooting method together with the fourth order Runge-Kutta Fehlberg integration scheme. A graphical representation of the pertinent parameters on the flow field and heat transfer characteristics are displayed and thoroughly discussed. To our best of knowledge, the investigations of the proposed problem are new and the results have not been published before.

6.2 Model Formulation

The steady laminar incompressible two-dimensional MHD boundary layer flow of an electrically conducting water-based nanofluid past a convectively heated porous vertical semi-infinite flat plate under the combined effects of buoyancy forces and Navier slip are considered. The nanofluids contain three different types of nanoparticles: Cu, Al_2O_3, and TiO_2. Let the *x*-axis be taken along the direction of plate and *y*-axis normal to it. The left side of the plate is assumed to be heated by convection from a hot fluid at temperature T_f, which provides a heat transfer coefficient h_f, while the right surface is subjected to a stream of an electrically conducting cold nanofluid at temperature T_∞ in the presence of a transverse magnetic field of strength B_0 applied parallel to the y-axis, as shown in Figure 6.1 below. The induced magnetic field due to the motion of the electrically conducting fluid is negligible. It is also assumed that the external electrical field is zero and that the electric field due to the polarization of charges is negligible.

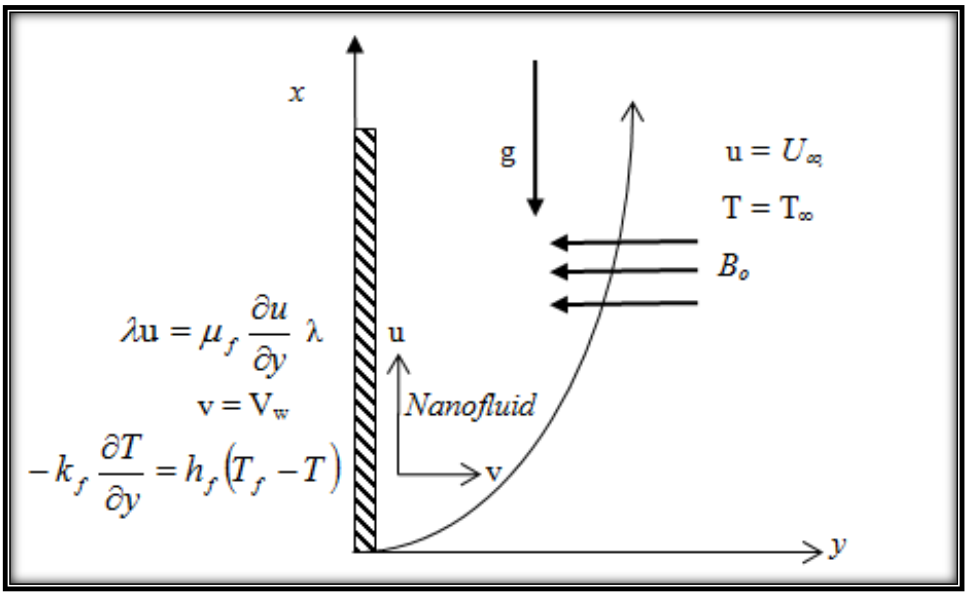

Figure 6.1: Flow Configuration and Coordinate System

Assuming a Boussinesq incompressible fluid model, the continuity, momentum, and energy equations describing the flow can be written as;

$$\frac{\partial u}{\partial x}+\frac{\partial v}{\partial y}=0, \tag{6.1}$$

$$u\frac{\partial u}{\partial x}+v\frac{\partial u}{\partial y}=U_\infty\frac{dU_\infty}{dx}+\frac{\mu_{nf}}{\rho_{nf}}\frac{\partial^2 u}{\partial y^2}+\beta_{nf}g(T-T_\infty)-\frac{\sigma_{nf}B_0^2(u-U_\infty)}{\rho_{nf}}, \tag{6.2}$$

$$u\frac{\partial T}{\partial x}+v\frac{\partial T}{\partial y}=\frac{k_{nf}}{(\rho c_p)_{nf}}\frac{\partial^2 T}{\partial y^2}+\frac{\mu_{nf}}{(\rho c_p)_{nf}}\left(\frac{\partial u}{\partial y}\right)^2+\frac{\sigma_{nf}B_0^2}{(\rho c_p)_{nf}}\left(u-U_\infty\right)^2. \tag{6.3}$$

The boundary conditions at the plate surface and at the free stream may be written as;

$$\begin{aligned}&\lambda u(x,0)=\mu_f\frac{\partial u}{\partial y}(x,0),\quad v(x,0)=V_w,\quad -k_f\frac{\partial T}{\partial y}(x,0)=h_f[T_f-T(x,0)],\\&u(x,\infty)=U_\infty(x),\qquad T(x,\infty)=T_\infty.\end{aligned} \tag{6.4}$$

where (u, v) are the velocity components of the nanofluid in the x- and y-directions respectively, T is the nanofluid temperature, $U_\infty(x) = ax$ is the free stream velocity (which implies that the free stream fluid velocity is increasing with axial distance along the plate surface), T_∞ is the free stream temperature, g is acceleration due to gravity, λ is the slip coefficient, μ_{nf} is dynamic viscosity of the nanofluid, ρ_{nf} is density of the nanofluid, k_{nf} is thermal conductivity of the nanofluid, σ_{nf} is electrical conductivity of the nanofluid, $(\rho c_p)_{nf}$ is heat capacity at constant pressure of the nanofluid, β_{nf} is volumetric expansion coefficient of the nanofluid which are defined as [153, 192],

$$\begin{aligned}&\mu_{nf}=\frac{\mu_f}{(1-\phi)^{2.5}},\quad \rho_{nf}=(1-\phi)\rho_f+\phi\rho_s,\ \beta_{nf}=(1-\phi)\ \beta_f+\phi\beta_s\\&\alpha_{nf}=\frac{k_{nf}}{(\rho c_p)_{nf}},\frac{k_{nf}}{k_f}=\frac{(k_s+2k_f)-2\phi(k_f-k_s)}{(k_s+2k_f)+\phi(k_f-k_s)},\\&(\rho c_p)_{nf}=(1-\phi)(\rho c_p)_f+\phi(\rho c_p)_s,\sigma_{nf}=(1-\phi)\sigma_f+\phi\sigma_s.\end{aligned} \tag{6.5}$$

where φ is the nanoparticle volume fraction ($\varphi = 0$ correspond to a regular fluid), ρ_f and ρ_s are the densities of the base fluid and the nanoparticle respectively, β_f and β_s are the thermal expansion coefficients of the base fluid and the nanoparticle respectively, k_f and k_s are the thermal conductivities of the base fluid and the nanoparticles respectively, $(\rho c_p)_f$ and $(\rho c_p)_s$ are the heat capacitance of the base fluid and the nanoparticle respectively, σ_s and σ_f are the electrical conductivities of the base fluid and the nanofluid respectively.

Table 6.1: Thermophysical Properties of Water and Nanoparticles [147,193]

Materials	ρ(kg/m^3)	c_p (J/kgK)	k (W/mK)	σ(S/m)
Pure water	997.1	4179	0.613	$5.5\text{x}10^{-6}$
Copper (Cu)	8933	385	401	$59.6\text{x}10^{6}$
Alumina (Al_2O_3)	3970	765	40	$35\text{x}10^{6}$
Titania (TiO_2)	4250	686.2	8.9538	$2.6\text{x}10^{6}$

In order to simplify the mathematical analysis of the problem, we introduce the following dimensionless variables;

$$\eta = \left(a/\upsilon_f\right)^{1/2} y, \quad \psi = \left(a\upsilon_f\right)^{1/2} xf(\eta), \quad \theta(\eta) = \frac{T - T_\infty}{T_f - T_\infty}, \tag{6.6}$$

where η is the similarity variable and ψ is the stream function defined as;

$$u = \frac{\partial \psi}{\partial y} \text{ and } v = -\frac{\partial \psi}{\partial x} \ . \tag{6.7}$$

After introducing equation (6.7) into equations (6.1)-(6.4) we obtain the following ordinary differential equations;

$$\begin{aligned} &f'''+(1-\varphi)^{2.5}(1-\varphi+\varphi\rho_s/\rho_f)\,ff''-(1-\varphi)^{2.5}(1-\varphi+\varphi\rho_s/\rho_f)(f')^2 \\ &+(1-\varphi)^{2.5}(1-\varphi+\varphi\rho_s/\rho_f) \\ &+\mathrm{Gr}(1-\varphi)^{2.5}(1-\varphi+\varphi\rho_s/\rho_f)(1-\varphi+\varphi\beta_s/\beta_f)\theta \\ &-Ha(1-\varphi)^{2.5}(1-\varphi+\varphi\sigma_s/\sigma_f)(f'-1)=0, \end{aligned} \tag{6.8}$$

$$\begin{aligned} &\theta''+\frac{\mathrm{Pr}\,k_f[1-\phi+\phi(\rho c_p)_s/(\rho c_p)_f]}{k_{nf}}\,f\theta'+\frac{\mathrm{Pr}\,Eck_f}{k_{nf}(1-\phi)^{2.5}}(f'')^2 \\ &+\frac{Ha\,\mathrm{Pr}\,Eck_f}{k_{nf}}(1-\phi+\phi\sigma_s/\sigma_f)(f'-1)^2=0. \end{aligned} \tag{6.9}$$

Taking into account the variable plate surface permeability and the hydrodynamic slip boundary functions defined respectively as;

$$V_w = -f_w\left(a\upsilon_f\right)^{1/2} \quad \text{and} \quad \lambda u(x,0) = \mu_f \frac{\partial u}{\partial y}(x,0). \tag{6.10}$$

the boundary conditions are;

$$f(0) = f_w,\ f'(0) = \beta f''(0),\ \theta'(0) = Bi[\theta(0)-1], \tag{6.11}$$

$$f'(\infty) = 1, \quad \theta(\infty) = 0. \tag{6.12}$$

where a prime symbol denotes derivative with respect to η, f_w is a constant with $f_w > 0$ representing suction rate at the plate surface, $f_w < 0$ corresponds to injection and $f_w = 0$ shows an impermeable surface, λ = 0 represents highly lubricated surface, λ = ∞ corresponds to a normal surface. The local Reynolds number Re_x, Grashof number *Gr*,

Hartmann number *Ha*, Prandtl number *Pr*, Eckert number *Ec*, Slip parameter *β*, and Biot number *Bi*, are defined as;

$$\begin{aligned} &\mathrm{Re}_x = \frac{U_\infty x}{\upsilon_f},\ Gr = \frac{\beta_f g\left(T_f - T_\infty\right)}{U_\infty a},\ \ Ha = \frac{\sigma_f B_o^{\ 2}}{\rho_f a},\ \ \mathrm{Pr} = \frac{\upsilon_\mathrm{f}}{\alpha_\mathrm{f}}, \\ &\mathrm{Ec} = \frac{\mathrm{U}_\infty^{\ 2}}{C_{p_f}\left(T_f - T_\infty\right)},\ \beta = \frac{\mu_f}{\lambda}\sqrt{\frac{\mathrm{a}}{\upsilon_f}},\ \ Bi = \frac{h_f}{k_f}\sqrt{\frac{\upsilon_f}{a}}. \end{aligned} \tag{6.13}$$

The physical quantities of practical significance in this work are the skin friction coefficient C_f and the local Nusselt number *Nu*, which are expressed as;

$$C_f = \frac{\tau_w}{\rho_f U_\infty^2},\ \ Nu = \frac{x q_w}{k_f (T_f - T_\infty)}, \tag{6.14}$$

where τ_w is the skin friction and q_w is the heat flux from the plate which are given by;

$$\tau_w = \mu_{nf}\left.\frac{\partial u}{\partial y}\right|_{y=0},\quad q_w = -k_{nf}\left.\frac{\partial T}{\partial y}\right|_{y=0}. \tag{6.15}$$

Putting equation (15) into equation (14), we obtain;

$$\mathrm{Re}_x^{1/2} C_f = \frac{1}{(1-\varphi)^{2.5}} f''(0),\quad \mathrm{Re}_x^{-1/2} Nu = -\frac{k_{nf}}{k_f}\theta'(0). \tag{6.16}$$

The set of equations (6.8)–(6.9) together with the boundary conditions (6.11)-(6.12) are a coupled nonlinear boundary value problems which are solved numerically using a shooting algorithm with a Runge-Kutta Fehlberg integration scheme. This method involves, transforming equations (6.8)–(6.9) and (6.11)-(6.12) into a set of initial value problems which contain unknown initial values that need to be determined by guessing, after which a fourth order Runge–Kutta iteration scheme is employed to integrate the set of initial valued problems until the given boundary conditions are satisfied. The entire computation procedure is implemented using a program written and carried out using MAPLE computer language. From the process of numerical computation, the fluid velocity, the temperature, the skin friction coefficient and the Nusselt number, are proportional to $f'(\eta),\ \theta(\eta),\ f''(\eta),\ \theta'(\eta)$, respectively.

6.3 Results and Discussion

Physically realistic numerical values were assigned to the pertinent parameters in the system in order to gain an insight into the flow structure with respect to velocity, temperature, skin friction and Nusselt's number. The results were presented graphically in Figures 6.2 – 6.15 and conclusions are drawn for the flow field. The Prandt number is kept constant at 6.2 [154]. *Ha* = 0 corresponds to absence of magnetic field and $\varphi = 0$ is regular fluid.

6.3.1 Dimensionless Velocity Profiles

Figures 6.2 – 6.4 illustrate the effects of various thermo physical parameters on the nanofluids velocity profiles. Generally, it is noted that the fluid velocity increases gradually from zero at the plate surface to the free stream prescribed value far away from the plate satisfying the boundary conditions. Figure 6.2 shows that the momentum boundary layer thickness for Cu-water nanofluid is smaller than the rest of the nanofluids, consequently, Cu-water nanofluid tends to flow closer to the convectively heated plate surface and serves as a better coolant than the other nanofluids. It is observed in Figures 6.3 – 6.4, an increase in the magnetic field intensity (*Ha)*, nanoparticle volume fraction (φ), Eckert number (*Ec*), Grashof number (*Gr*), and the suction/injection parameter (f_w) causes an overshoot of the fluid velocity towards the plate surface hence decreasing both the momentum boundary layer thickness and the fluid velocity. From the physics of the problem, an increase in the magnetic field intensity leads to an increase in the Lorentz force which is a retarding force to the transport phenomena. This retarding force can control the nanofluids velocity which is useful in numerous applications such as magneto-hydrodynamic power generation and electromagnetic coating of wires and metal, etc. We also note that the fluid velocity at the plate surface increases with an increase in the slip parameter (β). This is in agreement with the fact that higher β implies an increase in the lubrication and slipperiness of the surface.

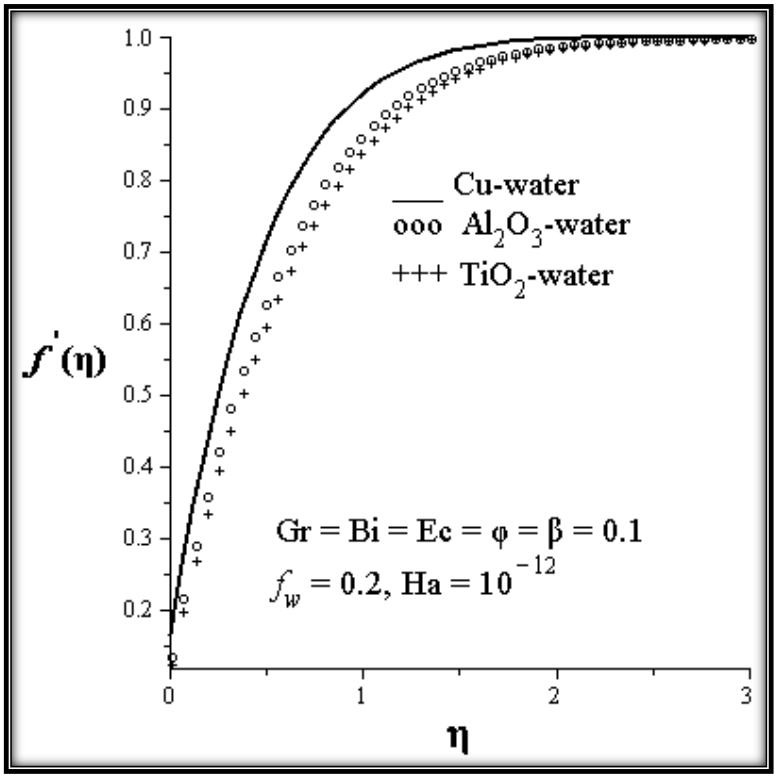

Figure 6.2: Velocity profiles for different nanofluids

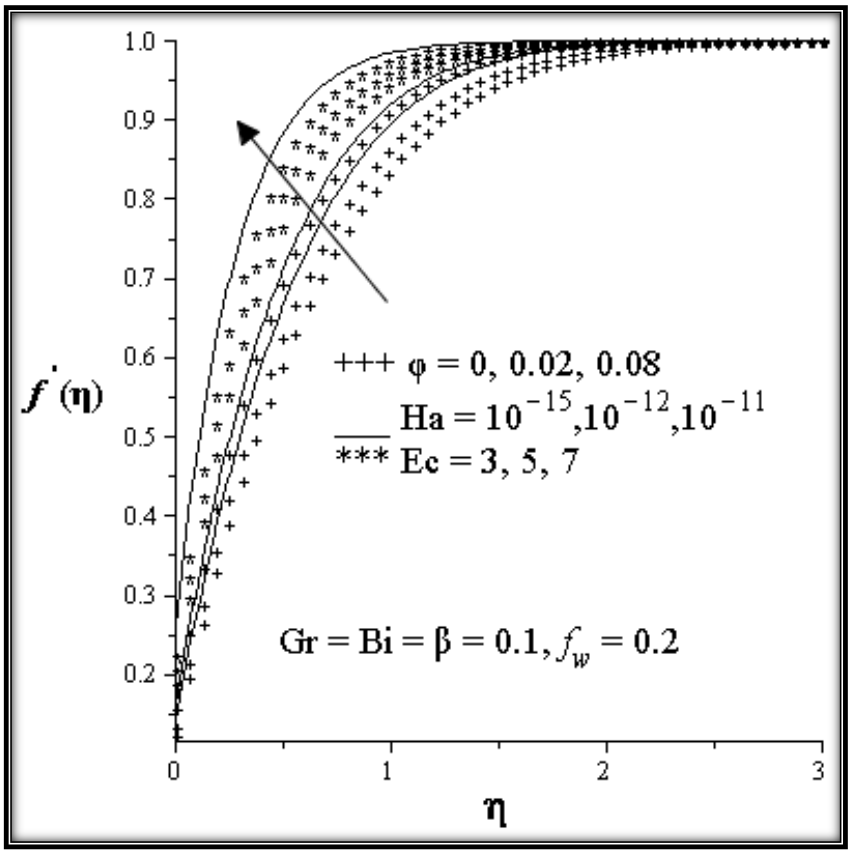

Figure 6.3: Velocity profiles with increasing *Ha*, *φ* and *Ec*.

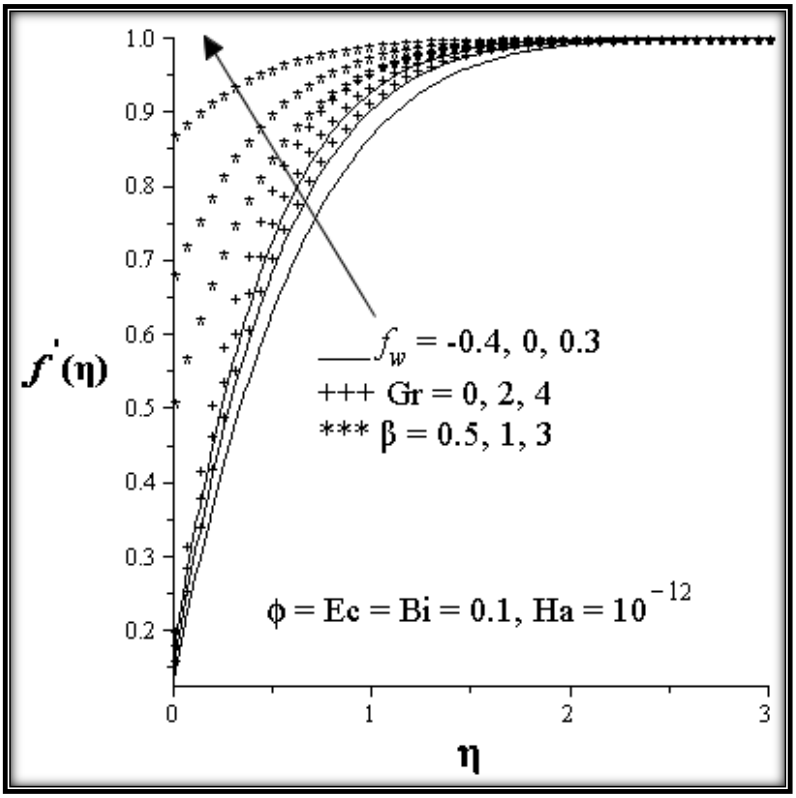

Figure 6.4: Velocity profiles with increasing *Gr*, *β* and f_w

6.3.2 Dimensionless Temperature Profiles

Figures 6.5 – 6.7 shows the effects of various parameters on the temperature profile. In general, the maximum fluid temperature is achieved at the plate surface due to the convectional heating but decreases exponentially to zero far away from the plate surface satisfying the free stream conditions. As expected, at the plate surface Cu-water has the highest temperature and a greater thermal boundary layer thickness than the other two nanofluids, as seen in Figure 6.5. This is in accordance with the earlier observation, since the Cu-water nanofluid is more likely to absorb more heat from the plate surface owing to its close proximity to the hot surface. It is observed from Figure 6.6, that increasing *Ha*, *φ*, *Bi* and *Ec* leads to an increase in both the fluid temperature and the thermal boundary layer thickness. This can be attributed to the additional heating due resistance of fluid flow as a result of the magnetic field, the presence of the nanoparticle, the increased rate at which the heat moves from the hot fluid to the plate and the additional heating as a result of the viscous dissipation.

On the other hand, it is evident that surface slipperiness and suction affect the temperature of the fluid inversely. This is clearly seen from Figure 6.7, where both temperature and thermal boundary layer decrease as f_w and *β* increases.

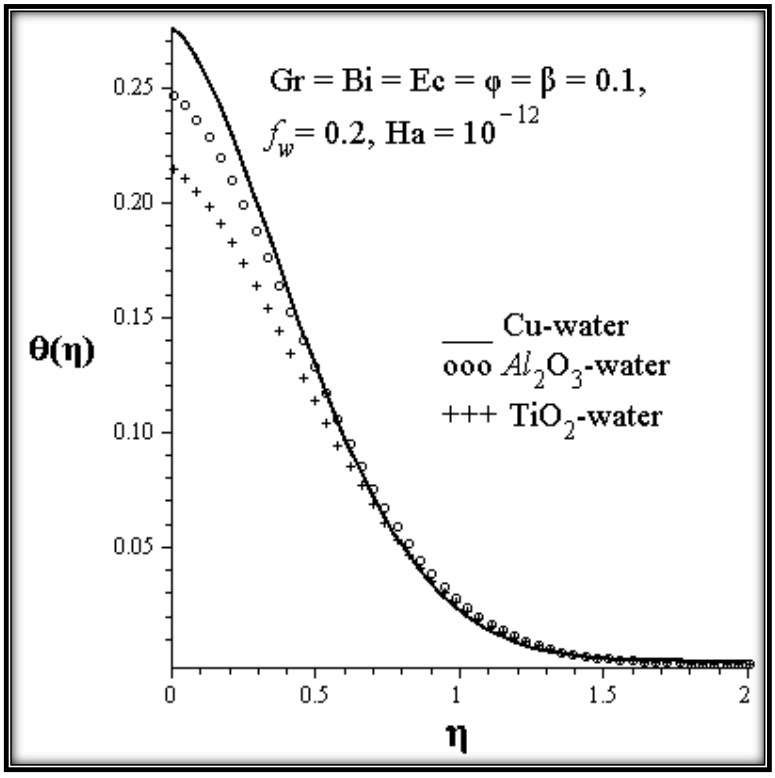

Figure 6.5: Temperature profiles for different nanofluids

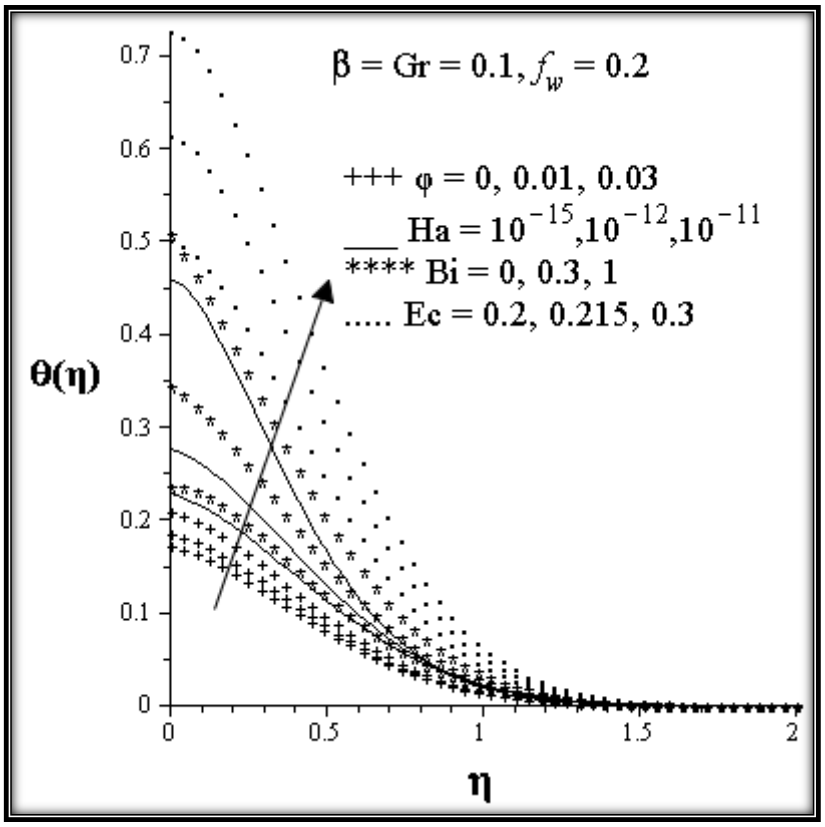

Figure 6.6: Temperature profiles with increasing *φ, Ha, Bi* and *Ec*

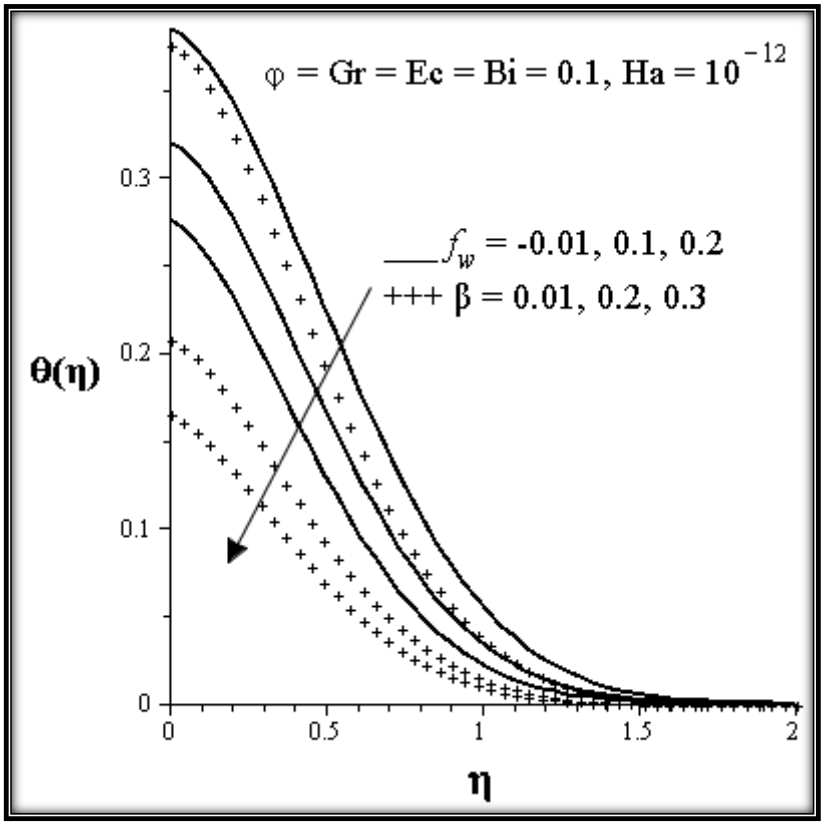

Figure 6.7: Temperature profiles with increasing *β*, *Gr* and f_w

6.3.3 Effects of parameters variation on the skin friction and Nusselt number

Figures 6.8 – 6.13 demonstrate the effects of the various pertinent parameters at the plate surface for both the skin friction coefficient and the local Nusselt number (rate of heat transfer). The presence of nanoparticle in the convectional fluid leads to an increase in the skin friction, as seen in Figure 6.8, where increasing the nanoparticle volume fraction increases the skin friction for the three nanoparticles (Cu, Al_2O_3, TiO_2) used, with Cu-water exhibiting the highest increment. This is as expected, since Cu-water moves closer to the plate surface leading to an elevation in the velocity gradient at the plate surface. As expected, increasing *Ha*, *Gr*, *Ec* and f_w leads to an increase in the skin friction coefficient, while an increase in *β* reduces the skin friction coefficient as shown in Figures 6.9 – 6.10. There is an increase in the rate of heat transfer with an increase in *φ*, *Bi* and f_w as seen in Figures 6.11 – 6.12, with Al_2O_3 exhibiting the highest increment. The converse is seen with increasing *Ha* as shown in Figure 6.13.

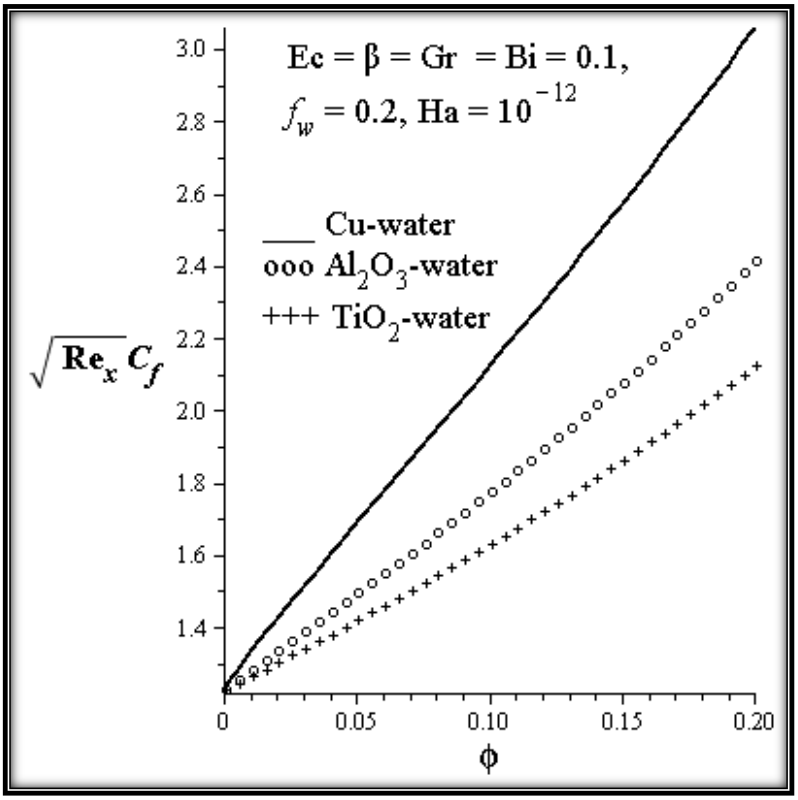

Figure 6.8: Local skin friction profiles for different nanofluids

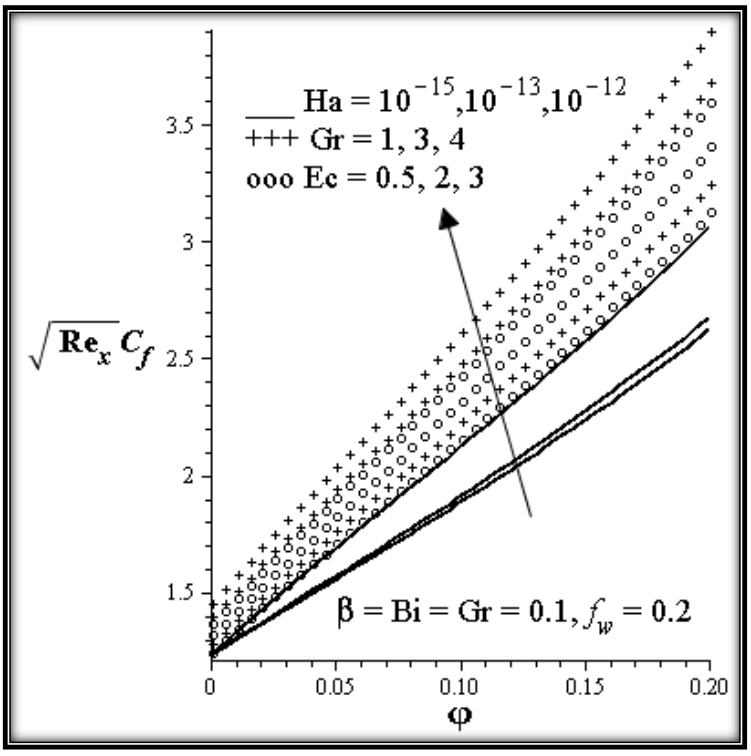

Figure 6.9: Effects of increasing *Gr*, *Ha* and *Ec* on local skin friction

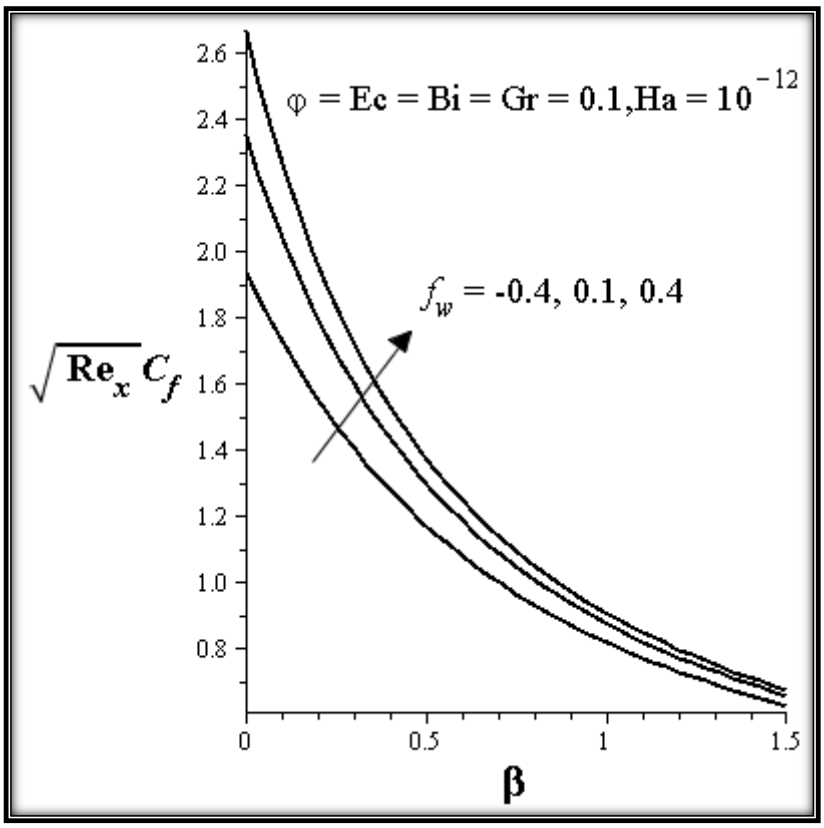

Figure 6.10: Effects of increasing β and f_w on local skin friction

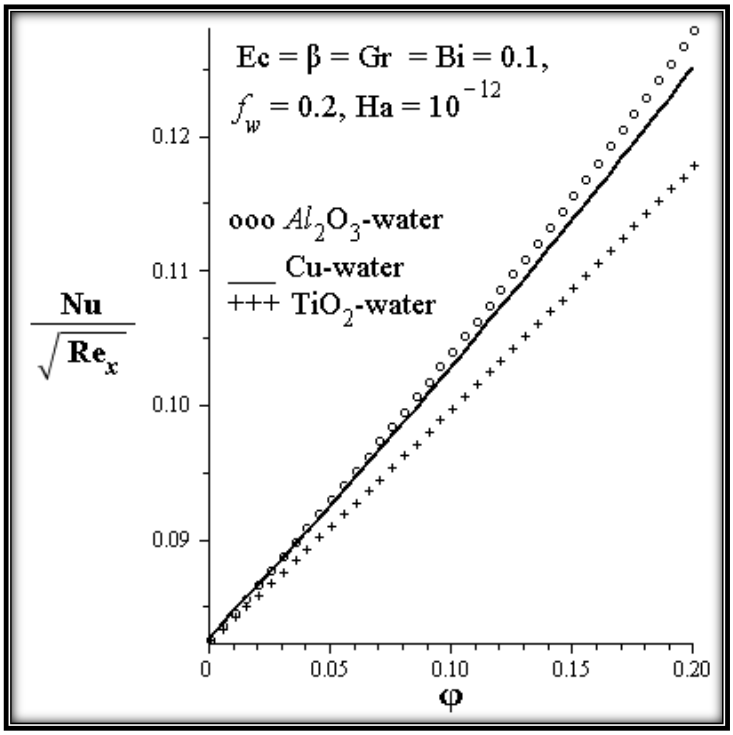

Figure 6.11: Local Nusselt number for different nanofluids

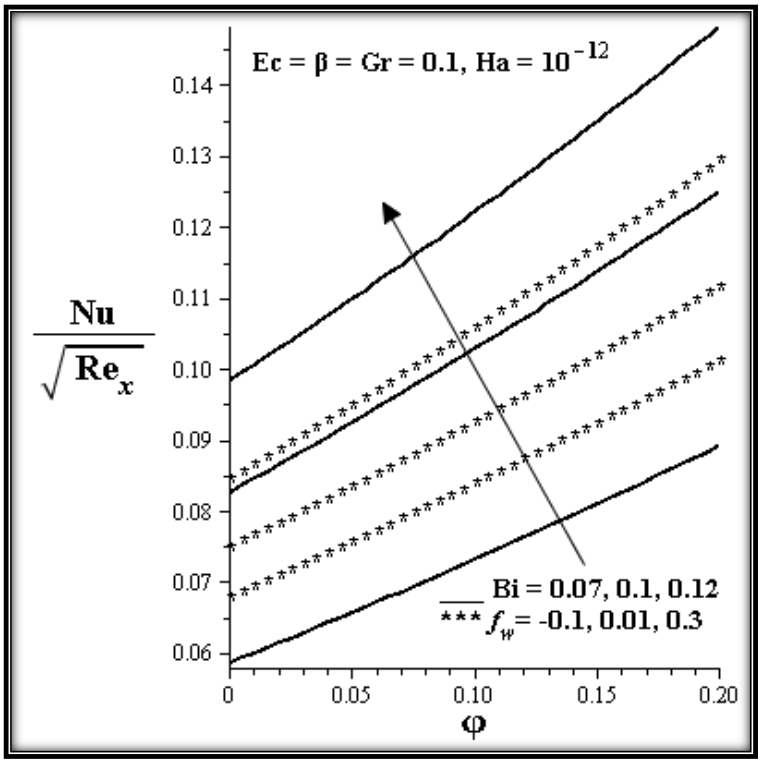

Figure 6.12: Effects of increasing *φ*, *Bi* and *Ha* on local Nusselt number

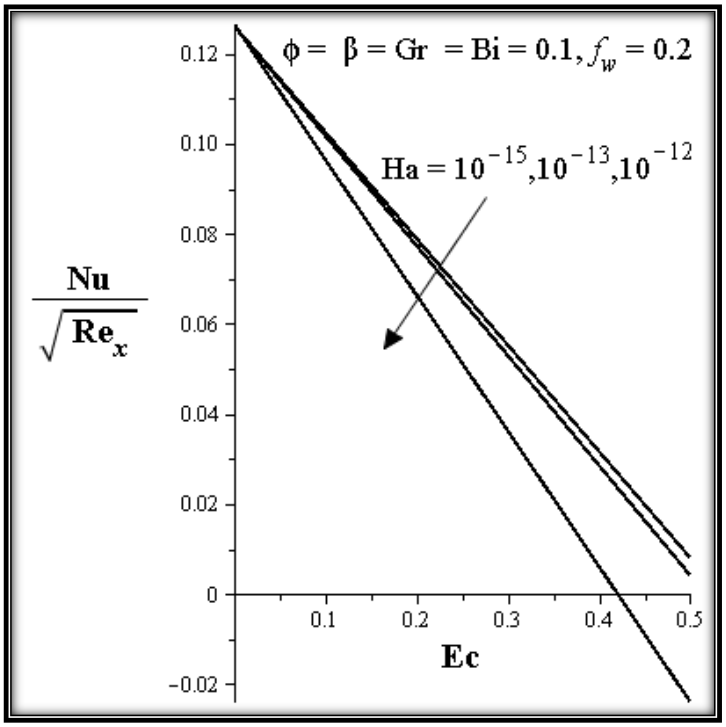

Figure 6.13: Effects of increasing *φ*, *Ha* and *Ec* on local Nusselt number

6.4 Conclusions

The problem of hydromagnetic boundary layer flow of an incompressible electrically conducting water based nanofluids past a convectively heated vertical porous plate with Navier slip boundary condition was studied. The governing nonlinear partial differential equations were transformed into a self-similar form and numerically solved using shooting technique with a fourth-order Runge-Kutta-Fehlberg integration scheme, putting into consideration the enhanced electrical conductivity of the convectional base fluid due to the presence of the nanoparticles. Our results showed that the fluid velocity increases, while the local skin friction decreases with increase in the slip parameter (β) but the reverse is observed with increase in the magnetic field intensity (*Ha)*, nanoparticle volume fraction (*φ*), Eckert number (*Ec*), Grashof number (*Gr*), and the suction/injection parameter (f_w). Both the temperature and the thermal boundary layer thickness are enhanced by increasing the magnetic field intensity (*Ha)*, nanoparticle volume fraction (*φ*), Eckert number (*Ec*) and the intensity of Newtonian heating (*Bi*), while the cooling effect on the convectively heated plate surface is enhanced by increasing the velocity slip (*β*) and suction parameter (f_w).

CHAPTER SEVEN

CONCLUSION AND RECOMMENDATIONS

7.1 Conclusion

In this thesis, we investigated a steady MHD boundary layer flow of nanofluids over a convectively heated surface. The governing partial differential equations for mass, momentum and energy are obtained and transformed to non-similar equations by using a similarity transformation. The resulting dimensionless nonlinear differential equations are solved numerically using the well-known fourth order Runge-Kutta-Fehlberg method with shooting technique taking into consideration the complex interaction between the electrical conductivity of the conventional base fluids and that of the nanoparticles. The Numerical results for the velocity and temperature profiles, as well as the skin-friction coefficient and Nusselt number, are studied and depicted graphically for the effect of pertinent parameter conditions.

Generally, our results revealed that the susceptibility of nanofluids to the influence of magnetic field is extremely high compared to conventional base fluid due to the complex interaction of electrical conductivity of nanoparticles with that of base fluid. There is an increase in the temperature and a decrease in the velocity due to the increase in the nanoparticle volume fraction and magnetic strength, which means that nanofluids in the presence of a magnetic field are important in the cooling and heating processes.

This study is of paramount importance as it highlights the significance of nanofluids which makes them have numerous applications involving heat transfer and other applications such as detergency, medicine and biomedicine. Nanofluids plays a very important role in engineering such as the next-generation solar film collectors, heat exchanger technology, geothermal energy storage, and all those processes which are greatly affected by a heat enhancement concept. Nanofluids are also used as heat transfer nanofluid, chemical nanofluids, bio nanofluids, medical nanofluids (drug delivery and functional tissue cell interaction), etc. The interdisciplinary nature of nanofluid research presents a great opportunity for exploration and discovery at the frontiers of nanotechnology

7.1 Further work

For future work, investigation can be carried out on the interaction of magnetic field and nanofluids for turbulent flow.

BIBLIOGRAPHY

[1] Choi, S.U.S.: Enhancing thermal conductivity of fluids with nanoparticles, in: D.A. Siginer, H.P. Wang (Eds.), developments and applications of non-Newtonian flows FED-vol. 231/MD-66, ASME, New York, 1995, 99–105.

[2] Choi, S.U.S.: Nanofluids: from vision to reality through research, Journal of Heat Transfer, 131(3), 2009, 1–9.

[3] Yu, W., France, D. M., Routbort, J. L., Choi, S.U.S: Review and comparison of nanofluid thermal conductivity and heat transfer enhancements, Heat Transfer Engineering, 29(5), 2008, 432–460.

[4] Tyler, T., Shenderova, O., Cunningham, G., Walsh, J., Drobnik, J., McGuire,G.: Thermal transport properties of diamond-based nanofluids and nanocomposites, Diamond and Related Materials,15(11-12), 2006, 2078–2081.

[5] Das, S.R., Choi, S.U.S., Patel, H.E.: Heat transfer in nanofluids–a review. Heat transfer engineering, 27(10), 2006, 3-19.

[6] Liu, M., Lin, M. C., Huang, I., Wang, C.: Enhancement of Thermal Conductivity with Carbon Nanotube for Nanofluids, International Communication on Heat Mass, 32(9), 2005, 1202-1210.

[7] Choi, S. U. S., Zhang, Z. G., Keblinski, P.: Nanofluids, in Encyclopedia of Nanoscience and Nanotechnology, American Scientific, 6, 2004, 757–737.

[8] Granqvist, C. G., Buhrman, R. A.: Journal of Applied Physics, 47(5), 1976, 2200.

[9] Choi, S. U. S., Zhang, Z. G., Yu, W., Lockwood, F. E., Grulke, E. A.: Anomalous Thermal Conductivity Enhancement in Nanotube Suspensions, Applications of Physics, 79(14), 2001, 2252-2254.

[10] Lee, S., Choi, U.S., Li, S., Eastman, J.A.: Measuring thermal conductivity of fluids containing oxide nanoparticles, Journal of Heat Transfer 121, 1999, 280–289.

[11] Eastman, J.A., Choi, U.S., Li, S., Thompson, L.J., Lee, S**.:** Enhanced Thermal Conductivity through the Development of Nanofluids. In *Nanophase and Nanocomposite Materials II.* Edited by Komarneni S, Parker JC, Wollenberger HJ. Pittsburg: Materials Research Society; 1997, 3-11.

[12] Li, Y. Zhou, J. Tung, S., Schneider, E., Xi, S.: A review on development of nanofluid preparation and characterization, Powder Technology, 196(2), 2009, 89–101.

[13] Yatsuya, S., Tsukasaki, Y., Milahama, K., Uyeda, R.: Journal of Crystal Growth, 43,1978, 490-494.

[14] Eastman, J.A., Choi, S.U.-S., Li, S. Yu, W., Thompson, L.J.: Anomalously increase effective thermal conductivities of ethylene glycol-based nanofluids containing copper nanoparticles, Appl. Phys. Lett. 78 (6), 2001, 718–720.

[15] M. Wilson, X. Hu, D. G. Cahill, P. V. Braun, “Colloidal metal particles as probes of nanoscale thermal transport in fluids,” Phys. Rev. B, 66, 2002, 224-301.

[16] Trisaksri, and Wongwises, V. S.: Critical review of heat transfer characteristics of nanofluids, renewable and sustainable energy reviews, 11, 2007, 512-523.

[17] Das, S.R., Choi, S.U.S., Patel, H.E.: Heat transfer in nanofluids–a review. Heat transfer engineering, 27, 2006, 3-19.

[18] Masuda, H., Ebata, A., Teramea, K., Hishinuma, N.: Alteration of thermal conductivity and viscosity of liquid by dispersing ultra-fine particles, *Netsu Bussei,* 4, 1993, 227-233.

[19] Eastman, J.A., Choi, U.S., Li, S., Thompson, L.J., Lee, S.: Enhanced Thermal Conductivity through the Development of Nanofluids. *In Nanophase and Nanocomposite Materials II.* Edited by Komarneni S, Parker JC, Wollenberger HJ. Pittsburg: Materials Research Society; 1997,3-11.

[20] Oztop, H.F., Abu-Nada, E.: Numerical study of natural convection in partially heated rectangular enclosures filled with nanofluids, International Journal of Heat Fluid Flow, 29, 2008, 1326-1336.

[21] http://en.wikipedia.org/wiki/Electrical_resistivity_and_conductivity (*13/06/2013).*

[22] Li, Y, Zhou, J., Tung, S., Shneider, E., Xi, S.: A Review of Development of Nanofluid Preparation and Characterization, Power Technology, 196, 89-101, 2009

[23] Abu-Nada, E., Chamkha, A.J.: Effect of nanofluid variable properties on natural convection in enclosures filled with a CuO-EG-Water nanofluid, International Journal of Thermal Sciences, 49, (2010), 2339-2352

[24] http://www.ndted.org/GeneralResources/MaterialProperties/ET/et_matlprop_index.hm.

[25] Jahanshahi, M., Hosseinizadeh, S.F., Alipanah, M., Dehghani, A., Vakilinejad, G.R.: Numerical simulation of free convection based on experimental measured conductivity in a square cavity using Water/SiO_2nanofluid, International Communications in Heat and Mass Transfer, 37 (2010), 687–694.

[26] Lee, S., Choi, S. U. S.: Application of metallic nanoparticle suspensions in advanced cooling systems, in recent advances in solids/structures and application of metallic materials, Vol. 342 /MD-Vol. 72, New York: ASME, 1996, 227-234.

[27] Wang, X., Xu, X., Choi, S. U. S.: Thermal conductivity of nanoparticle-fluid mixture, Journal of Thermophysics and Heat Transfer,13(4), 1999, 474-480.

[28] Murshed, S.M.S., Leong, K.C., Yang, C.: A Combined Model for the Effective Thermal Conductivity of Nanofluids, Applied Thermal Engineering, 29, 2009, 2477-2483.

[29] Khanafer, K., Vafai, K., Lightstone, M.: Buoyancy-driven heat transfer enhancement in a two-dimensional enclosure utilizing nanofluids, International Journal of Heat Mass andTransfer, 46, 2003, 3639 – 3663.

[30] Das, S.K., Putta, N., Thiesen, P., Roetzel, W.: Temperature dependence of thermal conductivity enhancement for nanofluids, ASME Trans. Journal of Heat Transfer, 125, 2003, 567–574.

[31] Abareshi, M., Goharshiadi, E.K., Zebarjad, S.M., Farafan, H.K., Youssefi A.: Fabrication, Characterization and Measurement of Thermal Conductivities of Fe_3O_4 Nanofluids,Journal of Magentism and Magentic Materials, 322, 2010, 3895-3901.

[32] Maxwell, J. C.: *A Treatise on Electricity and Magnetism*, Clarendon Press, Oxford, 1873.

[33] Xie, H., Wang, J., Xi, T., Liu, Y., Ai, F.: Dependence of the Thermal Conductivity of Nanoparticle-Fluid Mixture on the Base Fluid, Journal of Material Science, Nano Letters, 21(19), 2002, pp. 1469-1471.

[34] Chopkar, M., Sudarshan, S., Das, P., Manna, I.: Effect of Particle Size on Thermal Conductivity of Nanofluid, Metallic Material Transfer, 39(7), 2008, 1535-1542.

[35] Liu, M., Lin, M. C., Huang, I., Wang, C.: Enhancement of Thermal Conductivity with Carbon Nanotube for Nanofluids, International Communication on Heat Mass, 32(9), 2005, 1202-1210.

[36] Chopkar, M., Das, P. K., Manna, I.: Synthesis and Characterization of Nanofluid for Advanced Heat Transfer Applications, Scripta Mater., 55(6), 2006, 549-552.

[37] Moghadassi, A.R., Hosseini, S.M., Henneke, D.E.: Effect of CuO nanoparticles in enhancing the thermal conductivities of monoethylene glycol and paraffin fluids, Industrial Engineering and Chemistry Research, 49, 2010,1900-1904.

[38] Xie, H., Wang, J., Xi, T., Liu, Y.: Thermal Conductivity of Suspensions Containing Nanosized SiC Particles, International Journal Thermophysics, 23(2), 2002, 571-580.

[39] Murshed, S., Leong, K., Yang, C.: Enhanced Thermal Conductivity of TiO_2-Water Based Nanofluids, International Journal of Thermal Sciences, 44(4), 2005, 367-373.

[40] Zhu, H.T., Zhang, C.Y., Tang, Y.M., Wang, J.X.: Novel synthesis and thermal conductivity of CuO nanofluid, Journal of Physical Chemistry, 111,2007, 1646-1652.

[41] Zhu, D., Li, X., Wang, N., Wang, X., Gao, J., Li, H.: Dispersion behavior and thermal conductivity characteristics of Al_2O_3-H_2O nanofluids, Current Applied Physics, 9, 2009, 131-139.

[42] Hiegeister, R., Andra, W., Buske, N., Hergt, R., Hilger, I., Richter, U., Kaiser, : Applications of Magnetite ferrofluids for hyperthermia, Journal of Magenetism and Magentic Materials, 210,1999, 420-422.

[43] Li, C. H., Peterson, G. P.: Experimental Investigation of Temperature and Volume Fraction Variations on the Effective Thermal Conductivity of Nanoparticle Suspensions (Nanofluids), Journal of Applied Physics, 99(8), 2006, 084314.

[44] Beck, M., Yuan, Y., Warrier, P., Teja, A.: The Effect of Particle Size on the Thermal Conductivity of Alumina Nanofluids, Journal of Nanoparticles, 11(5),2009,1129-1136.

[45] Mintsa, H. A., Roy, G., Nguyen, C. T., Doucet, D.: New Temperature Dependent Thermal Conductivity Data for Water-Based Nanofluids, International Journal of Thermal Science, 48(2), 2009, 363-371.

[46] Turgut, A., Tavman, I., Chirtoc, M., Schuchmann, H., Sauter, C., Tavman, S.: Thermal Conductivity and Viscosity Measurements of Water-Based TiO_2 nanofluid, International Journal of Thermophysics, 30, 2009, 1213–1226.

[47] Choi, S. U. S., Zhang, Z. G., Yu, W., Lockwood, F. E., Grulke, E. A.: Anomalous Thermal Conductivity Enhancement in Nanotube Suspensions, Applications of Physics, 79(14), 2001, 2252-2254.

[48] Ding, Y., Alias, H., Wen, D., Williams, R. A.: Heat Transfer of Aqueous Suspensions of Carbon Nanotubes (CNT Nanofluids), International Journal Heat Transfer, 49, 2006, 240-250.

[49] Northrup, E. F.: Some Newly Observed Manifestations of Forces in the Interior of an Electrical Conductor, Physical Review, 24 (6), 1907, 474.

[50] Gravesen, P., Branebjerg, J., Jensen O.S., Microfluidics — review, Journal of Micromechanical Microengineering, 3, 1993, 168–182.

[51] Jang, J., Lee, S.S.: Theoretical and experimental study of MHD - magnetohydrodynamic/micropump, Sensors and Actuators, 80, 2000, 84–89

[52] Sporn, P., Kantrowitz, A.: Magnetohydrodynamics: Future Power Process?, Power 103 (11), 1959, 62–65.

[53] Steg, L., Sutton, G. W.: Prospects of MHD Power Generation, Astronautics 5, 1990, 22–25.

[54] Thess, A., Votyakov, E., Kolesnikov, Y.: Lorentz force velocimetry, Physical Review Letters, 96**,** 2006,164501.

[55] Faraday, M.: *Phil. Trans. R. Soc.* 15, 1832, 175.

[56] Shercliff, J.A.: The theory of Electromagnetic flow measurements; Cambridge university press, 1962.

[57] Feng, C. C., Deeds, W. E, Dodd, C. V.: Analysis of eddy current flow meters Journal of Applied Physics, 46, 1975, 2935–2940.

[58] Baumgartl, J., Hubert, A., Müller, G.: The use of magnetohydrodynamic effects to investigate fluid flow in electrically conducting melts, Physics of Fluids, 5 ,1993, 3280–3289.

[59] Stefani, F., Gundrum, T., Gerbeth, G.: Contactless inductive flow tomography, Physical Review, 70, 2002.

[60] Fabre, P.: Utilization des forces electromotices d'induction pour l'enregistrement des variations de vitesse des liquides conducteurs: un nouvel hemodromographe sans palette dans le sand, Compt. Rend. Acad. Sci ,194, 1097, 1932.

[61] Kolin, A.: Electromagnetic flow meter. Principles of the method and its application to blood flow measurements, Proc. Soc. Exper. Biol. Med,46(2) 35, 1936, 53.

[62] Kolesnichenko, A. F.: Electromagnetic Processes in Liquid Material in the USSR and Eastern European Countries, Iron and Steel Institute of Japan (ISIJ), 30 (1), 1990, 8–26.

[63] Khristinich, R.M., Timofeyev, V.N., Stafievskaya, V.V., Velenteyenko, A.V.: Molten Metal Electromagnetic Stirring in Metallurgy, International Scientific Colloquim,2003, 26-36.

[64] Wang, L., Fan,J.: Nanofluids Research: Key Issues, Nanoscale Research Letters, 5, 2010, 1241–1252.

[65] Kaufui, V. W., Omar D. L.: Applications of Nanofluids: Current and Future, Advances in Mechanical Engineering, 2010, Article ID 519659, 11 pages, doi:10.1155/2010/519659.

[66] Senthilraja, S., Karthikeyan, M., Gangadevi, R.: Nanofluid applications in future automobiles: comprehensive review of existing data", Nano-Micro Lett. 2, 306-310 (2010). doi:10.3786/nml.v2i4.p306-310.

[67] Yu, W., Xie, H.: A review of Nanofluids: Preparations, Stability Mechanisms and Applications, Journal of Nanomaterials, Vol 2012, Article ID 435873, 17pages, doi:10.1155/2012/435873.

[68] Trisaksri, V., Wongwises,S.: Critical review of heat transfer characteristics of nanofluids, Renewable and Sustainable Energy Reviews,11(3), 2007,512–523.

[69] zerinc, S. O., Kakac, S., YazIcIoglu, A. G.: Enhanced thermal conductivity of nanofluids: a state-of-the-art review, Microfluidics and Nanofluidics, 8(2), 2010, 145–170.

[70] Wong, K. V., Leon, O.: Applications of nanofluids: current and future, Advances in Mechanical Engineering, Article ID 519659, 11 pages, 2010.

[71] Arruebo, M., Fern´andez-Pacheco, R., Ibarra, M.R., Santamar´ıa, J.: Magnetic nanoparticles for drug delivery, Nano Today, 2(3),20017, 22–32.

[72] Routbort, J.L., Wu, Y., France, D.M, Singh, D., Timofeeva, E.V., Smith, D.S.: Argonne National Lab, Michellin North America, St. Gobain Corp., 2009, http://www1.eere.energy.gov/industry/nanomanufacturing/pdfs/nanofluids/industrial cooling.pdf.

[73] Nelson, I. C., Banerjee, D, Ponnappan, R.: Flow loop experiments using polyalphaolefin nanofluids, Journal of Thermophysics and Heat Transfer, 23(4), 2009, 752–761, 2009

[74] Ma, K. Q., Liu, J.: Nano liquid-metal fluid as ultimate coolant, Physics Letters Section A, 361(3), 2007, 252– 256.

[75] Donzelli, G., Cerbino, R., Vailati, A.: Bistable heat transfer in a nanofluid, Physical Review Letters, 102(10), Article ID 104503, 2009, 4pages.

[76] Kim, S. J., Bang, I. C., Buongiorno, J., Hu, L. W.: Study of pool boiling and critical heat flux enhancement in nanofluids, Bulletin of the Polish Academy of Sciences Technical Sciences, 55(2), 2007, 211–216.

[77] Kim, S. J. Bang, I. C., Buongiorno, J., Hu, L. W.: Surface wettability change during pool boiling of nanofluids and its effect on critical heat flux, International Journal of Heat and Mass Transfer, 50(19-20), 2007, 4105–4116.

[78] Boungiorno, J., Hu, L.W., Kim, S. J., Hannink, R. Truong, B., Forrest, E. :Nanofluids for enhanced economics and safety of nuclear reactors: an evaluation of the potential features issues, and research gaps, Nuclear Technology, 162(1), 2008, 80–91.

[79] Buongiorno, J., Hu, L. W., Apostolakis, G., Hannink, R., Lucas, T., Chupin, A.: A feasibility assessment of the use of nanofluids to enhance the in-vessel retention capability in light-water reactors, Nuclear Engineering and Design, 239(5), 2009, 941–948.

[80] Yu, W., Xie, H.: A Review on Nanofluids: Preparation, Stability Mechanisms, and Applications, Journal of Nanomaterials, Volume 2012, Article ID 435873,17pages, doi:10.1155/2012/435873

[81] Saidur, R. , leong, K.Y., Mohammed, H.A.: A review on applications and challenges of nanofluids, Renewable and Sustainable Energy Reviews, 15, 2011, 1646-1668

[82] Jang, Choi, S. U. S.: Cooling performance of a microchannel heat sink with nanofluids, Applied Thermal Engineering, 26(17-18), 2006, 2457–2463.

[83] Chen, Y. T., Wei, W.C., Kang, S.W., Yu, C.S.: Effect of nanofluid on flat heat pipe thermal performance, in Proceedings of the 24th IEEE Semiconductor Thermal Measurement and Management Symposium (SEMI-THERM ’08),March 2006.

[84] Vafaei, S., Borca-Tasciuc, T., Podowski, M.Z, Purkayastha, A., Ramanath, G., Ajayan, P. M.: Effect of nanoparticles on sessile droplet contact angle, Nanotechnology, 17(10), 2006, 2523–2527.

[85] Dash, R. K., Borca-Tasciuc, T., Purkayastha, A., Ramanath, G.: Electrowetting on dielectric-actuation of micro-droplets of aqueous bismuth telluride nanoparticle suspensions, Nanotechnology, vol. 18, no. 47, Article ID 475711, 6pages, 2007.

[86] Singh, D., Toutbort, J., Chen, G.: Heavy vehicle systems optimization merit review and peer evaluation, Annual Report, Argonne National Laboratory, 2006.

[87] Kao, M. J., Lo, C. H., Tsung, T. T., Wu Y. Y., Jwo, C. S., Lin, H. M.: Copper-oxide brake nanofluid manufactured using arc- submerged nanoparticle synthesis system, Journal of Alloys and Compounds, 434-435, 2007, 672–674.

[88] Kao, M. J., Chang, H., Wu, Y. Y., Tsung, T. T., Lin, H. M. : Producing aluminum oxide brake nanofluids using plasma charging system, Journal of the Chinese Society of Mechanical Engineers, 28(2), 2007, 123–131.

[89] Kulkarni, D. P., Das, D. K., Vajjha, R. S.: Application of nanofluids in heating buildings and reducing pollution, Applied Energy, 86(12), 2009, 2566–2573.

[90] Răcuciu, M.: Recent Advances in Biological and Medical Applications of Magnetic Fluids, Tomul II, s. Biofizică, Fizică medicală şi Fizica mediului, 2006.

[91] Alexiou, C., Arnold, W., Klein, R. J., Parak, F. G., Hulin, P., Bergemann, C., Erhardt, W. Wagenpfeil, S., Lübbe, A.S.: Locoregional cancer treatment with magnetic drug targeting, Cancer Res., 60, 2000, 6641-6648.

[92] R&D Digest, Using Magnetic Fluids to Repair Damaged Retinas, MDDI, New Technologies, 2002, 39.

[93] Shawgo, R. S., Grayson, A.C.R., Li, Y., Cima, M.J.: BioMEMS for drug delivery, Current Opinion in Solid State and Materials Science, 6(4), 2002, 329 - 334,.

[94] Cepheid, 2009, http://www.Cepheid.Com.

[95] Ovsianikov, A., Chichkov, B., Mente, P., Monteiro- Riviere, N.A., Doraiswamy, A, Narayan, R.J.: Two photon polymerization of polymer-ceramic hybrid materials for transdermal drug delivery, International Journal of Applied Ceramic Technology, 4(1), 2007, 22–29.

[96] Kim, K., Lee, J.-B.: High aspect ratio tapered hollow metallic microneedle arrays with microfluidic interconnector,Microsystem Technologies, 13(3-4), 2007, 231-235.

[97] Labhasetwar, V., Leslie-Pelecky, D.L.: Biomedical Applications of Nanotechnology, John Wiley & Sons, New York, NY, USA, 2007.

[98] Yan, J.-F., Liu, J.: Nanocryosurgery and its mechanisms for enhancing freezing efficiency of tumor tissues, Nanomedicine, 4(1), 2008, 9–87.

[99] Faraday, M.: Experimental Researches in Electricity, Second Series, Philos Tran Roy Soc. London, 122, 163-194.

[100] Alfven, H. L.: Existence of electromagnetic-hydrodynamic waves, Nature, 150, 1942, 405-406.

[101] Larmor, J.:A rotational origin of magnetic fields of sun and earth, Electrical Review 85: 412, Reprinted in Engineering, 108,1919, 461.

[102] Moreau, R. : *Magnetohydrodynamics, Kluwer Academic Publishers*, Dordrecht, 1990.

[103] Hartmann, J., Lazarus, J.: Hg-Dynamics II, Theory of Laminar Flow of Electrically Conductive Liquids in a Homogeneous Magnetic Field, 15(7), 1937.

[104] Smirnov, V.P.: Tokomak Foundation In Russia 1950-1990, Nuclear Fusion, 50, 2010.

[105] Alan, P.A.: An Introduction to Magnetohydrodynamics, Cambridge University Press, 2001.

[106] Rossow, V.J.: On the flow of electrically conducting fluids over a flat plate in the presence of a transverse magnetic field, NASA report No. 1358 (1958).

[107] Samad, M.A., Mohebujjaman, M.: MHD Heat and Mass Transfer Free Convection Flow along a Vertical Stretching Sheet in Presence of Magnetic Field with Heat Generation, Research Journal of Applied Sciences, Engineering and Technology 1(3), 98 106, 2009

[108] Sakiadis, B.C.: Boundary layer behavior on continuous solid flat surfaces. AICHE Journal, 7: 1961, 26-28.

[109] Tsou, F.K., Sparrow, E.M., Goldstein, R.J.. Flow and heat transfer in the boundary layer on a continuous moving surface. Int. J. Heat Mass Transfer, 10: 1967219-235.

[110] Ibrahim, S.Y., Makinde,O.D.: Chemically reacting MHD boundary layer flow of heat and mass transfer past a moving vertical plate with suction, Scientific Research and Essays, 5 (19), 2010, 2875-2882.

[111] Makinde, O.D.: On MHD heat and mass transfer over a moving vertical plate with a convective surface boundary condition, Canadian Journal of Chemical Engineering, 88, 2010, 983-990.

[112] Makinde, O.D.: On MHD boundary-layer flow and mass transfer past a vertical plate in a porous medium with constant heat flux, Engineering papers and reports, paper 13, 2009.

[113] Singh, A.K., Gholami, H.R., Soundalgekar, V.M.: Transient free convection flow between two vertical parallel plates, Heat and Mass Transfer, 31, 1996, 329-333.

[114] Jha, B.K.: Natural Convection in Unsteady MHD Couette Flow, Heat and Mass Transfer, 37, 2001, 329-331.

[115] Makinde, O.D.: Free-convection flow with thermal radiation and mass transfer past a moving vertical porous plate'', International Communications in Heat and Mass Transfer, 32, 2005, 1411-19.

[116] Hossain, M.M.T. , Mojumder, R.: Similarity solution for the steady natural convection boundary layer flow and heat transfer above a heated horizontal surface with transpiration, International Journal of Applied Mathematics and Mechanics, 6(4), 2010, 1-16.

[117] Ibrahim, S. Y, Makinde, O. D.: Chemically reacting MHD boundary layer flow of heat and mass transfer over a moving vertical plate with suction, Scientific Research and Essays, 5(19), 2010, 2875-2882.

[118] Makinde, O.D., Olajuwon, B.I., Gbolagade, A.W.: Adomian decomposition approach to a boundary layer flow with thermal radiation past a moving vertical porous plate. International Journal of Applied Mathematics and Mechanics, 3(3), 2007,62-70.

[119] Ali, M.E.: Heat transfer characteristics of a contious stretching surface. – Warme Stoffuberttragung, 29, 1994, 227-234.

[120] Li, Q., Xuan, Y.: Experimental investigation on transport properties of nanofluids, in Heat Transfer Science and Technology 2000 (ed. Wang Buxuan), Beijing: Higher Education Press, 2000, 757-762.

[121] Xuan, Y.M., Li, Q.: Heat transfer enhancement of nanofluids, International Journal of Heat Fluid Flow, 21, 2000, 58–64.

[122] Jang, S.P., Choi, S.U.S.: Role of Brownian motion in the enhanced thermal conductivity of nanofluids. Applied Physics Letters, 84,2004, 4316-4318.

[123] Evans, W., Fish, J., Keblinski, P.: Role of Brownian motion hydrodynamics on nanofluid thermal conductivity. Applied Physics Letters, 88, 2006, 093116-1 0931161-3.

[124] Chang, B.H , Mills, A.F: Natural convection of microparticle suspensions in thin enclosures. International Journal of Heat mass transfer. 51, 2008, 1332-1341.

[125] Putra, N., Roetzel, W., Das, S.K.: Natural convection of nanofluids. Heat Mass Transfer, 39, 2003,775–84.

[126] Bernaz, L.,Bonnet, J.M., Seiler, J.M.: Investigation of natural convection heat transfer to the cooled top boundary of a heated pool. Nuclear Engineering and Design 204 (2001), 413–427

[127] Khanafer, K., Vafai, K., Lightstone, M.: Buoyancy-driven heat transfer enhancement in a two-dimensional enclosure utilizing nanofluids, International Journal of heat Mass transfer, 46, 2003, 3639-3653.

[128] Wen, D., Ding, Y.: Experimental Investigation into Convective Heat Transfer of Nanofluids at the Entrance Region under Laminar Flow Conditions, International Journal Heat Mass Transfer, 47, 2004,5181–5188.

[129] Rong,Y. J, Sheng,C. T.:Numerical research of nature convective heat transfer enhancement filled with nanofluids in rectangular enclosures, International Journal, 33, 2006, 727-736.

[130] Ho, C.J.,Chen, M.W, Li, Z.W.: Numerical simulation of natural convection of nanofluid in a square enclosure: Effects due to uncertainties of viscosity and thermal conductivity, International Journal, 51, 2008, 4506–4516.

[131] Xuan, Y., Li, Q.: Investigation on Convective Heat Transfer and Flow Features of Nanofluids. ASME J HeatTransfer, 125, 2003, 151-5.

[132] Pak, B. C., Cho, Y. I.: Hydrodynamic and heat transfer study of dispersed fluids with submicron metallic oxide particles, Experimental Heat Transfer, 11, 1998, 51-170

[133] Tahery, A.A, Pesteei, S.M, Zehforoosh, A.: International Journal of Chemical Engineering and Applications, 1(1), June 2010.

[134] Hakan, F. O., Eiyad, A.: Numerical study of natural convection in partially heated rectangular enclosures filled with nanofluids, Int. J. 29, 2008, 1326–1336.

[135] Maïga, S.E.B, Palm, S.J, Nguyen, C.T., Roy, G., Galanis, N.: Heat transfer enhancement by using nanofluids in forced convection flows, Int. J. Heat and Fluid Flow, 26 (2005) 530–546.

[136] Peyghambarzadeh, S.M., Hashemabadi, S.H., Hoseini, S.M., Seifi Jamnani, M.: Experimental study of heat transfer enhancement using water/ethylene glycol based nanofluids as a new coolant for car radiators, International Communications in Heat and Mass Transfer, 38, 2011, 1283–1290

[137] Assael, M.J., Metaxa, I.N, Kakosimos, K., Konstadinou, D.: Thermal conductivity of nanofluids – Experimental and Theoretical, Chemical Engineering Department, Aristotle University, 54124 Thessaloniki, Greece.

[138] Anjali, S.P., Andrews, J.: Laminar Boundary Layer Flow on a Nanofluid over a flat plate, International Journal of Maths and Mechanics, 7(6), 2011, 52-71.

[139] Popa, C., Polidori, G., Arfaoui, A., Fohanno, S.: Heat and Mass Transfer in External Boundary Layer Flows Using Nanofluids, Heat and Mass Transfer – Modeling and Simulation, Intech, 5, 2011,95-116.

[140] Aziz A: A similarity solution for laminar thermal boundary layer over a flat plate with a convective surface boundary condition. Commun Nonlinear Sci Numer Simul, 14, 2009,1064-1068.

[141] Makinde OD, Aziz A: MHD mixed convection from a vertical plate embedded in a porous medium with a convective boundary condition. Int J Therm Sci, 49, 2010, 1813- 1820.

[142] Ishak A: Similarity solutions for flow and heat transfer over a permeable surface with convective boundary condition. Appl Math Comput, 217, 2010, 837-842.

[143] Nourazar, S.S, Habibi Matin, M., Simiari, M.: The HPM Applied to MHD Nanofluid Flow over a Horizontal Stretching Plate, Hindawi Publishing Corporation, Journal of Applied Mathematics, Volume 2011, Article ID 876437, 17 pages, doi:10.1155/2011/876437.

[144] Hamad, M.A.A, Pop, I., Ismail, A.I.: Magnetic field effects on free convection flow of a nanofluid past a vertical semi-infinite flat plate, Nonlinear Analysis: Real World Applications 12, 2011, 1338–1346.

[145] Hamad, M.A.A.: Analytical solution of natural convection flow of a nanofluid over a linearly stretching sheet in the presence of magnetic field, International Communications in Heat and Mass Transfer, 38, 2011, 487–492.

[146] Ghasemi, B., Aminossadati, S.M., Raisi, A.: Magnetic field effect on natural convection in a nanofluid-filled square enclosure, International Journal of Thermal Sciences, 50, 2011, 1748-1756.

[147] Kuznetsov, A.V., Nield, D.A.L Natural convective boundary- layer flow of a nanofluid past a vertical plate. International Journal of Thermal Sciences, 49, 2010, 243–247.

[148] Chaudhary, M.A., Merkin, J.H.: The effect of blowing and suction on free convection boundary layers on vertical surface with prescribed heat flux, J. Eng. Math, 27, 1993, 265–292.

[149] Al-Sanea, S.A.: Mixed convection heat transfer along a continuously moving heated vertical plate with suction or injection, Int. J. Heat Mass Transf, 47,2004, 1445–1465

[150] Ishak, A., Nazar, R., Pop, I.: Boundary layer on a moving wall with suction and injection, Chin.Phys. Lett., 24, 2007, 2274–2276.

[151] Bachok, N., Ishak, A., Pop, I.: Boundary layer flow over a moving surface in a nanofluid with suction or injection, Acta Mech. Sin., 281, 2012, 34–40.

[152] Bachok, N., Ishak, A., Pop, I.: Boundary layer flow of nanofluids over a moving surface in a flowing fluid, Int. J. Thermal Sci. 49, 2010, 1663-1668.

[153] Makinde, O.D., Aziz, A.: Boundary layer flow of a nanofluid past a stretching sheet with a convective boundary condition, Int. J. Thermal Sciences, 50, 2011,1326-1332.

[154] Ahmad, S., Rohni, A.M., Pop, I.: Blasius and Sakiadis problems in nanofluids, Acta Mechanica, 218, 2011, 195–204.

[155] Buongiorno, J.: Convective transport in nanofluids. ASME Journal of Heat Transfer, 128, 2006, 240–250.

[156] Motsumi, T. G., Makinde, O. D.: Effects of thermal radiation and viscous dissipation on boundary layer flow of nanofluids over a permeable moving flat plate. Phys. Scr. 86 (2012) 045003 (8pp). doi:10.1088/0031-8949/86/04/045003.

[157] Nachtsheim, P. R., Swigert, P.: Satisfaction of the asymptotic boundary conditions in numerical solution of the system of nonlinear equations of boundary layer type NASA Technical Report Server NASA TND-3004, 1965.

[158] Florio, L.A., Harnoy, A.: Combination technique for improving natural convection cooling in electronics, International Journal of Thermal Science, 46(1), 2007, 76–92.

[159] Lim, K.O., Lee, K.S., Song, T.H.: Primary and secondary instabilities in a glass melting surface, Numerical Heat Transfer A- Application, 36(3), 1999, 309–325.

[160] Singh, S., Sharif, M.A.R.: Mixed convective cooling of a rectangular cavity with inlet and exit openings on differentially heated side walls, Numerical Heat Transfer A Application, 44 (3), 2003, 233–253.

[161] Tan, F.L., Hosseinizadeh, S.F., Khodadadi, J.M., Fan, L.: Experimental and computational study of constrained melting of phase change materials (PCM) inside a spherical capsule, International Journal of Heat and Mass Transfer, 19–20, 2009, 4105–4116.

[162] Patil, P.M., Kulkarni, P.S.: Effects of chemical reaction on free convective flow of a polarfluid through a porous medium in the presence of internal heat generation, International Journal of Thermal Science, 47(8), 2008, 1043–1054.

[163] Lamsaadi, M., Naimi, M., Hasnaoui, M., Mamou, M.: Natural convection in a vertical rectangular cavityfilled with a non-Newtonian power lawfluid and subjected to a horizontal temperature gradient, Numerical Heat Transfer A-Application, 49(10), 2006, 969–990.

[164] Saha, L.K., Hossain, M.A., Gorla, R.S.R.: Effect of Hall current on the MHD laminar natural convection flow from a vertical permeable flat plate with uniform surface temperature, International Journal of Thermal Science, 46(8), 2007, 790–801.

[165] Uddin, M.J., Khan, W.A., Ismail, A. I.: MHD Free Convective Boundary Layer Flow of a Nanofluid past a Flat Vertical Plate with Newtonian Heating Boundary Condition, PLoS ONE, 7(11), 2012, 49499. doi:10.1371/journal.pone.0049499.

[166] Schaefer, H.: Nanoscience: The Science of the Small in Physics, Engineering. Chemistry, Biology and Medicine (Nanoscience and Technology), Publisher: Springer, 2010.

[167] Capretto, L., Cheng, W., Hill, M., Zhang, X.: Micro-mixing within microfluidic devices, Top Current Chemistry, 304, 2011, 27–68.

[168] Kleinstreuer, C., Li, J., Koo, J.: Microfluidics of nano-drug delivery, International Journal of Heat Mass Transfer, 51, 2008, 5590–5597.

[169] Chamkha, A.J., Aly, A. M.: MHD free convection flow of a nanofluid past a vertical plate in the presence of heat generation or absorption effects. Chem Eng Comm, 198, 2011, 425–441.

[170] Zeeshan, A., Ellahi, R., Siddiqui, A.M., Rahman, H.U.: An investigation of porosity and magnetohydrodynamic flow of non-Newtonian nanofluid in coaxial cylinders, International Journal of Physical Science, 7(9), 2012, 1353–1361.

[171] Matin, M.H., Nobari, M.R.H., Jahangiri, P.: Entropy analysis in mixed convection MHD flow of nanofluid over a non-linear stretching sheet. Journal of Thermal Science and Technology, 7, 2012, 104-109.

[172] Uddin, Md. J., Khan, W. A., Md. Ismail, A.I.: Scaling Group Transformation for MHD Boundary Layer Slip Flow of a Nanofluid over a Convectively Heated Stretching Sheet with Heat Generation, Mathematical Problems in Engineering, Volume 2012, Article ID 934964,20pages, doi:10.1155/2012/934964.

[173] Ferdows, M., Md. Khan, S., Md. Alam, M., Sun, S.: MHD Mixed Convective Boundary Layer Flow of a Nanofluid through a Porous Medium due to an Exponentially Stretching Sheet, Mathematical Problems in Engineering Volume 2012, Article ID 408528,21pages doi:10.1155/2012/408528.

[174] Rosmila, A. B., Kandasamy, R., Muhaimin, I.: Lie symmetry group transformation for MHD natural convection flow of nanofluid over linearly porous stretching sheet in presence of thermal stratification, Applied Mathematics and Mechanics, Appl. Math. Mech. -Engl. Ed., 33(5), 2012, 593–604, DOI 10.1007/s10483-012-1573-9.

[175] Aziz, A., Khan, W.A.: Natural convective boundary layer flow of a nanofluid past a convectively heated vertical plate, International Journal of Thermal Sciences, 52, 2012, 83-90.

[176] Na, T.Y.: Computational Methods in Engineering Boundary Value Problems, Academic Press, New York, 1979.

[177] Singh, K.R., Cowling, T.G.*:* Effect of magnetic field on free convective flow of electrically conducting fluids past a semi-infinite flat plate, Quarterly Journal of Mechanics and Applied Mathematics*,* 16, 1963, 1-15.

[178] Ahmmed, S. F., Alam Sarker, M. S., MHD natural convection flow of viscous incompressible fluid from a vertical flat plate, Journal of Physical Sciences*,* 13, 2009, 77-85.

[179] Anjali Devi, S.P., Kayalvizhi, M.: Analytical solution of MHD flow with radiation over a stretching sheet embedded in a porous medium, International Journal of Applied Mathematics and Mechanics, 6(7), 2010, 82 -106.

[180] Rajesh, V.: Radiation effects on MHD free convection flow near a vertical plate with ramped wall temperature, International Journal of Applied Mathematics and Mechanics, 6(21),2010, 60 – 77.

[181] Reddy, M.G., Reddy, N.B.: Soret and Dufour effects on steady MHD free convection flow past a semi-infinite moving vertical plate in a porous medium with viscous dissipation, International Journal of Applied Mathematics and Mechanics, 6(1), 2010, 1 – 12.

[182] Anjali Devi, S.P., Wilfred Samuel Raj, J.: Thermo-diffusion effects on unsteady hydromagnetic free convection flow with heat and mass transfer past a moving vertical plate with time dependent suction and heat source in a slip flow regime, International Journal of Applied Mathematics and Mechanics, 7(21), 2010, 20-51

[183] Makinde, O.D.: Computational Modelling of MHD unsteady Flow and Heat Transfer Towards a Flat Plate with Navier Slip and Newtonian Heating, Brazilian Journal of Chemical Engineering, 29(1), 2012, 159 – 166.

[184] Mukhopadhyay, S., Md. Uddin, S., Layek, G.C.: Lie Group Analysis on MHD Boundary Layer Slip Flow Past a Heated Stretching Sheet in Presence of Heat Source/Sink, International Journal of Applied Mathematics and Mechanic, 8(1), 2012, 51-66.

[185] Eldesoky, I.M.: Influence of slip condition on peristaltic transport of a compressible maxwell fluid through porous medium in a tube, International Journal of Applied Mathematics and Mechanics, 8(2), 2012, 99-117.

[186] Aziz, A.: Hydrodynamic and thermal slip flow boundary layers over a flat plate with constant heat flux boundary condition, Communications in Nonlinear Science and Numerical Simulations, 15, 2010, 573-580.

[187] Navier, C.L.M.H.: Mémoire sur les lois du mouvement des fluides. Mém, *A*cademic Research Science Institute of France, 6, 1823, 389-440.

[188] Singh, G., Makinde, O. D.: MHD Slip Flow of Viscous Fluid Over an Isothermal Reactive Stretching Sheet, Annals of Faculty Engineering Hunedora – Internal Journal of Engineering, Toxe XI, Fascile 2. ISSN 1584 – 2665, 2013.

[189] Md. Uddin, J., Pop, I., Md. Ismail, A.I.: Free Convection Boundary Layer Flow of a Nanofluid from a Convectively Heated Vertical Plate with Linear Momentum Slip Boundary Condition, Sains Malaysiana, 41(11), 2012,1475-1482.

[190] Martin, M.J., Boyd, I.D.: Falkner-Skan flow over a wedge with slip boundary conditions, AIAA Journal of Thermo physics and Heat Transfer, 24(2), 2010, 263-270.

[191] Bhattacharyya, K., Mukhopadhyay, S., Layek, G.C.: MHD boundary layer slip flow and heat transfer over a flat plate, China Physics Letters, 28(2), 2011, 024701.

[192] Tiwari, R.K., Das, M.K.: Heat transfer augmentation in a two-sided lid-driven differentially heated square cavity utilizing nanofluids, International Journal of Heat Mass Transfer, 50, 2007, 2002–18.

[193] Ahmed, S.E., Mahdy, A.: Natural Convection Flow and Heat Transfer Enhancement of a Nanofluid past a Truncated Cone with Magnetic Field Effect, World Journal of Mechanics, 2, 2012, 272-279.

APPENDIX

APPENDIX I: Articles Published or accepted for publication

1. W. N. Mutuku-Njane, O. D. Makinde, On Hydromagnetic Boundary Layer Flow of Nanofluids Over a Permeable Moving Surface with Newtonian Heating, Latin American Applied Research, Vol. 44, No.1, 2014.
2. W. N. Mutuku-Njane, O. D. Makinde, Hydromagnetic thermal boundary layer of nanofluids over a convectively heated flat plate with viscous dissipation and Ohmic heating, University Politehnica of Bucharest Scientific Bulletin – series A – Applied mathematics and physics - Accepted and in press, 2013.
3. Mutuku-Njane, W.N.; Makinde, O. D., MHD Nanofluids Flow over a Permeable Vertical Plate with Convective heating, Journal of Computational and Theoratical Nanoscience, Volume 11, No. 3, 667-675, 2014.
4. W. N. Mutuku-Njane, O. D. Makinde, Combined Effect of Buoyancy Force and Navier Slip on MHD Flow of a Nanofluid over a Convectively Heated Vertical Porous Plate, The Scientific World Journal, Volume 2013, Article ID 725643, 8pages, http://dx.doi.org/10.1155/2013/725643.

APPENDIX II: Letters of Acceptance of Articles

Acceptance Letters 1:

On Monday, July 15, 2013 1:27 PM, florentina minca <scientificbulletin@yahoo.com> wrote:

Dear Madam,
Your paper was accepted for publication.

Best regards,
Florentina Minca